A REASSESSMENT OF ANNUAL WATER BALANCES FOR OIL SANDS RECLAMATION SOIL COVERS PLACED OVER COKE

A Thesis Submitted to the College of

Graduate and Postdoctoral Studies

In Partial Fulfillment of the Requirements

For the Degree of Master of Science

In the Department of Civil, Geological and Environmental Engineering

University of Saskatchewan

Saskatoon, SK

By

Matthew Armoh

PERMISSION TO USE

In presenting this thesis in partial fulfilment of the requirements for a Postgraduate degree from the University of Saskatchewan, I agree that the Libraries of this University may make it freely available for inspection. I further agree that permission for copying of this thesis in any manner, in whole or in part, for scholarly purposes may be granted by the professor or professors who supervised my thesis work or, in their absence, by the Head of the Department or the Dean of the College in which my thesis work was done. It is understood that any copying or publication or use of this thesis or parts thereof for financial gain shall not be allowed without my written permission. It is also understood that due recognition shall be given to me and to the University of Saskatchewan in any scholarly use which may be made of any material in my thesis. Requests for permission to copy or to make other use of material in this thesis in whole or part should be addressed to:

Department of Civil, Geological and Environmental Engineering

University of Saskatchewan

3B48 Engineering building 57 Campus Drive

Saskatoon, Saskatchewan S7N 5A9

Alternatively, requests for permission to copy or to make other use of material in this thesis in whole or part may also be addressed to:

Dean

College of Graduate and Postdoctoral Studies

University of Saskatchewan

116 Thorvaldson Building, 110 Science Place

Saskatoon, Saskatchewan S7N 5C9 Canada

ABSTRACT

There were initial concerns that the soil covers constructed by Syncrude Canada on the Coke Beach Instrumented Watershed were experiencing elevated water losses which was limiting revegetation plant growth. Previous studies conducted on the site aimed at unravelling the cause of the accelerated water loss but failed in achieving this objective. However, these studies found that the enhanced drying of the covers may be due to other processes than the water balance components but not convective air flow. A bypass flow was hypothesised to be the likely cause of the accelerated drying of the covers. From this background, this study was designed to; Construct a daily water balance for long-term (2005-2017) monitoring data set based on field meteorological and soil monitoring data; a) develop a calibrated physics based model of the hydrologic performance of the two reclamation covers using a soil-vegetation-atmosphere transfer (SVAT) model; b) use this calibrated SVAT model to identify the key processes controlling the hydrological performance of the reclamation covers with a focus on identifying which processes (e.g. preferential flow, convective air flow) or hydraulic properties (e.g. dual porosity water flow storage) have the greatest influence over performance.

In achieving these objectives, this study adopted two approaches (system dynamics and physics-based model) in constructing the daily water balance and to identify which processes control the hydrological performance of the covers.

From the results of the water balance components using the system dynamics model, a mean AET of 38% of the annual mean PPT was found to be lost to the atmosphere on the shallow cover while on the deep cover, a mean AET of 44% of mean annual PPT was found to be lost. The mean net percolation for the shallow cover was 63% of annual PPT compared to the mean net percolation of 58% of annual PPT lost through the deep cover. Comparing the change in water ability of the covers, the shallow cover was found to be losing -2% of annual PPT while the deep cover lost -3% of the annual PPT.

From the detail evaluation of the water storage ability of the covers, it appears the SD approach underestimates the AET and overestimates net percolation in this scenario and hence the results by the SD approach may not be the reality.

With the simulated water balance approach (physics-based model) a mean AET of 76% of annual PPT was observed to be lost to the atmosphere on the shallow cover compared to a mean AET of 86% of annual PPT found to be lost on the deep cover. Similarly, the mean percentage of precipitation released as NP was 24% on the shallow cover and 21% on the deep cover. The predominant volume of NP was associated with snowmelt and rainfall while the cover was frozen. The higher AET on the deep cover than the shallow cover is an indication of the additional water stored within the thicker cover and available for use by vegetation.

From the water balance components volumes estimated by the physics-based model, evapotranspiration was identified by this study as the main component greatly influencing the performance of the covers and causing the elevated drying in the growing season, followed by the net percolation.

ACKNOWLEDGEMENT

My sincere gratitude to God Almighty for giving me the strength, understanding and directing me to achieve this feat. A special thank you to my supervisor and mentor, Dr Lee Barbour for his patience, encouragement, commitment, support and guidance through this journey. To my co-supervisor, Dr Mingbin Huang, I appreciate your time and directions to that has contributed to the success of the work. Again, my sincere appreciation goes to my committee members, Dr Warren Helgason and Dr Terrance Fonstad.

The success of this thesis has been possible by the funds and data supports provided in diverse ways by Syncrude Canada Ltd and its staffs. I say thank you to Amy Heidman of O'KANE Consultant for her willingness to provide data and information any time.

Also, my sincere appreciation goes to my lab friends, especially Yolanda Tang and Shahabul Alam for their assistance in diverse ways.

Again, I would like to thank my Mother, brothers and sisters and friends back home for their support and in diverse ways. My final appreciation goes to my wife, Vida and my son, Michael for their love, understanding, patience and encouragement. They have been a source of motivation for the successful completion of my degree.

TABLE OF CONTENTS

LIST OF TABLES

LIST OF FIGURES

LIST OF ABBREVIATIONS

AET	Actual Evapotranspiration
AE	Actual evaporation
AT	Actual transpiration
AW	Available soil water
AWC	Available water capacity of the soil
f	Functional relationship
FAO	Food and Agricultural Organisation
CNRL	Canadian Natural Resources
CEMA	Cumulative Environmental Management Association
ds	Average depth of snowpack
FFT	Fluid Fine Tailing
EPEA	Environmental Protection and Enhancement Act
LCCS	Land Capability Classification System
PWP	Permanent wilting point
PET	Potential Evapotranspiration
FC	Field Capacity
WP	Wilting Point
AWHC	Available water holding capacity
CS229	Campbell Scientific thermal conductivity sensors
CS616	Campbell Scientific TDR sensors
TDR	Time domain reflectometry
CBIW	Coke beach instrumented watershed
SCL	Syncrude Canada, ltd.
OKC	O'Kane Consultants, Inc.
cm	centimetres

cm^2	centimeter square
cm^3	Cubic centimetres
g	Gravitational constant
m^2	square metres
m3	Cubic metres
MLSB	Mildred Lake Settling Basin
NP	Net percolation
Pa	Pascals
kPa	Kilopascals
kg	Kilogramme
PPT	Precipitation
SWE	Snow-water equivalence
SWCC	Soil water characteristic curve
S	Degree of saturation
SVAT	Soil-Vegetation-Atmospheric Transport Model
RI	Runoff and interflow
VWC	Volumetric water content
ea	Actual vapour pressure vapour pressure
es	Saturated vapour pressure
RH	Relative humidity
q	flux
SBH	South Bison Hills
SW30	South West 30 Overburden Dump
ETo	Reference evapotranspiration
LAI	Leaf Area Index
DAS	Data acquisition system
FM-EL	Flow model with enhanced infiltration
*P*s	Average density of snow
*P*w	Density of water

Kφ	Hydraulic conductivity at suction
φ	Suction
i	Hydraulic gradient
θ_i	Soil water content
θ_r	Residual soil water content
θ_s	Saturated soil water content
S_e	Effective saturation
$\propto, m, n$	Empirical fitted parameters
h	Pressure head
SD	Systems Dynamics Model
IM	Inverse Modelling

CHAPTER 1

INTRODUCTION

Oil sands mining in northern Alberta generates large volumes of surface waste deposits such as overburden, sand tailings, fluid fine tailings (FFT) and petroleum coke (Lahmira et al.2013). Petroleum coke, or simply coke, is a by-product of oil sands upgrading that is considered as a potential future energy source and consequently must be disposed of in a manner that allows for future extraction. The coke is comprised primarily of carbon (over 90%) (Alberta Energy Regulator, 2015).

The oil sands mines operated by Syncrude, Canada Limited (SCL), Suncor and CNRL Horizon near Fort McMurray produce coke. A portion of the coke is used for energy production - Suncor uses about 10 percent of its annual coke production as site fuel while SCL used 21 percent of its annual coke production as site fuel in 2014. All the coke generated by CRNL at its Horizon mine is stockpiled. A 2014 coke inventory indicated that there was 90 million tonnes of stockpiled coke with an annual production of 6 million tonnes (Alberta Energy Regulator, 2015).

Mine closure design requires that disturbed land and mining waste must be reclaimed to an equivalent capability (e.g. ability to support flora and fauna) as to what existed prior to mining before the land is returned to the Crown (Government, 2011). Therefore, a key question to the design of mine closure landscapes containing coke is where this coke should be stored within the landscape and how it can be most effectively utilized as part of reclamation efforts. For example, Suncor and SCL have both used surplus coke as a lightweight fill material to cap soft tailings. SCL constructed two prototype reclaimed watersheds in which soil covers were placed directly on coke deposits placed overtop of FFT contained in the Mildred Lake Settling Basin (MLSB).

The purpose of these prototype covers was to develop an understanding of the hydrological performance of reclamation covers placed over coke based on monitoring of soil water dynamics within the cover soils and underlying coke. This research site is referred to as the Coke Beach Instrumented Watershed (CBIW).

The two soil covers were constructed in 2004 and were both comprised of a layer of salvaged peat/mineral soil placed over salvaged glacial clay. One cover was nominally 100 cm in thickness and the other cover was nominally 35 cm in thickness.

Research conducted by Fenske (2012) evaluated the preliminary performance of the CBIW covers with respect to the available water holding capacity based on monitoring of the soil profiles and climate at the site from 2005-2006. The result from this study, which is also reported by Huang et al. (2010), indicated that the soil cover was unable to store sufficient water necessary for optimal plant growth under dry conditions, although the deep cover performed better than the shallow cover.

Huang et al. (2010) speculated that the elevated water loss may be occurring because of some process other than net percolation, runoff, or surface evapotranspiration. Following this study, Lahmira et al. (2013) investigated a similar case of accelerated drying for a reclamation cover constructed over coke at the Suncor mine site. In this case, it appeared that density driven air flow may have caused dry surface air to move through the cover causing enhanced drying of the cover.

Koehler (2018) instrumented the Syncrude coke reclamation covers with gas pressure monitoring to define whether convective air flow across the covers was occurring. The results from this study confirmed the presence of convective air flow across the covers but these flows did not appear to be sufficient to account for observed drying within the covers. Koehler (2018) also attempted to close a daily water balance for the covers based on monitoring data collected from 2005-2014.

1.1 Study Objectives and Scope

The overall goal of this research is to undertake a re-evaluation of the hydrological performance of the Syncrude Coke Watershed covers with a view to identifying the key processes that control the water balance for these covers. The specific objectives are as follows;

1. Construct a daily water balance for long-term (2005-2017) monitoring data set based on field meteorological and soil monitoring data;

2. Develop a calibrated physics-based model of the hydrologic performance of the two reclamation covers using a soil-vegetation-atmosphere transfer (SVAT) model which includes dual porosity flow dynamics;
3. Use this calibrated SVAT model to identify the key processes controlling the hydrological performance of the reclamation covers with a focus on identifying which processes (e.g. preferential water flow, convective air flow) or hydraulic properties (e.g. dual porosity water flow storage) have the greatest influence over performance.

1.2 Thesis Layout

The thesis outline is as follows:

- Literature Review (Chapter 2); a summary of relevant literature with a focus on similar cases of fine-textured, clay rich, covers placed over well-drained substrate and findings from these studies related to processes controlling water dynamics.
- Study Site Description (Chapter 3); a summary of the current study site
- Methodology (Chapter 4); a description of the modelling methodology used to re-interpret the field monitoring data
- Presentation of Monitoring Data (Chapter 5); a synthesis and discussion of the field monitoring data collected
- Presentation of Water Balance Model (Chapter 6); a presentation of the modelling results
- Conclusions and Recommendations (Chapter 7)

CHAPTER 2

LITERATURE REVIEW

This chapter synthesizes the relevant literature associated with mine reclamation covers, the processes affecting the water balance of these covers, as well as a summary of the properties of petroleum coke. This review also attempts to synthesize observations from literature case studies of fine-textured, clay rich, covers placed over well-drained substrate to identify the key processes that might control water dynamics within these soil profiles.

2.1 Mine Reclamation and Soil Cover Systems

The extraction of bitumen from oil sands deposits can result in environmental consequences. To safe guard the environment and ensure sustainability, land taken for oil sand extraction is reclaimed at the earliest time, and to a standard required for the intended use (DCLG, 1996). One of the techniques for reclaiming of oil sand mining after closure is the construction of soil covers. Covers are aimed at providing adequate water and nutrients for vegetation as well as protecting the root zone from high salinity and sodicity (Meiers; *et al.*, 2011; Huang; *et al.*, 2015).

2.1.1 Regulatory Underpinning

The Environmental Protection and Enhancement Act (EPEA) together with other documents created by Cumulative Environmental Management Association (CEMA), Alberta, provides a directive used in regulating the activities of oil sands mine reclamation and closure planning (Alberta Environment and Sustainable Resource Development, 2013). The Alberta Environment and Sustainable Resources Development is the office responsible for the implementation of this regulation. The main goal set by EPEA, Alberta, to govern reclamation activity states;

> "The approval holder shall reclaim the land so that the reclaimed soils and landforms are capable of supporting a self-sustaining, locally common boreal forest, regardless of the end land use" (Alberta Environment and Sustainable Resource Development, 2013).

For a reclamation certificate to be given by the government to the oil sand operator, the operator must demonstrate that the reclaimed land capability is equivalent to that which existed before mining. Land capability is defined by Alberta Environmental Protection (1994) as:

> "the ability of the land to support a given land use, based on an evaluation of the physical, chemical and biological characteristics of the land including topography, drainage, hydrology, soils and vegetation (Alberta Environmental Protection, 1997).

2.1.2 Types of Covers

There are basically two general types of covers used to cover mining waste; conventional mine closure covers used to control oxygen or water fluxes and reclamation water balance covers used to support re-vegetation. Conventional covers, also known as resistive covers, are normally designed for waste containment facilities. These covers often utilize a layer or layers of materials which restrict water or gas (i.e. oxygen) ingress into the underlying waste (Albright, 2009).

The design of reclamation or water balance covers could be monolithic barriers (single) or capillary barriers (multilayer). The monolithic barriers use a layer of fine-textured soil as its water storage layer (Milind Vishnu Khire, 1995) while the capillary barriers comprise of multiple layers of contrasting texture (Khire, 1997). The contrasting texture could range from simple two-layer designed with a finer textured layer above a coarser-textured layer to multiple layer design comprising of finer-textured and coarser-textured soils. The distinction between monolithic cover and a capillary barrier is the presence of a capillary break comprised of a finer-textured cover layer overlying a coarser-textured layer resulting in elevated water storage within the finer textured cover layer. (Apiwantragoon, 2007; Apiwantragoon, 2015).

Most of the research work conducted into soil covers have focused on the use of conventional covers to prevent the movement of water and gases into the underlying waste. However, some of the studies that considered the use of water balance covers are discussed in section 2.5 below.

2.1.3 Cover Selection and Design

The primary purpose of a reclamation cover is to provide a topsoil/subsoil system which will provide adequate nutrients and water storage to support the growth of boreal forest vegetation where these capabilities are defined by the Land Capability Classification System (LCCS) (Cumulative Environmental Management Association (CEMA), 2006; Meiers, 2011). The above

objective is achieved by selecting a cover thickness that supports similar rates of evapotranspiration rates as existed before mining (Huang, 2015).

The available water holding capacity (AWHC) is the main indicator used in assessing the suitability of the soil water content for an ecosystem. AWHC is the representation of the volume of water stored within the cover (i.e. over the rooting depth) between field capacity (FC) and the permanent wilting point (PWP), taking into account enhanced water storage associated with the effect of layering (e.g. low hydraulic conductivity layer or a capillary break layer) or shallow depths to a permanent water table (Keshta, 2010; Huang, 2015). Layered soils have been found to be more successful in storing an appreciable amount of water in oil sand reclamations design (Zettl et al. 2011; Elshorbagy and Barbour 2007; Huang et al. 2015).

The hydraulic conductivity and the water storage capacity of the cover soils are the two main parameters that affect the performance of reclamation covers (Meiers; *et al.,* 2011). It is important to note that these properties can change with time following placement of the covers due to chemical, biological and physical processes at the specific site (International Network for Acid Prevention, 2003; Meiers; *et al.,* 2011). Reclamation soil covers are therefore designed in layers to control the expected increase in the hydraulic conductivity and to enhance water storage within these covers.

2.3 Factors that affect the performance of reclamation covers

The key soil properties responsible for the performance of reclamation soil covers are the water storage characteristics and the hydraulic conductivity. These properties are known to change with time following placement because of changes in physical, chemical, biological processes at the site (Meiers; *et al.,* 2011).

2.3.1 Water storage characteristics

Water storage in reclamation soil covers for mine closure is often estimated to assess the viability of these covers to sustain vegetation growth and to enhance the promotion of biodiversity. Several researchers have estimated water balance in soil covers using various methods. Two of the most common methods are a System Dynamics approach and physics based numerical modelling. In the System Dynamics approach the cover is envisaged as a series of water storage reservoirs between which water passes based on semi-empirical rules, (Elshorbagy and Barbour 2007;

Fenske, 2012). In the physics based modelling, the physical mechanisms controlling water storage and water flow are described mathematically and then simulated using numerical methods (Huang et al. 2011; Keller et al. 2009; Khire; et al. 1997; Keller et al. 2015; Milczarek et al. 2000; Woyshner and Yanful 1995; M.O'Kane; et al. 2003). Both System Dynamics and physics-based models have been found to be capable of representing the water balance dynamics in reclamation soil covers.

The stored water within a reclamation soil cover can be expressed in terms of the various processes controlling the water balance (Figure 2.1) as follows:

$$\Delta S = PPT - R - AET - NP - I \quad (2.1)$$

where: ΔS is the change in water storage (mm); *PPT* is the precipitation (rainfall plus snowmelt as measured using the snow water equivalent (SWE) (mm) of the snow pack; *R* is the surface runoff (mm); *AET* is the actual evapotranspiration (mm); *NP* is the net percolation (mm); and I is the interflow (mm).

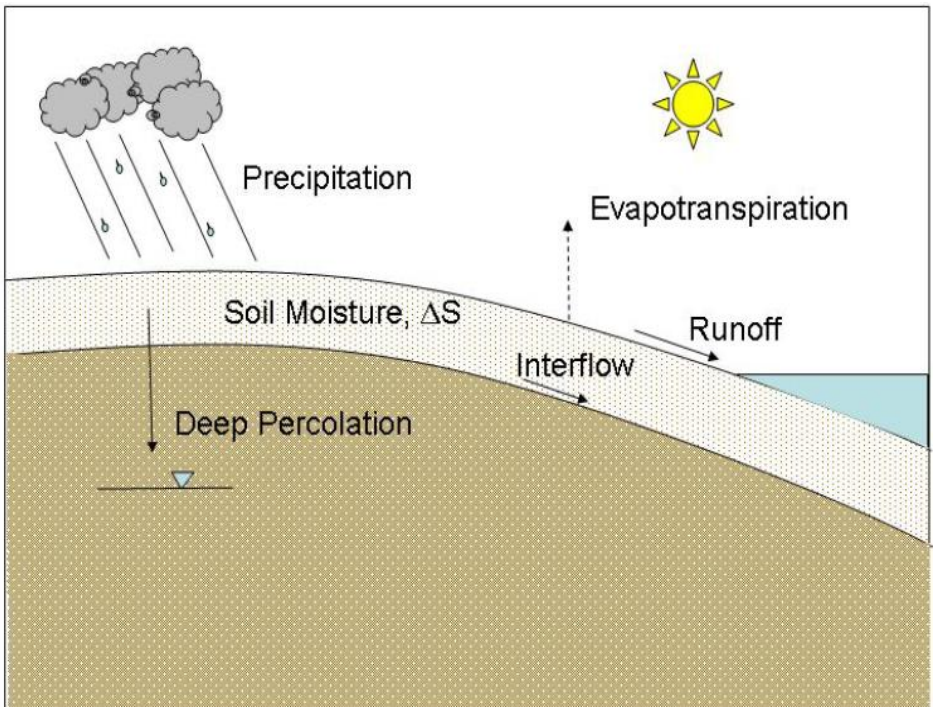

Figure 2.1: Water Balance (Fenske, 2012)

2.3.1.1 Soil Water Storage

The change in soil water storage is calculated from changes in the measured volumetric water content over time (e.g. weeks, months, years, etc.) (Brooks, 2013). Since soil covers are generally unsaturated and the water stored within the soil profile is held primarily by capillarity and adhesive/cohesive forces (molecular attraction) to resist gravity drainage or evapotranspiration (World Meteorological Organization 2008).

Soil water storage is affected by a wide range of factors including, soil texture, type of clay present in the soil, the content of organic matter, the soil structure, the depth of wetting and antecedent water content, the presence of impermeable layers in the profile, and the rate of evapotranspiration (Hillel, 1998). Quantitative methods of measuring volumetric water content include gravimetric water contents (with density measurements), dielectric, gamma-ray attenuation, and neutron scatter method. More qualitative or index methods include inference from measurements of soil suction (i.e. tensiometric) or through indirect measurements such as electrical resistance and remote sensing (World Meteorological Organization 2008).

2.3.1.2 Precipitation

Precipitation can be of different forms, namely rain, snow, hail, dew, and frost. There are different methods for the measurement of the precipitation and the accuracy of the measurement is important for the calibration and validation of hydrologic models and for the estimation of available water in a watershed (Dingman, 2015). These methods are broadly categorised as point measurements (standard rain gauges) and measurement over the entire area through radar and satellite. Similarly, the advancement of technologies has made it possible for unconventional recording gauges to measure both rain and snow. Some of these methods are optical gauges (measures rain and snow differently), capacitance gauges (records precipitation electronically), acoustical gauges (uses sound spectra to measure rainfall rates), disdrometers (Dingman, 2015). The accurate measurement of precipitation is foundational to quantitative hydrologic analyses, such as real-time flood forecasting or calibration and validation of hydrologic models.

During the winter period, when precipitation normally falls as snow, the method of measurement of precipitation is different compared to rainfall measurement. It is possible to measure snowfall using gauges, but the measurement is often not reliable. This is because the snowfall is more likely to be redistributed by wind due to its low density and high surface area. Hence, snow surveys are

conducted along transects across the site in which snow depth is measured at multiple sampling points using a cylindrical tube with a cutting edge (Brooks, 2013) and snow density is measured by melting a known volume of snow. The amount of water in the snowpack (snow water equivalent-SWE) is calculated using the method described by Pomeroy; and Gray (1995) as follows:

$$SWE = \frac{ds * \rho s}{\rho w} \qquad (2.2)$$

where; SWE is the snow water equivalent, (mm), ds is the average depth of snow pack, (cm), ρs is average density of the snow, (kg/m^3), ρw is the density of water, (kg/m^3).

2.3.1.3 Surface Runoff and Interflow

Surface water excess occurs when the rate of precipitation (rain or snowmelt) exceeds the rate of infiltration. This excess water collects in depressions, forming pools. The quantity of the pool per unit area is known as the surface storage capacity. This is affected by the irregularities of the shape of the surface and the gradient of the land. Surface (overland) runoff occurs only when the surface storage is filled. It could be defined as the quantity of precipitation which is neither infiltrated into the soil, nor stored on the surface, but flows down gradient through channels and ultimately ends up in streams (Hillel, 1980). This characteristic is generally difficult to accurately estimate from natural soil surfaces (Boese, 2003).

Interflow or subsurface flow is the water that flows laterally above some layer that impedes downward water migration. Interflow consist of both saturated and unsaturated flows in either vertical or down-gradient (e.g. slope) directions (Morel-Seytoux, 1989). The saturated component of the interflow may form above the unsaturated soil or rock where there exists a hydraulic conductivity break within the profile or below isolated depressions within the surface of the bedrock (Morel-Seytoux, 1989; Boese, 2003). However, the mechanisms of interflow are difficult to accurately understand.

2.3.1.4 Evapotranspiration

Potential evapotranspiration (PET) could be defined as the maximum quantity of evaporation that could occur from a large area completely covered by actively growing vegetation with adequate supply of water. Defined in this manner, it represents the maximum value of the actual

evapotranspiration (AET) (Armstrong, 2008; Donohue, 2010). The water loss from the soil surface is known as actual evaporation (AE). The water loss from the stomata of plant canopies to the atmosphere is called actual transpiration (AT) (Hillel, 1998) with the water taken up through a root distribution within the soil profile.

AET is affected most by available energy, vapour pressure deficit and stomatal resistance though other variables such as wind speed, air temperature could affect it weakly (Jarvis, 1976). Generally, the higher the AET, the lower the volume of water storage or water release by net percolation or interflow. AET is generally less than potential evapotranspiration (PET) with water availability in the soil being the determinant factor (Armoh 2015; Boese 2003).

There are several methods used to estimate AET in the field; these are generally categorised as either direct or indirect methods. Eddy covariance methods, weighing lysimeter methods, and portable chambers are examples of the direct methods whereas soil water balance, energy balance and Bowen ratio are examples of the indirect methods (Rana and Katerji, 2000). These methods differ in terms of accuracy, cost, and availability of weather data (Tabari, Grismer and Trajkovic, 2013). Though the Food and Agriculture Organisation, (FAO) recommends the use of FAO Penman-Monteith Equation (micrometeorological approach) as a standard method for the estimation of reference PET (Allen *et al.*, 1998).

2.3.1.5 Net Percolation

Infiltration is the process by which water enters the soil surface by the combined effect of capillarity and the force of gravity. This water could be precipitation (rain and snowmelt) or irrigated water. However, when the infiltrated water exceeds the field capacity of the soil, the excess water drains downwards due to gravity. This volume of water that drains past the rooting zone and into the underlying saturated flow system is defined as net percolation (NP) (Brooks, 2013).

There are different methods in estimating net percolation rate. These methods include Darcy law method (using monitored soil suction or negative pressures), the water balance method, tracer methods, lysimetry, inferences based on trend analysis, the zero-flux plane method and the field capacity-based method. For this study, the water balance method will be used primarily to estimate net percolation supported where possible by calculations based on Darcy's Law or from tracking

the release of water volumes stored temporarily in excess of field capacity. Details about the other methods are discussed by King (2015) and Benson et al. (2001).

2.3.1.5.1 Water Balance Method

In the water balance method, all the water balance components are estimated and then the water balance equation is used to estimate the percolation component as stated in equation 2.1. The accuracy of this method depends on the accuracy of which the various components (AET, precipitation, change in soil water storage and surface run-off are measured or calculated. Benson et al. (2001) suggests that given the limitations in measurement accuracy for ET and precipitation components of the water balance, these estimates of NP have a precision of 230 mm/year for a humid site and 75 mm/year for semiarid site. These values change to 100 mm/yr. for the humid site and 50 mm/yr. for the semiarid site when error in precipitation is assumed to be negligible.

2.3.1.5.2 Darcy Law Method

The estimation of net percolation rate using the Darcy Law is based on estimates of the hydraulic conductivity of the soil at any suction (i.e. hydraulic conductivity function) as well as measurements of the hydraulic gradients from measurements of soil suction. The NP rate is then calculated based on Darcy's Law as follows:

$$NP = -K_{\varphi}\mathrm{i} \tag{2.3}$$

where K_{φ} is the hydraulic conductivity at suction (φ) and i is the hydraulic gradient (Benson *et al.*, 2001; Zhan *et al.*, 2014).

The hydraulic gradient could also be estimated from measured water contents if the water retention curve (i.e. relationship between volumetric water content and suction) is known.

Some of the limitations to the use of this method are;

1. The inability of soil moisture sensors to measure or detect preferential flows through macropores, fractures or cracks. This leads to the underestimation of percolation rate on sites with macroscopic features.
2. Errors in the estimation of hydraulic conductivity at matric suction and the omission of hysteresis in the estimation of WRC are other limitations to the use of the approach.

However, the errors in this approach is reduced in cases where preferential flow is considered in the estimation of percolation rate as can be done in the dual porosity model (Hydrus 1-D).

2.3.1.5.3 Field Capacity based Method of Estimating NP

In this approach, the water volumes stored within the profile at water contents greater than the field capacity of the specified layer are assumed to drain and represent a net percolation water volume.

$NP = (\theta_i - FC_i)$ when $\theta_i > FC$ (2.4)

$NP = 0$ when $\theta_i \leq FC$

Subsequently, water draining below the root zone is considered lost and not accounted for.

In summary, Benson et al. (2001) found the lysimetry method to be the best method for the estimation of percolation rate. The precision of the water balance method is about 100 mm/yr in humid climates, however, the precision could be worse in many instances. The Darcy's Law method was found to have a precision of about two orders of magnitude or higher than the calculated percolation rate. Subsequently, this method can be used when preferential flow is not required. The accuracy of the tracer method depends on the concentration of the solute used, percolation rate and the sensitive of the chemical extraction and analysis adopted. The trend analysis method was found to be the least accurate method for the estimation of percolation rate because soil water content data alone cannot be used to assess percolation rate. The trend analysis method infers the occurrence of percolation rate based on the changes or variation of soil water content at a particular depth within the soil profile.

2.3.1.5.4 Preferential Flow

A key process that can increase net percolation is preferential flow which includes all forms of water flow in paths bypassing the finer pores within the soil matrix in which capillary forces are dominant. These preferential flow paths can include macropore flow, funnel flow, or finger flow with the macropore flow being the major concern to reclamation soil covers (Saravanathiiban, 2014).

Reclamation soil covers, similar to conventional covers are subject to potential cracks resulting from soil desiccation because they are often designed with soils which contain a plastic clay fraction which can undergo changes in volume with changes in water content (Hardt, 2008; Welter, 2009). This often leads to the formation of secondary pore structures (e.g. macropores or fractures) as a result of wet/dry or freeze/thaw cycles (Meiers; *et al.*, 2011). Macropores can also be formed by plant roots, or the activities of insects and earthworms present in the soil covers.

Macropores have a greater hydraulic conductivity than the surrounding soil matrix (micropores). They also have comparatively low water-entry suctions and are often linked to the surface which allows easy entry of water especially during long and high rainfall and snowmelt events. The depth of the macropores determines its ability to transport appreciable amount of water at some orders of magnitude higher than the surrounding soil matrix. However, disregarding the flow of water through macropores in the estimation of water balance in reclamation soil covers can result in the underestimation of the percolation component of the water balance and subsequently wrong prediction of the cover performance (Hardt, 2008).

2.2 Hydraulic Properties of Reclamation covers

2.2.1 Water Retention Curve

The water retention curve (WRC) describes the functional relationship that exists between the volumetric of water content of the soil and the matric suction (Figure 2.2). This relationship defines available water storage within the soil at any given range of suction but also can be interpreted through the capillary model to describe the distribution of fluid filled pores. This subsequently forms the basis for the methods of estimating the hydraulic conductivity function for the soil (Barbour, 1998).

Figure 2.1 depicts a typical WRC with its important attributes, namely; saturated volumetric water content, $\theta_{s,}$ the residual water content, θ_r and the air entry value. At saturation, the volumetric water content is equal to porosity. Residual water content is the point where liquid flow becomes increasingly discontinuous and reduction of the water content through drainage increasingly difficult. The air-entry value is the minimum value of suction that has to be applied to cause drainage of the largest pores, which then allows air to enter the soil (Tarboton, 2003). Generally, coarse-textured and well-graded soil have smaller air-entry values. However, since there is often more nearly uniformity of pores size in coarse-textured soils, the soil could display a critical air - entry phenomenon more uniquely and abruptly compared to fine-textured soils.

The volumetric moisture content could be expressed with regards to dimensionless moisture content or relative degree of saturation, effective saturation, S_e (moisture content between saturation and the residual moisture content) as described by van Genuchten (1980):

$$\Theta = Se = \frac{\theta - \theta r}{\theta s - \theta r} \tag{2.5}$$

where θ_s and θ_r are the saturated and residual water content respectively.

Out of the several models that have been developed to estimate the various SWCC parameters, one of the most recognised models was developed by van Genuchten (1980) as follows:

$$\Theta = \left[\frac{1}{1+(\alpha h)^n}\right]^m \quad (2.6)$$

where α, n and m are empirical fitted parameters and h is the pressure head.

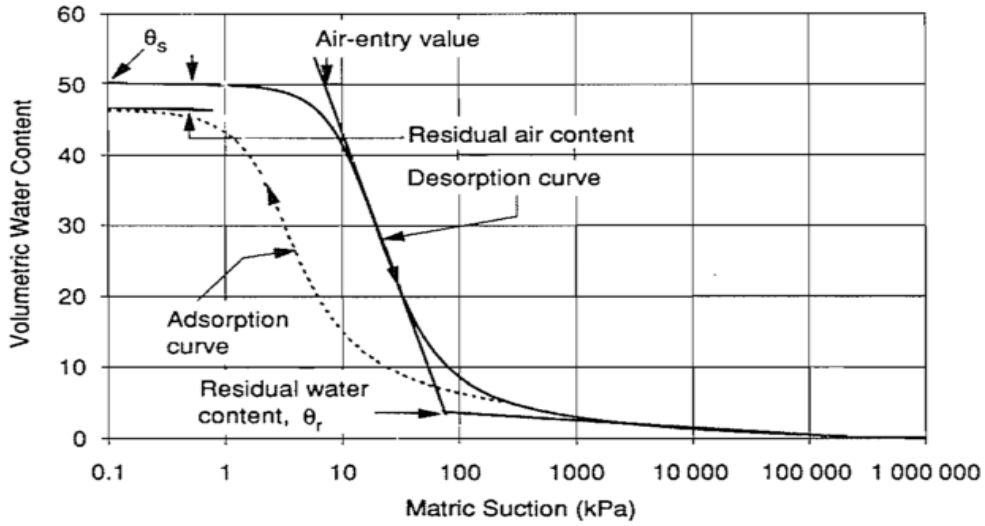

Figure 2.2. A typical SWCC for silty soil (Fredlund; and Xing 1994)

2.2.2 Hydraulic Conductivity

The saturated hydraulic conductivity of a soil is among the most variable of all engineering soil properties, ranging over 10 orders of magnitude for a range of typical soils encountered in engineering practice (Fredlund, Xing and Huang, 1994). When a soil undergoes a decrease in volumetric water content, the hydraulic conductivity also decreases due to a decrease in both the area and the effective pore-size of the remaining fluid filled pores. This functional relationship for hydraulic conductivity has been shown to be comparatively distinct function of the soil water content in both the desorption and the absorption processes especially when volume change of the soil structure is negligible.

Several researchers have suggested methods to estimate the unsaturated hydraulic conductivity function; however, there exists a great disparity between empirical models and between these models and field-based measurements. As a consequence, field-based measurements, when

available, better characterize the hydraulic conductivity of the soil. Some of the field measurement methods include sprinkling infiltration (Youngs, 1964), infiltration through an impeding layer Hillel and Gardener (1970), internal drainage Richards and Weeks (1953); and the instantaneous profile method developed by Watson (1966), the latter method considered to be the best and most commonly used method. The instantaneous profile method is based on the application of theories of soil physics in predicting the actual processes in the field and is dependent on the understanding of the hydraulic characteristics of the unsaturated soil.

There are other tested field methods for measuring hydraulic conductivity including sorptivity methods (White and Perroux, 1989); the use of Guelph permeameter (Elrick and Reynolds, 1992); and the inverse methods (Kool and Parker 1988).

2.4 Petroleum Coke

2.4.1 Description and Uses of Petroleum Coke

Petroleum coke is a solid material that is rich in carbon and is a by-product of oil sand refining and other cracking processes. This process results in the breakdown of other complex organic molecules such as heavy hydrocarbons into simpler, and more valuable lighter petroleum products (Tao, 2015). Coke is considered a dirty fuel. As well as having a very elevated carbon content (over 90%), a lot of the tar sand bitumen develops into concentrated coke (Stockman, 2013).

Coke has economic value as a source of energy or as carbon for industrial applications. The quality of the coke determines its specific use, as a fuel or as a source of carbon in an industrial manufacturing process (Stockman, 2013). However, because of higher production of coke than demand by Syncrude Canada, most of the coke produced is stored for possible future extraction.

The saturated hydraulic conductivity of coke has been found in various publications to be varying from $1x10^{-6}$ m/s to $1.12x10^{-4}$ m/s (Fenske 2012). However, Fenske (2012) found a mean saturated hydraulic conductivity of $1.12x10^{-4}$ m/s for the Syncrude coke.

2.4.2 Hydrophobicity of Coke

The hydrophobic property is the ability of a polar molecule like water to be repelled by non-polar molecules like coke or coal. Soils which exhibit the properties of hydrophobicity (water repellent soils) such as coke could repel water infiltration. The high carbon content of coke is the property that facilitate the exhibition of hydrophobicity (Bauters, 1999; Bauters *et al.*, 2000; Debano, 2000;

Doerr *et al*., 2000). Water repellent soil has significant hydrological and geomorphological consequences. These consequences include a reduction in the infiltration capacity of the soil, increased overland flow, promotion of soil erosion, unequal wetting patterns, an occurrence of preferential flow and increased leaching of agrichemicals (Bauters *et al.*, 2000; Doerr *et al*., 2000).

A water-repellent layer (coke) causes infiltrated water to pond over that layer and if the infiltration rate exceeds the infiltration capacity of the layer, there can be lateral flow. However, the rate of gaps (such as drying or structural cracks, root holes or burrows) through the layer would determine if there would be lateral flow or preferential flow. Subsequently, hydrophobic soils could be useful in preventing downward flow of water, directing water through structural or preferential flow paths or producing an unstable irregular wetting front. This may lead to incomplete soil wetness with the passage of wetting front (Debano, 2000), with the water being channeled through macropores and cracks, diverting water from the soil matrix (Doerr, 2000).

2.5 Literature examples of the control of cover and waste texture on water balance components

Key studies related to the current work were those conducted on multilayer reclamation covers over saline-sodic overburden at the South Bison Hills (SBH) site at Syncrude's Mildred Lake mine site. The cover soils used at this site were the same as those used at the current study site. Actual evapotranspiration and net percolation were the main components considered while reviewing various similar case studies. Aside from these two components, the saturated hydraulic conductivity was considered, as it could be an indication of the cover's ability to allow the flow of water and contribute to the performance of the cover.

In 2018, Huang et al. used different models including fully coupled water and heat flow model and water flow model to assess the performance of the SBH covers of which FM-EI (flow model with enhanced infiltration) model was found to be the best model. Results from the study using FM-EI model found an average annual simulated AET of 317 mm which accounted for 87% of the mean annual precipitation (365 mm) for the study site for study duration (15 years). The simulated AET was found to increase with increased stored water from snowmelt infiltration. Mean net percolation was found to be about 14 mm per year (Huang et al., 2018) with runoff (from both snowmelt + rainfall) accounting for 26 mm (24 mm from snowmelt) with mean water lost being 40 mm (percolation + runoff) together with a change in storage of 8 mm. The mean simulated AET for

the growing season was higher than the mean measured AET on an adjacent, younger, reclaimed plateau area (AET of 251 mm) using eddy covariance (Carey, 2008).

In a related study to access the transport of stable isotopes of water and sulphate within this same study site, Huang et al. (2015) found mean net percolation rates estimated from a stable isotope of water profiles ranged from 24 mm/yr to 43 mm/yr for a plateau area. This study considered measured data from the SBH plateau area.

Similarly, Huang et al (2015) calibrated a physics-based water balance model to simulate the water balance components for the site over the historical monitoring period as well as for a typical 60-year climate cycle. They found that the mean potential evapotranspiration was 496 mm with a mean growing season precipitation of 426 mm. Actual evapotranspiration was found to be ranging from 63% to 84% of precipitation with total runoff and percolation amounting to about 42 mm, varying with cover thickness and assumed Leaf Area Index (LAI). The result obtained was based on 60-year climate data.

This study found an optimised mean saturated hydraulic conductivity of 1.0×10^{-5} m/s, 1.0×10^{-6} m/s and 3.0×10^{-8} m/ for peat mineral mix, glacial clay soil and shale, respectively. These optimised Ks values were found to correspond to the measured Ks values on the same site by Meiers; et al. (2011). Meiers, et al. (2011) obtained these Ks values through repeated measurement within a five-year period using Guelph permeameter. The mean measured Ks were 5.0×10^{-5} m/s (peat mineral mix), 1×10^{-6} m/s (glacial till) and 3.0×10^{-8} m/s (shale) and were observed to evolve over 3-5 years and then stabilize (Meiers, et al. 2011).

Shurniak (2003), working on the same site only a few years after cover construction, estimated AET to be 293 mm with a PET of 508 mm for the 50 cm thick soil cover (20 cm peat and 30 cm till) and 35 cm thickness (15 cm peat and 20 cm till) South Hill overburden piles. The AET for the 100 cm cover (20 cm of peat and 80 cm of glacial till) was 296 mm. This study found a mean Ks of 6.6×10^{-5} m/s for peat mineral mix and 2.75×10^{-5} m/s for glacial till material.

The studies described above for SBH were fine textured covers placed over a fine textured shale overburden located in a humid continental climatic region. In contrast to that work, the work described by Milczarek; *et al.*, (2015) highlights the hydrological performance of cover systems constructed over coarse textured waste rock. The mean annual precipitation during the study period

(2006 to 2009) was 1290 mm with mean pan evaporation and reference evapotranspiration (ETo) been 935 mm/yr and 745 mm/yr respectively. The covers were comprised of topsoil material placed over borrowed clay/silt material. According to the study, AET accounted for 54% of the study site precipitation while net percolation accounted for 28% of the precipitation. It was also noted that the Ks of the soil cover systems were observed to be changing over time. It is important to note that the water balance component results by this study were estimated using the water balance equation (system dynamic approach).

The studies described by Barber, *et al.* (2015) for reclamation soil cover systems at the Cluff Lake mine in northern Saskatchewan's Athabasca Basin included both soil covers constructed on waste rock (waste rock cover systems) as well as finer textured tailings (tailing cover systems). The tailing cover system comprised of 100 cm thick layer of non-compacted, silty-sand till with a grass and legume vegetation cover while the waste rock cover system consisted of 20 cm compacted waste rock overlain by non-compacted 100 cm silt-sand till with grass and legume vegetation cover. From the water balance component results, a mean growing season AET of 268 mm (75% of growing season precipitation) and mean net percolation of 82 mm (22% of PPT) were obtained for the waste rock cover system for the plateau area. On the sloping areas of the rock waste cover system, a mean AET of 281 mm (78% of PPT) with mean net percolation accounting for 61 mm (16% of PPT) were obtained. Similarly, on the water balance fluxes for the tailing cover system, a mean growing season AET of 258 mm (72% of PPT) whereas net percolation was 45 mm (12% of PPT) were obtained.

Preferential flow has been observed to be the major setback on the hydrological performance of soil covers. Kelln, *et al.* (2007) also conducted research on the South Bison Hills covers discussed previously. The study found the snowmelt infiltration was occurring as preferential flow through the frozen cover during spring melt and on occasion when the antecedent soil water was high through the unfrozen cover. Subsequently, preferential flow was observed to impose control on the discharge rate and cumulative volumes of interflow.

Similarly, Welter, (2009) found the existence of preferential flow within soil columns and as a result, serve as the path for solute transport within soil covers which affect the performance of soil covers. This study was also conducted on South West 30 Overburden Dump (SW30) with the cover properties and climate the same as described in SBH.

Saravanathiiban, (2014) found measured annual percolation rate increased by an order of magnitude within a four-year period due to preferential flow. The existence of preferential flow was confirmed by conduction of controlled irrigation test. In addition, the estimated effective field hydraulic conductivity increased by an order of magnitude during the fourth year of operation compared with the first year of service (Saravanathiiban, 2014). This study was conducted on a cover comprising of 30 cm topsoil underlain by 150 cm thick clay in sub-humid climate.

In a summary, various studies on multilayer reclamation covers over saline-sodic overburden at the South Bison Hills (SBH) site at Syncrude's Mildred Lake mine site found net percolation rate ranging from 13 mm/yr to 48 mm/yr. The mean AET for the growing season for the same study site ranged from 268 mm to 358 mm. These results were obtained using simulated approach. The mean Ks obtained for the SBH cover ranged from 1.0×10^{-5} m/s to 6.6×10^{-5} m/s for the peat soil and 2.75×10^{-5} m/s to 1×10^{-6} m/s for the glacial till material.

AET and net percolation results estimated using the water balance equation from other study sites either than SBH site ranged from 248 mm/yr to 697 mm/year while net percolation ranged from 45 mm/yr to 361 mm/yr.

CHAPTER 3

STUDY SITE DESCRIPTION

The field instrumentation at the CBIW was designed to establish a water balance for each of the soil covers. The instrumentation set up was designed and installed by O'Kane Consultants in 2004 (O'Kane, 2004) and was elaborated upon by Fenske (2012). Koehler (2018) augmented the instrumentation at the Syncrude coke reclamation covers with gas pressure monitoring to define whether convective air flow across the covers was occurring. This chapter presents a summary of the various field programs undertaken on the CBIW (southwest corner of the MLSB) since the inception of the project.

3.1 Description of Test Covers and Existing Instrumentations

This study location is at the Mildred Lake mine site, operated by Syncrude Canada Limited in the Athabasca oil sands area of northern Alberta (Figure 3.1). The location of installed meteorological stations on the CBIW and other adjacent sites (30 Hill Top/South Bison Hill, Southwest Sand storage covers (SWSS C32) and W1 dump sites) are shown in Figure 3.2. The CBIW was constructed within the Mildred Lake Settling Basin (MLSB) on Cell 4 and 5 (Figure 3.3 and Figure 3.3) where Coke had been deposited over top of fine tailings in the south-west corner of the MLSB, an area referred to as the coke beach (Fenske, 2012).

Two prototype rehabilitation soil covers were constructed directly on the coke deposit in 2004. Both covers were comprised of a peat/mineral mix layer placed over glacial clay. The 'deep' cover was nominally 100 cm in thickness and comprised of 20 cm of peat- mineral mix and 80 cm of glacial clay, while the 'shallow' cover was nominally 35 cm in thickness comprised of 15 cm of peat-mineral mix and 20 cm of clay (O'Kane, 2016) as shown in Figure 3.5.

Figure 3.1: Location of Athabasca Oil Sands Area in Northern Alberta, Canada. (wikipedia.org)

Figure 3.2: Location of Nearby Site Meteorological Stations

The field instrumentation was installed by O'Kane Consultants in 2004 and was augmented by Fenske (2012) and Koehler (2018). The original O'Kane instrumentation included a meteorological station, soil profile monitoring, and a tank lysimeter under the covers. The instrumentation installed by Koehler (2018) included both atmospheric gas pressure monitoring as well as pressure monitoring at various depths across the covers. However, this study used only data from instrumentation installed by O'Kane Consultants in 2004. Shown in Table 3.1 is a summary of all the instrumentation carried out by O'Kane Consultants and other researchers at the study site

Figure 3.3. Aerial view of MLSB and project study area (Fenske, 2012)

Figure 3.4. Aerial view of project study area (Fenske, 2012)

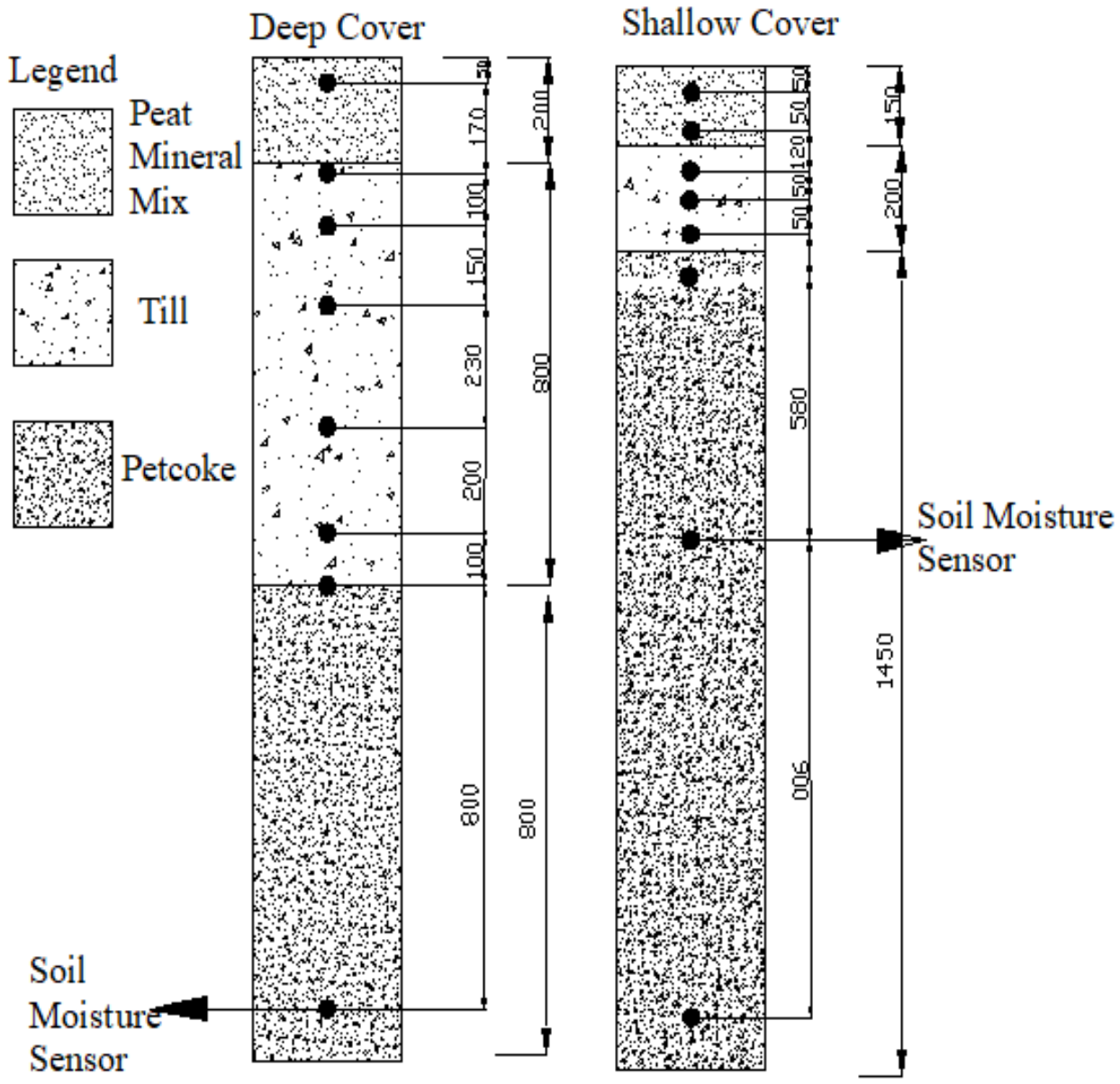

Figure 3.5: A cross section through both deep and shallow covers

Table 3.1: Summary of Data Monitoring Installations for the CBIW monitoring site

Location	Instrumentation	Reference	Instrument
Shallow and Deep Covers	• Soil volumetric water content sensors (8) • Soil matric suction and temperature sensors (8) • Data acquisition system • Tank lysimeter • Two soil gas and temperature monitoring stations • Two standpipe piezometers • Three manual water content access tubes	OKC (2004) Installed in summer 2005 by Fenske (2012)	• Time domain reflectometry (TDR) CS616 sensors (soil water content) • CS229 thermal conductivity (TC) sensors (suction and temperature)
Deep Cover	• Differential gas pressure sensors, 3 locations (D01, D02, D03), 3 sensors each location	Installed in Spring 2013 by Koehler (2018)	

Shallow Cover	• Meteorological station • Data acquisition system (DAS) • Differential gas pressure sensors, 3 locations (S01, S02, S03), 3 sensors each location	OKC (2004) Installed in Spring 2013 by Koehler (2018)	• CR10X datalogger, component of DAS Rain gauge (TE525), CS705 snowfall adapter

3.1.1 Meteorological Station

A fully automated meteorological station installed at the CBIW by O'Kane Consultants Inc. (OKC) in the fall of 2004 is used to monitor standard meteorological data including precipitation (rainfall and snowfall), wind speed and direction, air temperature, relative humidity (RH), and net radiation.

Attached to the meteorological station mast/tripod are various sensors for meteorological data measurements (Figure 3.6). A temperature and relative humidity sensor (Model HMP45CF) with an operating temperature range of -55 ^{o}C to +50 ^{o}C and RH measurement range of 0 to 1 is used to measure temperature and RH. Net radiation is measured with NT-Lite Net Radiometer. This is a high-output thermocouple sensor and it's mounted about 2.5 m higher above the ground surface. Wind speed and direction are measured with an R.M Young Model 05103 wind monitor. Precipitation is measured with a tipping bucket rain gauge (model TE525) with a snowfall adapter (model CS705) which contains ethylene glycol which function is to melt snowfall and then measure the SWE (O'Kane, 2004). However, the snowfall adapter was removed on the 7th April 2005 and only daily measurement of rainfall by TE525 was recorded. Snow surveys were therefore conducted at regular intervals for the study site each winter to determine the snow water equivalent. This snow survey was carried out by technicians from O'Kane Consultants Inc at a designated station following a permanent marked traverse.

All the data collected by the meteorological station is connected to an automated data acquisition system (DAS) which consist of a data logger, (CR10X). This is powered by a rechargeable/ solar panel system. Meteorological data is measured on an hourly time steps and then averaged to represent the day while noting the maximum and the minimum values. Data is then collected from the DAS using a laptop for processing.

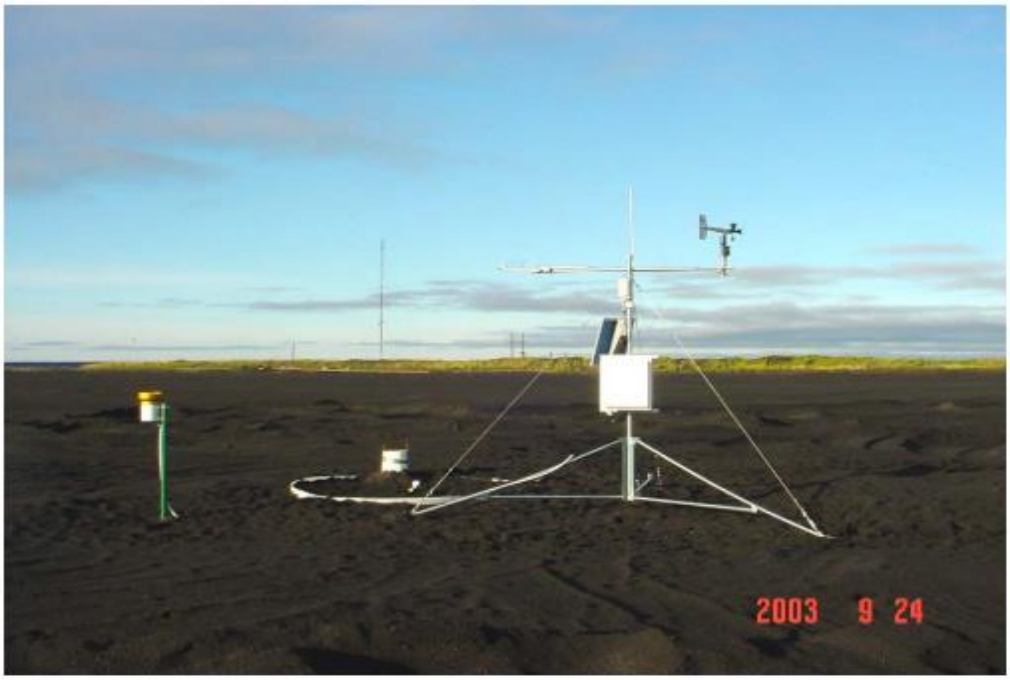

Figure 3.6: A Meteorological Station Installed on the Shallow Cover on the MSLB, (O'Kane, 2004)

3.1.2 Automated Soil Monitoring System

Soil monitoring sensors were installed across the cover profile for both the shallow and the deep covers in summer/fall 2004 with data acquisition system commencing in March 2005. The various parameters measured by these sensors were soil water content, soil temperature and soil matric suction. Soil temperature and suction were measured by Campbell Scientific (CS) CS229 thermal conductivity (TC) sensors while soil volumetric water content was measured by time domain reflectometry (TDR) CS616. The installation was done at a depth of 5, 10, 20, 25, 30, 40, 90 and 180 cm for the shallow cover. Similarly, for the deep cover, the depth of installation of the sensors were 5, 20, 30, 45, 70, 90, 100, and 180 cm.

To more fully capture the changes in water content or suction immediately next to the interface between soil layers, monitoring sensors were installed directly above and beneath the peat mineral mix/till interface and the till/coke interface. In the shallow cover, these interfaces occurred at depths of 15 cm and 35 cm; while in the deep cover, these interfaces were at depths of 25 cm and 95 cm. Data measurements were recorded every 6 hours and stored in the memory of DAS for following data collection (Fenske, 2012).

This installation was carried out close to the tank lysimeters on the deep cover and about 10 m from the middle of the meteorological station on the shallow cover.

3.1.3 Net Percolation

An attempt was made to directly measure NP through the covers by installing two tank lysimeters near the centre of both covers. These lysimeters had a diameter 2.44 m and a height of 2.5 m and were filled with the same material and thickness as the surround covers. The lysimeters were installed at a depth of 2.5 m beneath the coke with the top of the lysimeter being at the same level as the base of the covers. Measurement of percolated water was carried by the installing wells within the tanks from which water was pumped using a peristaltic pump (O'Kane, 2004; Fenske, 2012; Koehler, 2018).

The lysimeters were only operated over the 2005 and 2006 seasons. Fenske (2012) noted that no percolation rate was recorded at the shallow cover at the end of 2006 while the deep cover recorded 21.6 mm of percolated water through the deep cover.

3.1.4 Volumetric Water Content

Campbell Scientific 616 (CS616) time-domain reflectometry (TDR) sensors are used in measuring the volumetric water content for the study. With the CS616 time-domain reflectometry (TDR) method, two parallel stainless-steel rods (300 mm long) are inserted into the soil (Fenske, 2012; Koehler, 2018). The steel rod act as an electrode, with the soil between and around the rod acting as the dielectric material. A signal is reflected from one steel rod to the other and then back to a receiving station. The receiving station then measures the time between sending the signal and receiving the reflected wave. The propagation velocity can be calculated using the length of the cable. The speed of the propagation velocity depends on the average volumetric water content of the soil adjacent to the steel rod. This device is comparatively expensive, after installation, it is very accurate. (World Meteorological Organization 2008; Hillel 1998).

3.1.5 Soil Temperature and Matric Suction

Campbell Scientific 229 (CS229) matric potential sensors were used to measure the soil matric suction. The principle underlying this sensor is that a heating element and a thermocouple is encapsulated in epoxy inside a hypodermic needle. The system is subsequently enclosed in a ceramic matrix with pores to achieve equilibrium with the surrounding soil water. The senor has a

minimum and maximum measurement potential of 10 and 2500 kPa suction respectively (Koehler, 2018).

The CS229 sensor induces an electrical current within the thermocouple. The induced current then causes an upsurge in the temperature of the thermocouple. The rise of temperature is dependent on the amount of water content of the ceramic matrix surrounding the thermocouple system and as consequence the corresponding suction value can be correlated to this rate of rise through laboratory calibration of the sensor. The temperature of the soil surrounding the CS229 is also recorded before each measurement by the sensor to give a reference temperature for the total temperature increase. This is the reason for the dual functioning of the sensor as a matric suction and a soil temperature sensor (Koehler, 2018).

3.2 Summary of Field Data used in Current Study

The current study is a re-evaluation of the collected climate and soil monitoring data from the study site and no additional field work or monitoring was undertaken. The specific data sets used as part of this study is summarised in Table 3.2.

Table 3.2: Summary of Specific Data Set used for this Study

Location	Specific Data	Reference
Shallow and Deep Covers	1. Meteorological Data Daily air temperature Daily relative humidity Daily wind speed Daily net radiation Daily precipitation Yearly SWE 2. Soil Monitoring Data Soil temperature Soil matric suction Soil water content	OKC (2004)

The various possible sources of error for the meteorological and soil monitoring data used for this study include SWE (possible error in snow survey), error in rainfall measurement. Soil water content measurements by the uppermost sensor (5 cm depth) may also be subjected to errors due to its closeness to the surface. Similarly, a possible sensor failure could occur at other depth within the soil cover profile and may result in erroneous measurement. These possible sources of error appear to be more prevalent, especially from 2007 to 2008 and 2010 in the shallow cover. The possible sources of the errors within these years may be due to;

- poor contact with the soil, resulting from improper installation or disturbance and;
- calibration that is inappropriate for the soil in which the sensor is installed.

CHAPTER 4

METHODOLOGY

A description of the modelling methodology used to re-interpret the field monitoring data is discussed in this chapter.

4.1 General Overview of Study Approach

The first two objectives of this study were focused on the development of water balance models for the CBIW covers for the entire (2005-2017) monitoring data set. Two different methods of constructing this water balance were used; a system dynamics model and a physics-based model. The first method was based on a daily accounting of changes in storage based on estimated daily actual evapotranspiration and monitored precipitation. Rather than simulate soil water dynamics this method utilizes a 'box' or system dynamics approach to close the daily and seasonal water balances. The second method used a numerical, physics based, soil water dynamics model (Hydrus). Model optimization was used to characterize the material properties followed by a validation simulation to verify the model performance. The calibrated model was then used in a sensitivity analyses to evaluate key controls on the water balance. The last objective of the study was to use the developed models to identify the key processes controlling the hydrological performance of the CBIW covers with a particular focus on identifying and quantifying the role of preferential flow on net percolation.

This chapter first provides an overview of how the monitoring data collected from 2005-2017 was collected, checked, and prepared for the analyses. The methodology used to develop the water balance models is then presented and discussed in detail. For both methods, key hydraulic properties of the soil covers were collected from existing information and adapted for use in these models.

These field and laboratory derived hydraulic properties were the hydraulic conductivity and water retention curves from previous research on similar soils at the South Bison Hills study site by: Huang et al. (2015), Meiers; and Barbour (2002), Meiers; et al. (2011), Shurniak (2003), Boese (2003) and Fenske (2012). Similarly, vegetation heights and LAI values for the study was obtained from field vegetation inventory survey conducted by Syncrude Canada Ltd.

4.2 Data Management

Prior to developing the water balance models, the data set was checked for erroneous data and incoherencies in trend as a result of instrumentation failure. For instance, in the cases of missing data, a linear interpolation approach was used to fill in the missing data set. The measured meteorological data from the study site (CBIW) was compared with similar data sets from adjacent sites to assess the validity or the correctness of the CBIW data. These adjacent sites were 30 Hill Top, SWSS C32 and W1. Pearson correlation coefficient was used to obtain the relationship between the CBIW data and data from all the neighbouring sites using ™SPSS Statistics 20. The sample correlation coefficient, r, between two variables, x and y, which is denoted by r_{xy}.

$$r_{xy}=\frac{cov(xy)}{\sqrt{var\,(x)}\sqrt{var\,(y)}} \tag{4.1}$$

where cov(xy) is the sample variance of *x* and *y*; var(x), is the sample variance of x*;* var(y), is the sample variance for y

The correlation coefficient, r, and coefficient of determination, R^2, is related by $r = \sqrt{R^2}$ (Pallant, 2010).

4.3 System Dynamics Model

The system dynamics model calculates daily changes in storage based on meteorological data together with the soil monitoring data without the application of physics based models. The daily water balance equation presented earlier (Equation 2.3) is modified by assuming that interflow and runoff is negligible:

$$\Delta S = PPT - AET - NP \tag{4.2}$$

The reason for assuming that surface runoff and interflow were negligible is that based on previous research, the study site has an average topographic slope of less than 1%. With this gradient, the runoff for most of the year would be insignificant and therefore will be greatly improbable that

inflow would occur at significant quantities; although it is possible that extreme rainfall events or rapid spring melt could generate at least localized runoff, given the surface roughness it is likely minimal.

4.3.1 Water Storage

Water storage within both the shallow and the deep covers were estimated only for the unfrozen/growing periods (last week of April to third/last week of November) of the year. This was to prevent the use of erroneous measurement by the sensors at temperatures below 0 ^{o}C. The water storage was calculated using the water content data measured in each of the covers. The covers were divided into depth increments associated with each sensor. Each of the increments covered a depth interval extending between the midpoint between the sensor and sensors above and below. The volume of water was calculated by multiplying the thickness of each increment by its corresponding measured water content. The water volumes were summed up to obtain the total volumes of water storage in the cover profile. The thickness of the shallow and the deep covers were nominally 35 cm and 100 cm respectively. The actual thickness at the sensor locations was 37 cm and 95 cm, respectively, were used for calculating water volumes.

The water content at permanent wilting point and field capacity for both peat mineral mix and glacial till material used for this study was adopted from the research work of Shurniak, (2003). These values which have been used by Koehler, (2018) for a similar study on the same study site are summarised in Table 4.1.

Table 4.1: Summary of Cover System Material Properties

Cover System	FC (cm^3/cm^3)	WP (cm^3/cm^3)
Shallow Cover, Peat	0.30	0.20
Shallow Cover, Till	0.35	0.21
Deep Cover, Peat	0.30	0.20
Deep Cover, Till	0.35	0.21

A study by Huang et al. ((2015) also on SBH site with the same cover system material properties found the FC and WP to be 0.47 and 0.20 respectively for peat mineral mix and 0.37 and 0.178, respectively for the glacial till material. The glacial till values are comparable with the FC and WP values obtained by Shurniak, (2003) but the FC value for the peat mineral is higher than that of

the FC for peat obtained by Shurniak, (2003) but the WP values for both studies are the same. The FC and WP values obtained by Huang et al. (2015) were used to estimate the water balance components for 2005 and 2006, the reason being that the results obtained using the values in Table 4.1 were unrealistic.

4.3.2 Precipitation

The total precipitation measured on the MLSB site for both the shallow and the deep covers was comprised of daily measured rainfall and Snow Water Equivalent (SWE). However, the water balance estimation for this study only considered the unfrozen or the growing season of the year and subsequent the growing season precipitation (rainfall) was used for the water balance estimations. The estimates of net percolation and change in storage associated with spring freshet were calculated independently.

4.3.3 Potential Evapotranspiration Estimation

Prior to the estimation of daily AET of the soil covers, the daily potential evapotranspiration (PET) was calculated using the Penman equation (combination of an energy balance and an aerodynamic formula). This model was adopted because it is known to be the most suitable model for the estimation of potential evapotranspiration from bare soil, and grass (Donohue et al. 2010; Maidment, 1993) .

The PET was estimated as follows;

$$E_p = \frac{\Delta}{\Delta+\gamma} Q_n + \frac{\gamma}{\Delta+\gamma} \frac{6430\,(1+0.536u_2)\,D}{\lambda} \tag{4.3}$$

where Q_n is the net radiation (the unit here is mm/day); Δ is the slope of the saturation vapour pressure curve (Pa/K); γ is the psychrometric constant (Pa/K); λ is the latent heat of vapourization (J/kg); D is the vapour pressure deficit (Pa).

The slope of the saturation vapour pressure curve was calculated as follows;

$$\Delta = \frac{4098\left[0.6108exp\left(\frac{17.27\,T}{T+237.3}\right)\right]}{(T+237.3)^2} \tag{4.4}$$

Saturation and actual vapour pressure were calculated as follows;

$$e_s = \frac{e_{T_{max}} + e_{T_{min}}}{2} \quad (4.5)$$

where $e_{T_{max}}$ and $e_{T_{min}}$ are the saturation vapour pressure at daily maximum and minimum air temperatures respectively and was calculated following the procedure described by Zotarelli et al. (2015) and ASCE-EWRI Task Committee (2005).

$$e_a = \frac{e_{(T_{min})}\left[\frac{RH_{max}}{100}\right] + e_{(T_{max})}\left[\frac{RH_{min}}{100}\right]}{2} \quad (4.6)$$

where RH_{max} and RH_{min} are the daily maximum relative humidity and daily minimum relative humidity.

The psychrometric constant and the latent heat of vapourisation were calculated following the procedure described by Zotarelli et al. (2015); ASCE-EWRI Task Committee (2005).

4.3.4 Estimation of Actual Evapotranspiration

The actual evapotranspiration (AET) was not measured directly but was estimated as function of PET. AET relates to PET by a function of the ratio of available soil water (AW) and the available water capacity of the soil (AWC). This is one of the most widely used method (Dingman, 2015) and it is expressed mathematically as:

$$AET = (PET) f\left(\frac{AW}{AWC}\right) \quad (4.7)$$

where; f is the functional relationship; *AW* = (soil moisture content – permanent wilting point) *(rooting depth of matured vegetation) (mm); *AWC* = (field capacity – permanent wilting point) * (rooting depth of matured vegetation) (mm) (Brooks;, Ffolliott; and Magner, 2013).

Specifically, AET was estimated using this approach as follows;

$$AET = PET * \theta_{relative} \quad (4.8)$$

where $\theta_{relative}$ is the relative water content of a soil relative to its FC and WP.

$$\theta_{relative} = \frac{\theta - \theta_{WP}}{\theta_{FC} - \theta_{WP}} \quad (4.9)$$

where θ is the weighted average of the measured soil water content within the rooting zone of the soil, $\theta_{FC}$and θ_{WP} are the water content at field capacity and wilting point respectively.

A field vegetation inventory survey by Syncrude Canada Ltd revealed that there are about twenty-seven different species of plants on the study site. Some of these plants are *Calamagrostis canadensis* (bluejoint reedgrass), *Agrostis stolonifera* (creeping bentgrass), *Elymus trachycaulus* (slender wheatgrass), *Medicago sativa* (alfalfa), *Hordeum jubatum* (foxtail barley), *Lotus corniculatus* (birds-foot trefoil), *Picea glauca* (white spruce), *Cornus stolonifera* (red-osier dogwood), *Populus tremuloides* (trembling aspen) (Farnden, 2018). Based on the field vegetation inventory survey by Syncrude, the mean vegetation height after the age of six to 2017 ranged from 0.56 m to 1.28 m. Similarly, Syncrude Canada Ltd found a mean LAI of 2.23 ~ 2.2 for the study site during the study duration.

Found in Appendix E is the study site photos from 2006 to 2017, showing the growth of vegetation on only the deep cover since the photograph on the shallow cover was unavailable. These photos do not show the growth stages of vegetation within a year due to unavailable photographs. However, they show the yearly trend of vegetation growth (O'Kane, 2018).

Prior to the establishment of vegetation at the study site in late June 2005 (Fenske, 2012), soil evaporation was assumed to be occurring on the study site, i.e., right after spring (April/May 2005) to 26 June 2005. The soil evaporation was estimated as a function of the vapour pressure gradient between the atmosphere and the cover surface as follows (Shurniak, 2003);

$$E = \frac{\tau Q + \nu E_a}{\tau + A\nu} \tag{4.10}$$

where E is the vertical evaporating flux (mm/day); τ is the slope of saturation vapour pressure versus temperature curve at the mean temperature of the air (kPa/^{o}C); Q is net radiation (mm/day); ν is the psychrometric constant (kPa/^{o}C); A is the inverse of the relative humidity at the soil surface.

$$E_a = f(u)\, P_a(B - A) \tag{4.11}$$

where $f(u)$ is a function that depends on wind speed, surface roughness and the eddy diffusion.

$$f(u) = 0.35\,(1 + 0.15\,u_a) \tag{4.12}$$

where P_a is the vapour pressure in the air above the evaporating surface (kPa); u_a is the wind speed (km/hr); B is the inverse of the relative humidity of the air.

The relative humidity of the soil surface (h_r) as a function of total suction and temperature and was estimated as follows;

$$h_r = e^{\left(\frac{\varphi g W_v}{RT}\right)} \quad (4.13)$$

where φ is the total suction(m) - measured soil matric suction at 5 cm depth of the soil was used; W_v is the molecular weight of water (0.18 kg/k mole); g is the acceleration due to gravity (9.81 m/s^2); R is the universal gas constant (8.314 J/mole/K); T is the temperature (K) – measured temperature at 5 cm depth of the soil cover was used (Shurniak, 2003; Han and Zhou, 2013).

4.3.5 Estimation of Net Percolation

The net percolation was estimated using the water balance method. The daily NP was calculated for each day by comparing a single day precipitation, AET and change in soil water storage as follows;

$$NP = PPT - AET - \Delta S \quad (4.14)$$

The difference between the volume of the precipitation event, AET and the change in soil water storage volume in either ascending or descending order was assumed to be the water that percolated through the root zone of the covers.

4.4 Estimation of water balance using physics-based model

HYDRUS-1D is a physics based, finite element numerical model, which is used to simulate soil water dynamics in unsaturated soils. It was selected to simulate the water balance within the soil covers in this study due to its successful application in similar applications (Keller *et al.*, 2009; Huang, Elshorbagy, *et al.*, 2011).

4.4.1 The Governing Equation

HYDRUS-1D can simulate two different physical descriptions of the water flow through unsaturated soils. The first model is based on the concept that water flow occurs within a single porosity medium as defined by a hydraulic conductivity function and a water retention function. The second model is based on the concept that water flow is occurring through macropores (i.e.

mobile phase) and water storage is associated within a matrix of finer pores in which there is no water flow (i.e. immobile phase). In this dual porosity approach, the water flow and storage properties are assigned to separate mobile and immobile regions.

$$\theta = \theta_m + \theta_{im} \tag{4.15}$$

where θ_m mobile volumetric water content; θ_{im} immobile volumetric water content

The governing equation for the single porosity approach can be described by the following equation (Simunek; *et al.*, 2013):

$$\frac{d\theta}{dt} = \frac{d}{dx}\left[K\left(\frac{dh}{dx} + cos\,\alpha\right)\right] - S \tag{4.16}$$

where h is the soil pressure head (L); θ is the volumetric water content (cm^3/cm^3); t is time (T); x is the spatial coordinate (L) (positive upward); S is the sink term ($L^3\ L^{-3}\ T^{-1}$); α is the angle between the flow direction and the vertical axis (α = 0 for vertical flow, 90^0 for horizontal flow, while for an inclined flow $0^0 < \alpha < 90^0$); and K is the unsaturated hydraulic conductivity function [L/T^1]

Clay rich soils are often characterized by the presence of macropores formed as the result of aggregate formation or cracking as the result of freeze/thaw or wet/dry cycles. In these types of soils, the single porosity approach requires that the presence of this secondary structure is reflected in hydraulic conductivity and water retention functions which are 'double humped'. This approach was used by Huang et al. ((2015) to simulate water flow and solute transport for the South Bison Hill covers on the Syncrude mine site, soils which are similar to those in the present study. However, the use of inverse modelling (IM) is difficult for these double hump functional relationships. Inverse modelling utilizing the simpler monotonic single hump hydraulic conductivity and water retention curves was attempted initially for this study but was found to provide a poor fit to the observe water content variations.

Huang et al. (2015) did find that the IM with the dual porosity approach was able to capture the observed water content variations for the South Bison Hills cover soils. As a consequence, a similar approach was adopted for this study.

The governing equation for the dual porosity approach is described by the following equations(Simunek; *et al.*, 2013):

$$\frac{\partial \theta_m}{\partial t} = \frac{\partial}{\partial z}\left[K(hm)\ \left(\frac{\partial h_m}{\partial z}\right) + 1\right] - S_m - \ \Gamma_w \tag{4.17}$$

$$\frac{\partial \theta_{im}}{\partial t} = -S_{im} + \ \Gamma_w$$

where; t is the time; $K(hm)$ is the unsaturated hydraulic conductivity function in the mobile region; z is the elevation; S_m and S_{im} are the sink term for both regions; and Γ_w is the transfer rate for water from the fractures to the matrix pores.

The water transfer coefficient was assumed to be having a proportional relationship with the difference between the soil water content of the macropores and the soil matrix systems as described by Gerke and Genuchten (1993)

$$\Gamma_w = \ \alpha_w(\theta_m - \theta_{im}) \tag{4.18}$$

where α_w is a first order transfer coefficient ($L^{-1}T^{-1}$); and the soil water content of both the mobile and the immobile region were estimated from the water retention curves for peat and glacial till materials for both regions. However, water flow was only considered in the mobile region for the coke material and subsequently the saturated and residual water content was estimated from the water retention curve. The equation 4.18 is solved numerically by Hydrus 1-D by applying Galerkin-type linear finite element schemes with specified initial and boundary conditions (Simunek; *et al.*, 2013).

4.4.2 Model Description

The primary parameter sets used within HYDRUS include soil hydraulic parameters, vegetative parameters, and meteorological parameters. The boundary conditions include both initial conditions (e.g. initial water content distribution) and domain boundary conditions (e.g. suction or water flow). The soil hydraulic parameters include the functional relationships defining hydraulic conductivity and soil water storage. The vegetation parameters include leaf area index (LAI), root

distribution, and limiting suction values for evaporative and transpiration water losses. The meteorological parameters include precipitation and solar radiation.

The soil profile in each model included the cover soils (peat and glacial clay) and the underlying coke to a depth of 1 m below the cover/coke interface. The spatial discretization used in the model was 1 cm. Within this model domain, a number of sub-domains were identified to use as observation points. The entire model domain was divided into 8 different observation sites (for a 1.8 m domain) where the thickness of each domain were as follows: deep cover; 8, 8, 9, 5, 7, 29 and 69 cm, and for the shallow cover; and 14 cm, 14 cm, 13 cm, 19 cm, 21 cm, 15 cm, 45 cm. These observation points were the depth interval extending between the midpoint between the sensor and sensors above and below. The average time step for the model was approximately 72 minutes with a maximum time step of 144 minutes.

4.4.3 Initial and Boundary Conditions

The simulation was carried out only for the unfrozen periods (growing season) of the year with the measured soil water content of the soil profile after unfrozen used as the initial water content values.

For both covers, the initial water content was assigned to each layer of the soil cover, surface-atmosphere boundary was assigned as the upper boundary condition (precipitation, potential evapotranspiration fluxes and LAI used). The potential evapotranspiration (PET) was calculated using the Penman equation. The base of the soil column was assumed to be a unit gradient boundary (i.e. the pressure head gradient was zero).

4.4.4 Soil hydraulic Parameters

The unsaturated hydraulic conductivity for the macropores was estimated using the van Genuchten (VG)-Mulaem model as follows:

$$\theta(h) = \begin{cases} \theta_r + \frac{\theta_S - \theta_r}{[1 + [\alpha h]^n]^m} & h < 0 \\ \theta_s & h \geq 0 \end{cases} \quad (4.19)$$

where θ is the volumetric water content [L3/L3]; θ_r is the residual water content; θ_s is the saturated water content; α [L^{-1}], n , m are shaped parameters; h is the pressure head which is assumed to be positive (van Genuchten, 1980); and m is estimated as:

$$m = 1 - \frac{1}{n}$$

$$K(h) = \begin{cases} K_S S_e^{\frac{1}{2}} + \left[1 - \left(1 - S_e^{\frac{1}{m}}\right)^m\right]^2 & h < 0 \\ K_S & h \geq 0 \end{cases} \quad (4.20)$$

where K_S [L/T^1] is the saturated hydraulic conductivity; S_e is the effective saturation and it is estimated as:

$$S_e = \frac{\theta - \theta_r}{\theta_e - S_r} \quad (4.21)$$

4.4.5 Root Water Uptake

The roots of vegetation cover were assumed to penetrate through the entire soil cover to a depth of the cover/coke interface. A water flux down across this interface was considered to be percolated water (i.e. net percolation).

The sink term for both regions, (the root water uptake) accounts for the volume of water taken up by plant roots per unit bulk volume of the soil per unit time and it is estimated by the HYDRUS-1D using the formula by Feddes; et al. (1974);

$$S(h) = \mu(h) \frac{b(i)}{\sum_{i=1}^{\prime} b(i)} T_p \quad (4.22)$$

where $\mu(h)$ is the root water uptake stress response function; T_p is the potential transpiration; pressure head for deciduous plants (*h1* and *h2*) of 500 cm and 15296 cm were used for the study site (Simunek; *et al.*, 2013). This was on the basis of the definition of h1 which is the value of the limiting pressure head below which the plant root cannot longer extract water at the maximum rate while h2 is the value of the pressure head below which root water uptake stops (normally taken as the wilting point) (Simunek; *et al.*, 2013)

$$\mu(h) = \begin{cases} 1 & h \geq h_1 \\ \dfrac{h_2 - h}{h_2 - h_1}, & h_2 < h < h_1 \\ 0, & h \leq h_2 \end{cases} \quad (4.23)$$

The factors influencing the root water uptake by plants are the potential transpiration, T_p, the root distribution function as have been described before, *b(z)* and the rate at which soil can supply water to the roots, *u(h)*.

4.4.6 Estimation of Potential Soil Evaporation and Plant Transpiration

The Hydrus 1 D model calculated potential evaporation and transpiration fluxes from PET using Beers law that partitions the solar radiation components of the energy budget as follows (Simunek; *et al.*, 2013):

$$T_P = ET_p\left(1 - e^{(-k * LAI)}\right) \quad (4.24)$$

$T_{p\,=}\, ET_p$ SCF

where T_P is the potential transpiration (LT^{-1}); ET_p is the potential evapotranspiration (LT^{-1})

$$E_P = ET_p\left(e^{(-k * LAI)}\right) \quad (4.25)$$

$$E_P = ET_p(1 - SCF)$$

where SCF = 1- exp (-a_i *LAI*); a_i = 0.54 (White *et al.*, 2000); E_P is the potential evaporation; LAI = 2.2 (obtained from site inventory survey by Syncrude Canada Ltd)

4.4.7 Estimation of Actual Soil Evaporation and Plant Transpiration

The actual plant transpiration and soil evaporation were estimated in Hydrus 1-D as explained below.

4.4.7.1 Actual Transpiration

Hydrus-1-D applies actual transpiration (Ta) as a sink term to the Richard equation over the rooting depth, z_R (L, using positive values) (Feddes;, Kowalik; and Zaradny, 1978). Using positive values

because z which is the vertical coordinates has its origin at the soil surface and directed positive upwards. This is expressed as follows (Huang, Barbour, *et al.*, 2011);

$$Ta = \int_{zr}^{0} S(h)dz \tag{4.26}$$

where z_R is the root depth (L); Ta is the actual transpiration (LT^{-1})

4.4.7.2 Actual Evaporation

The flow of soil water (Darcian flux, q) at the surface of the soil is controlled by the meteorological conditions. The only factor that controls the potential rate of soil evaporation from a given soil is the atmospheric conditions. However, actual flux over the soil surface depends on the ability of the porous medium to transfer water from the lower depth of the soil surface (Feddes;, Kowalik; and Zaradny, 1978). Thus, actual infiltration is limited by the antecedent soil water content whereas potential rate of infiltration depends on the atmospheric or other external conditions. As a result of this phenomenon, the boundary condition at the soil surface may alternate from a prescribed head and vice versa.

Numerical solution of the Richard equation is obtained by constraining the absolute value of the evaporation flux by satisfying the underlisted conditions.

$$\left|-K\ \frac{\partial h}{\partial x}\ - K\right| \leq E \qquad \text{at} \quad x = 0 \tag{4.27}$$

$$h_A\ \leq h \leq h_s \qquad \text{at} \quad x = 0$$

At the surface of the soil x = 0 and at the bottom of the soil profile x = -z

where E is the maximum potential rate of infiltration or evaporation under current atmospheric condition (LT^{-1}), h_A and h_s are the minimum and maximum pressure head at the soil surface under prevailing soil condition and K is the hydraulic conductivity (LT^{-1}), h is the total head (L) and x is the length of the soil column (L). The value of h_A was determined from the equilibrium conditions between soil water and the atmospheric vapour, h_s is usually set to zero; if positive, h_s represent a small layer of ponded water (Simunek; *et al.*, 2013).

4.4.8 Model Calibration and Validation

Prior to the simulation of the daily water balance using the Hydrus-1D model, the van Genuchten (VG) parameters were obtained by calibrating the model against water content monitoring data.

The simulation of water flow using the dual porosity model in Hydrus 1-D requires $K_s, \theta_{rm}, \theta_{sm}, \alpha, n$ in the mobile, θ_{rim} and θ_{sim} in the immobile, and water transfer coefficient, ω_w between two regions for each material.

In the calibration process, the K_s θ_{sm}, α, n and ω_w parameters were optimised yearly by applying the inverse procedure for the peat and till materials, while θ_{rm} and θ_{rim} were for each material. In addition, all the required parameters for the coke were obtained from the research work of Fenske (2012) and O'Kane (2004).

The values of θ_{rim} and θ_{sim} for each material were obtained from the research work of Huang, Barbour and Carey, (2015) while the value θ_{rm} was 0 for peat mineral mix and the secondary till material. The θ_{sm} value was decided based on the soil water content data from the study site. The Ks and optimised VG parameters for the three materials for both covers are shown in section 6.2. After the yearly calibration, the Ks was found to be evolving, similar to what was reported by Huang et al. (2015). This Ks values for all years were plotted together with the measured Ks values obtained by Meiers; et al. (2011) from South Bison Hill. The Ks value at which the covers were assumed to have stabilised was selected together with its corresponding θ_{sm}, n and $\propto$ values.

These calibrated Ks, θ_{sm}, n and $\propto$ values were used to simulate the soil water content and subsequently the water balance components for both covers at the CBIW site (validation process). To improve the simulation in the validation process, Ks and $\propto$ values were fixed while the θ_{sm} and n values were not fixed in the mobile region. Similarly, in the immobile region, the θ_{sim} and θ_{rim} were fixed while the ω_w was not fixed.

4.4.9 Statistical Analysis

The simulated water content for the various soil cover observation sites at different time lapse were compared with the measured water content values. In assessing the accuracy of the model, the root-mean-square error (RMSE) and coefficient of determination (R^2) were calculated.

The actual deviation between the simulated and the measured values are provided by the RMSE which ranges from 0 to infinity as it has no higher bounds. However, the lower the RMSE, the better the agreement.

$$RMSE = \left(\frac{\sum_{i=1}^{n}(x_i - y_i)^2}{n}\right)^{0.5} \quad (4.28)$$

where x_i is the i[th] measured soil water content; y_i is the i[th] simulated soil water content; n is the total number of observations (ASCE-EWRI Task Committee, 2002).

CHAPTER 5

PRESENTATION OF MONITORING DATA

This chapter presents the various field measurement data including meteorological and soil monitoring data. The meteorological data include ambient temperature, relative humidity, wind speed and direction, net radiation and precipitation data. These data were measured at a height of 2 m. The soil monitoring data to be discussed are the soil water content and soil temperature. Meteorological data is presented in the form of potential evapotranspiration followed by the soil measurement data obtained from the shallow and the deep covers respectively.

5.1 Potential Evapotranspiration

Shown in Table C.1 in Appendix C is the potential evapotranspiration (PET) data for both covers. It is important to note that based on the soil temperature results, the shallow cover thawed earlier than the deep cover and hence has long growing season period which reflect into higher PET and precipitation for the shallow cover than the deep cover. The results of the PET for the shallow cover ranged from 611 mm to 719 mm with a mean of 660 mm. The highest PET of 719 mm was obtained for the shallow cover in 2006 with the lowest PET of 611 mm obtained in 2014. Similarly, the range of PET for the deep cover during the study duration was 574 mm to 668 mm with a mean of 620 mm. The highest PET of 668 mm was obtained in 2015 while the lowest in 2013.

The measured meteorological data obtained from the MLSB site for this study was verified for its accuracy before it was used to estimate PET.

The Pearson correlation coefficient (r) results between the meteorological data obtained at CBIW and data from the adjacent environment were found to have a strong correlation with data from the neighbouring sites. A Pearson correlation coefficient value of 0.99 and 0.88 were obtained for temperature and RH respectively for the study site and 30 Hill Top, SWSS C32 and W1 sites. A correlation coefficient of 0.93 was obtained for net radiation between the CBIW site and 30 Hill Top and W1 site, while r of 0.90 was obtained for net radiation between the CBIW and SWSS C32

site. The r of wind speed was 0.8 between CBIW and 30 Hill Top, 0.64 between CBIW and SWSS C32 and 0.77 between MLSB and W1 site.

5.2 Precipitation

A summary of precipitation data for both covers during the study duration are shown in Figure 5.1 and Table C.2 in Appendix C. The highest annual rainfall of 397 mm was obtained in 2005 and 2016 with a minimum annual rainfall of 169 mm obtained in 2009. Similarly, the highest annual SWE of 120 mm was obtained in 2007 with a minimum SWE of 25 mm obtained in 2017. However, highest annual precipitation (annual rainfall + SWE) was 464 in 2005 with the lowest annual precipitation of 260 mm obtained in 2011.

The highest growing season rainfall for the shallow cover was 385 mm in 2016 while the minimum growing season precipitation was 161 mm in 2009 (Figure 5.1 and Table C.2). In the case of the deep cover, the highest growing season rainfall was 382 mm was obtained in 2016 with the minimum of 154 mm obtained in 2009. The growing season rainfall was slightly higher for the shallow cover due to the longer growing season (i.e. unfrozen cover) utilized for the shallower cover.

Generally, out of the mean annual precipitation of 369 mm, the annual mean rainfall accounted for 307 mm while 62 mm was snow water equivalent. Of the mean annual rainfall of 307 mm, 291 mm occurred during the growing season period for the shallow cover while 277 mm was for the deep cover.

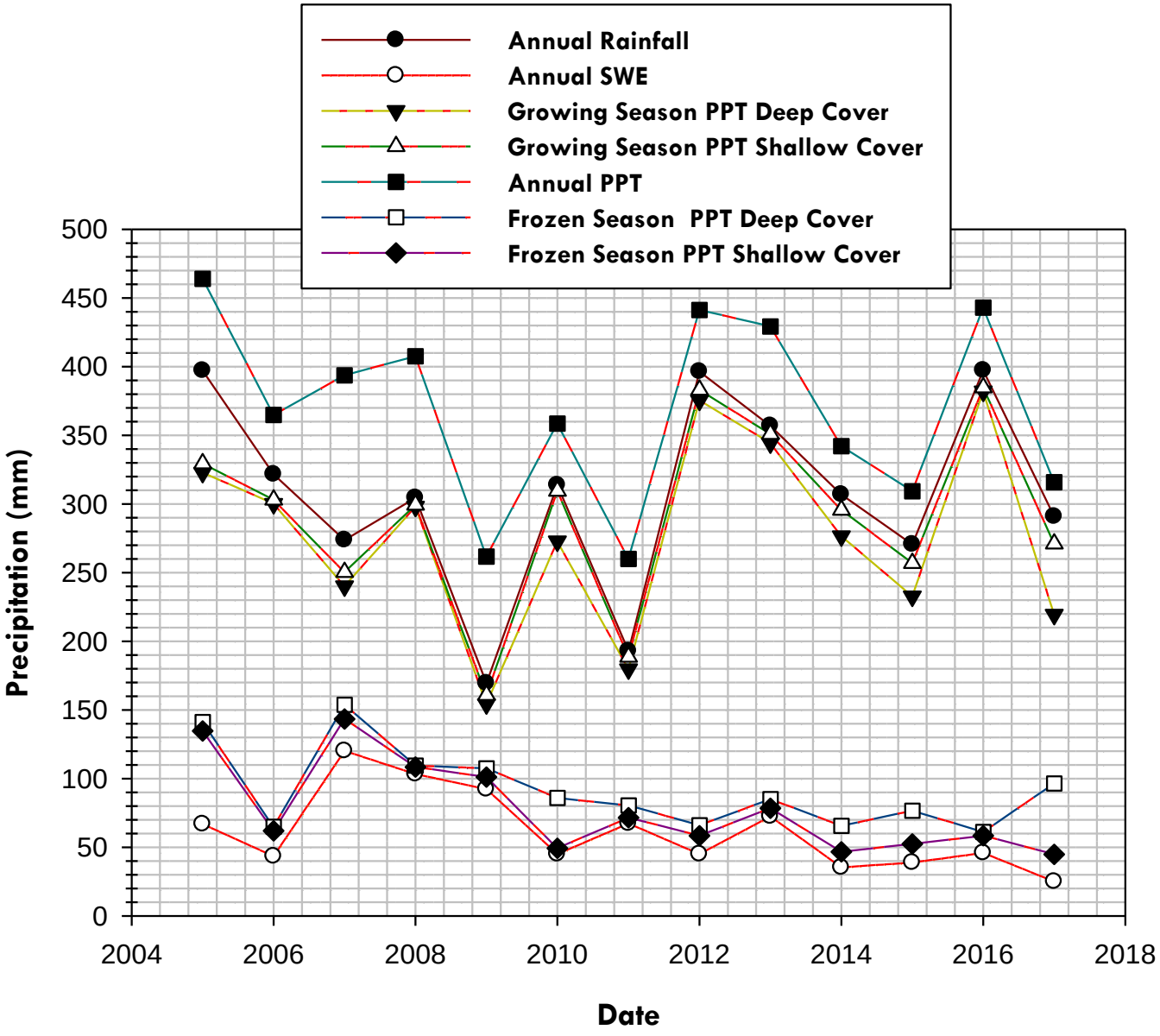

Figure 5.1: Annual rainfall, growing season PPT and SWE depth during the study period

5.3 Soil Monitoring Data

Presented in this section is the soil monitoring data including soil temperature and soil water content along the soil profile. The soil temperature measurements were the basis for defining the start and end of the growing season period for both covers.

5.3.1 Soil Temperature

Shown in Figure 5.2 and Figure A.1 to Figure A.3 in Appendix A is the soil temperature measurements of the soil profile for the shallow cover. The figures highlight the differences in temperatures between the soil cover and the underlying coke. The cover and underlying coke generally freeze to approximately the 90 cm depth annually, depending on the duration of winter for the year. The coke at depths greater than 100 cm never freezes. The soil temperature was observed to be above 0 from the surface layer to 90 cm depth around April/May yearly, highlighting that the base of the cover remains frozen during freshet. The temperature increased sharply to about 22 ^{o}C in July (peak temperature for the year) and declined from July to 0 ^{o}C around October/November yearly. During the frozen period of the year (October/November and April/May) a peak minimum temperature ranging from -2 ^{o}C to -10 ^{o}C depending on the year were observed. The coke at a depth of 100 cm was observed to have a minimum temperature of about 1^{o}C in May each year and increased to a maximum temperature of around 19 ^{o}C each year in August. Likewise, the coke at a depth of 180 cm had a minimum temperature of about 4 ^{o}C in April and a maximum yearly temperature of about 18 ^{o}C in September.

The temperature profiles for the deep cover exhibited a similar pattern to those for the shallow cover. The soil temperature measurements of the soil profile for the deep cover are shown in Figure 5.3 and Figure A.4 to A.6 in Appendix A. In contrast to the shallow cover, it is apparent that although the base of the cover (i.e. 90 cm depth) and the coke below the covers (e.g. 100 cm depth) freezes in most years, the coke below the cover (i.e. 100 cm depth) only approaches near freezing temperatures in 2007 and 2013.

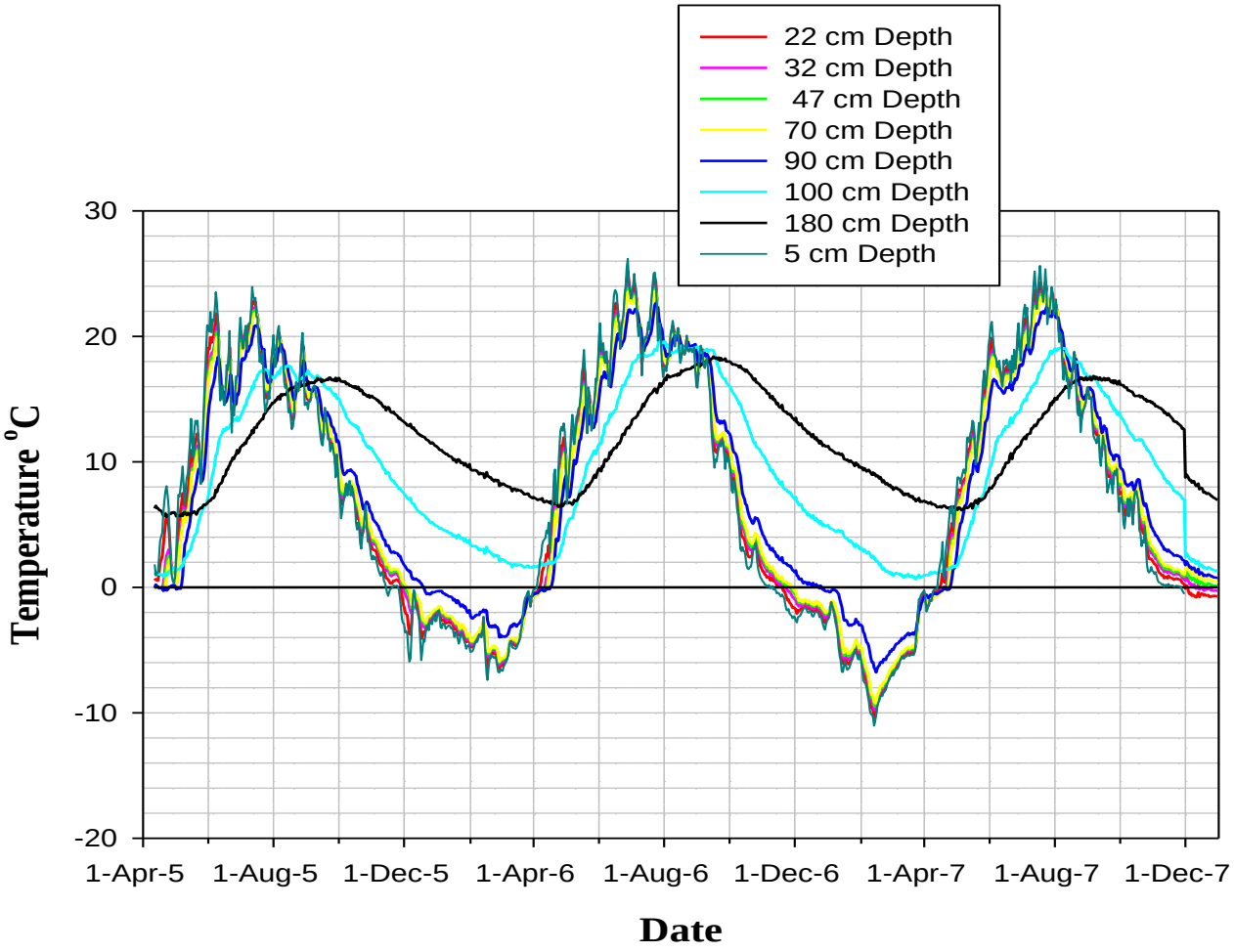

Figure 5.2: Measured Soil Temperature of Soil Profile for the Shallow Cover (2005-2007)

Like the shallow cover, the frozen period of the deep cover was observed to be consistently occurring between late October/early November to late April/early May each year. The coke at a depth of 180 cm remained unfrozen in winter period during the study duration. The soil temperature was found to be higher than 0 ^{o}C from the surface layer to a depth of 100 cm in late April/early May and increased sharply to about 20 ^{o}C in late July/early August (peak temperature) and decreased to 0 ^{o}C in late October/early November yearly. During the frozen period, a peak minimum temperature ranging from -2 ^{o}C to about -8 ^{o}C was observed for the study duration. The coke at a depth of 180 cm was observed to have a minimum temperature of around 3 ^{o}C in May and a yearly maximum temperature of about 15 ^{o}C in September.

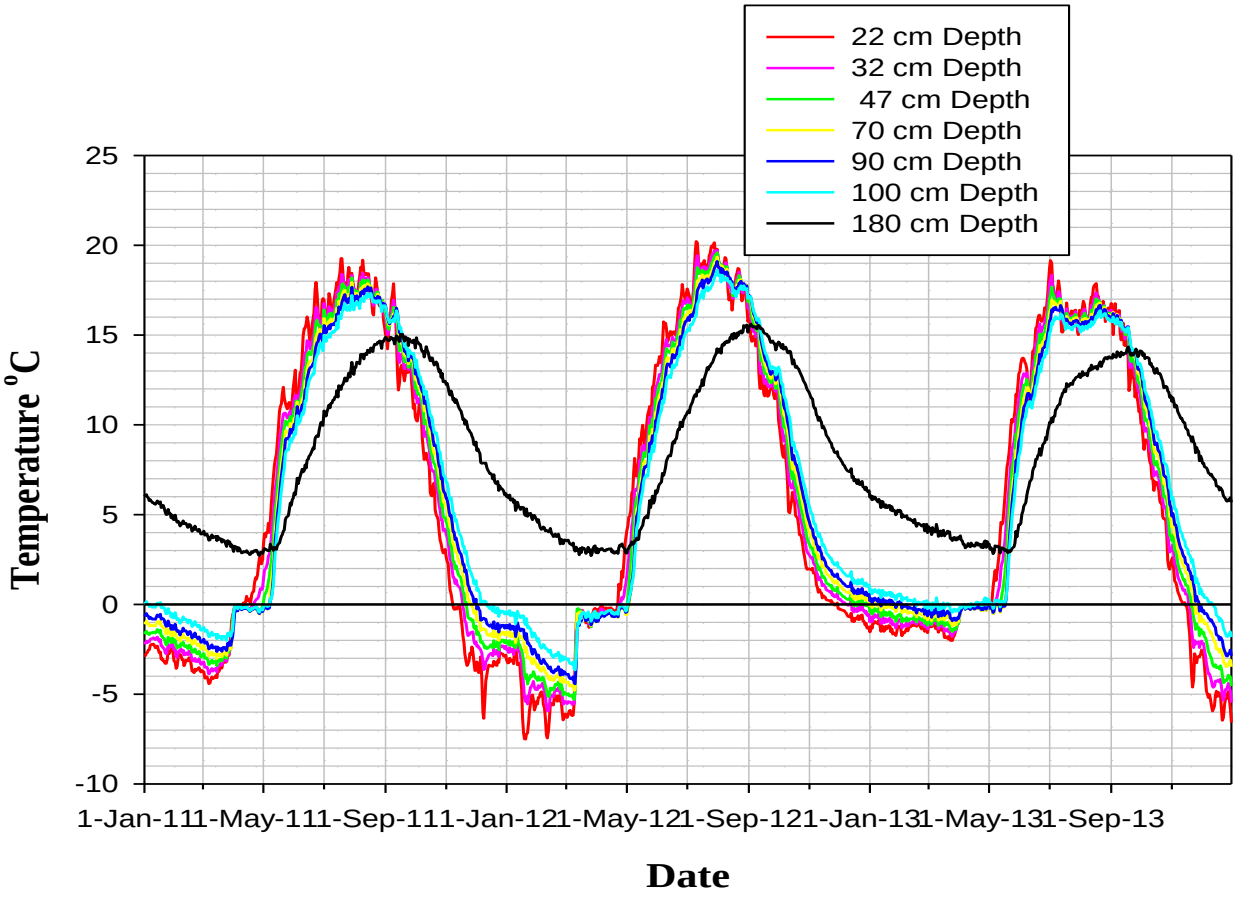

Figure 5.3: Measured Soil Temperature of Soil Profile for the Deep Cover (2011-2013)

5.3.2 Volumetric Soil Water Content and Storage for Both Unfrozen and Frozen Seasons

Presented in this section is the trend of the measured volumetric soil water content of the soil profile for both the shallow and the deep covers of the MLSB site. This section also presents a preliminary evaluation of the covers ability to store water from individual precipitation events (snowmelt or daily rainfall) but without taking into consideration losses due to AET. The trend of the measured soil water content is presented first followed by the cover's ability to store water for the shallow and the deep covers respectively.

5.3.2.1 Volumetric Soil Water Content Dynamics for both Covers

Shown in Figure 5.4, Figure 5.5 and Figure A.7 to A.18 in Appendix A are the volumetric soil water content of the shallow cover. A general overview of the trends of the soil water content for the shallow cover shows that the peat at 10 cm depth has a consistently higher volumetric water content than the peat at 5 cm depth. This may be due to the peat at the 10 cm depth being near the

interface between the peat mineral mix and the glacial till layer which has a lower hydraulic conductivity than the peat material, hence the slow infiltration rate through the till material results in increased water content at the 10 cm depth.

Similarly, the water content at the 32 cm depth of the till material was observed to be higher than the measurement at 22 cm and 27 cm depth. The reason for this occurrence is that the coke layer underneath the till material serves as a capillary break, resulting in a lower value of suction within the coke below the base of the till layer, enabling an increased water content in the till layer immediately above the coke (32 cm depth).

The higher observed volumetric water content at a deeper depth of 180 cm than shallow depth (42 cm and 90 cm) of the coke during the study duration is as a result of the presence of a water table at that depth and associated capillary fringes. The water table within the coke was generally observed to be at a depth of 180 cm below the surface (Figure 5.4, Figure 5.5 and Figure 5.7 – Figure 5.8; Figure A.7 to A.28 in Appendix A). A typical example of the soil water content across the cover profile is shown in Figure 5.6.

Another observation from the figures is the increase in the volumetric soil water content from the previous fall to the next spring. This increase is a clear indication of an increase in storage due to snowmelt infiltration from pre-freeze up to post-thaw (which will be evaluated later). This initial increase in soil water content subsequently decreases as a result of increasing rates of evapotranspiration over the growing season. The lowest volumetric water for the year was consistently recorded around July/August. However, it was observed from the figures that, this reduced soil water content was increased whenever there was a precipitation event, predominantly at the shallow depth of the cover (i.e. from surface to 22 cm depth), highlighting the capacity of the cover for water storage. Rarely, does the measurement points at a deeper depth within the cover respond to a precipitation event which might suggest either the absence of preferential flow or an inability of the deeper soil profile to capture water infiltrating through macropores.

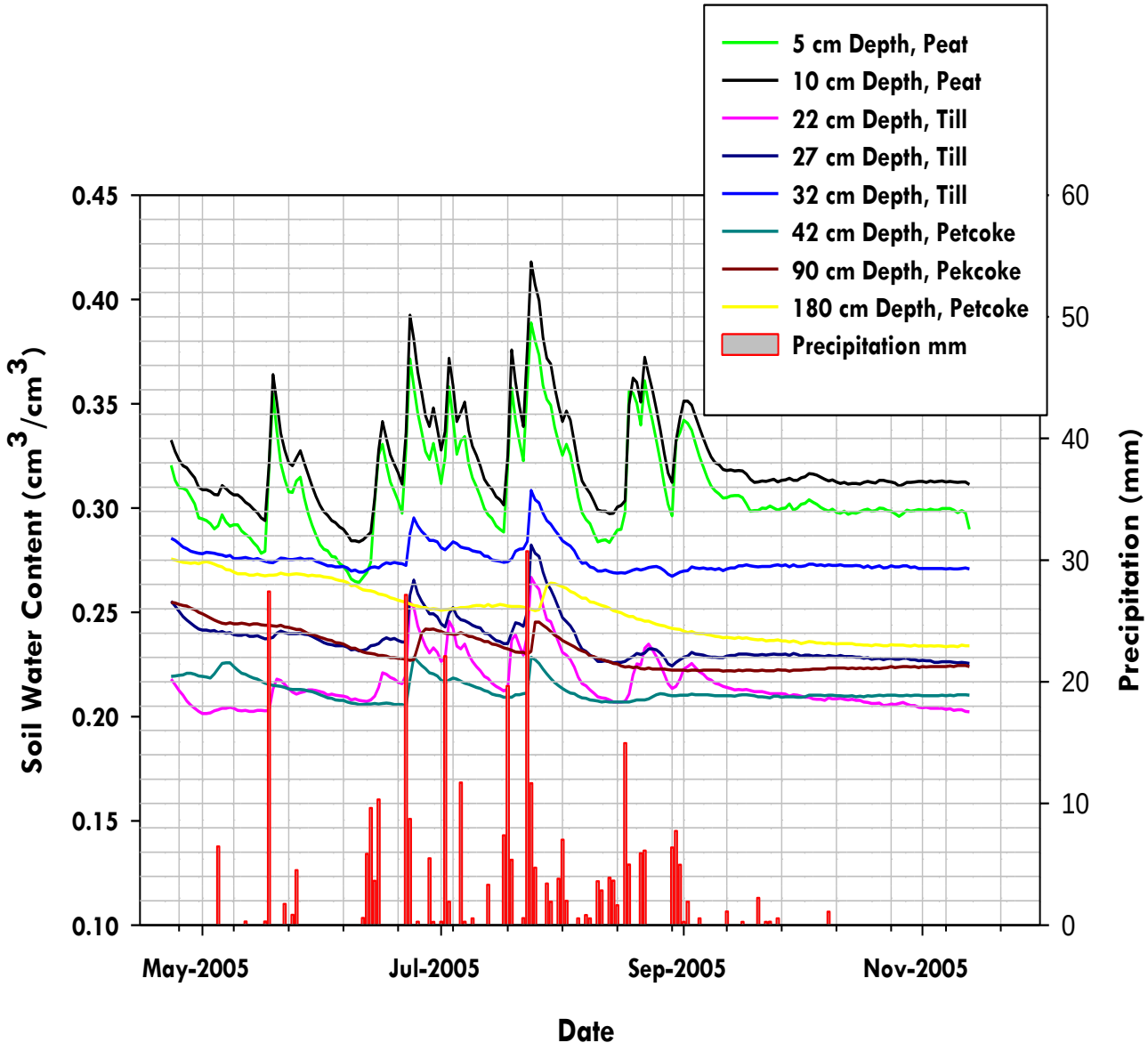

Figure 5.4: Volumetric Soil Water Content with Precipitation for the Shallow Cover (2005)

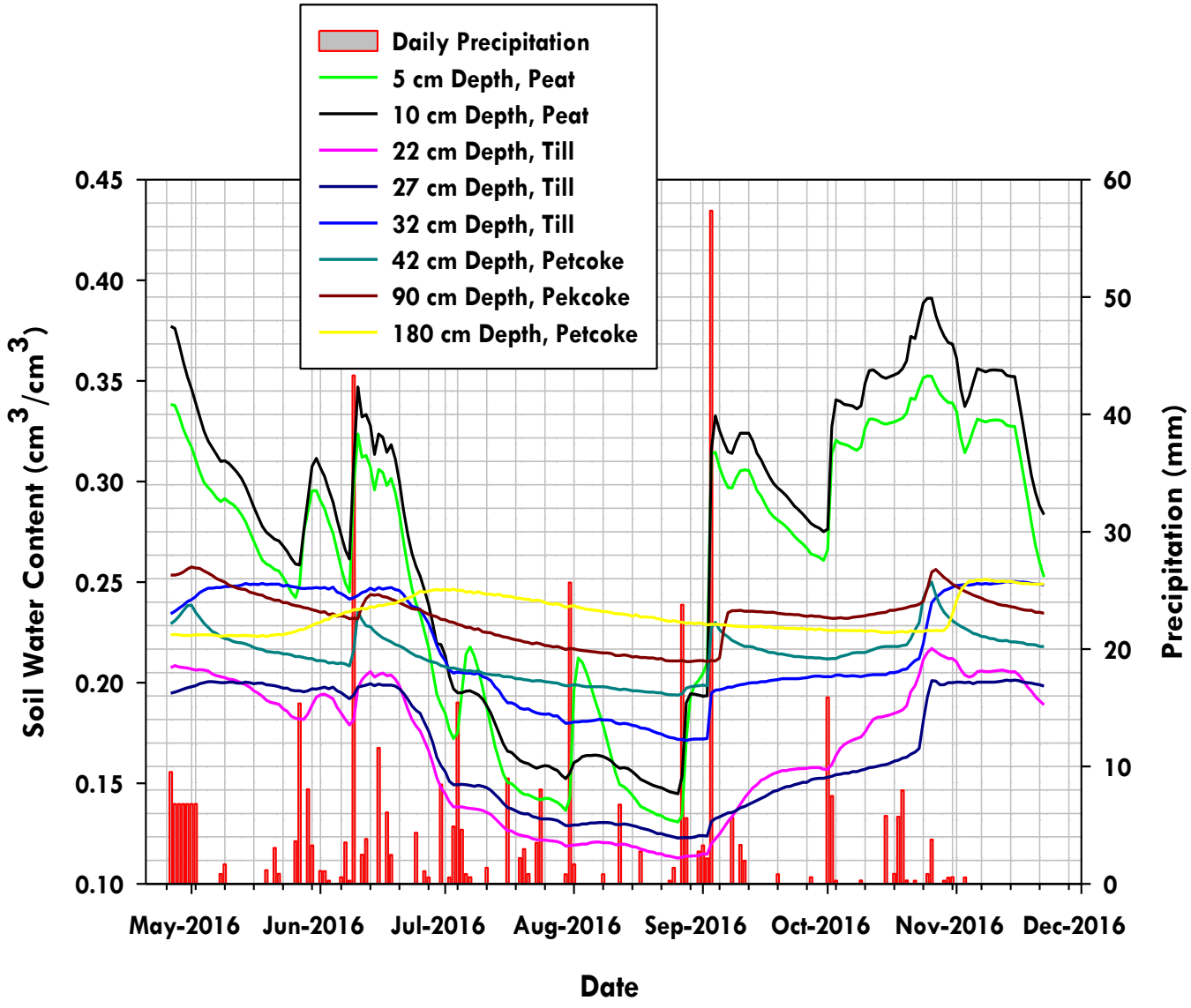

Figure 5.5: Volumetric Soil Water Content with Precipitation for the Shallow Cover (2016)

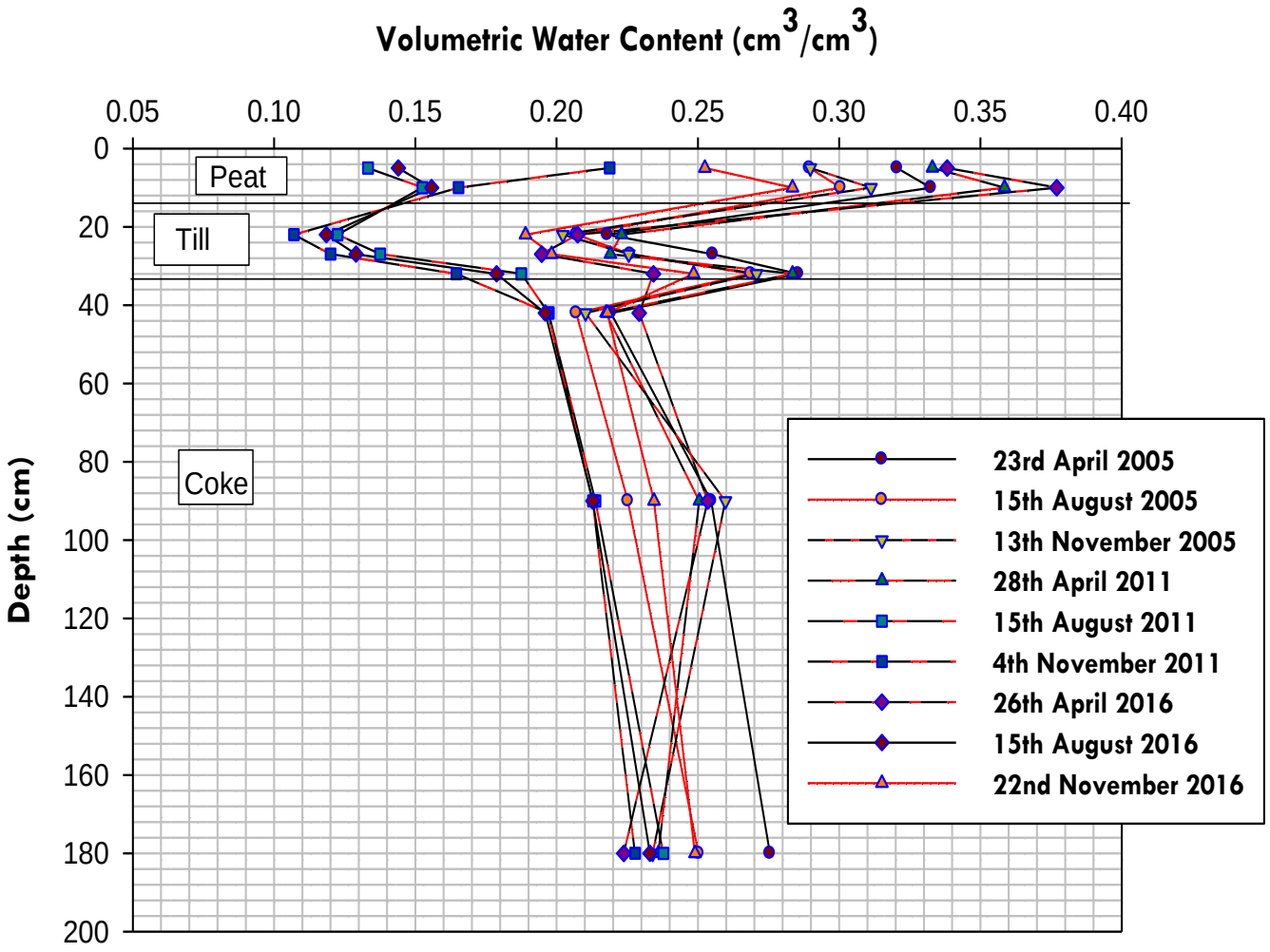

Figure 5.6: Volumetric Soil Water Content Profile, Shallow Cover

Figures 5.7, 5.8 and Figure A.18 to A.28 in Appendix A shows the measured volumetric water content of the soil profile for the deep cover. The general trends of the soil water content were similar to the observation made at the shallow cover.

For most of the years, an increase in soil water content was observed immediately after spring as a result of the contribution of snowmelt. This increased in soil water content decreased to a minimum around August, probably as a result of high evapotranspiration rate. However, it was generally observed that increases in water content occurred consistently with precipitation events as shown in Figure 5.7 and Figure 5.8.

It is important to note that in most instances the observation points at surface layers including 5 cm, 22 cm responded to a precipitation event. But the observation points at a deeper depth of the cover profiles including 47 cm, 70 cm, and 90 cm rarely responded to a precipitation event. This could be possibly due to the lag time required for infiltrating water to reach the deeper depth while water losses due to evapotranspiration are continuing. In a few instances, the observation points at deeper depth responded to precipitation event with high intensity. A typical example of the soil water content profile for the deep cover is shown in Figure 5.9.

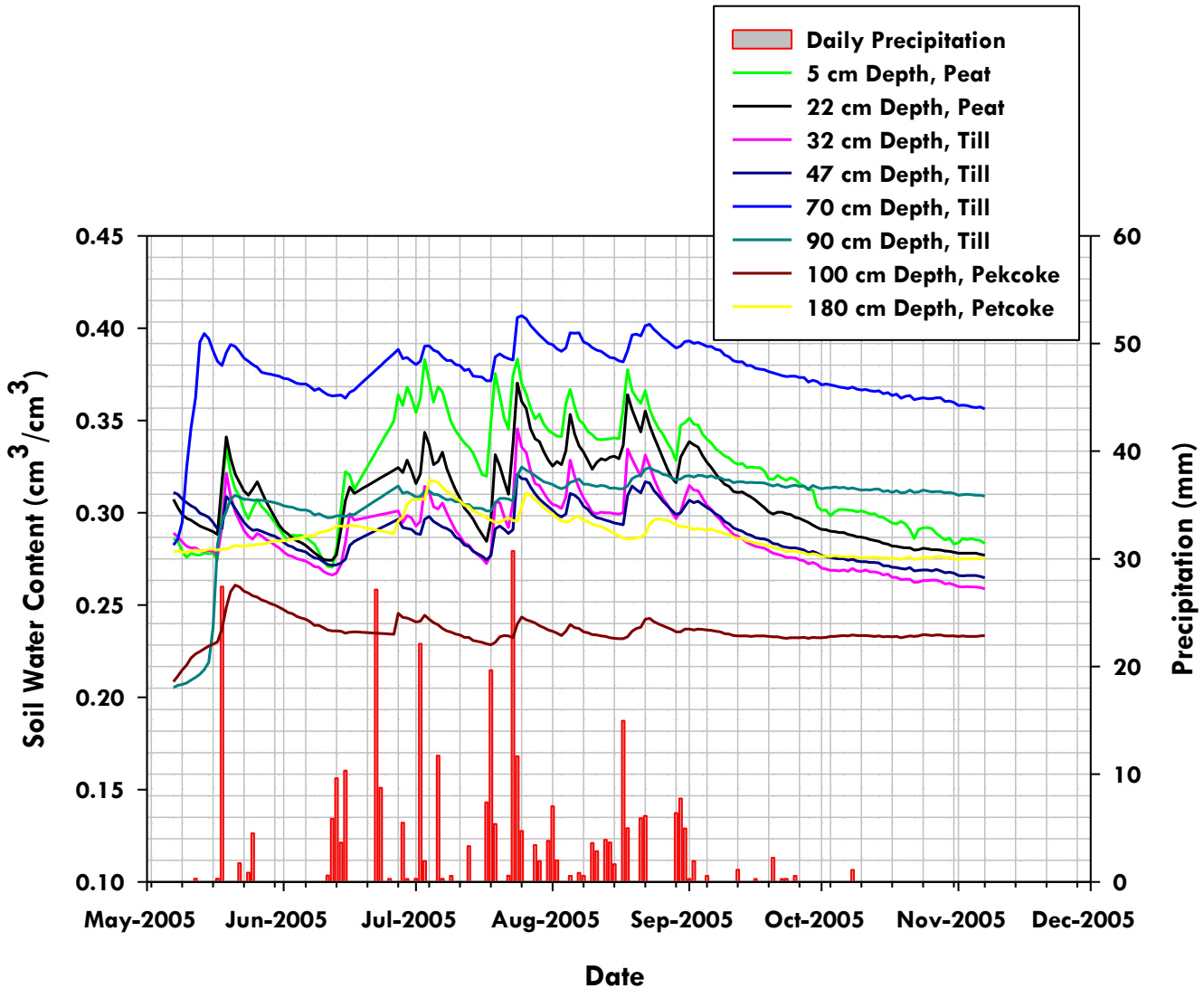

Figure 5.7: Volumetric Soil Water Content with Precipitation for the Deep Cover (2005)

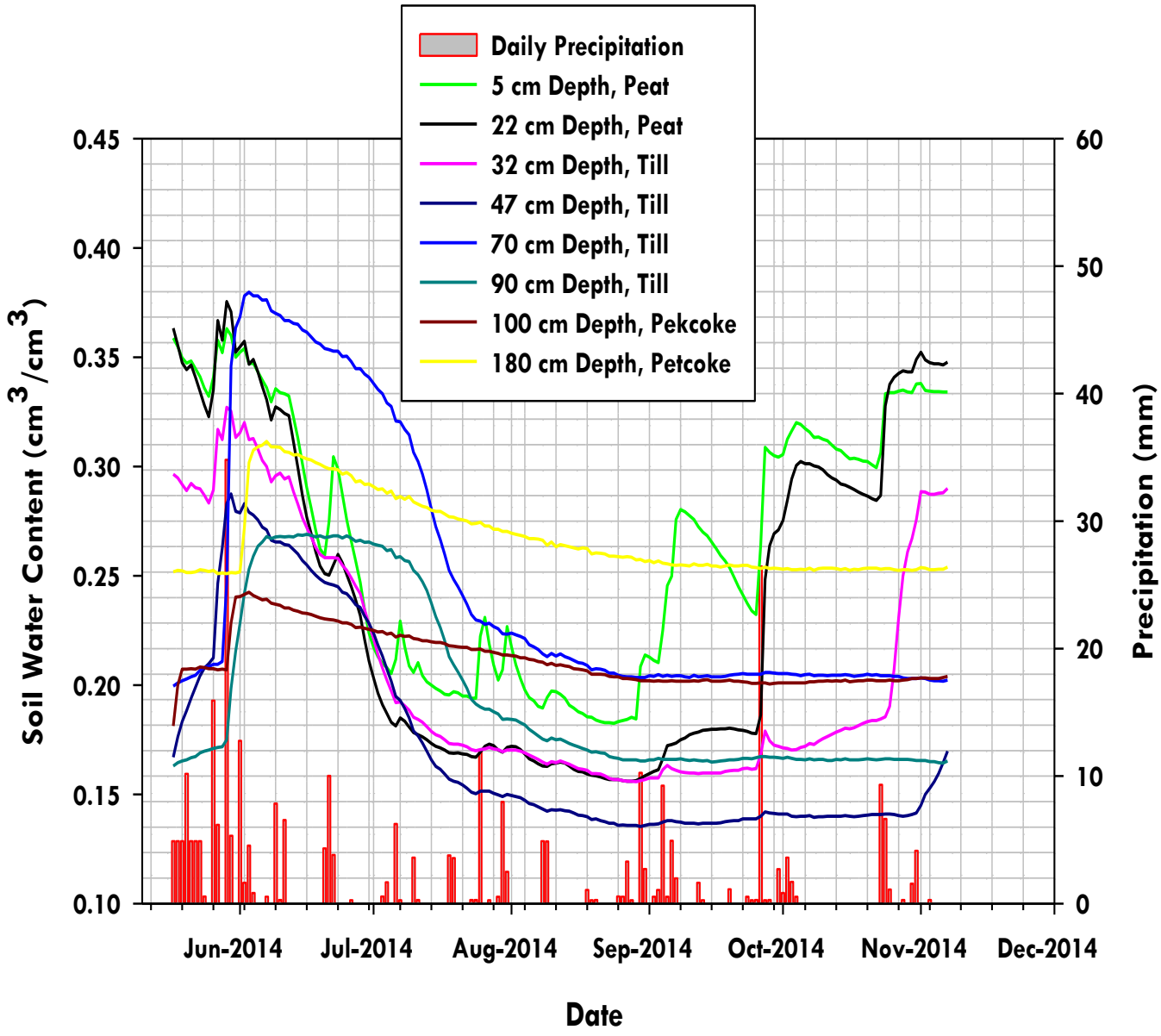

Figure 5.8: Volumetric Soil Water Content with Precipitation for the Deep Cover (2014)

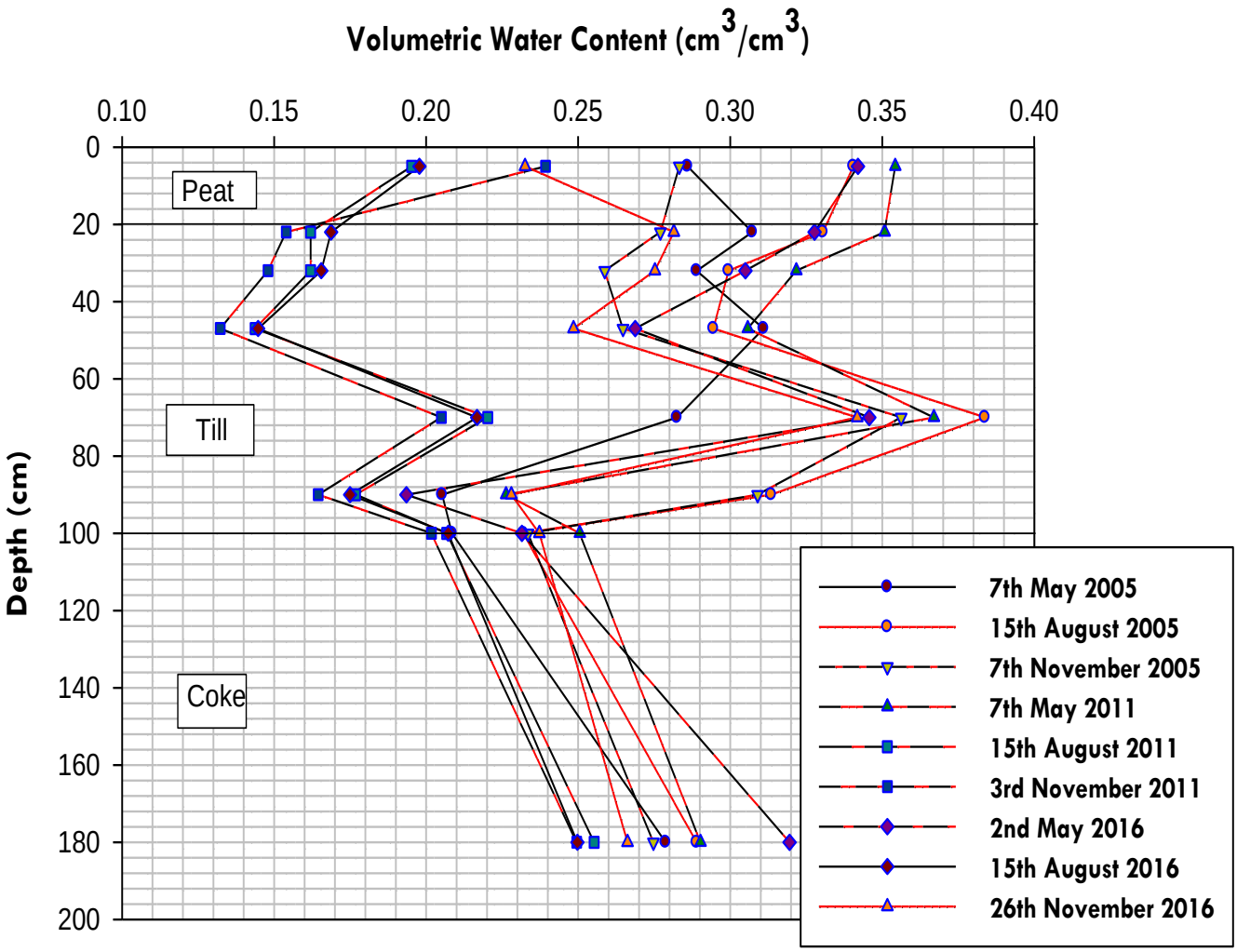

Figure 5.9: Volumetric Soil Water Content Profile, Deep Cover

5.3.2.2 Water Storage Abilities by the Covers for both Unfrozen and Frozen Seasons

The changes in water storage within the covers in response to precipitation events (e.g. daily rainfall or snowmelt) were evaluated by comparing the change in stored water volume across a precipitation event to the magnitude of the precipitation event. The daily estimated change in water storage explained in section 4.3.1 was used as the basis to estimate the daily captured infiltrating water. The difference between the volume of the precipitation event and the change in stored water volume represents water that either did not enter the soil profile (i.e. interception or evaporation) or could not be stored within the soil profile (i.e. net percolation). All obtained results with

negatives which is an indication of water lost either due to percolation or evapotranspiration or both (lost or missing PPT) were removed from the summary.

A similar analysis was also conducted to evaluate the capture of snowmelt water (and rain on frozen ground). In that analyses, the change in storage within the cover from just freeze up to ground thaw the following spring was compared to the volume of water provided to the cover as a result of snowmelt (SWE) and rain on frozen ground.

This analysis does not attempt to replicate the more detailed SD or physics-based models presented later but rather provides only an indication of the capacity of the covers for water capture and storage.

Figure 5.10 to Figure 5.13 provide examples of the results by plotting the infiltration event that was detected as a change in water storage within the shallow and the deep covers. The infiltration event stored is plotted against both the magnitude of the infiltration event as well as the antecedent average water content within the cover to evaluate if there were any consistent trends.

The results show that there does not appear to be any consistent pattern between captured infiltrating water and precipitation event. This is an indication that the net percolation cannot be characterized by the change in storage that is observed following a precipitation event. A key assumption of the system dynamic approach as shown in Equation 4.14.

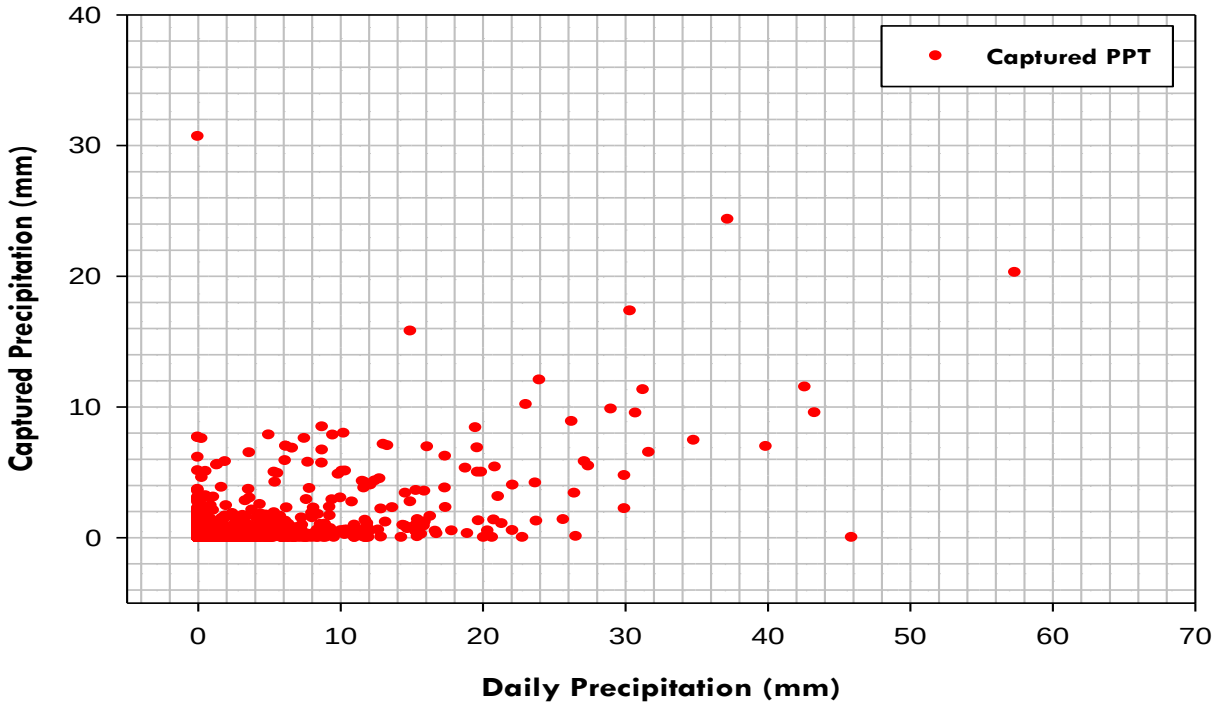

Figure 5.10: Captured Growing Season Precipitation-Shallow Cover (All years)

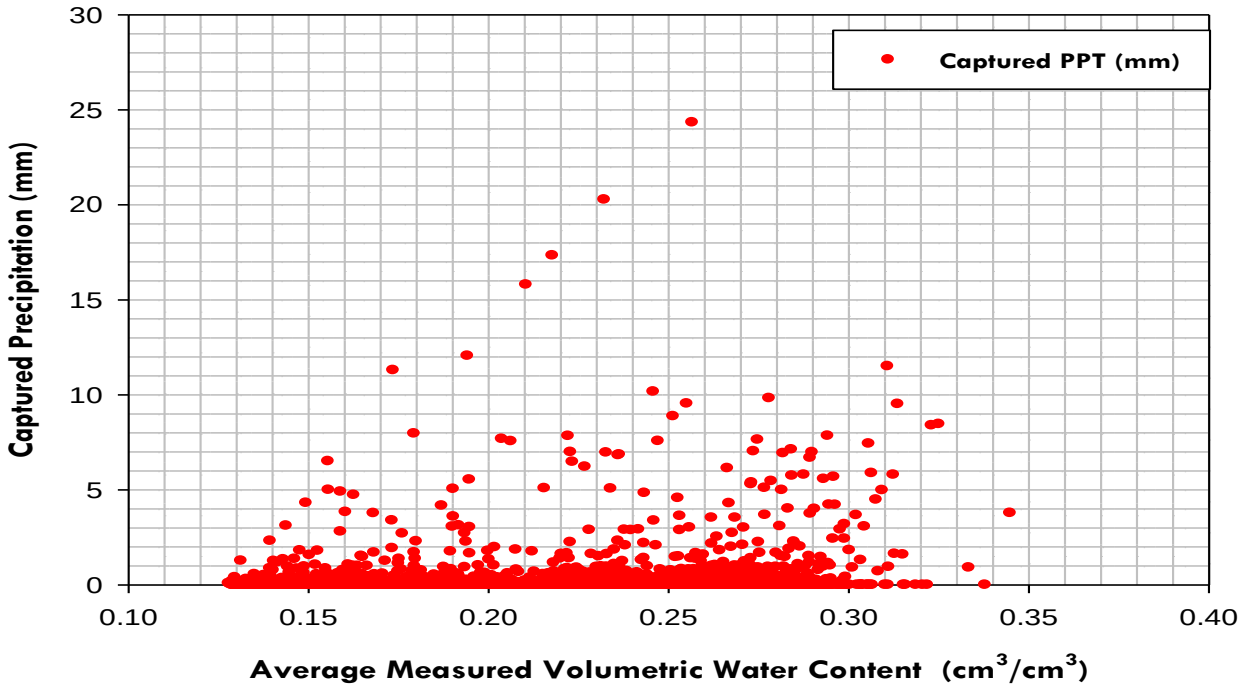

Figure 5.11: Average Water Content -Shallow Cover (All years)

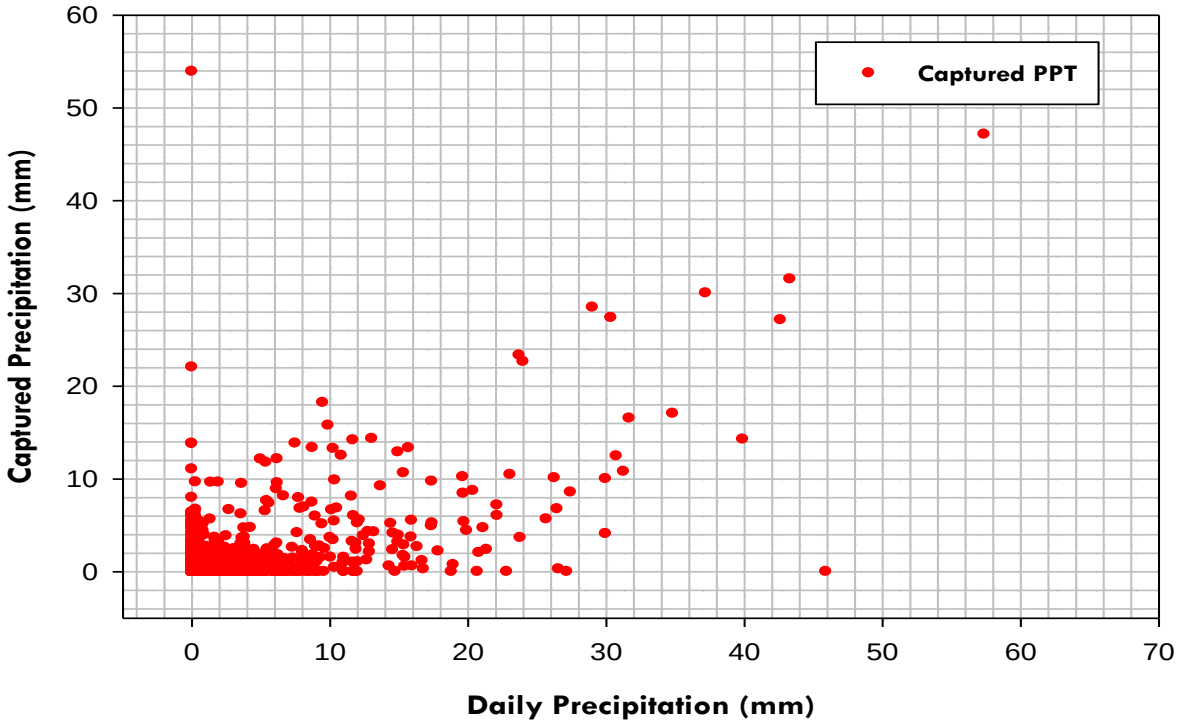

Figure 5.12: Captured Growing Season Precipitation-Deep Cover (All years)

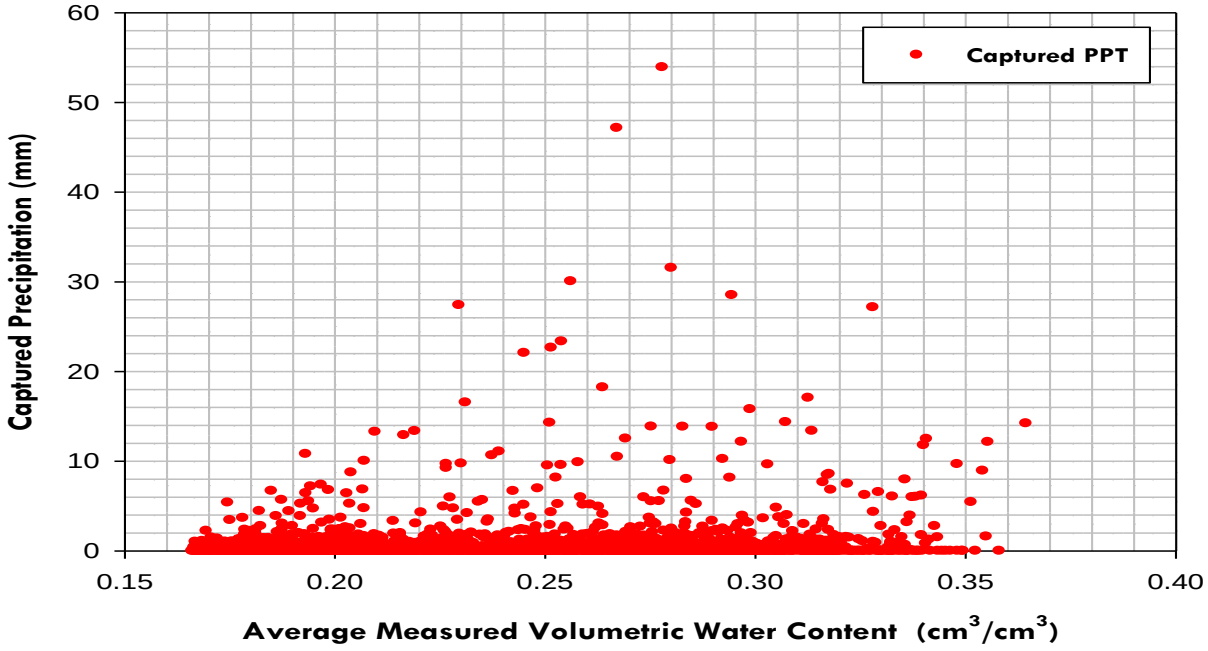

Figure 5.13: Average Water Content -Deep Cover

The cumulative captured infiltrating water for the growing season for the study duration for both covers were evaluated and discussed. Shown in Figure 5.14, Figure 5.15 and Table C.3 in Appendix C is the summary of the growing and frozen PPT, captured PPT and percentage of captured PPT for the shallow cover. From Table C.3 and Figure 5.14, the highest growing season captured precipitation of 121 mm (37% of growing season PPT) was observed to be stored by the shallow cover in 2005. The remaining 208 mm (63% of growing season PPT) was found to be missing. In 2006, the shallow cover captured 105 mm (35% PPT) of the growing season PPT with the remaining 195 mm (75 % PPT) lost. From 2007 to 2017, the captured PPT by the shallow cover ranged from 32 mm (18% PPT) in 2011 to 124 mm (32% PPT) in 2012. Whereas the lost PPT for the same period ranged from 119 mm (69% PPT) in 2009 to 289 mm (75% of PPT) in 2016.

In summary, if true, these analyses would suggest that of the mean growing season precipitation of 291 mm, only 27% (79 mm) was stored by the shallow cover whereas 212 mm (73% of mean growing PPT) was found missing. Given the lack of consistency in the measurements with either the magnitude of the precipitation event of the antecedent water content, this result is highly unlikely. However, if it was true, it would suggest that there was a large volume of the growing season PPT that was not being stored and consequently used for AET by the shallow cover.

Some attempt was made to separate the changes of water storage associated with each cover layer as well as the underlying coke. The peat material is the 160 mm surface layer of the cover beneath it is 210 mm thickness of a glacial till material. The results from this evaluation shows that the peat layer captured an infiltrating water ranging from 26 mm (2017) to 95 mm (2005) with a mean of 48 mm which is 16% of growing season PPT (Figure 5.15). The range of infiltrating water captured by the glacial till material ranged from 10 mm (2008) to 36 mm in 2005 with an average of 20 mm during the study duration. The 20 mm mean infiltrating water for the till material forms 7% of growing season PPT, which is less than half the volume captured by the surface layer. The volume of water stored by the underlying coke ranged from 8 mm in 2011 to 32 mm in 2017 with a mean of 22 mm (8% of growing season PPT). The higher water storage within the coke than the till material is due to the presence of a water table at that depth and related capillary fringes.

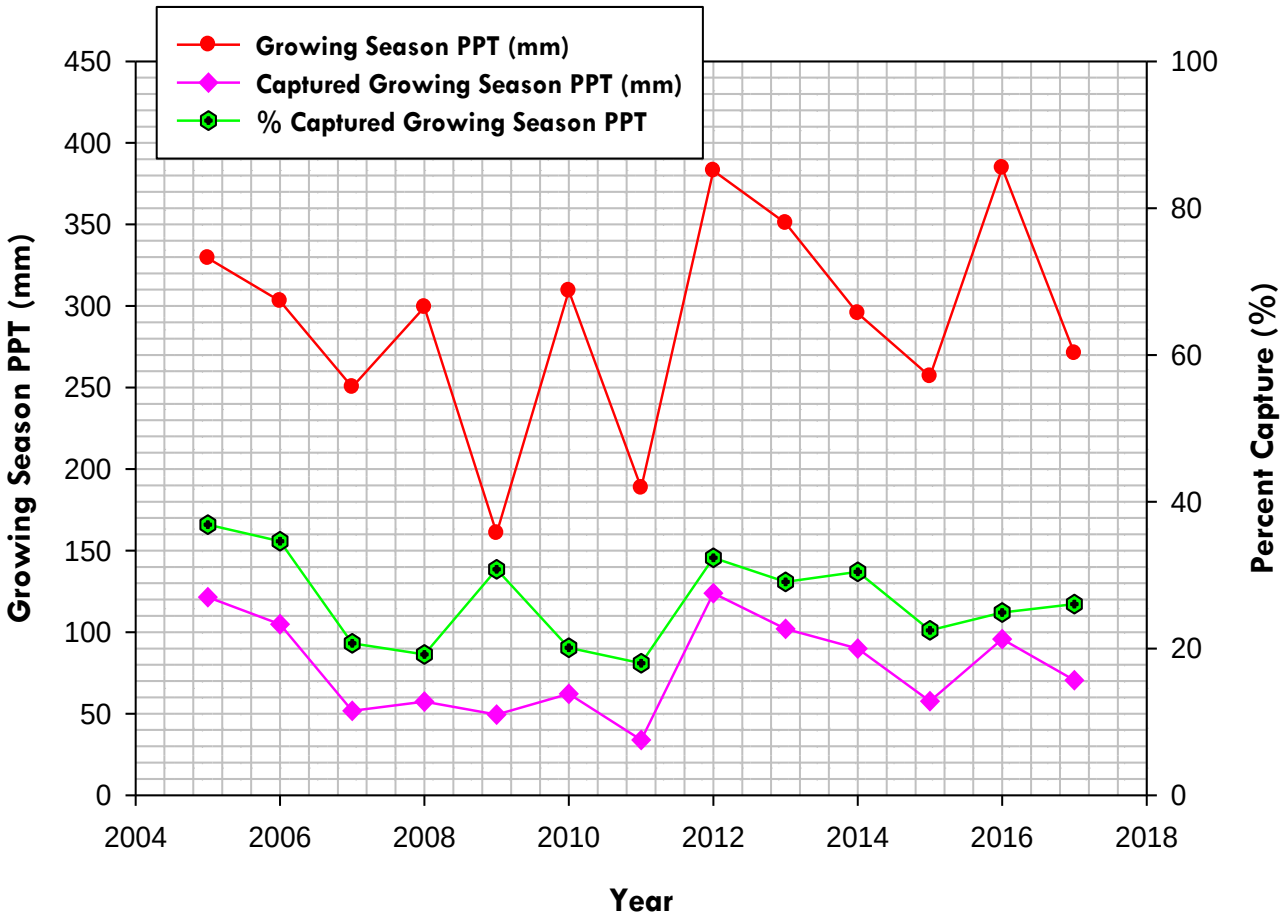

Figure 5.14: Summary of Growing Season Precipitation Component -Shallow Cover

One reason for this anomalous result may be the pre-dominance of the water storage within the peat layer and its subsequent release by both evaporation and transpiration from this layer. The thinness of the layer and the inability of the two sensors to fully capture the water storage dynamics within this layer would render this analysis prone to large errors. Whereas the low volumes of captured infiltrating water at the till material (lower depth) signifies the less likelihood of higher occurrence of percolation through the cover.

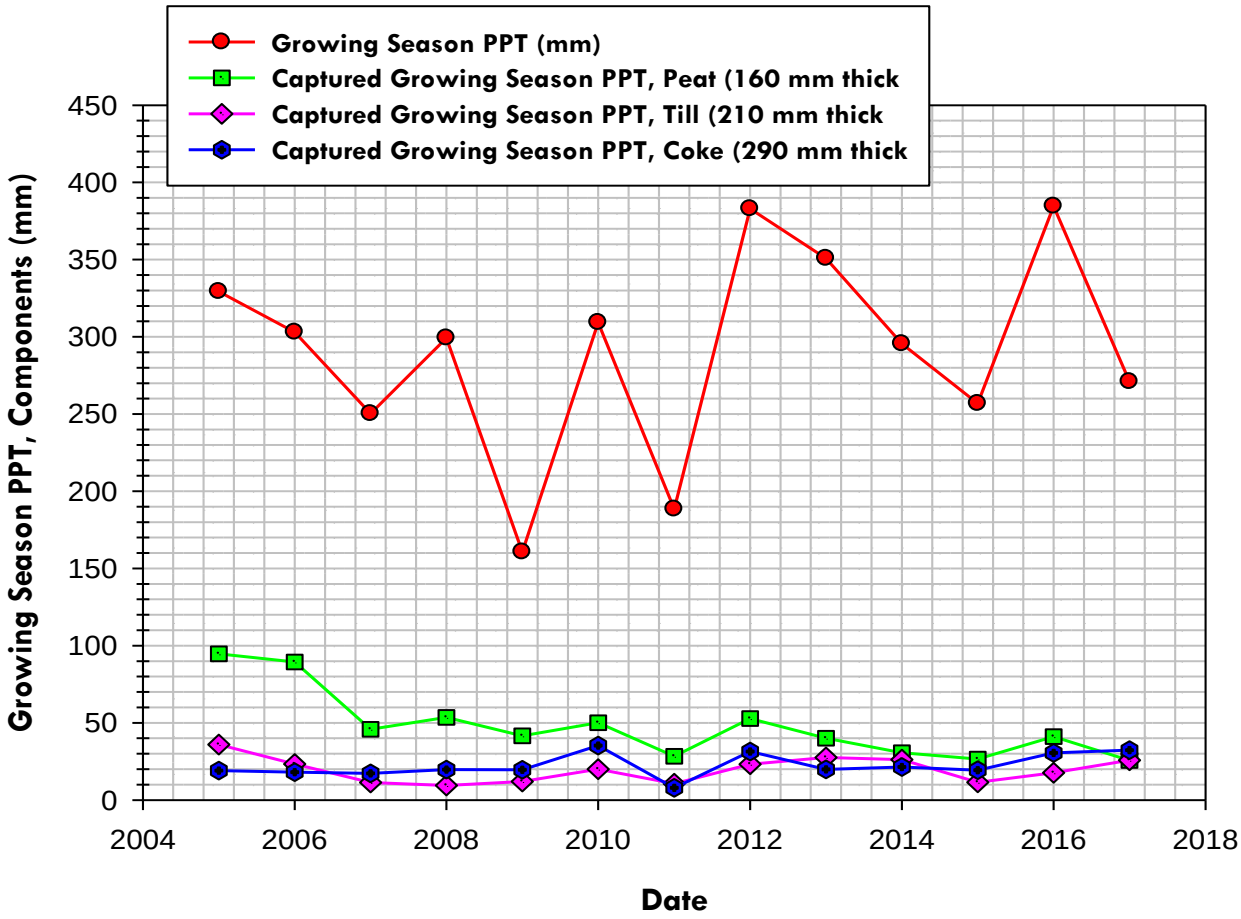

Figure 5.15: Captured Infiltrating Water for Peat, Till and Coke Layers -Shallow Cover

The results of the evaluation of changes in water storage associated with snowmelt is shown in Table C.3 in Appendix C and Figure 5.16. The highest change in storage was 48 mm (82% of SWE plus rain during the frozen period) in 2016 which would release 11 mm of this water as NP (18% of frozen season PPT). The minimum change in storage was 4 mm (6% of frozen season PPT) in 2006 together which corresponds to a NP of 58 mm (94% of PPT). Overall, the change in storage over the frozen season for the shallow cover ranged from 4 mm to 48 mm with a mean change in storage of 16 mm (22% PPT) out of mean frozen PPT of 78 mm. The mean NP obtained for the same period for the shallow cover was 61 mm (78% of frozen PPT). It is important to note that the water volume losses expressed as NP following freshet are possibly a combination of winter runoff and infiltrating water below the cover profile.

The high volumes of observed percolated water during the frozen season is in agreement with the observation by Kelln, (2007) which found an infiltration rate to be occurring along the path of preferential flow during the frozen period of the year or when an antecedent soil water persists before a precipitation event. The volumes of SWE during the study period also correspond with those observed at South Bison Hills by Hills by Huang et al. (2018) of approximately 74 mm. These authors also observed that approximately 36 mm infiltrated and was stored within the macropores of the frozen cover, and since the cover was underlain by a low hydraulic conductivity shale, most of this water was available for AET during the growing season. The amount of runoff from snowmelt was 24 mm.

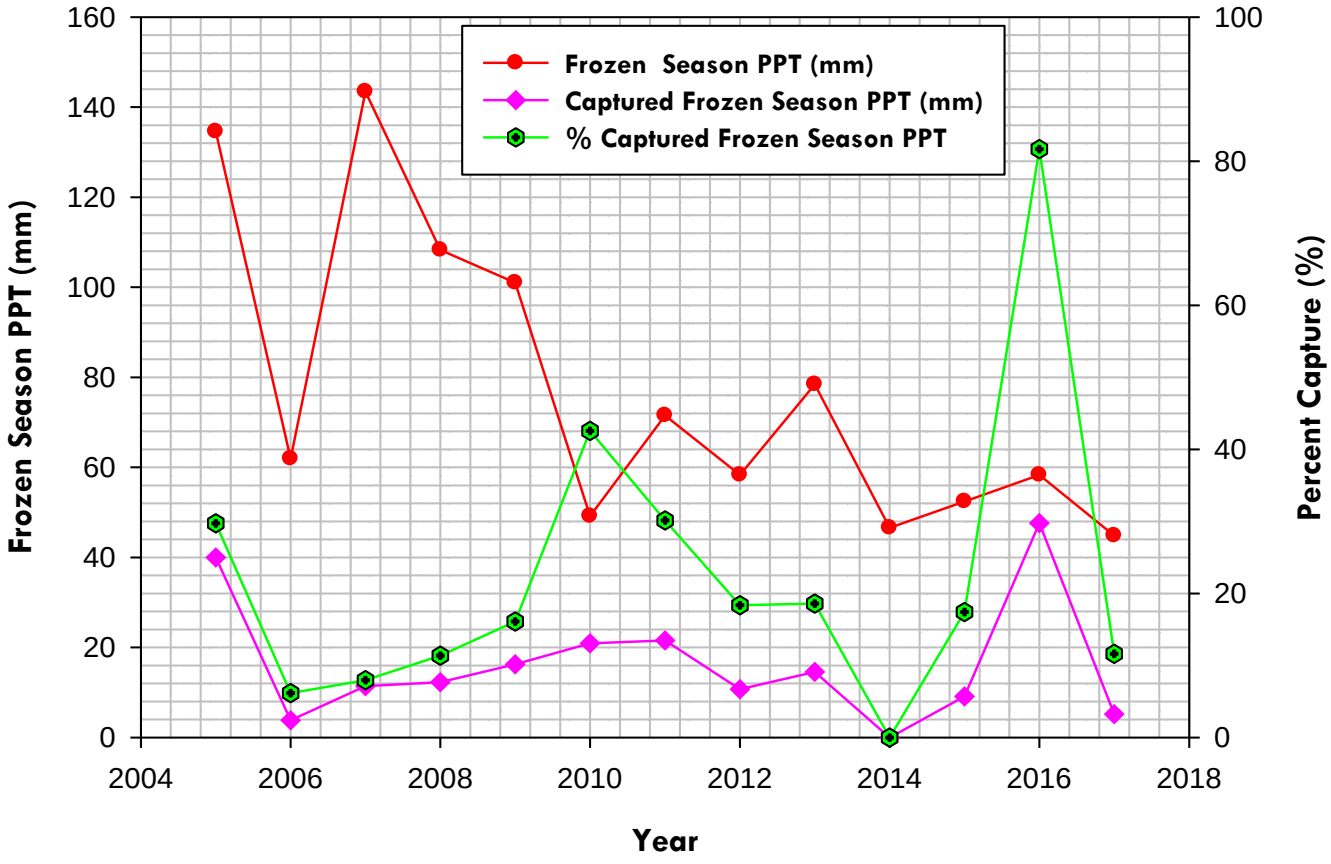

Figure 5.16: Summary of Frozen Season Precipitation Component -Shallow Cover

The parallel set of analyses for the deep cover are shown in Figures 5.17 and Figure 5.18 and summarized in Table C.4 in Appendix C. The years 2005, 2006 and 2009 were observed to be the years with the highest stored water like the shallow cover. In 2005, out of the growing season precipitation of 324 mm, 216 mm (67% of precipitation) was captured by the cover with 107 mm (33% of growing season PPT) been lost PPT for the year. Similarly, out of 300 mm of growing season precipitation for 2006, 198 mm (66%) was stored by the cover while 102 mm (34%) lost. In 2009, 127 mm (80% of PPT) out of 154 mm of growing season precipitation was captured by the deep cover while 31 mm (20% of PPT) lost.

The higher volumes of water storage detected for the deep cover are likely related to the thicker peat layer (~ 270 mm) as well as the overall thickness of the deep cover (100 cm thick) compared to the shallow cover. The thicker peat from 2007 to 2017, the captured PPT ranged from 86 mm to 221 mm. The year with the least soil water storage was found to be 2010. Out of the 273 mm of growing season precipitation, 101 mm (37% PPT) was stored by the cover together with the remaining 172 mm (63% PPT) lost.

To sum up, out of the mean growing season PPT of 277 mm obtained for the study duration,154 mm (56% PPT) was stored by the cover with 123 mm (44% of PPT) lost. Essentially the deep cover's water storage ability appears to be better than the shallow cover. The years found to have the highest water storage and least lost PPT are 2005, 2006 and 2009. Like the shallow cover, the high component of 123 mm of PPT that was lost may have been used for AET by the deep cover.

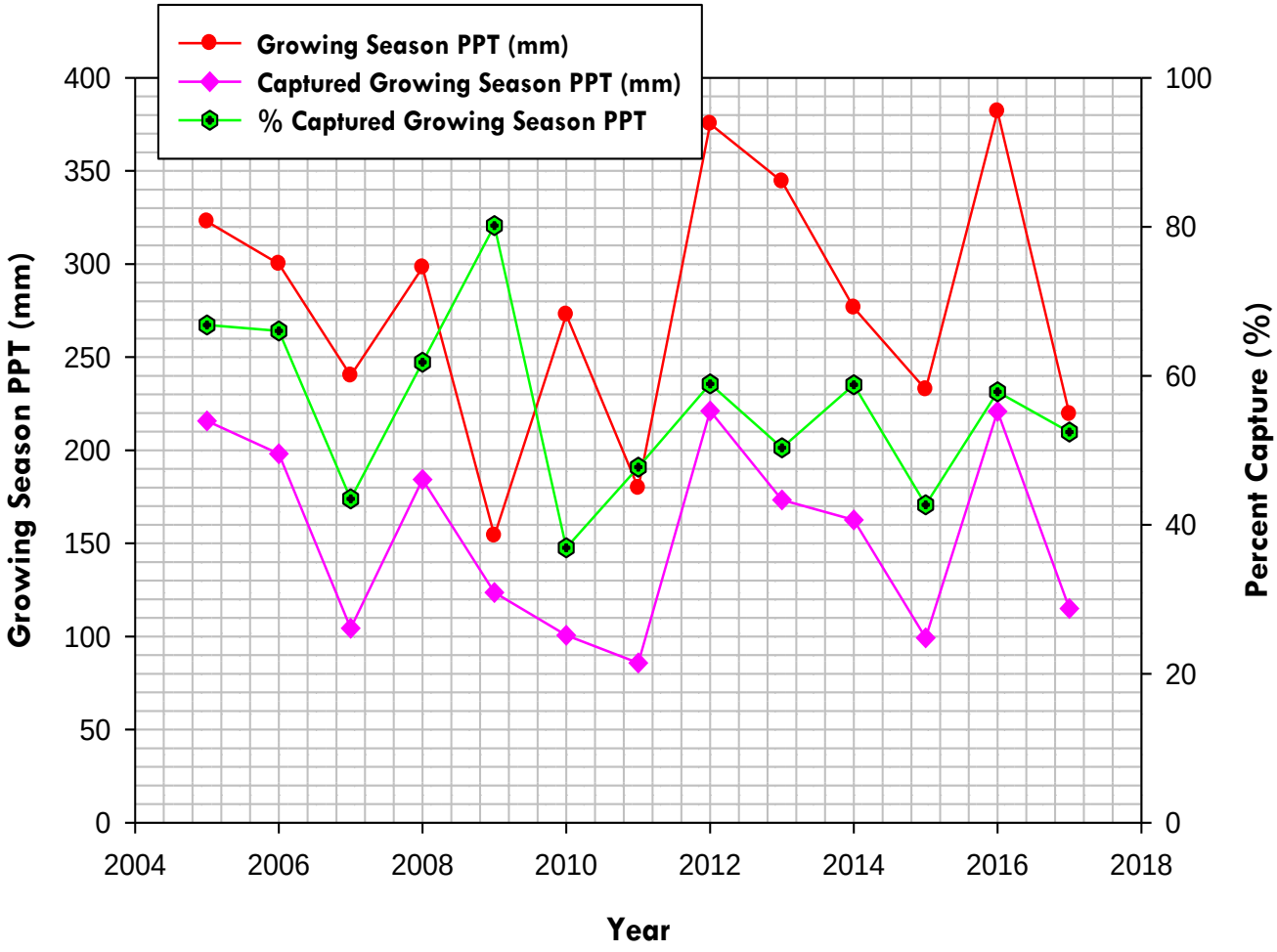

Figure 5.17: Summary of Growing Season Precipitation Component -Deep Cover

Like the shallow cover, the ability of the peat, till and the underlying coke to store water independently was evaluated for the deep cover. The thickness of the surface peat layer is 270 mm, with a glacial till layer 610 mm thick underneath and an underlying coke layer of 450 mm. From Figure 5.18, the volume of infiltrating water captured by the peat layer ranged from 56 mm in 2011 to 153 mm (2012 and 2016) with an average of 101 mm (36% of growing season PPT) for the study duration. The glacial till material captured an infiltrating water ranging from 40 mm in 2011 to 135 mm (2005) with a mean of 70 mm (25% growing season PPT). The underlying coke captured an infiltrating water ranging from 12 mm to 35 mm with a mean of 20 mm (7% of growing season PPT). Similar to the case of the shallow cover, the higher volumes of captured infiltrating water within the peat material is an indication of a possible occurrence of evapotranspiration from the surface with less percolation occurring through the covers.

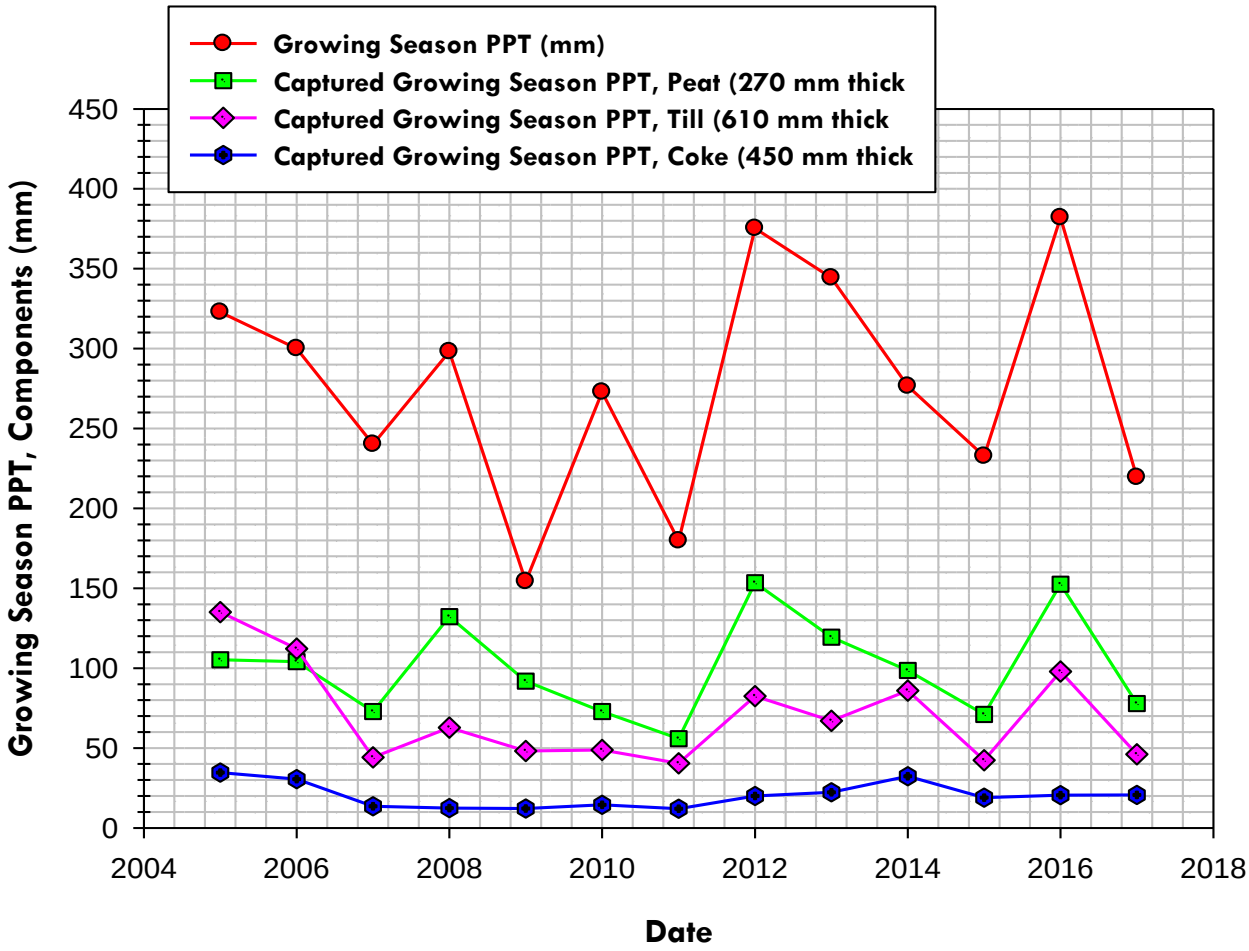

Figure 5.18: Captured Infiltrating Water for Peat, Till and Coke Layers -Deep Cover

The analyses of water storage changes as a result of snowmelt and rainfall over the frozen period are shown in Figures 5.19 and Table C.4 in Appendix C for the deep cover. The frozen season storage by the deep cover ranged from 29 mm to 116 mm representing 19% and 190% of frozen season PPT while percolated PPT ranged from 16 mm (15% PPT) to 124 mm (81% PPT). It was observed from Figure 5.19 that the frozen season storage by the cover exceeds the frozen precipitation in 2010, 2011, 2012 and 2016. The reason for this occurrence may be due to stored water by the cover from the previous year (antecedent soil water) as well as an error from snow survey leading to underestimation of SWE.

The stored water for the deep cover during the study duration ranged from 29 mm to 116 mm with a mean frozen season storage of 62 mm (75% PPT) out of mean frozen PPT of 92 mm. The mean NP obtained for the same period for the deep cover was 30 mm (25% of frozen PPT).

The mean frozen season percolation of 30 mm compares well with the combined percolation of 14 mm and runoff of 24 mm from snowmelt obtained by Huang et al. (2018). Similarly, most of the stored water during the frozen season was available for AET during the growing season as observed by Huang et al. (2018). According to Kelln, (2007) an infiltration rate occurs along the path of preferential flow during the frozen period of the year.

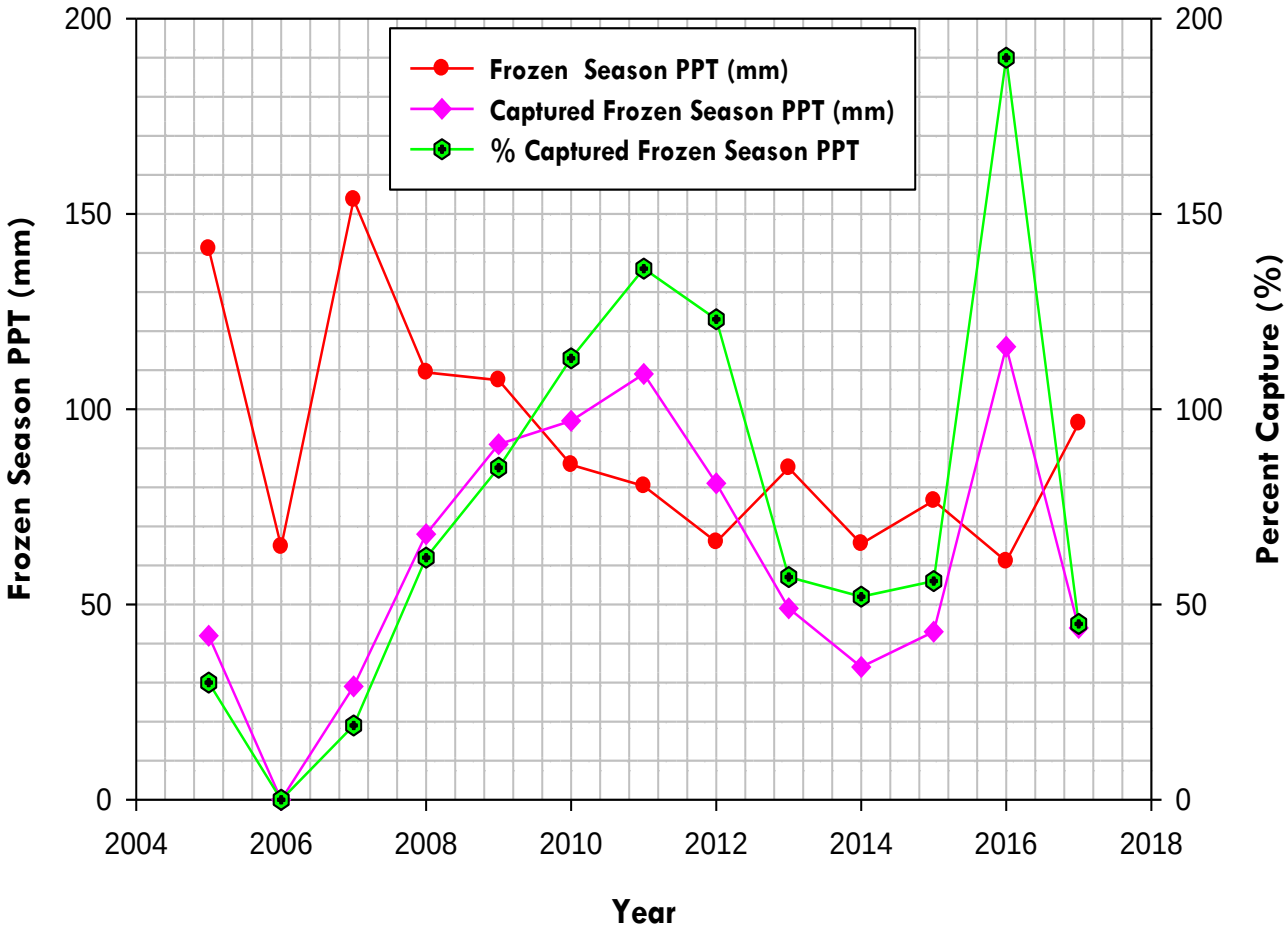

Figure 5.19: Summary of Frozen Season Precipitation Component -Deep Cover

In summary, the results for the changes in water storage associated with precipitation events during the growing season cast some significant doubts over the ability of daily changes in water storage to be characterized using the existing monitoring system. This is likely to cause difficulties with the system dynamics modelling results presented in the next chapter since the daily changes in storage are fundamental to the method used to define NP. The results suggest that the shallow cover captured 79 mm (27% of growing season PPT) out of 291 mm mean growing season PPT during the study duration. The volume of growing season PPT lost was 212 mm (73% of mean growing PPT). The deep cover captured 154 mm (56% mean growing season PPT) with 123 mm (44% of PPT) lost out of the mean 277 mm PPT. Out of the 79 mm captured infiltrating water by the shallow cover, 56 mm was captured by the surface layer (peat). Likewise, for the deep cover, out of the mean 277 mm captured 60% was captured by the surface peat material.

In the case of the changes in storage associate with frozen season precipitation, the shallow cover stored 16 mm (22% frozen PPT) out of the 78 mm mean frozen PPT during the study duration. The mean NP obtained for the shallow cover for the same period was 61 mm (78% of frozen PPT). The volume of water available from SWE and frozen season precipitation are comparable to those observed by Huang et al. (2018). However, in that case only 14 mm of SWE percolated through the covers as while 24 mm reported as runoff or interflow from the sloping covers together with 36 mm was captured and stored by the covers.

The water storage ability of the deep cover showed an improvement over the shallow cover. During the study duration, the deep cover stored 62 mm (75% PPT) of the mean growing season PPT of 92 mm. Net percolation accounted for 25% of the growing season PPT (30 mm).

CHAPTER 6

PRESENTATION OF WATER BALANCE MODEL

Annual water balances for the CBIW were estimated using two approaches: a system dynamics model and a physics-based model. The daily and growing season water balance were estimated for both covers for each year over the study period (2005 to 2017). These water balances were used as a basis for identifying which of the key processes (e.g. preferential flow, convective airflow) or hydraulic properties (e.g. dual porosity water flow storage) have the greatest influence over the cover performance. The system dynamics water balance model is presented first in this section followed by the physics-based model. The chapter concludes with a comparison of the water balance based on the two models along with a summary of the key learnings from these models as it pertains to the controls on the CBIW water balance.

6.1 Water Balance Based on System Dynamics Model

6.1.1 Shallow Cover System

The cumulative water volumes associated with the various components of the water balance are presented for all years in Figure B.1 to B.10 in Appendix B. A few typical years have been selected for presentation and discussion within this section. Figures 6.1 to 6.3 are the system dynamics water balance results for the shallow cover for the study site in years 2006, 2011 and 2016.

The reclamation cover should store water from snowmelt and/or precipitation so that is available for transpiration by vegetation during drier seasons of the year. A key failure mode for covers, consequently, is the inability to store water as a result of these infiltration processes. This is generally reflected by the NP component. The other potential failure mode proposed by Koehler, (2018) was that stored water is also lost as a result of convective air flow leading to enhanced drying of the cover. This process would occur primarily as enhanced drying beyond that expected based on transpiration or surface evaporation alone.

It is also important to note the water balance is developed for only non-frozen conditions from unfrozen conditions in the spring until freeze up in the fall. The capture of snowmelt infiltration by soil storage is not calculated in the water balance directly. Rather it was calculated separately as described in section 5.3.2.

The summary of the system dynamics water balance components for the shallow cover is shown in Table D.1 in Appendix D. From Table D.1 and Figure 6.4, growing season AET for 2005 was found to be 92% of the growing season precipitation while net percolation accounted for 10%. Measured change in storage accounted for -2% of the precipitation. The percentage of AET for 2006 reduced to 68% of growing season precipitation while net percolation and measured change in storage at 34% and -2% of precipitation respectively (Figure 6.1). The percentage of AET for 2007 and 2008 reduced considerably to 58% and 34% of precipitation respectively. While net percolation increased to 51% and 70% with measured change in storage being -9% and -4% of precipitation. There was a considerable improvement in AET in 2009 as it was found to be 68% of precipitation while net percolation was 54% of precipitation with measured change in storage being -22% of precipitation. The AET from 2010 to 2017 remained in the range of 34% to 56% while net percolation for the same period ranged from 52% to 85% of precipitation. Measured change in soil water storage from 2010 to 2017 was also found to be in the range of -26% to 0. Similarly, the percentage of AET to PET for the study duration for the shallow cover ranged from 11% to 43% with a mean of 21% with the highest AET/PET ratio (43% and 29%) found in the first two years of the cover after construction (Figure 6.5). The least AET/PET of 11% and 16% was obtained in 2011 and 2015 respectively.

The highest obtained AET rate in 2005 and 2006 is justified considering that these years were observed to be the years with the highest water storage by the shallow cover and hence, enhances the occurrence of evapotranspiration as discussed in section 5.3.2. The reduction in AET and increase in the rate of net percolation rates over time is due to the reduced soil water content within the cover as the approached to estimate the AET is heavily dependent on the soil water content.

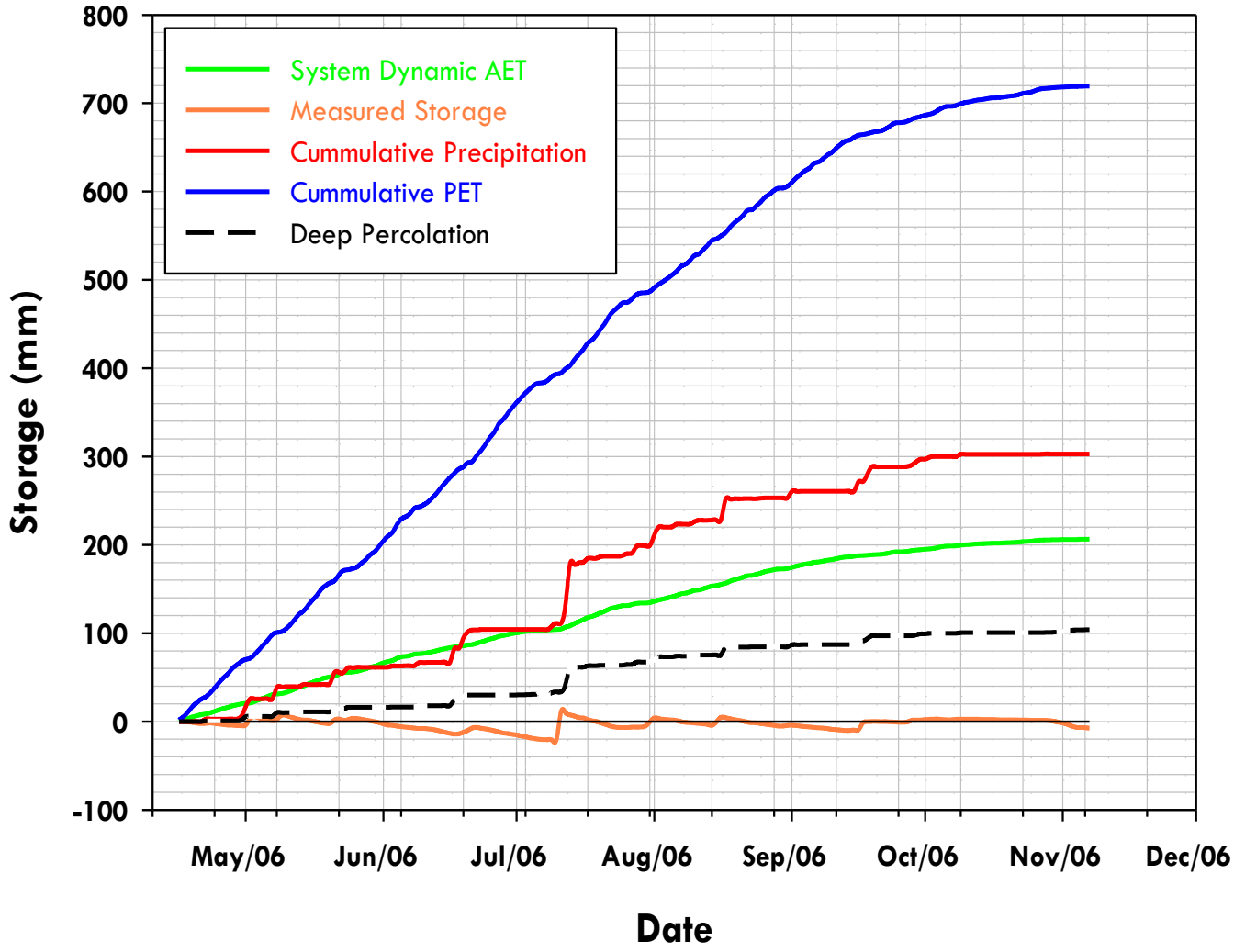

Figure 6.1: System Dynamic Water balance for Shallow Cover System for 2006

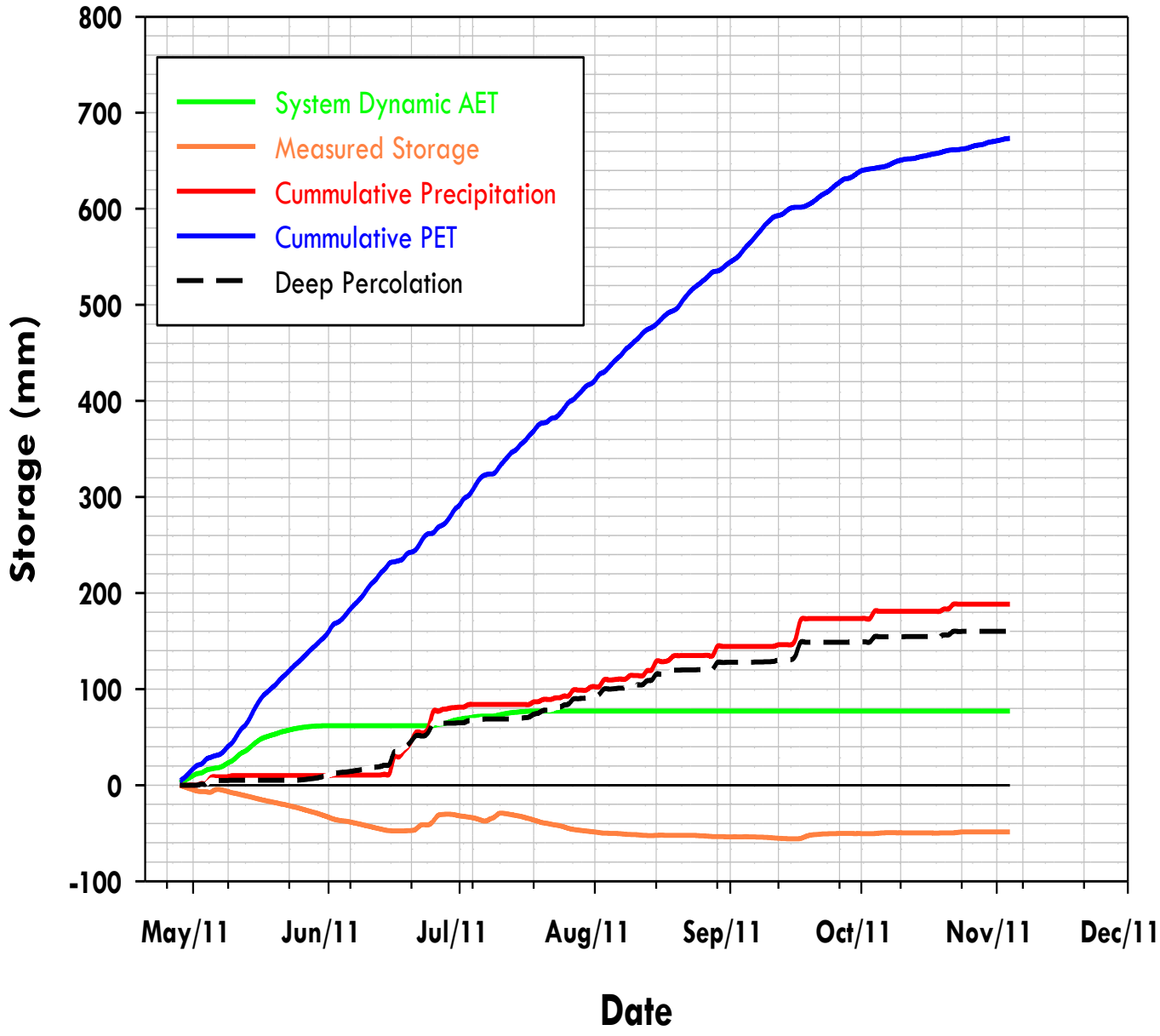

Figure 6.2: System Dynamic Water balance for Shallow Cover System for 2011

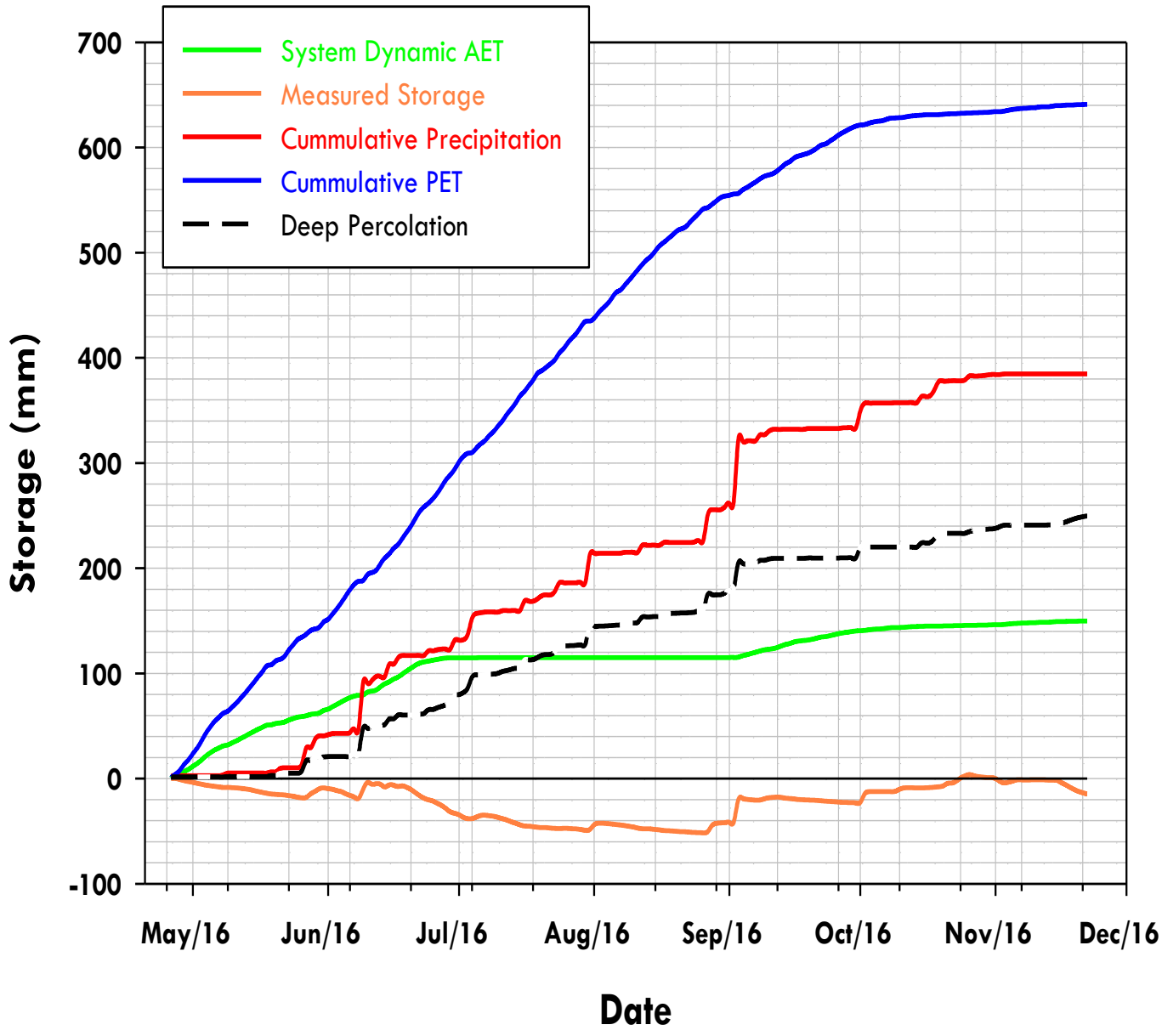

Figure 6.3: System Dynamic Water balance for Shallow Cover System for 2016

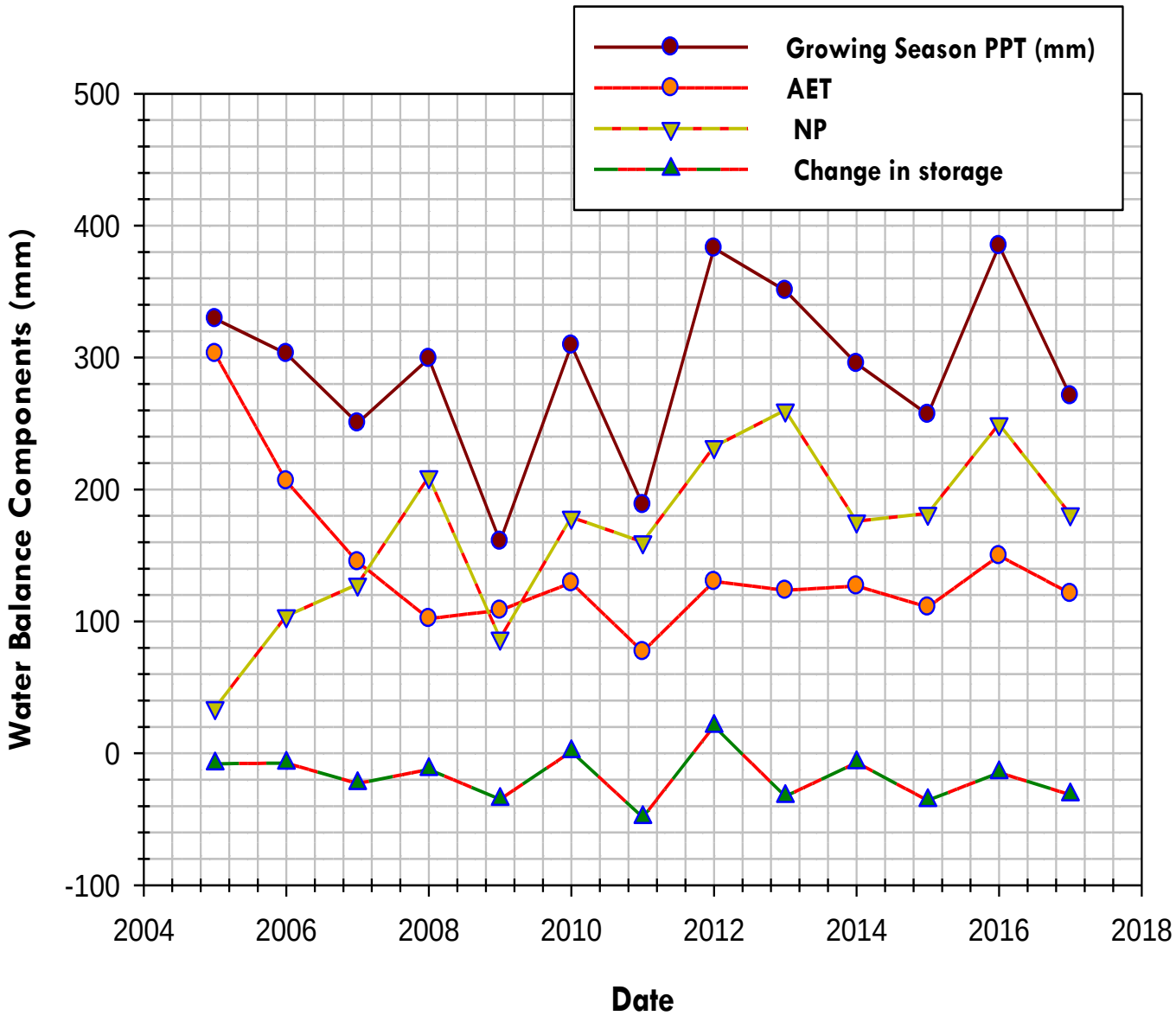

Figure 6.4: Summary of System Dynamics Seasonal Water Balance Components Results, Shallow Cover

Found in Figure 6.8 and Table D.2 in Appendix D is the summary of the annual system dynamics water balance volumes for the study duration for the shallow cover. The annual system dynamics water balance was obtained by adding the frozen season water balance volumes for the shallow cover (estimated in section 5.3.2) and the system dynamics water balance volumes for the growing season.

From Table D.2, annual AET was found to be 38% (141 mm) of annual precipitation and 21% of PET for the shallow cover during the study duration. Net percolation was found to be 63% (229 mm) of annual precipitation with annual measured change in storage accounting for -1% (-2 mm) of the annual precipitation for the study duration.

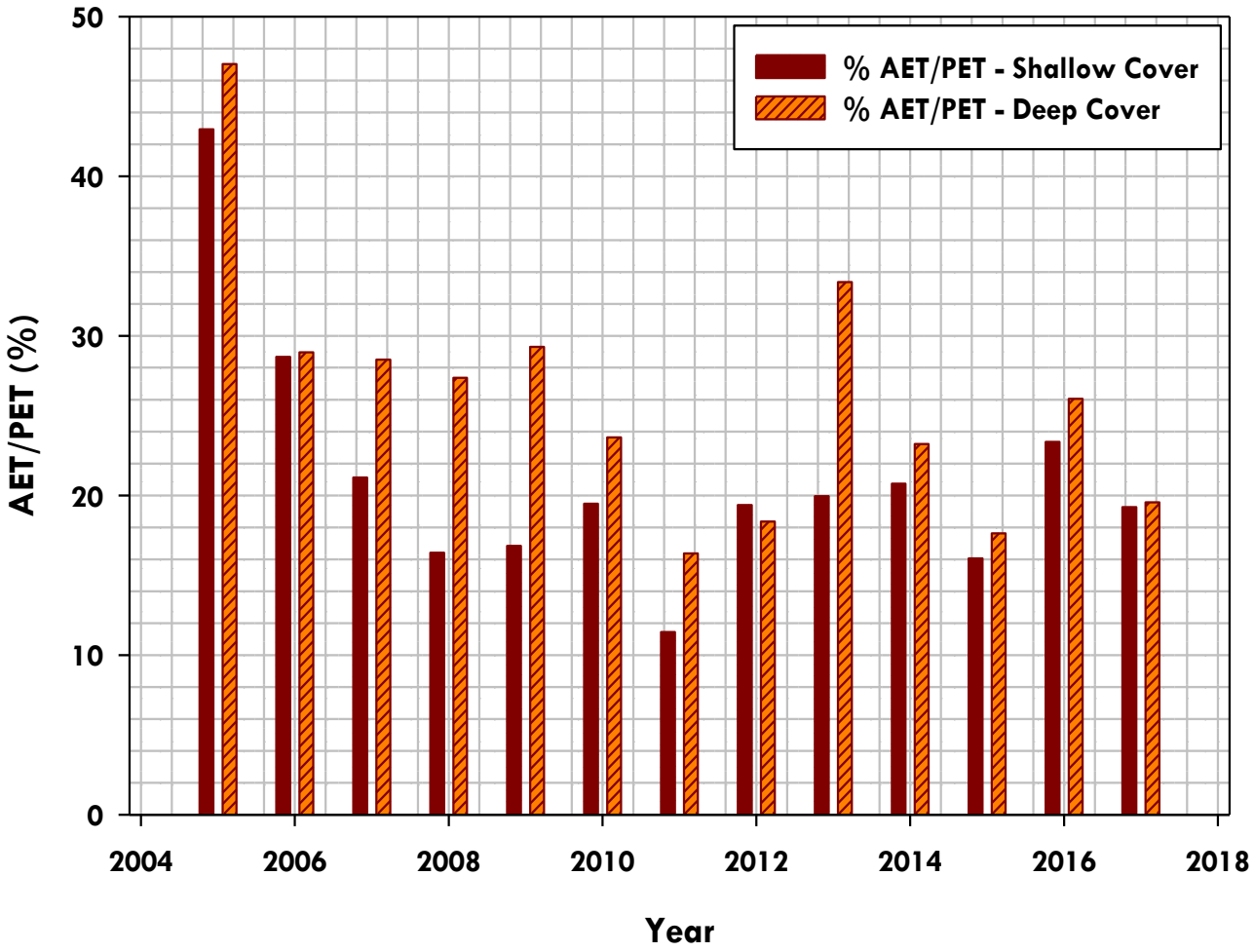

Figure 6.5: Percent AET/PET for System Dynamic Annual Water Balance, Shallow and Deep Cover System

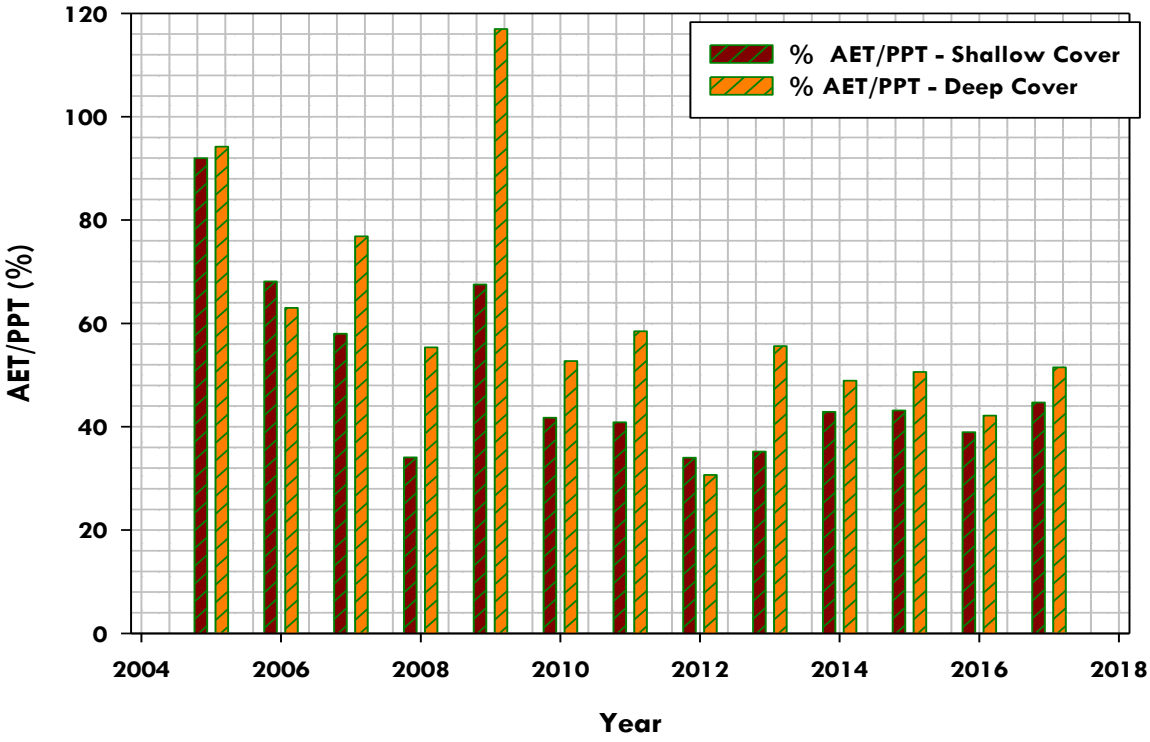

Figure 6.6: Percent AET/PPT for System Dynamic Seasonal Water Balance, Shallow and Deep Cover System

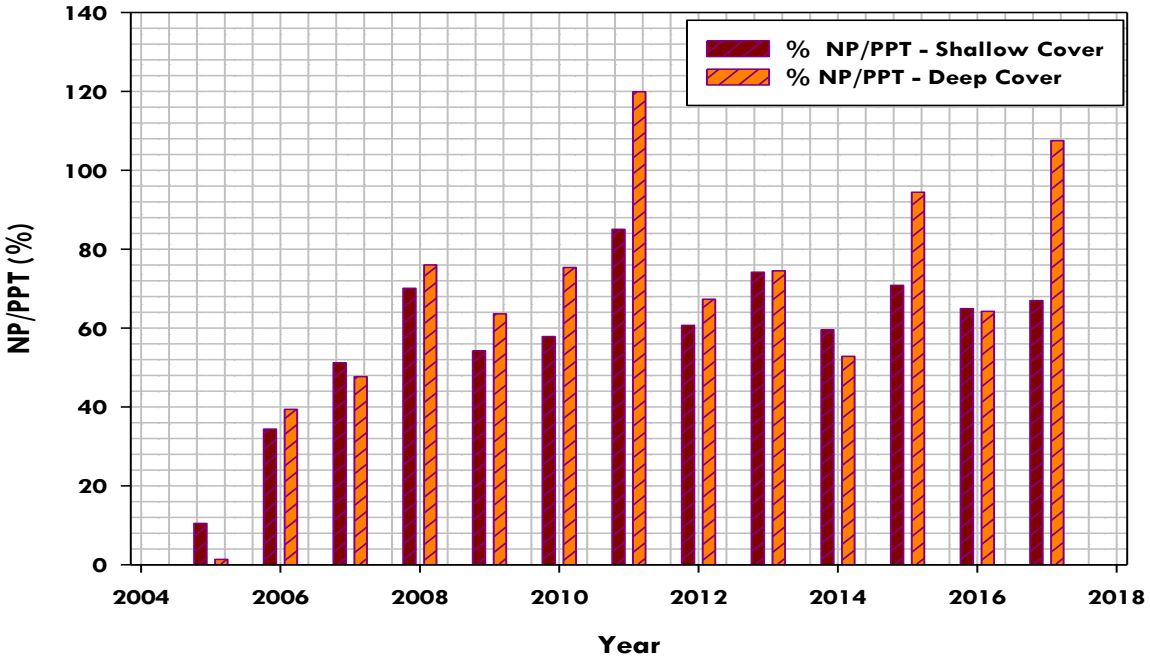

Figure 6.7: Percent NP/PPT for System Dynamic Seasonal Water Balance, Shallow and Deep Cover System

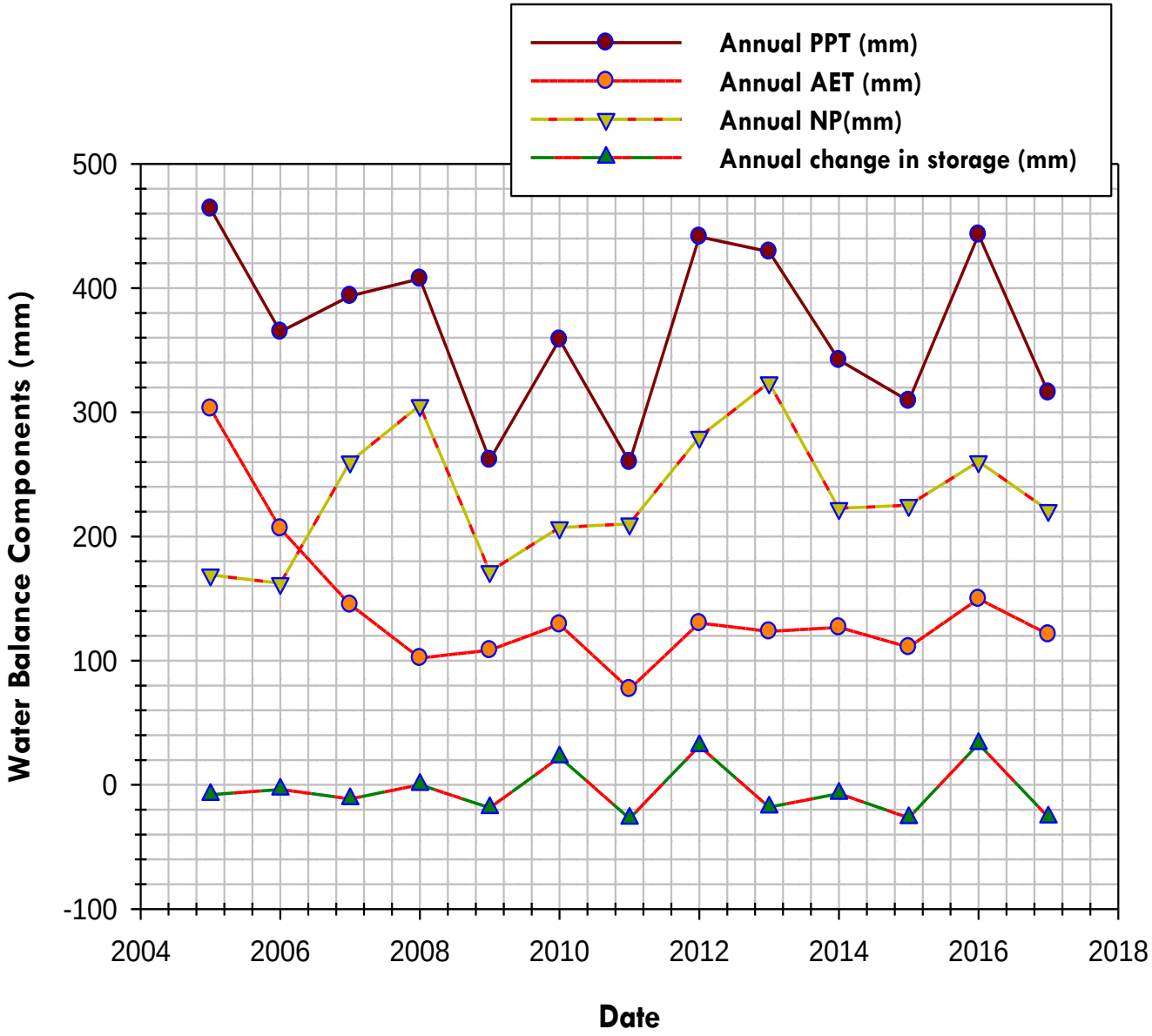

Figure 6.8: Summary of System Dynamics Annual Water Balance Components Results Including Frozen Period Precipitation and NP, Shallow Cover

6.1.2 Deep Cover System

The results of the cumulative volumes of system dynamics water balance for the deep cover for the study duration are presented in Figure B.11 to B.20 in Appendix B. Figure 6.9 to Figure 6.11 are typical examples selected for presentation in this section. From Figure 6.12 and Table D.3 in Appendix D, AET was found to be 94% of the growing season precipitation while net percolation was observed to be 1% of precipitation in 2005. Measured change in soil water storage for the

same year was found to be 5% of the precipitation. In 2006, AET was found to be 63% of precipitation while net percolation was found to be 39% with the change in measured storage been -2% of precipitation. The percentage of AET of precipitation for 2007 increased from that of 2006. The AET of 2007 was found to be 77% of the growing season precipitation while the net percolation was found to be 48% of precipitation. Measured change in storage for 2007 was found to be -25 of precipitation. The percentage of AET to precipitation from 2008 to 2017 ranged from 31% to 58% except in 2009 when the AET was 117% of growing season PPT. The net percolation for the same period ranged from 53% to 120% with change in measured storage ranging from -81% to 2% of the growing season precipitation. The percentage of AET to PET for the deep cover during the study duration ranged from 16% (2011) to 47% (2005). A mean per cent AET/PET of 26 was found for the deep cover (Figure 6.5). The reason for the high AET obtained in the first two years after the construction of the deep cover is as explained in section 6.1.1.

The trend of the system dynamic water balance for the deep cover shows that, in the first two years after construction of the cover, a significant amount of the growing season precipitation was found to be lost due to AET (63% to 94%). The cover's ability to store water during these initial years after construction was relatively fine. However, the water storage ability of the deep cover after the first two years started decreasing which resulted in increased net percolation through the cover with decreased AET for most of the study duration as explained earlier.

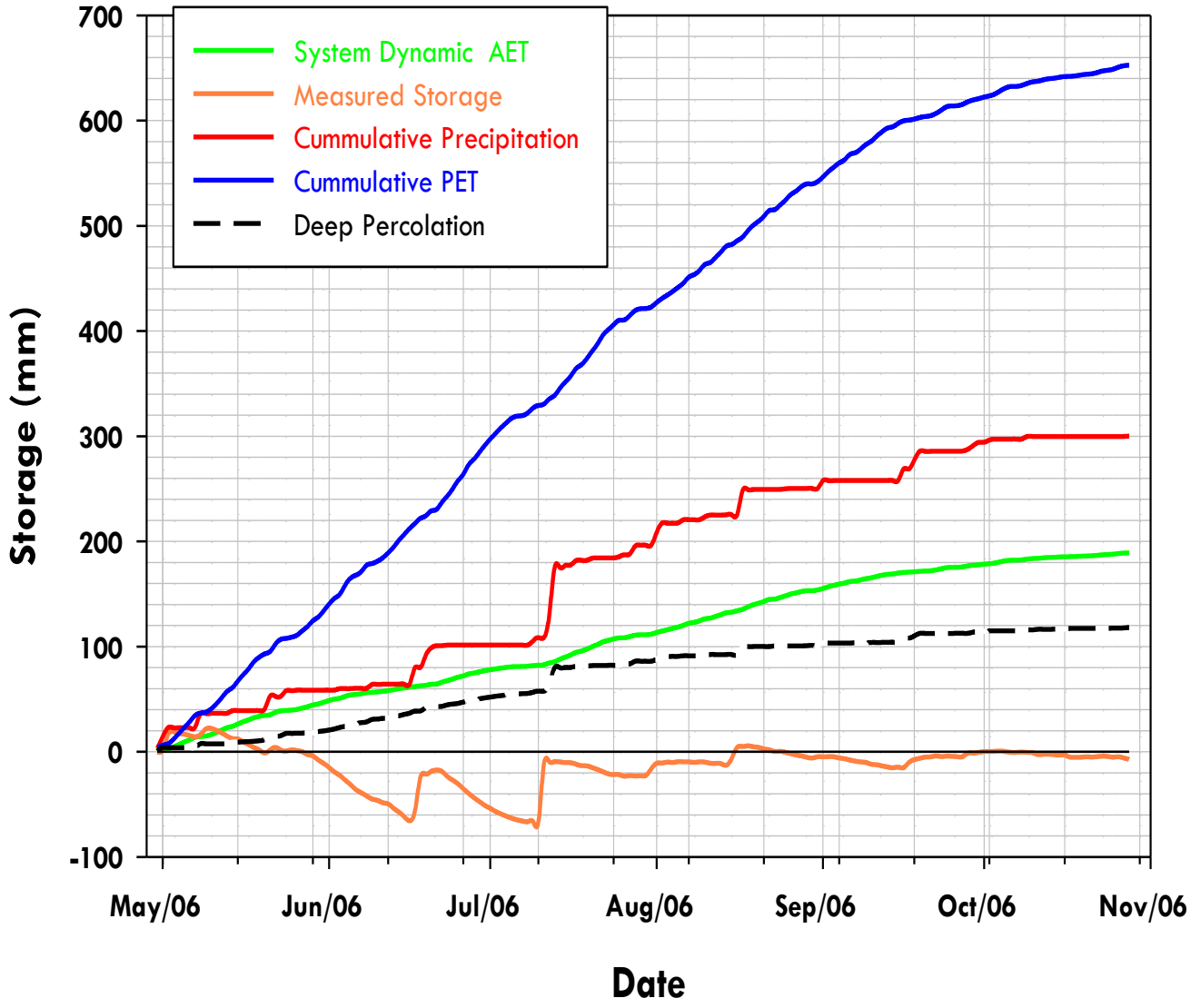

Figure 6.9: System Dynamic Water balance for Deep Cover System for 2006

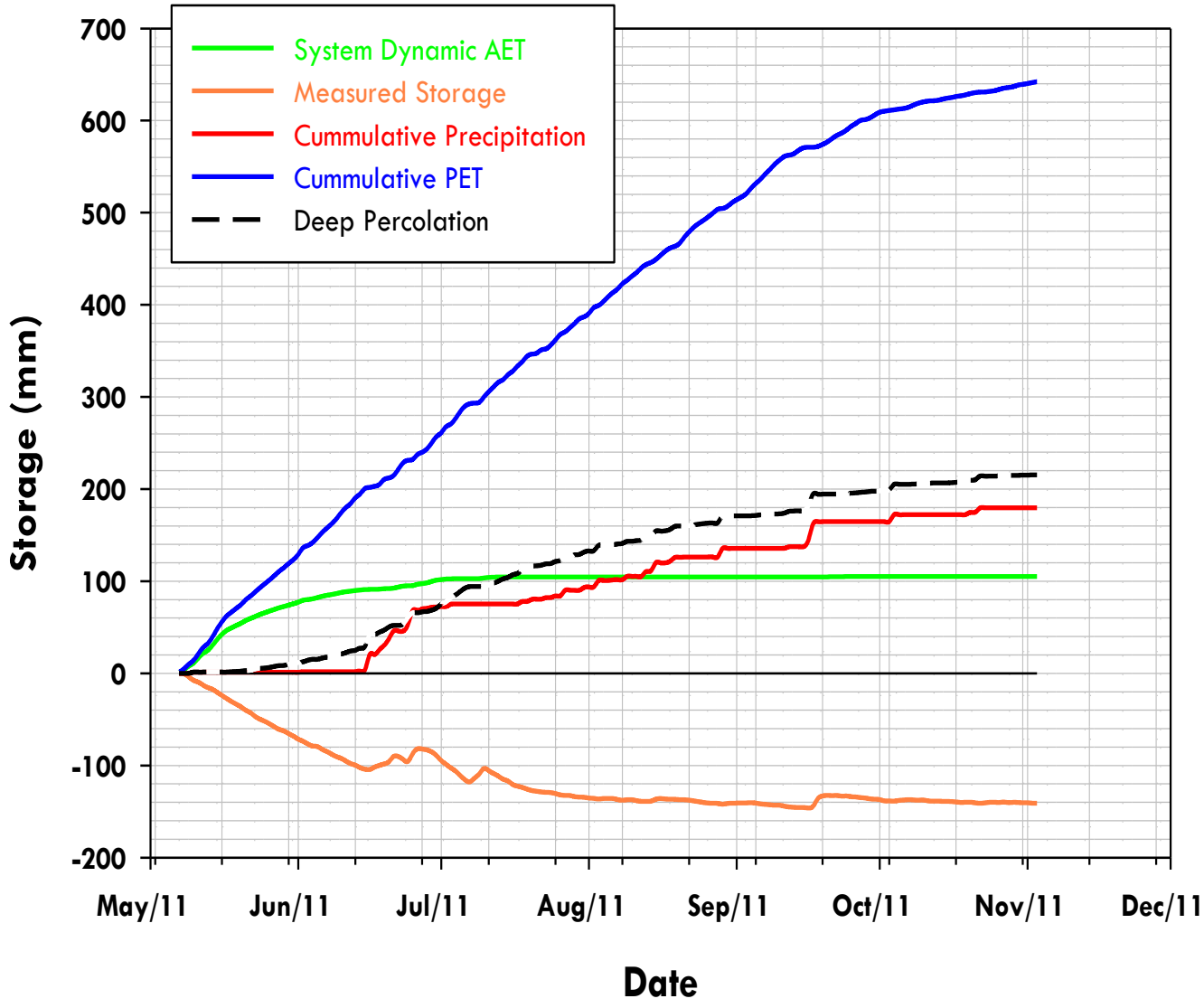

Figure 6.10: System Dynamic Water balance for Deep Cover System for 2011

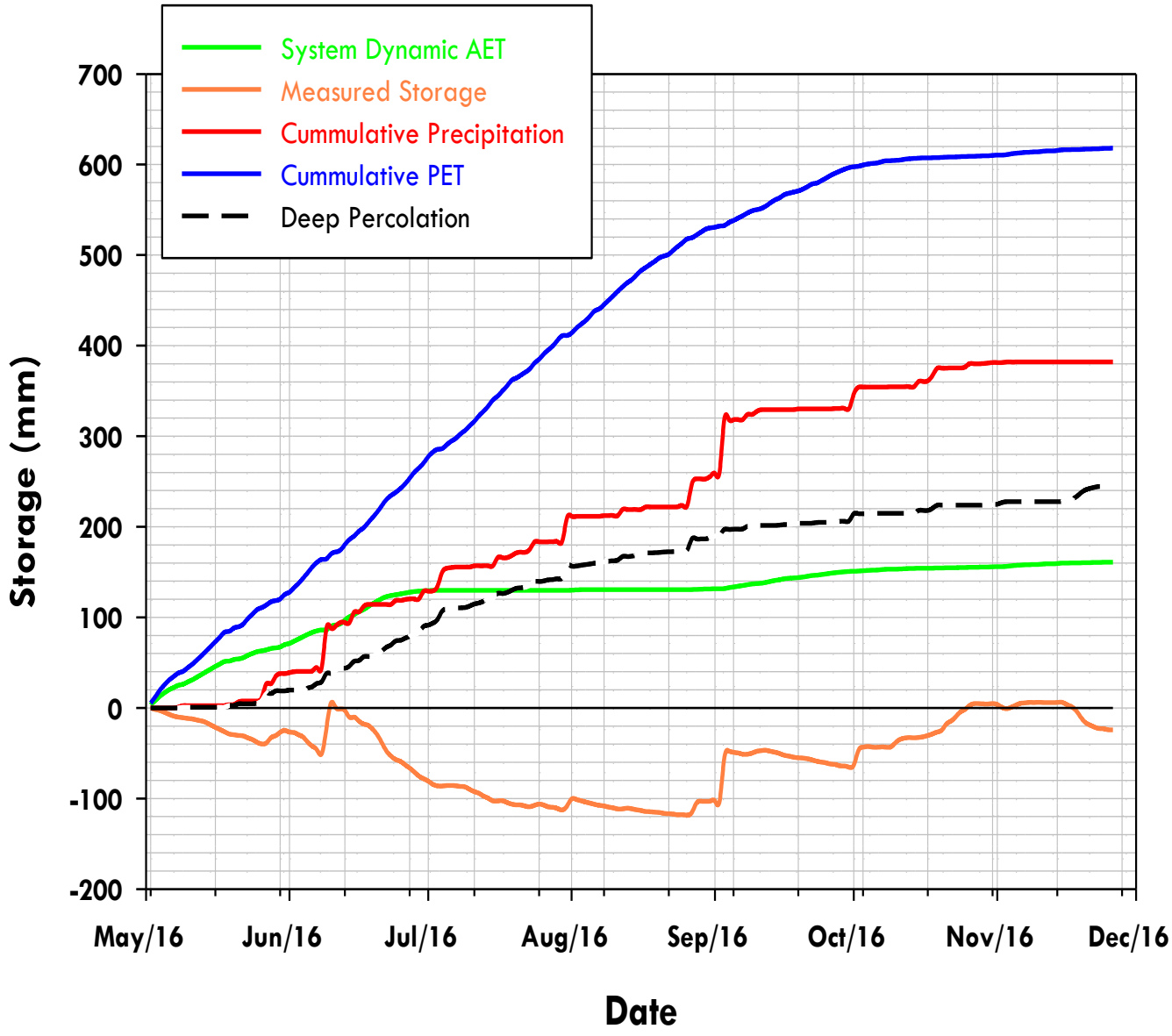

Figure 6.11: System Dynamic Water balance for Deep Cover System for 2016

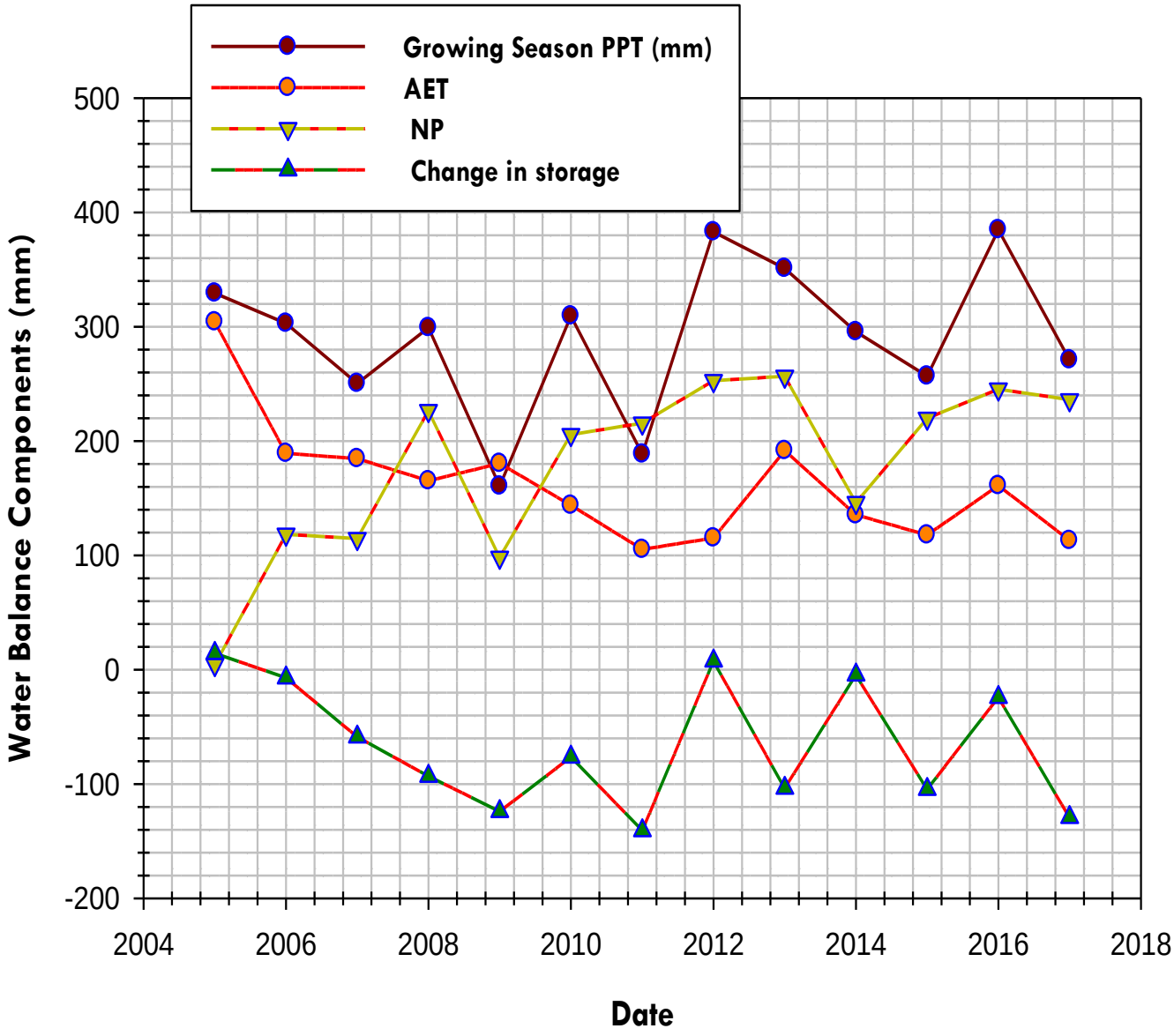

Figure 6.12: Summary of System Dynamics Seasonal Water Balance Components Results, Deep Cover

In summary, the mean percentage of AET of the growing season precipitation for the deep cover during the study period was found to be 61% while net percolation was found to be 68% of precipitation (Figure 6.6 and Figure 6.7). The measured change in soil water storage was found to be -29% of the precipitation.

The annual water balance components volumes for the study duration for the deep cover is shown in Figure 6.13 and Table D.4. An annual AET was found to be 44% (162 mm) of the annual precipitation and 26% of PET while annual net percolation was 58% (210 mm) of precipitation. Annual change in water storage of -2% (-3) was obtained for the deep cover during the study duration.

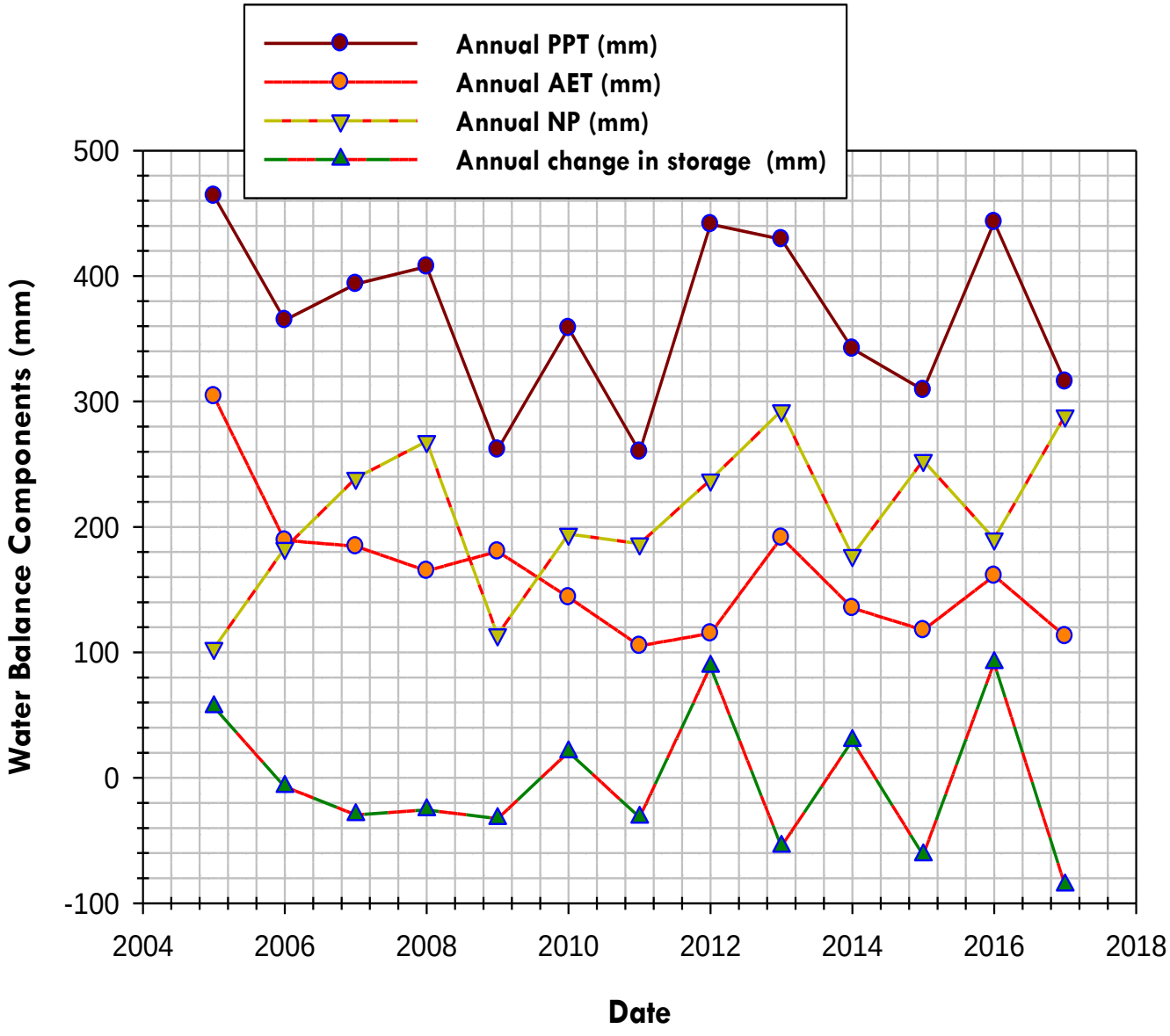

Figure 6.13: Summary of System Dynamics Annual Water Balance Components Results Including Frozen Period Precipitation and NP, Deep Cover

6.2 Simulated Water Balance

6.2.1 Optimization Results

Before simulating the soil water content and the water balance components for both covers at the CBIW site, an attempt was made to use the single porosity approach in Hydrus-1-D, but no reasonable fit was obtained for the water content and storage. Hence, the dual porosity approach was adopted. The optimized Ks and VG parameters used in the dual porosity approach and provided a reasonable fit for the water content and storage is shown in Table 6.1.

Table 6.1. The Optimized Ks and van Genuchten (VG) parameters for the three materials

VG parameters	Peat soil		Till material		coke material (both covers)
	shallow cover	deep cover	shallow cover	Deep Cover	
Mobile					
θ_{rm} (cm^3/cm^3)	0	0	0	0	0.018
θ_{sm} (cm^3/cm^3)	0.061	0.080	0.016	0.058	0.324
$\propto$ (1/cm)	0.004	0.00363	0.016	0.0277	0.029
n	2.25	2.292	2.46	2.08	1.29
Ks (m/s)	2.03×10^{-5}	4.21×10^{-5}	1.25×10^{-6}	3.09×10^{-6}	8.37 x 10-7
Immobile					
θ_{rim} (cm^3/cm^3)	0.147	0.147	0.132	0.132	0
θ_{sim} (cm^3/cm^3)	0.45	0.45	0.367	0.367	0
ω_w (1/cm per day)	0.017	0.00732	0.014	0.0071	0

The results of saturated hydraulic conductivity for both covers are presented (Figure 6.14 and 6.15). The Ks values for both peat and glacial till material were found to be increasing or evolving over the first five years following cover placement. The reasons for the evolution of the Ks values after placement could due to freeze thaw cycles and the development of root systems by plants. Similar observation has been reported by Huang, (2015) and Meiers; et al. (2011). Peat optimized mean Ks values ranging from 4.82×10^{-6} m/s to 6.22×10^{-5} m/s with an average value of 2.03 x

10^{-5} m/s was obtained for the shallow cover. Likewise, the till optimized mean Ks values for the shallow cover ranged from 1.35 x 10^{-8} m/s to 1.74 x 10^{-6} m/s with an average of 1.25 x 10^{-6} m/s (Figure 2.17). The Ks values for the deep cover did not deviate much from the shallow cover. Ks values ranging from 9.19 x 10^{-6} m/s to 2.15 x 10^{-4} m/s with an average of 4.21 x 10^{-5} m/s was obtained for peat mineral mix for the deep cover. Similarly, Ks values for the till material for the deep cover ranged from 5.01 x 10^{-8} m/s to 1.76 x 10^{-5} m/s with an average of 3.09 x 10^{-6} m/s (Figure 6.18) was obtained for the deep cover. The Ks values obtained for both peat and till for both covers are highly correlated. Similarly, these obtained optimized Ks values are correlated with the Ks values obtained by Huang, (2015) (1.0 x 10^{-5} m/s -peat, 1.0 x 10^{-6} m/s, till-simulated), Meiers; et al. (2011) (5.0 x 10^{-5} m/s - peat, 1.0 x 10^{-6} m/s till-measured) and Shurniak (2003) (6.62 x 10^{-5} m/s -peat, 2.75 x 10^{-5} m/s till-simulated). The summary of these Ks values is found in Table 6.2.

Table 6.2.: Summary of Ks Values for Peat Mineral Mix and Glacial Till Material for the Covers

Ks values obtained by this study (m/s – simulated)		Ks values by Huang etal., (2015) (m/s – simulated)		Ks values by Meiers; et al. (2011) (m/s – measured)		Ks values by Shurniak (2003) (m/s – simulated)	
Peat	Till	Peat	Till	Peat	Till	Peat	Till
3.1 x 10^{-5}	2.2 x 10^{-6}	1.0 x 10^{-5}	1.0 x 10^{-6}	5.0 x 10^{-5}	1.0 x 10^{-6}	6.6 x 10^{-5}	2.8 x 10^{-5}

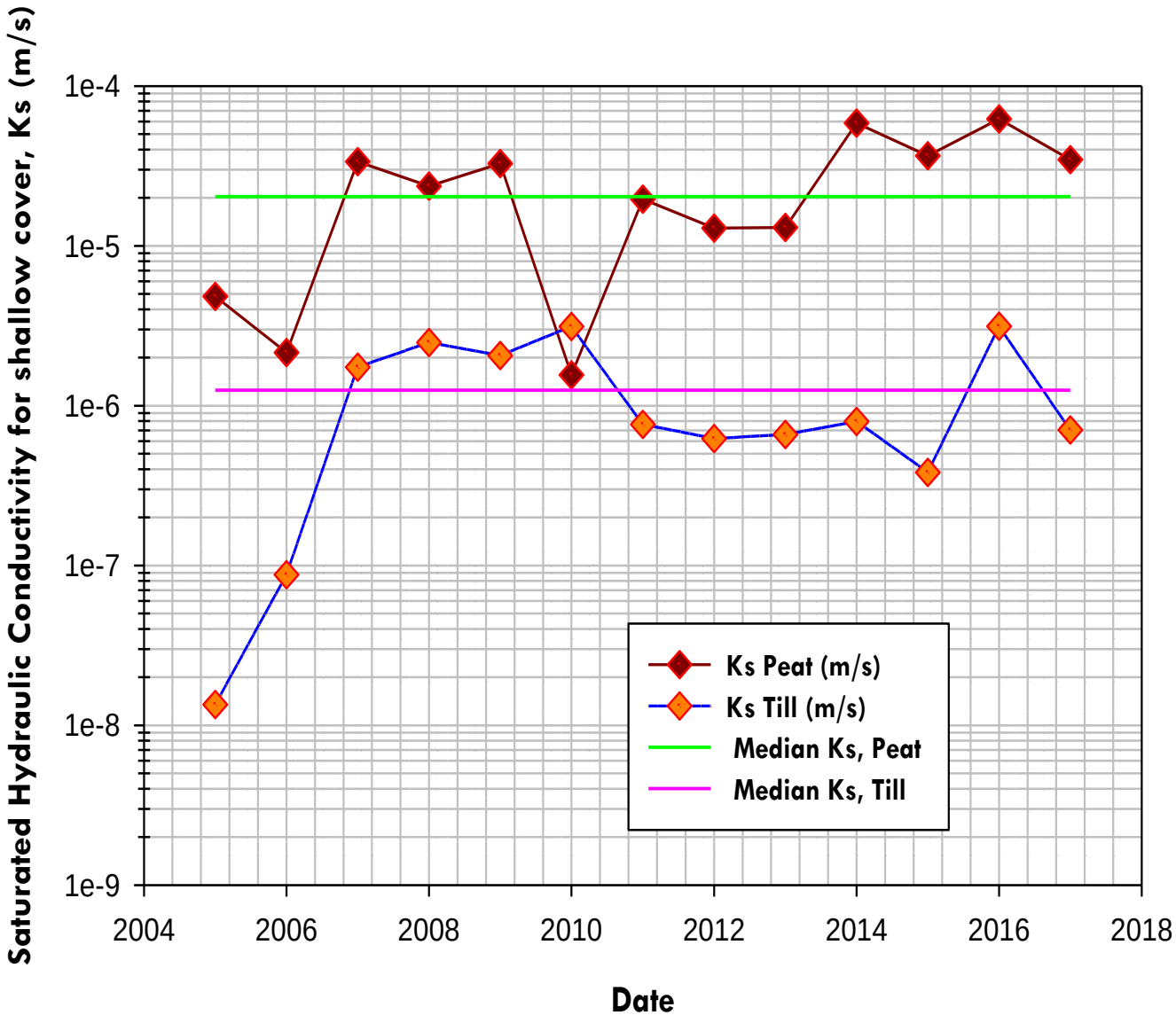

Figure 6.14: Optimized Ks for Both Peat and Till with Their Respective Average Values, Shallow Cover

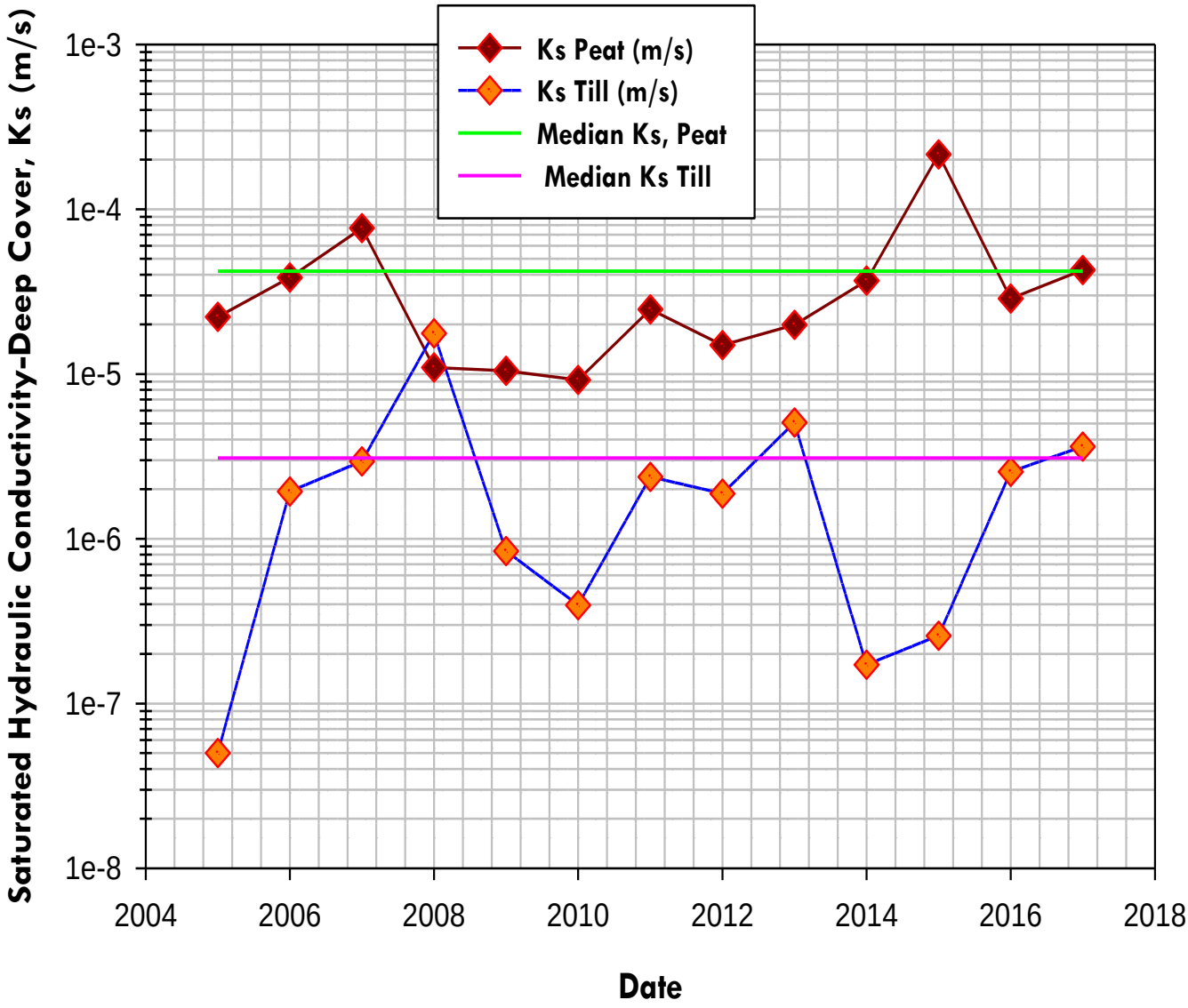

Figure 6.15: Optimized Ks For Both Peat and Till with Their Respective Average Values, Deep Cover

6.2.2 Model Accuracy

The accuracy of the model to the measured data for both covers were assessed using the coefficient of determination, (R^2) and the root mean square error (RMSE). The R^2 result shows the relationship between the simulated and the measured soil water content and storage which ranges from 0 to 1. An R^2 close to 1 signifies a better performance, whereas 1 means a perfects match of the simulated soil water content values and subsequently the soil water storage to the observed soil water content

and storage data. The obtained R^2 result for the shallow cover ranged from 0.3 to 0.8 (Table D.5 in Appendix D). The best R^2 was obtained in 2006 while the least obtained in 2007. The mean R^2 for the shallow cover was 0.7. However, the R^2 value may not necessarily be the best indicator of an agreement between the model and the measured data. RMSE for the shallow cover also ranged from 0.01 to 0.02 with a mean of 0.02.

Similarly, the R^2 result obtained for the deep cover ranged from 0.3 to 0.7 with a mean of 0.5 (Table D.5). The best R^2 was obtained in 2017 with the least obtained in 2005. The RMSE for the deep cover also ranged from 0.02 to 0.05 with an average of 0.02.

Typical examples, showing the relationship between simulated and measured soil water content for both covers are shown in Figure 6.16 to Figure 6.19.

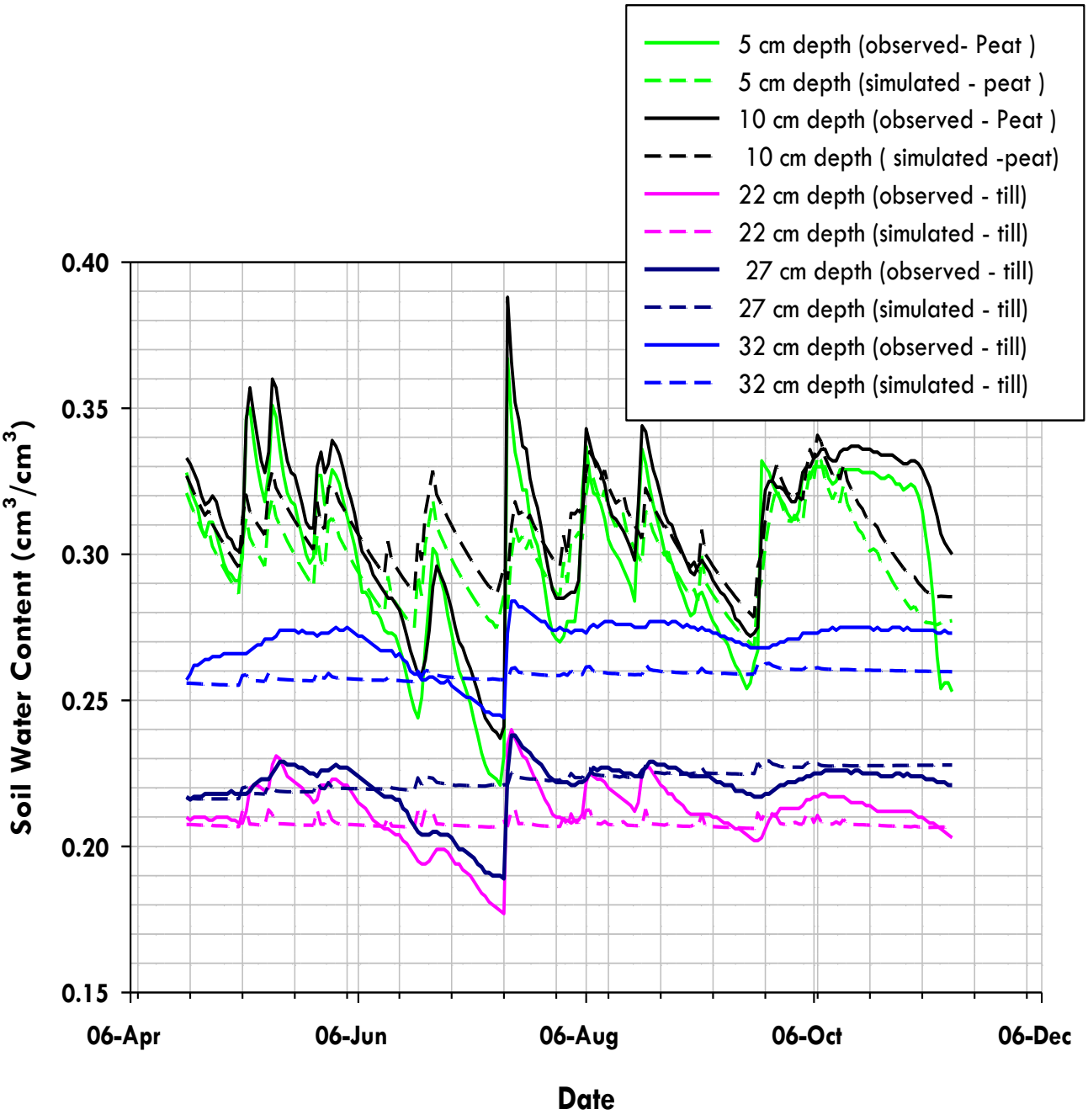

Figure 6.16: Simulated and Measured Soil Water Content-2006, Shallow Cover

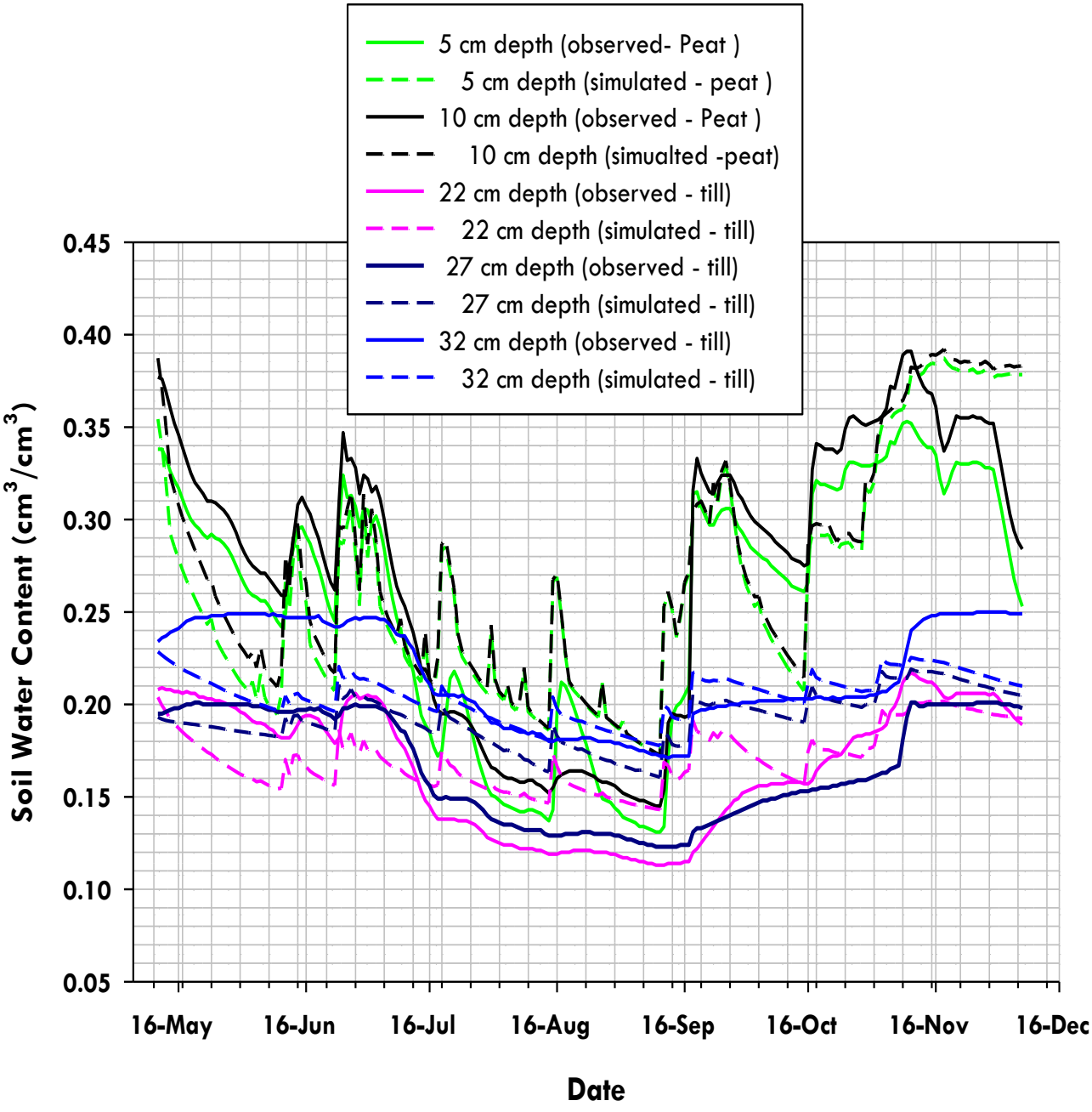

Figure 6.17: Simulated and Measured Soil Water Content-2016, Shallow Cover

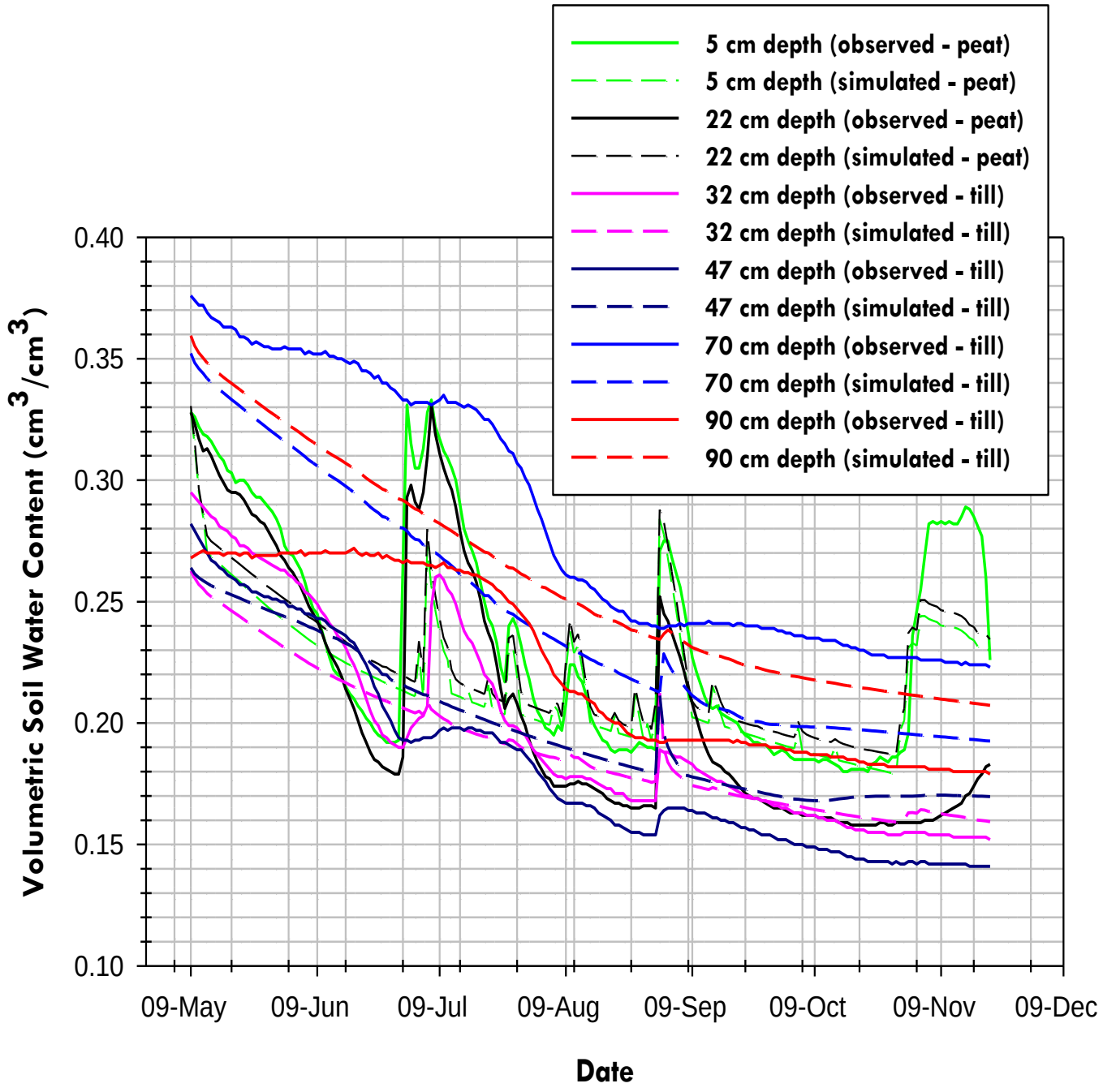

Figure 6.18: Simulated and Measured Soil Water Content-2009, Deep Cover

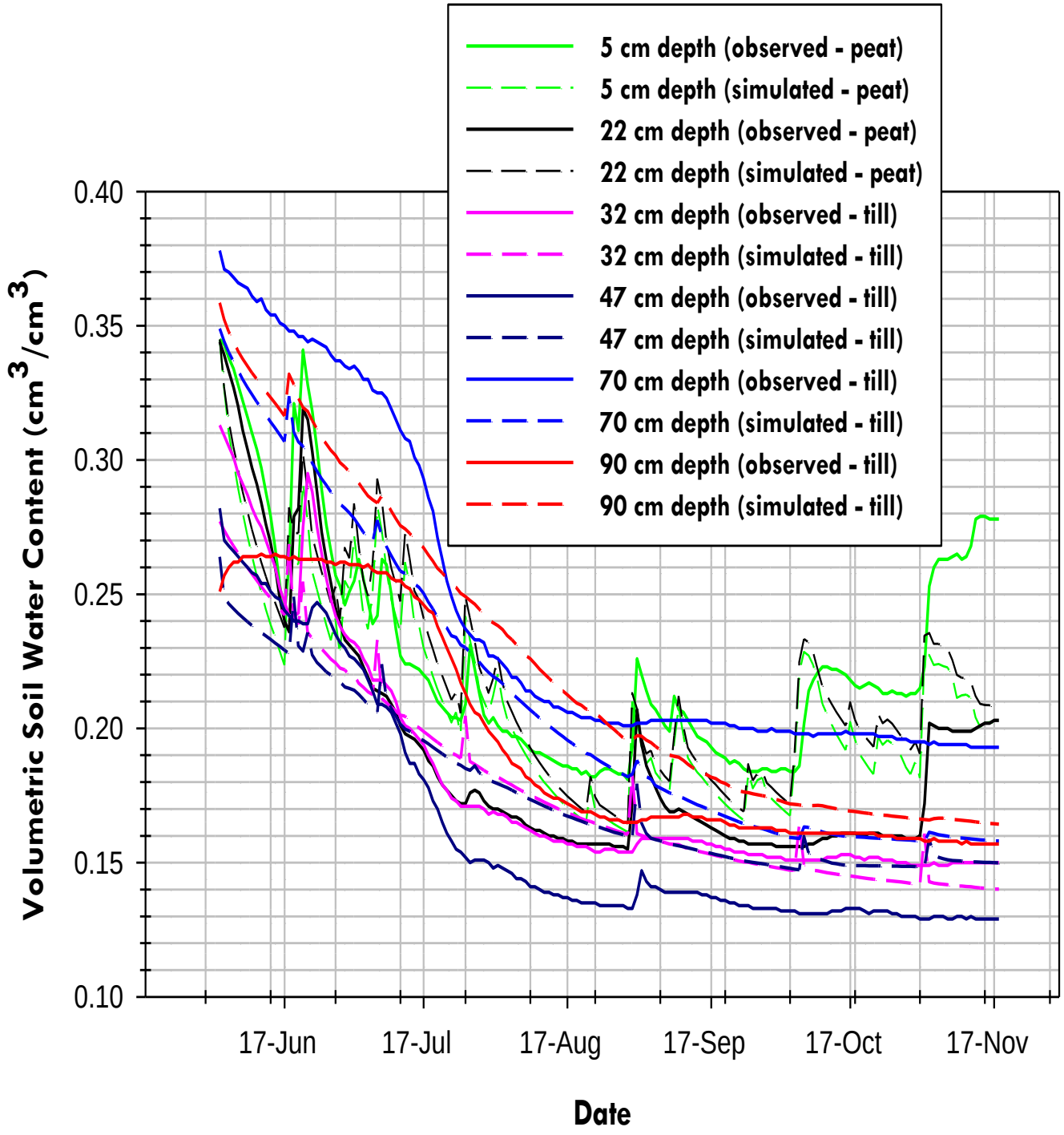

Figure 6.19: Simulated and Measured Soil Water Content-2017, Deep Cover

6.2.3 Shallow Cover System

The results of the simulated water balance for the shallow cover for the study duration are shown in Figure B.21 to B.30 in Appendix B with few selected years shown in Figures 6.20 to 6.22. From the simulated water balance component results (Figure 6.23 and Table D.6), AET accounted for 102% of growing season precipitation for 2005, while net percolation was 2% of the precipitation with -4% accounting for change in soil water storage. In 2006, 94% of growing season PPT was found to be the loss by AET with percolation accounting for 8% of precipitation. Simulated change in water storage accounted for -2% of precipitation. The percentage of AET of precipitation for 2007 was found to be 98% while net percolation was 8% with change in soil water storage accounting for -7% of precipitation. The trend of percentage AET from 2008 to 2017 ranged from 89% to 105% while the percentage of net percolation to precipitation ranged from 4% to 18% with the percentage of simulated change in soil water storage to precipitation found within the range of -21% to 0%. From 2008 to 2017, the highest percentage of AET to precipitation of 105% was obtained in 2015 while a minimum percentage of AET of 86% obtained in 2012. During the same study period, the highest percentage of net percolation of 19% was obtained in 2011 with a minimum of 2% obtained in 2005. The highest percentage of simulated change in soil water storage of 0 was obtained in 2016 while a minimum percentage of change in soil water storage of -21% obtained in 2011. The highest AET/PET ratio of 0.54 was obtained in 2016 with the lowest AET/PET ratio of 0.28 obtained in 2011. A mean AET of 43% PET was obtained for the shallow cover during the study duration (Figure 6.24).

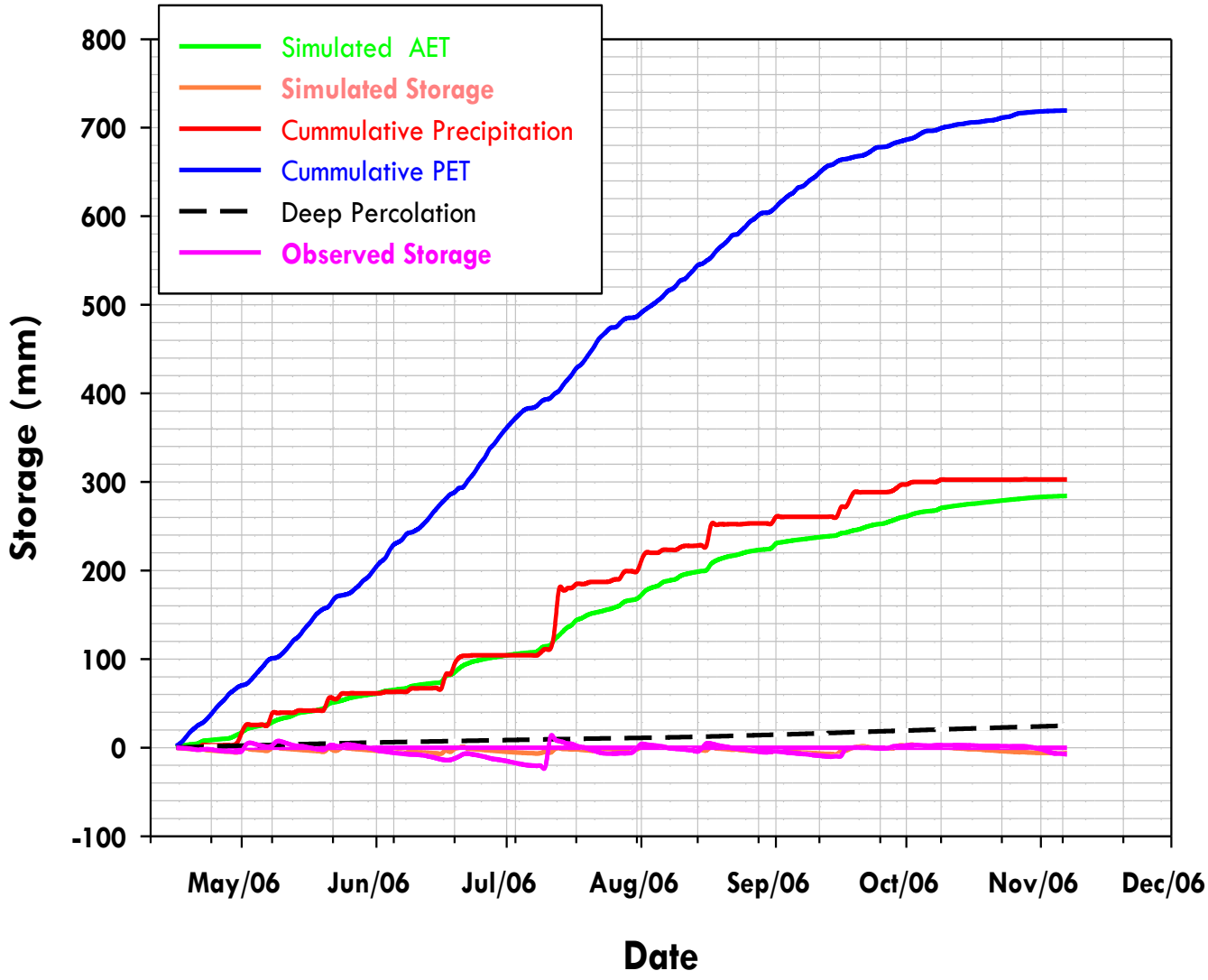

Figure 6.20: Simulated Water balance for Shallow Cover System for 2006

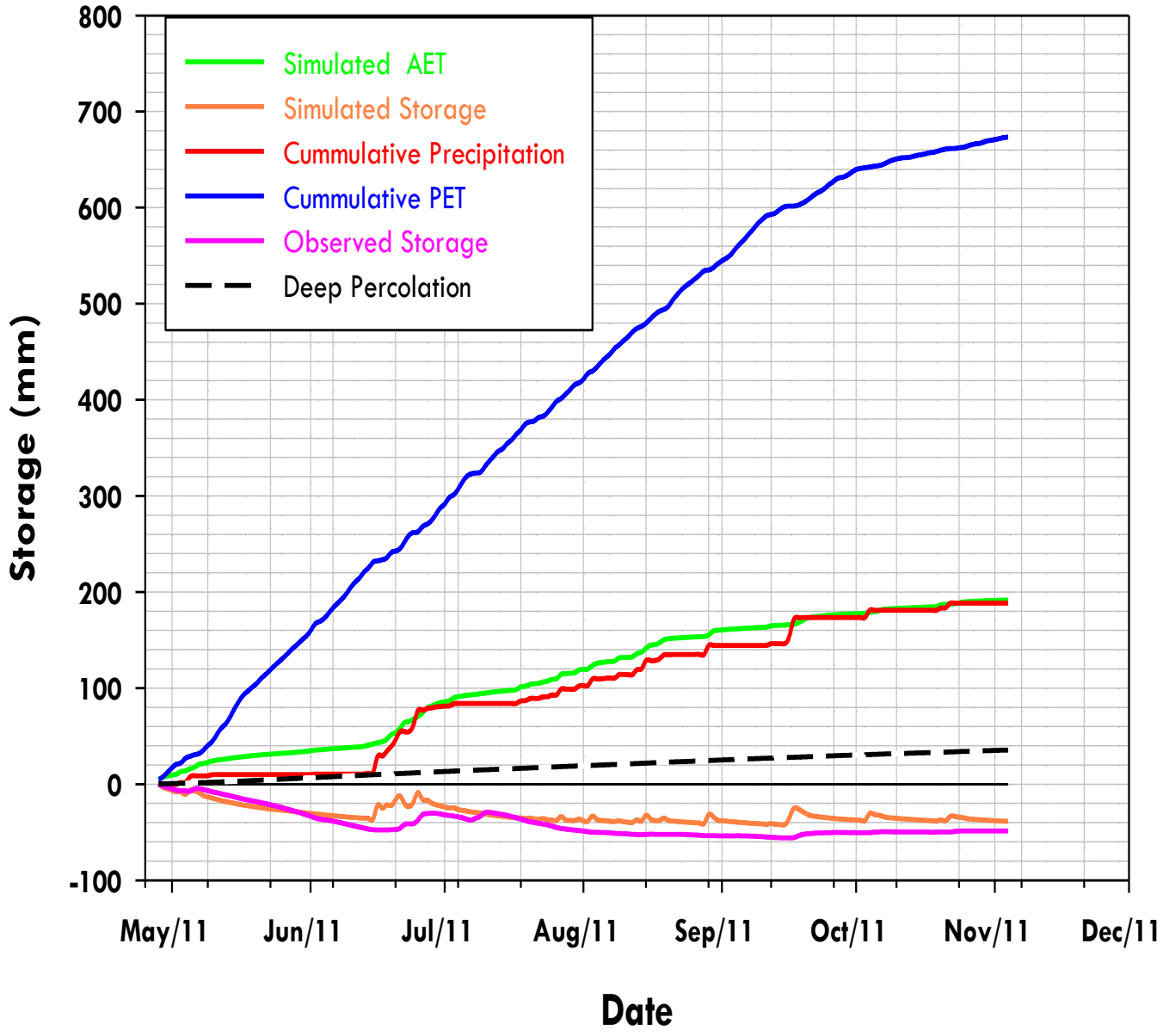

Figure 6.21: Simulated Water balance for Shallow Cover System for 2011

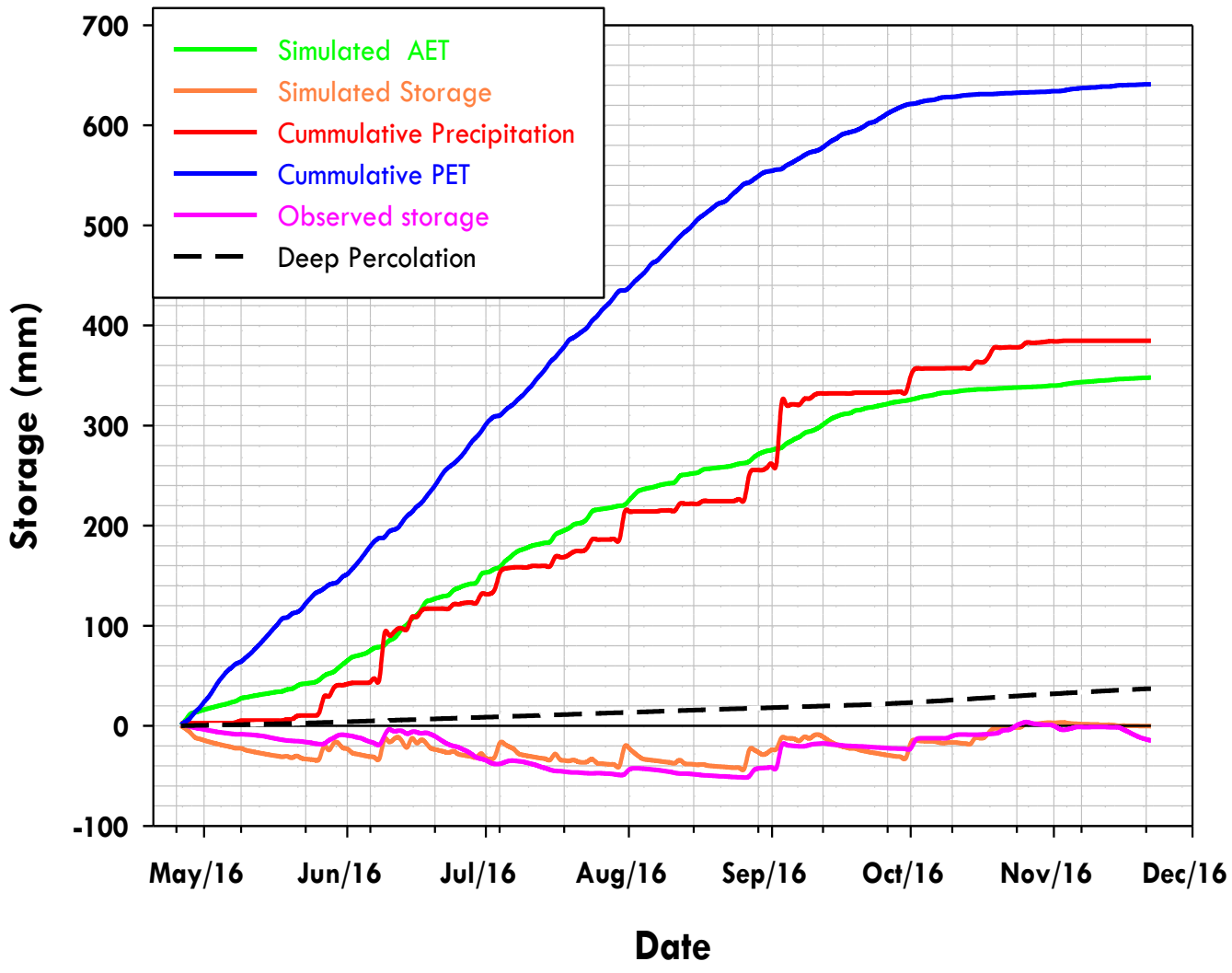

Figure 6.22: Simulated Water balance for Shallow Cover System for 2016

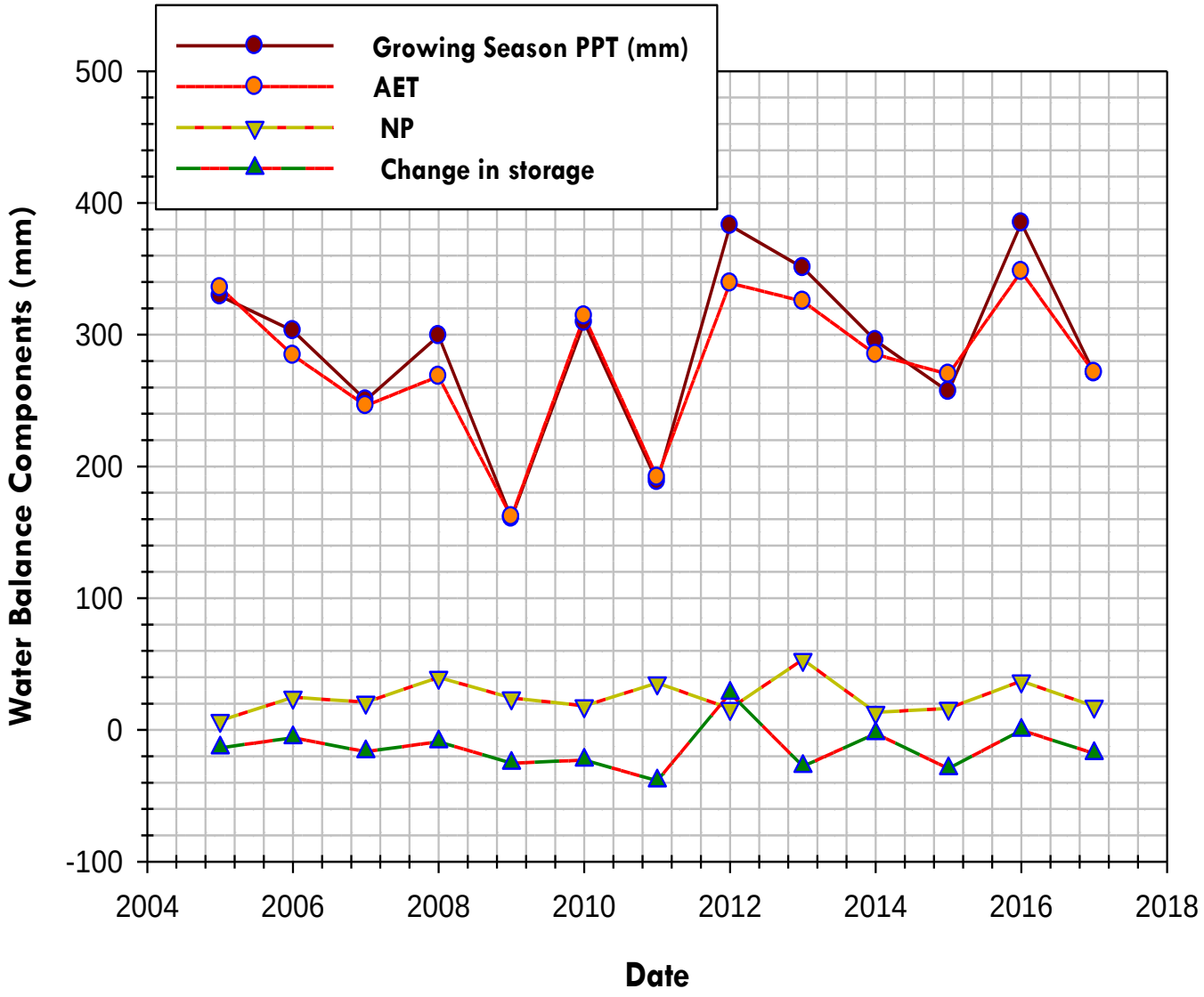

Figure 6.23: Summary of Simulated Seasonal Water Balance Components Results, Shallow Cover

The mean percentage of the simulated AET of the growing season precipitation for the shallow cover during the study period was found to be 97% while net percolation was found to be 9% of precipitation (Figure 6.25 and Figure 6.26). The mean simulated change in soil water storage was found to be -6% of the precipitation.

For the annual simulated water balance for the shallow cover, a mean annual AET was found to be 76% (280 mm) of mean annual precipitation of 368 mm (growing season + frozen season precipitation) and 43% of PET while a mean net percolation was 24% (86 mm) of annual PPT. The mean annual change in soil water storage was found to be 0 (2 mm) of precipitation (Figure 6.27 and Table D.7).

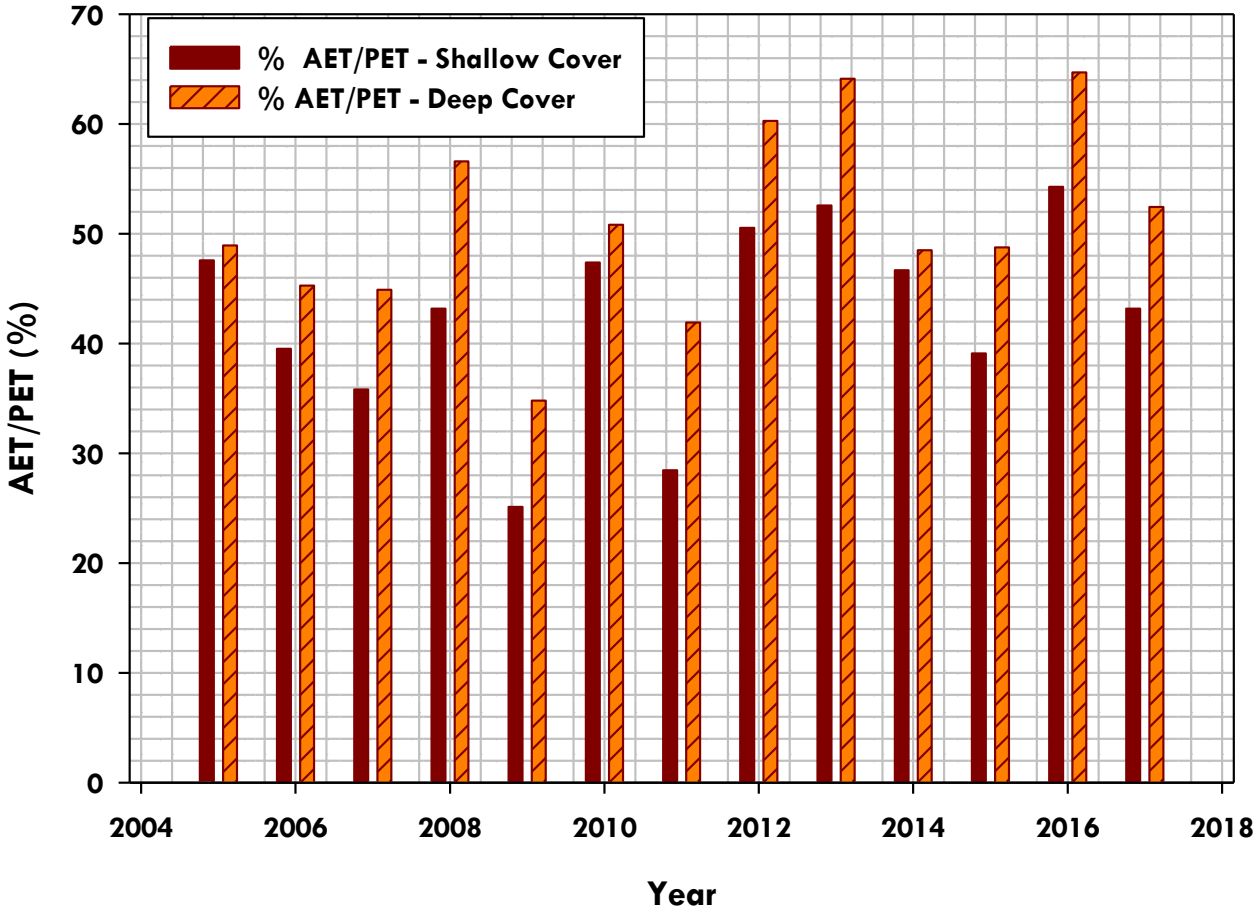

Figure 6.24: Percent AET/PET for Simulated Annual Water Balance, Shallow and Deep Cover System

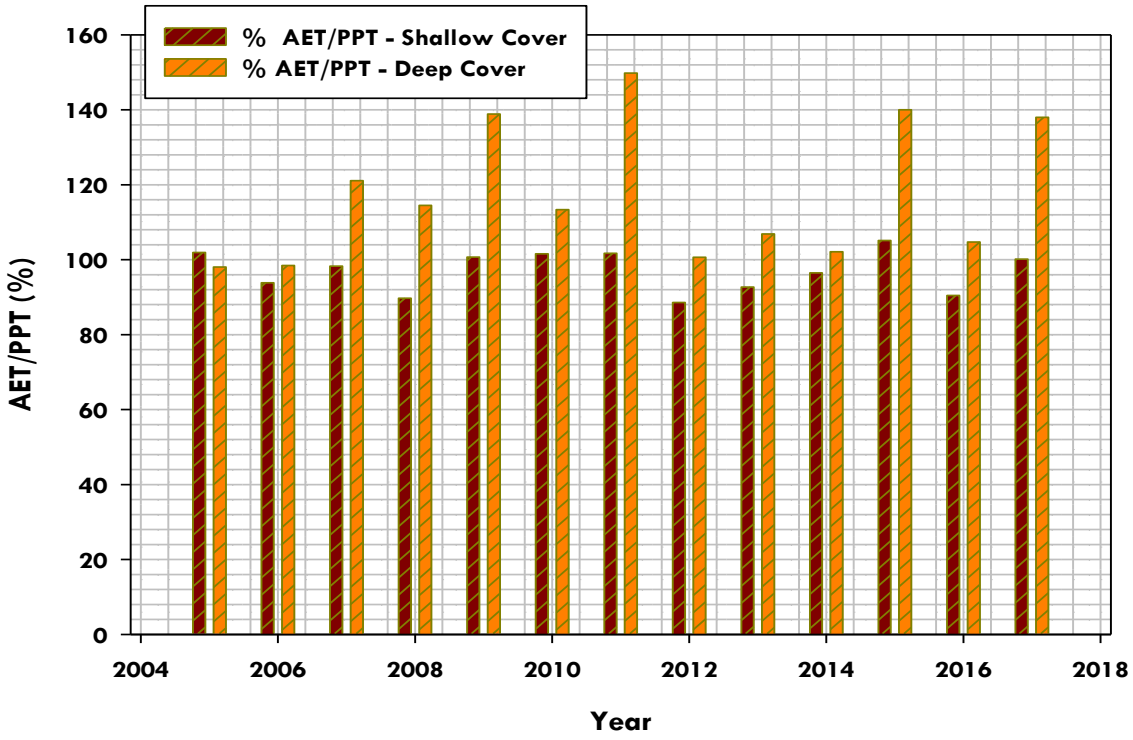

Figure 6.25: Percent AET/PPT for Simulated Seasonal Water Balance, Shallow and Deep Cover System

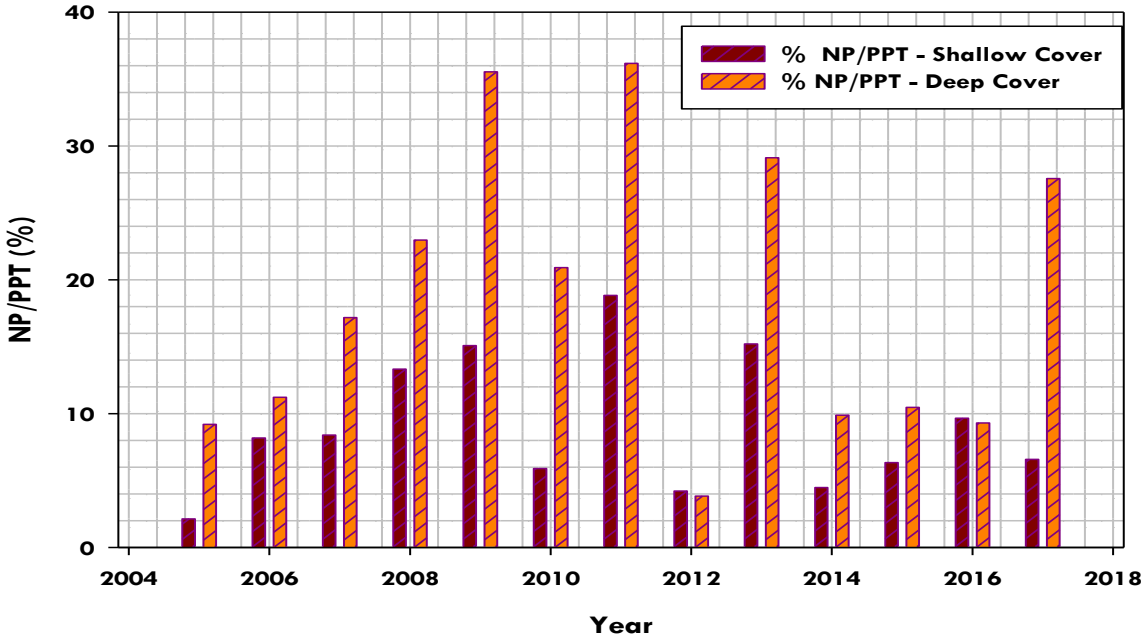

Figure 6.26: Percent NP/PPT for Simulated Seasonal Water Balance, Shallow and Deep Cover System

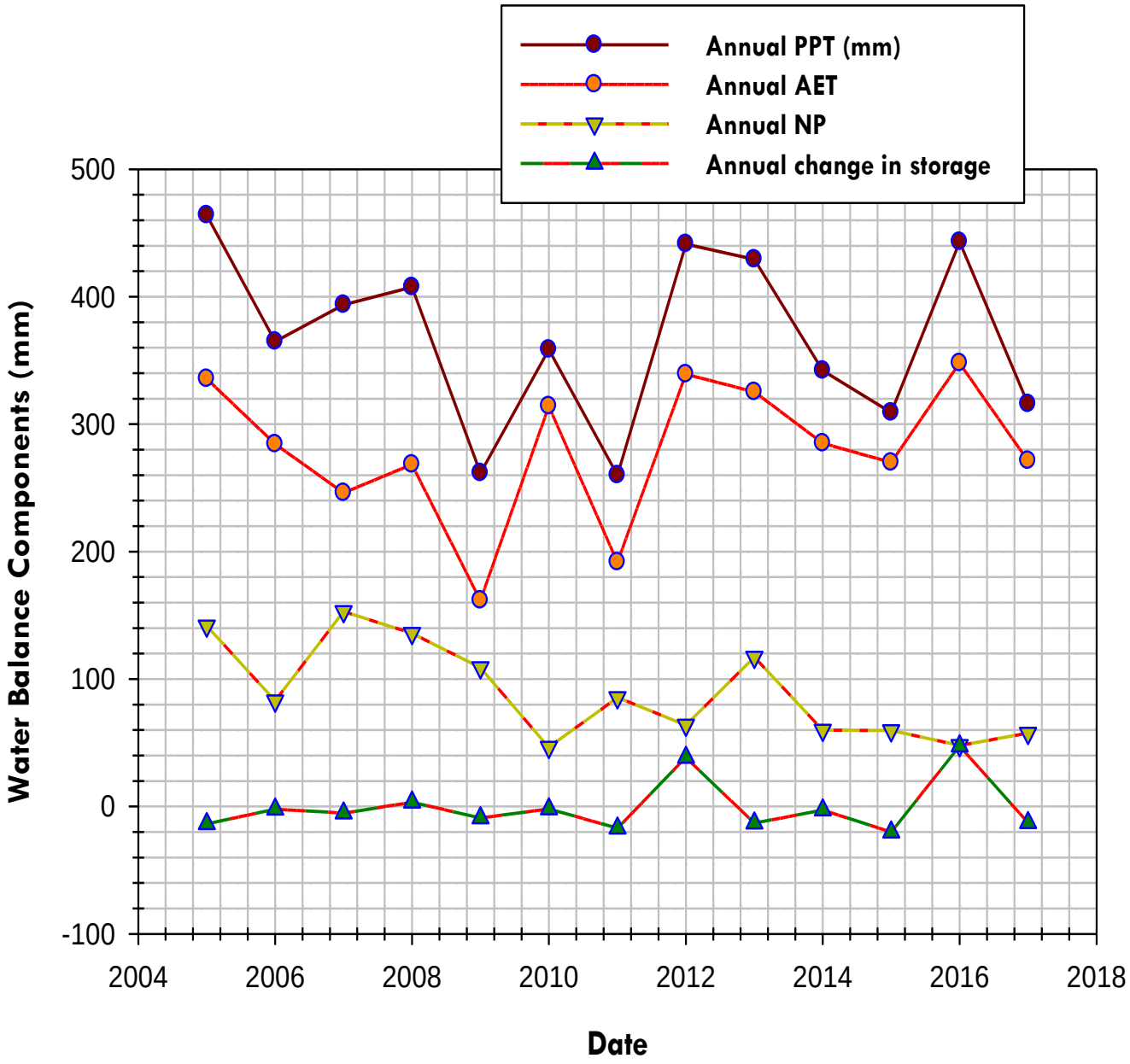

Figure 6.27: Summary of Simulated Annual Water Balance Components Results Including Frozen Period Precipitation and NP, Shallow Cover

6.2.4 Deep Cover System

In Figure B.31 to B.40 in Appendix B are the results of the yearly simulated water balance volumes for the deep cover. Few selected years as a reference are shown in Figure 6.28 to Figure 6.30. The summary of the yearly water balance component volumes for the deep cover is shown in Figure 6.31 and Table D.8 in Appendix D.

From Figure 6.31 and Table D.8, the AET was found to be 98% of growing season precipitation while net percolation was 9% of precipitation with change in soil water storage accounting for -7% of the precipitation. The percentage of AET to precipitation remained constant from 2005 to 2006 at 98% of growing season PPT. However net percolation increased from 9% in 2005 to 11% in 2006 due to a further reduction in change in soil water storage from -7% (2005) to -10% in 2006. In 2007, AET was found to be 121% of precipitation while net percolation accounted for 17% of the precipitation and the remaining -38% was losses due to change in soil water storage. The percentage of AET of precipitation from 2008 to 2017 ranged from 101% to 150% with the highest percentage of AET obtained in 2011 while the minimum percentage of AET to precipitation was obtained in 2005. But the AET in 2005 remained the highest volume of AET for the study duration. In the same way, the percentage of net percolation of precipitation for the duration under consideration ranged from 4% to 36% with 36% (the highest NP/PPT ratio) obtained in 2011 while 4% (the lowest NP/PPT ratio) obtained in 2012. The simulated change in soil water storage from 2008 to 2017 ranged from -86% to -4% with -86% (the lowest ΔS/PPT ratio) obtained in 2011 while -4 (the highest ΔS/PPT ratio) obtained in 2012. Similarly, the percentage of AET to potential evapotranspiration for the study duration for the deep cover ranged from 35% to 65% with a mean of 51% (Figure 6.24).

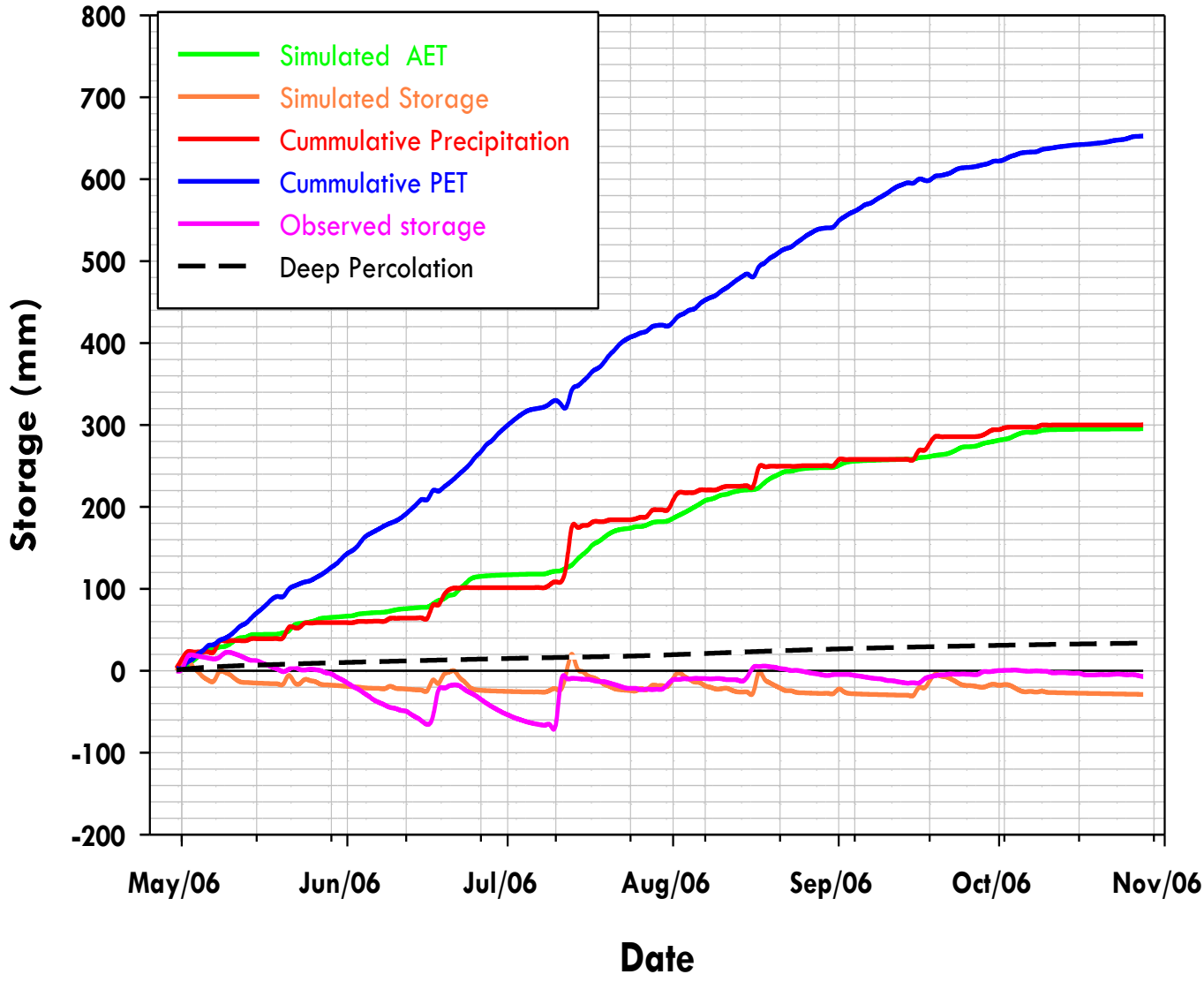

Figure 6.28: Simulated Water balance for Deep Cover System for 2006

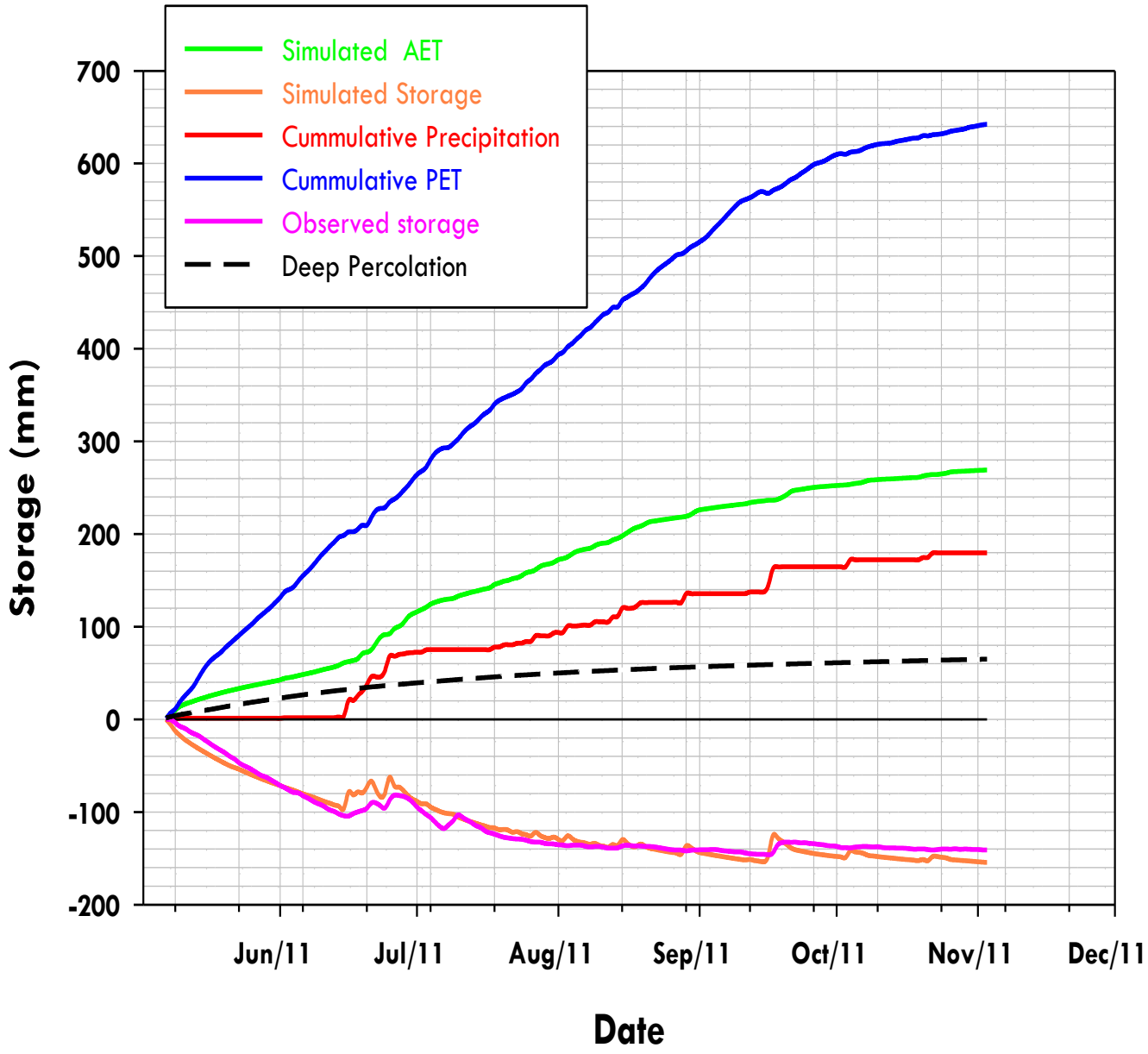

Figure 6.29: Simulated Water balance for Deep Cover System for 2011

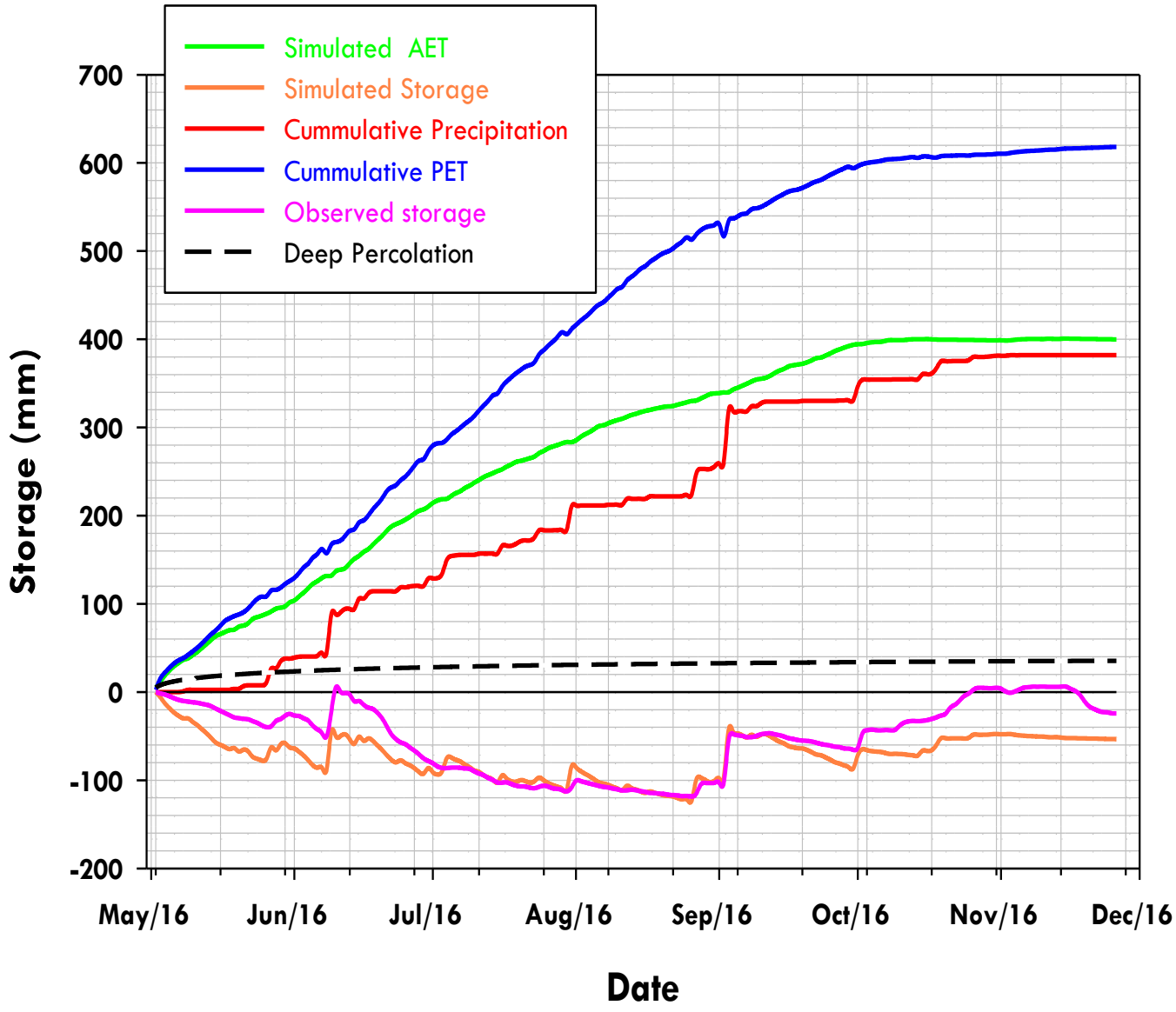

Figure 6.30: Simulated Water balance for Deep Cover System for 2016

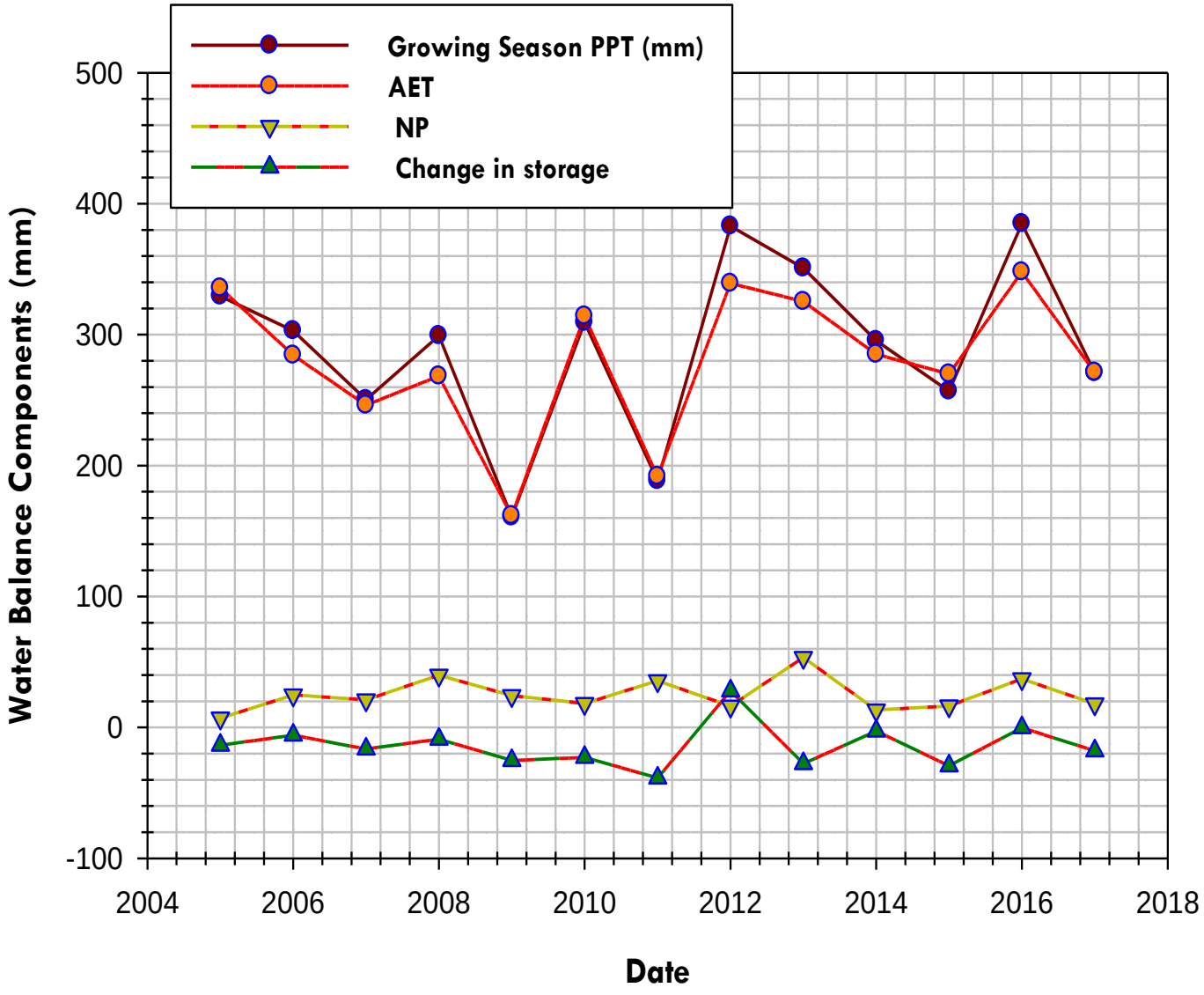

Figure 6.31: Summary of Simulated Seasonal Water Balance Components Results, Deep Cover

For the entire study duration (2005- 2017), a mean percentage of the simulated AET of the growing season precipitation for the deep cover was found to be 117%. The mean percentage of the net percolation to precipitation was found to 19% while the mean simulated change in soil water storage was found to be -36% of precipitation (Figure 6.25 and Figure 6.26).

The annual water balance for the complete year (frozen and growing season) found a mean per cent AET of 86. The net percolation was 21% of precipitation while change in soil water storage was -7% of precipitation for the deep cover during the study period (Figure 6.32 and Table D.9).

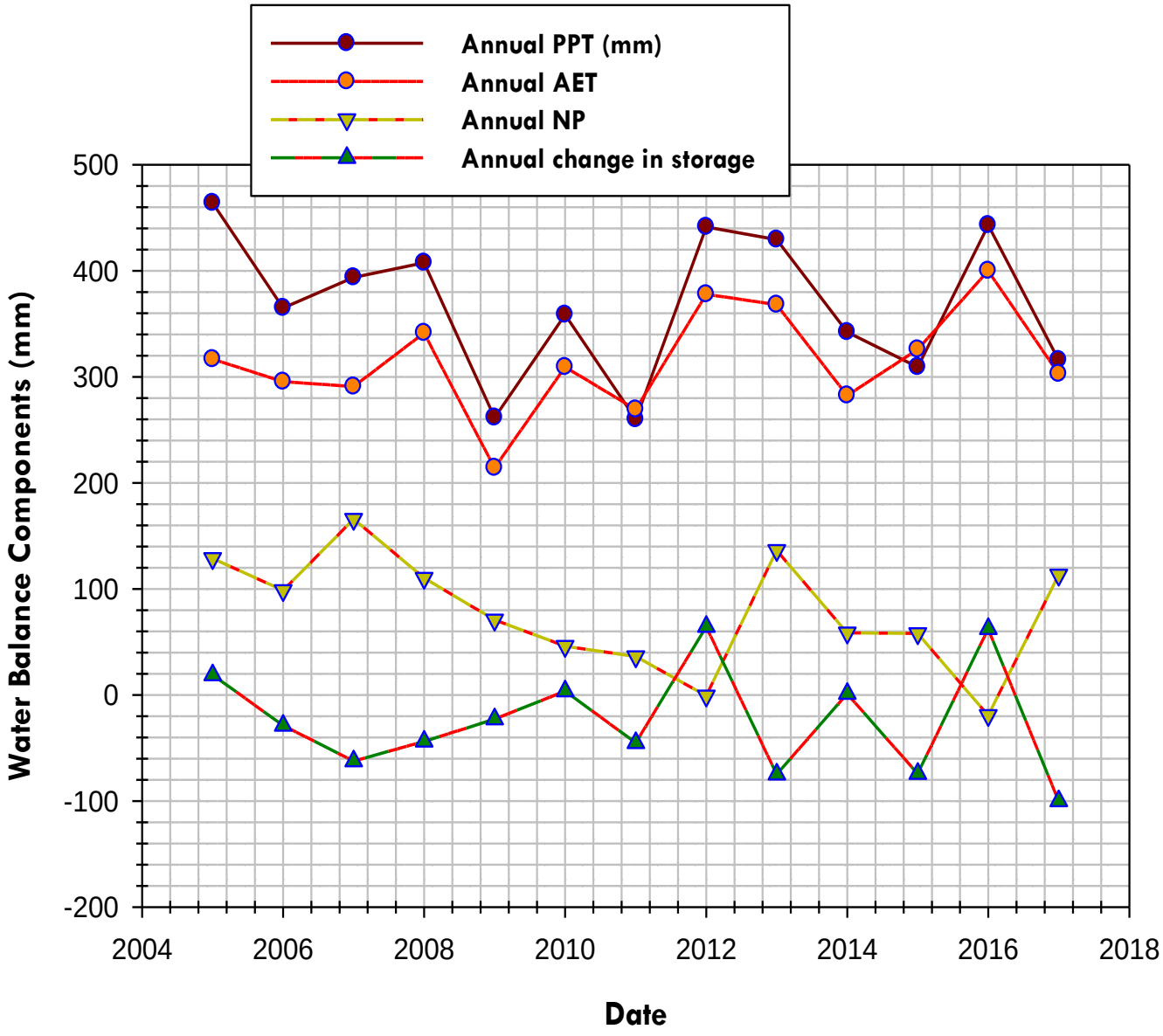

Figure 6.32: Summary of Simulated Annual Water Balance Components Results Including Frozen Period Precipitation and NP, Deep Cover

6.3 Comparison between Estimates of Water Balance Components by System Dynamics and Physics Based Approaches

The mean of the water balance components results for the study duration (2005 to 2017) for both the shallow and the deep covers were compared; i.e. comparison between estimates by system dynamics approach of the shallow cover and the deep cover, as well as the comparison between the estimates by the simulated approach for the two covers. The comparison is carried using the annual water balance component volumes since it incorporates the water storage and net percolation volumes for both the frozen into the unfrozen condition of the year.

For the system dynamics approach, the mean AET was 141 mm (38% of mean PPT) on the shallow cover whereas, on the deep cover, the mean AET was 162 mm (44% of PPT) (Figure 6.33 and Table D.10 in Appendix D). It would be expected that the deeper cover would have had a much higher annual AET since its ability to store infiltrating water, particularly water associated with snowmelt, should be much higher. The mean net percolation of 229 mm (63% of PPT) for the shallow cover was similar to that estimated for the deep cover of 210 mm (58% of PPT). The changes in soil water storage in both covers were also similar: a mean change in storage -2 mm (-1% of PPT) for the shallow cover and -3 mm (-2% of PPT) for the deep cover. Based on this analysis, both covers, regardless of cover depth, appear to be unable to capture water from either rainfall or snowmelt infiltration events and consequently are limited to similar rates of AET restricted by this lack of storage.

The results from physics-based simulations are quite different from those obtained by the system dynamics model. The mean AET for the shallow cover was 280 mm (76% of PPT) and 315 mm (86% of PPT) for the deep cover (Figure 6.33). The mean net percolation was 86 mm (24% of PPT) for the shallow cover and 77 mm (21% of PPT) for the deep cover with changes in storage of 2 mm (0% of PPT) and -23 mm (-7% of PPT) for the shallow and the deep cover respectively. Separately, a mean net percolation of 61 mm (79% of frozen PPT) was for the shallow cover and 30 mm (25% of frozen PPT) for the deep cover during the frozen season. In the growing season, mean net percolation was 25 mm (9% growing season PPT) for the shallow cover and 47 mm (19% of growing season PPT) for the deep cover.

The results from the physics-based modelling is more indicative of covers that are more efficient in capturing precipitation from rainfall and snowmelt with somewhat greater capacity for water capture and storage by the thicker cover as reflected in higher AET rates and lower NP rates.

Considering that AET may have started before the growing season start date used for both covers by this study, the study tried to project the potential AET that may have occurred but have not been accounted for by this study. Thus, the AET from when the average daily air temperature was sufficient for plant growth to the growing season start date used by this study. This potential AET was estimated considering the modelled AET results for the first weeks of the growing season used by this study. Based on this approach, an adjusted mean potential AET of 13 mm was obtained for the shallow cover while 21 mm obtained for the deep cover for the study duration.

The two modelling approaches present quite different pictures of the controls on the water balance for the two covers. The SD model suggests that both covers experience high, and similar amounts of preferential flow which results in a lack of water available for AET. The amount of this net percolation as a percentage of the available precipitation is as high or higher during the summer months (when the infiltration events are of relatively small magnitude and the soil is dry and able to readily store water) compared to just before spring.

The physics-based model suggests that the covers are capturing nearly all of the summer precipitation and making use of it for AET and that the dominant mechanism for NP is that associated with the infiltration and storage at freshet. This is in agreement with the observation by Kelln, (2007) which found that snowmelt infiltration into the covers at South Bison Hill was only captured as a result of ponding on the shale surface. If that low K barrier is not present, as it would not be in the case of well drained or unfrozen coke, then that water might continue to drain through the covers into the coke and be lost to cover water storage as observed by Huang et al. (2018). This study found 14 mm of snowmelt percolated through the covers with 24 mm runoff while a 36 mm captured and stored by the covers.

The high volumes of net percolation and low AET estimated by the SD approach may not be the true reflection of the reality for the following reasons;

- The SD model (as well as the analyses of infiltration event storage changes) relies heavily on the accurate and rapid response of the water content sensors to the individual event. If there was a long-time delay in these sensors it maybe that changes in storage associated with short term infiltration events (e.g. rainfall during growing season) are under-estimated and consequently the NP is over-estimated. This would be true for the growing season analyses presented in section 5.3.2 as well as the SD model in section 6.1. The physics-based model relies on a 'best fit' for all times and consequently is not heavily dependent on the daily response as used in the SD model.

- It would be expected that drainage of the profile should occur when the water content within the cover rises close to field capacity, and in addition, the occurrence of preferential flow should be greater for higher antecedent water contents. In the water content data available for the site, the water contents are generally much lower than field capacity indicating that percolation is unlikely to occur. In addition, the analyses presented in section 5.3.2 does not appear to support the concept of higher NP events when antecedent water contents are elevated.

From the above reasons, it appears the high estimated net percolation volumes were the volumes needed to close the water balance equation in the SD model. The reason for the possible low AET values in the SD reflects a problem with the method of AET calculation which requires the use of the measured soil water content which was low in volumes compared to the choice of the water content at FC and WP values.

Finally, it is possible that the SD model is not effectively calculating the high volumes of water storage (and subsequent source of water for AET) provided by the upper peat layer (section 5.3.2). The SD model calculates an average AET across the cover profile while the actual observations (and the physics-based model) highlight the large volume and dynamic nature of water storage within the uppermost peat layer. High volumes of the PPT is likely captured near the surface of the covers and returned into the atmosphere and therefore not available for storage. In effect, the SD approach appears to underestimate the AET and overestimates net percolation in this scenario and hence the results by the SD approach may not be the reality.

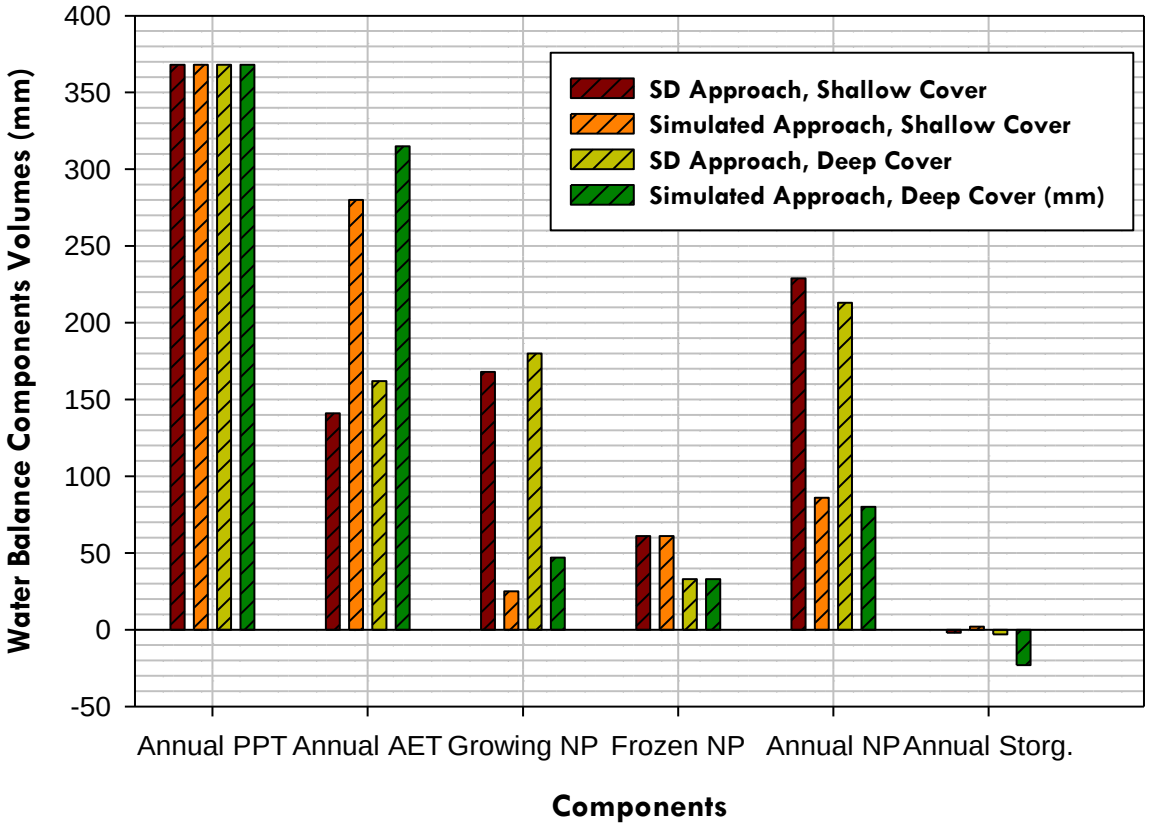

Figure 6.33: Mean Water Balance Components Results for the MLSB Site

On these bases, if we assume that the SD model is not capturing the water balance dynamics accurately, we can then focus on a comparison of the results from the physics-based model with similar studies conducted on similar cover soils. For instance, Huang *et al.*, (2018) found an average simulated AET of 317 mm for the growing season which accounted for 87% of the mean annual rainfall. The mean net percolation obtained was 34 mm / year for flat lying cover areas (i.e. plateau). The average SWE volume was 74 mm which was partitioned generally into 14 mm of snowmelt infiltration into macropores with an average of 24 mm reporting as runoff and/or interflow while a 36 mm was captured and stored.

These results are comparable to the mean simulated AET of 315 mm (86% annual PPT) and 280 mm (76% of annual PPT) for both the deep and the shallow covers in this study. The net percolation of 25 mm and 47 mm obtained for the growing season by this study is also similar to the mean growing season net percolation of 34 mm for flat areas obtained by Huang *et al.*, (2018).

In a similar study conducted on South Bison Hills using stable isotopes, Huang, (2015) found a mean growing season net percolation ranging from 24 mm/year to 43 mm/year for a plateau area. This is approximately the same as the growing season net percolation results obtained by this study.

In a related Huang et al. (2015) found mean AET ranging from 63% to 84% of precipitation with total runoff and percolation amounting to about 41 mm which varied with cover thickness and different LAI. The mean potential evapotranspiration which resulted in the mean AET was 496 mm. The obtained net percolation result by this study agrees with the runoff and percolation result obtained by Huang, (2015), however, the obtained AET appears to be lower than the AET of this study. The reason for the low AET may be due to the low mean PET used compared to the mean PET of 620 mm used by this study. A similar study by Shurniak (2003) also found AET of 293 mm to be evaporating from the shallow cover with 296 mm AET evaporating from the deep cover on South Hill overburden piles. The results of Shurniak (2003) correlates well with the results AET results obtained by this study.

CHAPTER 7

CONCLUSIONS AND RECOMMENDATIONS

7.1 Conclusions

There were initial concerns that the soil covers constructed by Syncrude Canada on the Coke Beach Instrumented Watershed were experiencing elevated water losses which was limiting revegetation plant growth. Previous studies conducted on the site aimed at unravelling the cause of the accelerated water loss but failed in achieving this objective. However, these studies found that the enhanced drying of the covers may be due to other processes than the water balance components but not convective air flow. The reason was that the occurrence of convective air flow through the covers was not enough to cause enhanced drying. A bypass flow was hypothesised to be the likely cause of the accelerated drying of the covers. From this background, this study was designed to; Construct a daily water balance for long-term (2005-2017) monitoring data set based on field meteorological and soil monitoring data;

- Develop a calibrated physics-based model of the hydrologic performance of the two reclamation covers using a soil-vegetation-atmosphere transfer (SVAT) model;
- Use this calibrated SVAT model to identify the key processes controlling the hydrological performance of the reclamation covers with a focus on identifying which processes (e.g. preferential flow, convective air flow) or hydraulic properties (e.g. dual porosity water flow storage) have the greatest influence over performance.

In achieving these objectives, this study adopted two approaches (system dynamics and physics-based model) in constructing the daily water balance and to identify which processes control the hydrological performance of the covers. Various field measurement data including ambient temperature, relative humidity, wind speed and direction, net radiation, precipitation (meteorological data) and the measured soil water content, soil matric suction and soil temperature

(soil monitoring data) were used as the basis for the construction of the water balance.

The measured meteorological data obtained from the MLSB site for this study was verified for its accuracy by comparing it with the same data set obtained from neighbouring sites such as 30 Hill Top, SWSS C32 and W1 sites.

The system dynamics approach adopted the water balance model stated in equation 4.2 in estimating the various water balance components. Closure of the daily water balance resulted in over-estimation of the net percolation rate and consequently lower values of AET obtained throughout most of the year. The use of the physics-based model became necessary for two reasons.

- To corroborate the water balance component results obtained by the system dynamic approach; and
- To identify if the preferential flow was occurring due to changes in hydraulic properties of the covers.

This is because the dual porosity model in Hydrus-1-D assumes that the water flow within the soil covers only occurs through the macropores while water storage is primarily associated with the fine pores within an immobile soil fine textured matrix. Based on this principle, all the simulated net percolation component of the water balance components could be considered as resulting from the preferential flow. Also, the use of Hydrus-1-D model helped to characterise the behaviour of the hydraulic properties (hydraulic conductivity of the various soil types, the V-G parameters, saturated and residual soil water content) of the soil covers over time.

7.1.1 Research Findings

From the results of the water balance components using the system dynamics model, a mean AET of 38% of the annual mean PPT was found to be lost to the atmosphere on the shallow cover while on the deep cover, a mean AET of 44% of mean annual PPT was found to be lost. The mean net percolation for the shallow cover was 63% of annual PPT compared to the mean net percolation of 58% of annual PPT lost through the deep cover. Comparing the change in water ability of the covers, the shallow cover was found to be losing -1% of annual PPT while the deep cover lost -2% of the annual PPT.

Based on the estimation of the water balance component using the system dynamics approach, more water was found to be lost to the atmosphere through AET on the deep cover than the shallow cover. Likewise, more water was observed to percolates through the shallow cover than the deep.

From the detail evaluation of the water storage ability of the covers, it appears the SD approach underestimates the AET and overestimates net percolation in this scenario and hence the results by the SD approach may not be the reality.

With the simulated water balance approach (physics-based model) a mean AET of 76% of annual PPT was observed to be lost to the atmosphere on the shallow cover compared to a mean AET of 86% of annual PPT found to be lost on the deep cover. Similarly, the mean percentage of precipitation released as NP was 24% on the shallow cover and 21% on the deep cover. The predominant volume of NP was associated with snowmelt and rainfall while the cover was frozen. The volume of net percolation for both the shallow and the deep cover during the frozen period was 61 mm and 30 mm respectively, compared to the growing season net percolation of 25 mm and 47 mm. The higher AET on the deep cover than the shallow cover is an indication of the additional water stored within the thicker cover and available for use by vegetation.

From the water balance components volumes estimated by the physics-based model, evapotranspiration was identified by this study as the main component greatly influencing the performance of the covers and causing the elevated drying in the growing season, followed by the net percolation. This is evident in the volumes of AET observed to be occurring through both covers during the growing season as shown by the simulated approach. The volumes of net percolation obtained using the simulated approach, were still higher compared to volumes of net percolation reported by other studies on similar cover systems.

7.2 Recommendations and Limitations

7.2.1 Limitations

- Volumetric soil water content at field capacity and the permanent wilting point is a major factor that controls the accuracy of the estimated water balance components by the system dynamics approach. Subsequently, the results obtained by the system dynamics approach may be misleading should the FC and WP for the MLSB site be different the adopted FC and WP figures from SBH site.

- The LAI is an important parameter for the simulation of the water balance components by Hydrus - 1- D model, used for this study. There the result by the simulated approach could be affected should the adopted LAI be different from the actual LAI on site. It is important to note that, the adopted LAI for this study was obtained from a field inventory survey by Syncrude Canada Limited.

7.2.2 Recommendations

From the results of this study, the following recommendations are identified for consideration in future studies;

- Installation of eddy covariance system at the MLSB site to directly measure evapotranspiration to serve as a check on estimated AET on the site.
- Field instrumentation should be augmented to directly measure net percolation through the covers as a check for net percolation.

REFERENCE

Alberta Energy Regulator (2015) *2015 Alberta ' s Energy Reserves 2014 and Supply/Demand Outlook 2015-2024*. Calgary.

Alberta Environment and Sustainable Resource Development (2013) *Criteria and Indicators Framework for Oil Sands Mine Reclamation Certification*.

Alberta Environmental Protection (1997) *A Guide for Oil Production Sites, Pursuant to the Environmental Protection and Enhancement Act and Regulations. Alberta Environmental Protection, Land Environmental Protection, 1994. A Guide for Oil Production Sites, Pursuant to the Environmental Protecti*. Edmonton.

Albright, W. H., Benson, C. H. and Waugh, W. J. (2009) *Water Balance Covers for Waste Containment : Principles and Practice*. Nevada, USA.

Allen, R. G. *et al.* (1998) 'FAO Irrigation and Drainage Paper No. 56, Crop Evapotranspiration', *Irrigation and Drainage*, 300(56), p. 300. doi: 10.1016/j.eja.2010.12.001.

Apiwantragoon, P. (2007) *Field Hydrologic Evaluation of Final Covers for Waste Containment*. University of Wisconsin-Madison.

Apiwantragoon, P., Benson, C. H. and Albright, W. H. (2015) 'Field Hydrology of Water Balance Covers for Waste Containment', *Journal of Geotechnical and Geoenvironmental Engineering*, 141(2), pp. 1–20. doi: 10.1061/(ASCE)GT.1943-5606.0001195.

Armoh, M. (2015) *Determination of Evaporation rate in a Sabkha in the Eastern Province, Saudi Arabia*. King Fahd University of Petroleum and Minerals.

Armstrong, R. N., Pomeroy, J. W. and Martz, L. W. (2008) 'Evaluation of three evaporation estimation methods in a Canadian prairie landscape', *Hydrological Processess*, pp. 1–15. doi: 10.1002/hyp.

ASCE-EWRI Task Committee (2002) *The ASCE Standardized Reference Evapotranspiration Equation: Appendices A - F*.

ASCE-EWRI Task Committee (2005) *The ASCE Standardized Reference Evapotranspiration Equation*.

Barber;, L. A., Ayres, B. K. . and Schmid, B. (2015) *Performance Evaluation of Reclamation Soil Cover Systems at Cluff Lake Mine in Northern Saskatchewan, Mine Closure 2015 – A.B. Fourie, M. Tibbett, L. Sawatsky and D. van Zyl (eds) © 2015 InfoMine Inc., Canada,*.

Barbour, S. L. (1998) 'Nineteenth Canadian Geotechnical Colloquium: The Soil-water Characteristic Curve: a Historical Perspective', *Canadian Geotechnical Journal*, 35(5), pp. 873–894. doi: 10.1139/t98-040.

Bauters, T. W. J. (1999) *Preferential Flow in Water Repellent and Moist Sands, Order A Journal On The Theory Of Ordered Sets And Its Applications*. Cornell University.

Bauters, T. W. J. *et al.* (2000) 'Physics of Water Repellent Soils', *Journal of Hydrology*, 231–232, pp. 233–243. doi: 10.1016/S0022-1694(00)00197-9.

Benson, C. *et al.* (2001) 'Field Evaluation of Alternative Earthen Final Covers', *International Journal of Phytoremediation*, 3(1), pp. 105–127. doi: 10.1080/15226510108500052.

Boese, C. D. (2003) *The Design and Installation of a Field Instrumentation Program for The Evaluation of Soil-Atmosphere Water Fluxes in a Vegetated Cover Over Saline/Sodic Shale Overburden*. University of Saskatchewan. Available at: n:%5CAdmin%5Cgeoscience%5CReferences%5CE006.pdf.

Brooks;, K. N., Ffolliott;, P. F. and Magner, J. A. (2013) *Hydrology and the Management of Watersheds, 3rd ed.,*. Fourth Edi, *Soil Science*. Fourth Edi. Oxford: John Wiley & Sons, Inc. doi: 10.1097/01.ss.0000100476.96182.cd.

Carey, S. K. (2008) 'Growing season energy and water exchange from an oil sands overburden reclamation soil cover, Fort McMurray, Alberta, Canada', *Hydrological Processes*, 22(November 2008), pp. 2847–2857. doi: 10.1002/hyp.

Cumulative Environmental Management Association (CEMA) (2006) *Land Capability Classification System for Forest Ecosystems in The Oil Sands - Volume 1: Field Manual for Land Capability*.

DCLG (1996) *Minerals Planning Guidance 7: Reclamation of mineral workings*.

Debano, L. F. (2000) 'Water Repellency in Soils: A Historical Overview', *Journal of Hydrology*,

231–232, pp. 4–32. doi: 10.1016/S0022-1694(00)00180-3.

Dingman, S. L. (2015) *Physical Hydrology*. Third Edit. Long Grove: Waveland Press, Inc.

Doerr, S. H., Shakesby, R. A. and Walsh, R. P. D. (2000) 'Soil Water Repellency: Its Causes, Characteristics and Hydro-Geomorphological Significance', *Earth Science Reviews*, 51(1–4), pp. 33–65. doi: 10.1016/S0012-8252(00)00011-8.

Donohue, R. J., Mcvicar, T. R. and Roderick, M. L. (2010) 'Assessing the ability of potential evaporation formulations to capture the dynamics in evaporative demand within a changing climate', *Journal of Hydrology*. Elsevier B.V., 386(1–4), pp. 186–197. doi: 10.1016/j.jhydrol.2010.03.020.

Elshorbagy, A. and Barbour, L. (2007) 'Probabilistic Approach for Design and Hydrologic Performance Assessment of Reconstructed Watersheds', *Journal of Geotechnical and Geoenvironmental Engineering*, 133(9), pp. 1110–1118. doi: 10.1061/(ASCE)1090-0241(2007)133:9(1110).

Farnden, C. J. (2018) *Field Vegetation Inventory Survey*. Edmonton.

Feddes;, R. A., Bresler;, E. and Neuman, S. . (1974) 'Field Test of a Modified Numerical Model for Water Uptake by Root System', 10(6).

Feddes;, R. A., Kowalik;, P. J. and Zaradny, H. (1978) *Simulation of Field Water Use and Crop Yield, John Wiley & Sons*. New York, NY: John Wiley & Sons.

Fenske, D. (2012) *A Study to Evaluate The Performance of Reclamation Soil Covers Placed Over an Oil Sands Fluid Coke Deposit*. University of Saskatchewan. Available at: %5C%5Cgolder.gds%5Ccalgary%5CAdmin%5CGROUPS%5COil Sands%5CReferences and Glossary%5CReference Manager%5CElectronic References%5C100017.pdf.

Fredlund;, D. G. and Xing, A. (1994) 'Equations for the Soil-Water Characteristic Curve', *Canadian Geotechnical Journal*, 31, pp. 521–532. doi: 10.1139/t94-120.

Fredlund, D. G., Xing, A. and Huang, S. (1994) 'Predicting the Permeability Function for Unsaturated Soils Using the Soil-Water Characteristic Curve', *Canadian Geotechnical Journal*, 31(4), pp. 533–546. doi: 10.1139/t94-062.

van Genuchten, M. T. (1980) ‘A Closed-form Equation for Predicting the Hydraulic Conductivity of Unsaturated Soils’, *Soil Science Society of America Journal*, 44(5), p. 892. doi: 10.2136/sssaj1980.03615995004400050002x.

Gerke;, H. H. and Genuchten, M. T. Van (1993) ‘Evaluation of a First-Order Water Transfer Term for Variably Saturated Dual-Porosity Flow Models’, *Water Resources*, 29(4), pp. 1225–1238.

Government, U. S. (2011) ‘Tailings Mine Waste ’10’, in Francis and Taylor (eds) *Proceedings of The 14th International Conference on Tailings and Mine Waste, Vail, Colorado, USA, 17-20 October 2010*. Proceeding. London: CFC Press, pp. 1–472.

Han, J. and Zhou, Z. (2013) ‘Dynamics of Soil Water Evaporation during Soil Drying: Laboratory Experiment and Numerical Analysis’, *The Scientific World Journal*, 2013, pp. 1–10. doi: 10.1155/2013/240280.

Hardt, C. M. (2008) *Numerical Evaluation of Preferential Flow Through Evapotranspirative Landfill Covers*. Michigan State University.

Hillel, D. (1980) *Applications of Soil Physics, Soil Science*. New York: Academic Press. doi: 10.1097/00010694-198109000-00011.

Hillel, D. (1998) *Environmental Soil Physics*. 1st edn. Academic Press.

Hillel, D. and Gardener, W. R. (1970) ‘Measurement of Unsaturated Conductivity and Diffusivity by Infiltration Through an Impeding Layer’, *Soil Science*, 109(3).

Huang;, M., Barbour, L. and Zettl, J. (2010) *Draft Report: Summary of Cover Performance and Hydrology – Mildred Lake COke Watershed*.

Huang, M., Elshorbagy, A., *et al.* (2011) ‘System Dynamics Modeling of Infiltration and Drainage in Layered Coarse Soil’, *Canadian Journal of Soil Science*, 91, pp. 185–197. doi: 10.4141/cjss10009.

Huang, M., Barbour, S. L., *et al.* (2011) ‘Water availability and forest growth in coarse-textured soils’, *Canadian Journal of Soil Science*, 91, pp. 199–210. doi: 10.4141/CJSS10012.

Huang, M. *et al.* (2018) ‘Fully coupled heat and water dynamics modelling of a reclamation cover for oil sands shale overburden’, *Journal of Hydrology*. Elsevier, 566(June), pp. 250–263. doi:

10.1016/j.jhydrol.2018.09.026.

Huang, M., Barbour, S. L. and Carey, S. K. (2015) 'The Impact of Reclamation Cover Depth on the Performance of Reclaimed Shale Overburden at an Oil Sands Mine in Northern Alberta, Canada', *Hydrological Processes*, 29(12), pp. 2840–2854. doi: 10.1002/hyp.10229.

Huang, M., Hilderman, J. N. and Barbour, L. (2015) *Transport of stable isotopes of water and sulphate within reclaimed oil sands saline-sodic mine overburden*, *Journal of Hydrology*. Elsevier B.V. doi: 10.1016/j.jhydrol.2015.08.028.

International Network for Acid Prevention (2003) *Evaluation of the Long-Term Performance of Dry Cover Systems*.

Jarvis, P. G. (1976) 'The Interpretation of the Variations in Leaf Water Potential and Stomatal Conductance in the Field', *Society, Royal Sciences, Biological*, 273(927), pp. 593–610.

Keller, J. *et al.* (2009) 'Characterization and Modeling of Macro-pore Flow in Heap Leach and Waste Rock Material', *8th International Conference on Acid Rock Drainage*, 8th Intern, pp. 1–10.

Keller, J., Milczarek, M. and Zhan, G. (2015) 'Water Balance Modeling of Preferential Flow in Waste Rock Materials', *10th International Conference on Acid Rock Drainage & INWA Annual Conference*, pp. 1–10.

Kelln, C., Barbour, L. and Qualizza, C. (2007) 'Preferential Flow in a Reclamation Cover: Hydrological and Geochemical Response', *Journal of Geotechnical and Geoenvironmental Engineering*, 133(10), pp. 1277–1289. doi: 10.1061/(asce)1090-0241(2007)133:10(1277).

Keshta, N., Elshorbagy, A. and Barbour, L. (2010) 'Comparative Probabilistic Assessment of the Hydrological Performance of Reconstructed and Natural Watersheds', *Hydrological Processes*, 24(10), pp. 1333–1342. doi: 10.1002/hyp.7596.

Khire;, M. V., Benson;, C. H. and Bosscher, P. J. (1997) 'Water Balance Modeling of EARTHEN FINAL COVERS', *Journal Geotechnincal Geoenvironmental Engineering*, 123(August), pp. 744–754.

King, J. (2015) *Comparison of Alternative Estimators of Deep Percolation in Full and Deficit Irrigation*. Colorado State University.

Koehler, B. (2018) *An Evaluation of Accelerated Drying of Reclamation Soil Covers by Convective Airflow*. University of Saskatchewan.

Kool, J. B. and Parker, J. C. (1988) 'Analysis of The Inverse Problem for Transient Unsaturated Flow', *Water Resources Research*, 24(6), pp. 817–830. doi: 10.1029/WR024i006p00817.

Lahmira, B., Barbour, L. and Huang, M. (2013) 'Numerical Modeling of Gas Flow in the Suncor Coke Stockpile Covers', *Vadose Zone Journal*, 0, p. 0. doi: 10.2136/vzj2013.07.0119.

M.O'Kane;, Wilson;, G. W. and Barbour, S. L. (2003) 'Soil Cover, A New Computer Model to Aid in The Design of Soil Cover Systems for Acid Generating Waste Rock and Tailings', *Proceedings of the 17th Annual British Columbia Mine Reclamation Symposium in Port Hardy, BC, 1993. The Technical and Research Committee on Reclamation*, pp. 1–13. Available at: papers2://publication/uuid/E68B2BCF-C987-458C-8F09-0E03DCB48A8D.

Meiers;, D. E. and Barbour, S. L. (2002) 'Monitoring of Cover and Watershed Saline-Sodic Shale Overburden From Oilsands Mining', in *National Meeting of the American Society of Mining and Reclamation*, pp. 602–622. doi: 10.21000/JASMR02010602.

Meiers;, G. P. *et al.* (2011) 'Evolution of the Hydraulic Conductivity of Reclamation Covers Over Sodic/Saline Mining Overburden', *Journal of Geotechnical and Geoenvironmental Engineering*, 137(1), pp. 968–976. doi: 10.1061/(ASCE)GT.1943-5606.0000523.

Meiers G, Barbour SL, Qualizza C, D. B. 2011. (2011) 'Evolution of the hydraulic conductivity of reclamation covers over sodic/saline mining overburden', *Journal of Geotechnical and Geoenvironmental Engineering*, 137(1), pp. 968–976. doi: 10.1061/(ASCE)GT.1943-5606.0000523.

Milczarek;, M. *et al.* (2015) 'Efficacy of Cover Systems in High Elevation Andean Climates', in *10th International Conference on Acid Rock Drainage & INWA Annual Conference*, pp. 1–9.

Milczarek, M., Hammermeister, D. and Vinson, J. (2000) 'Myths, Models, and Realities Infiltration and Seepage Control In Mine Reclamation Covers In The U. S. Southwest', *Proc. 5th International Conference on Acid Rock Drainage.*, pp. 1–7.

Milind Vishnu Khire (1995) *Field Hydrology and Water Balance Modeling of Earthen Final Covers for Waste Containment*. University of Wisconsin-Madison.

Morel-Seytoux, H. J. (1989) *Unsaturated Flow in Hydrologic Modeling*. Dordrecht: Kluwer Academic Publishers. doi: 10.1007/978-94-009-2352-2.

O'Kane, C. I. (2004) *As-Built Report for the Meteorological Station and Net Percolation Monitoring System Installed at the Mildred Lake Coke Watershed*. Calgary.

O'Kane, C. I. (2016) *Instrumented Watershed Monitoring Program at the Mildred Lake Setting Basin Reclamation Sites : Performance Monitoring Report for the Period January 2015 to December 2015*. Fort McMurray.

O'Kane, C. I. (2018) *Syncrude Watershed Research Database*.

Pallant, J. (2010) *SPSS Survival Manual*. 4th Editio, *Training*. 4th Editio. Mc Graw Hill.

Pomeroy;, J. W. and Gray, D. M. (1995) *Snowcover-Accumulation, Relocation and Management*. Saskatoon.

Rana, G. and Katerji, N. (2000) 'Measurement and Estimation of Actual Evapotranspiration in the Field Under Mediterranean Climate: A Review', *European Journal of Agronomy*, 13(2–3), pp. 125–153. doi: 10.1016/S1161-0301(00)00070-8.

Saravanathiiban, D. S. (2014) *Preferential Flow Through Earthen Landfill Covers*. Michigan State University.

Shurniak, R. E. (2003) *Predictive Modeling of Moisture Movement within Soil Cover Systems for Saline/Sodic Overburden Piles*. University of Saskatchewan.

Simunek;, J. *et al.* (2013) *The Hydrus-1D Software Package for Simulating the One-Dimensional Movement of Water, Heat, and Multiple Solutes in Variably-Saturated Media, Version 4.16 March 2013*. Riverside.

Stockman, L. (2013) *Petroleum Coke : The Coal Hiding in The Tar Sands*. Washington DC, USA. Available at: http://priceofoil.org/content/uploads/2013/01/OCI.Petcoke.FINALSCREEN.pdf.

Tabari, H., Grismer, M. E. and Trajkovic, S. (2013) 'Comparative Analysis of 31 Reference Evapotranspiration Methods Under Humid Conditions', *Irrigation Science*, 31(2), pp. 107–117. doi: 10.1007/s00271-011-0295-z.

Tao, W. (2015) *Managing China's Petcoke Problem*. Beijing. Available at:

http://carnegietsinghua.org/2015/05/31/managing-china-s-petcoke-problem-pub-60023.

Tarboton, D. (2003) *Rainfall-Runoff Processes, Utah State University*. Edited by David G Tarboton. Lake Salt: COMET. Available at: http://ceefsl.engr.usu.edu/cee6400/TarbotonRainfallRunoffProcesses.pdf.

Watson, K. K. (1966) 'An Instantaneous Profile Method for Determining the Hydraulic Conductivity of Unsaturated Porous Materials', *Water Resources Research*, 2(4), pp. 709–715. doi: 10.1029/WR002i004p00709.

Welter, D. (2009) *Evaluation of Preferential Flow Processes in Reclamation Soil Covers*. University of Saskatchewan. Available at: http://ecommons.usask.ca/bitstream/handle/10388/etd-07142009-155627/DanielleWelterThesis2009.pdf.

White, M. A. *et al.* (2000) 'Parameterization and Sensitivity Analysis of the BIOME – BGC Terrestrial Ecosystem Model : Net Primary Production Controls', *Earth Interactions*, 4(3), pp. 1–85.

World Meteorological Organization, W. (2008) *Guide to Hydrological Practices, Volume 1*. Sixth, *World meteorological Organization*. Sixth. Swizerland: World Metrorological Organization. doi: 10.1017/CBO9781107415324.004.

Woyshner, M. R. and Yanful, E. K. (1995) 'Modelling and Field Measurements of Water Percolation Through an Experimental Soil Cover on Mine Tailings', *Canadian Geotechnical Journal*, 32(4), pp. 601–609.

Zettl, J. *et al.* (2011) 'Influence of Textural Layering on Field Capacity of Coarse Soils', *Canadian Journal of Soil Science*, 91(2), pp. 133–147. doi: 10.4141/cjss09117.

Zhan, G. *et al.* (2014) '11 Years of Evapotranspiration Cover Performance at the AA Leach Pad at Barrick Goldstrike Mines', *Mine Water and the Environment*, 33(3), pp. 195–205. doi: 10.1007/s10230-014-0268-6.

Zotarelli, L. *et al.* (2015) 'Step by Step Calculation of the Penman-Monteith Evapotranspiration (FAO-56 Method)', pp. 1–10.

APPENDIX A

Soil Monitoring Data

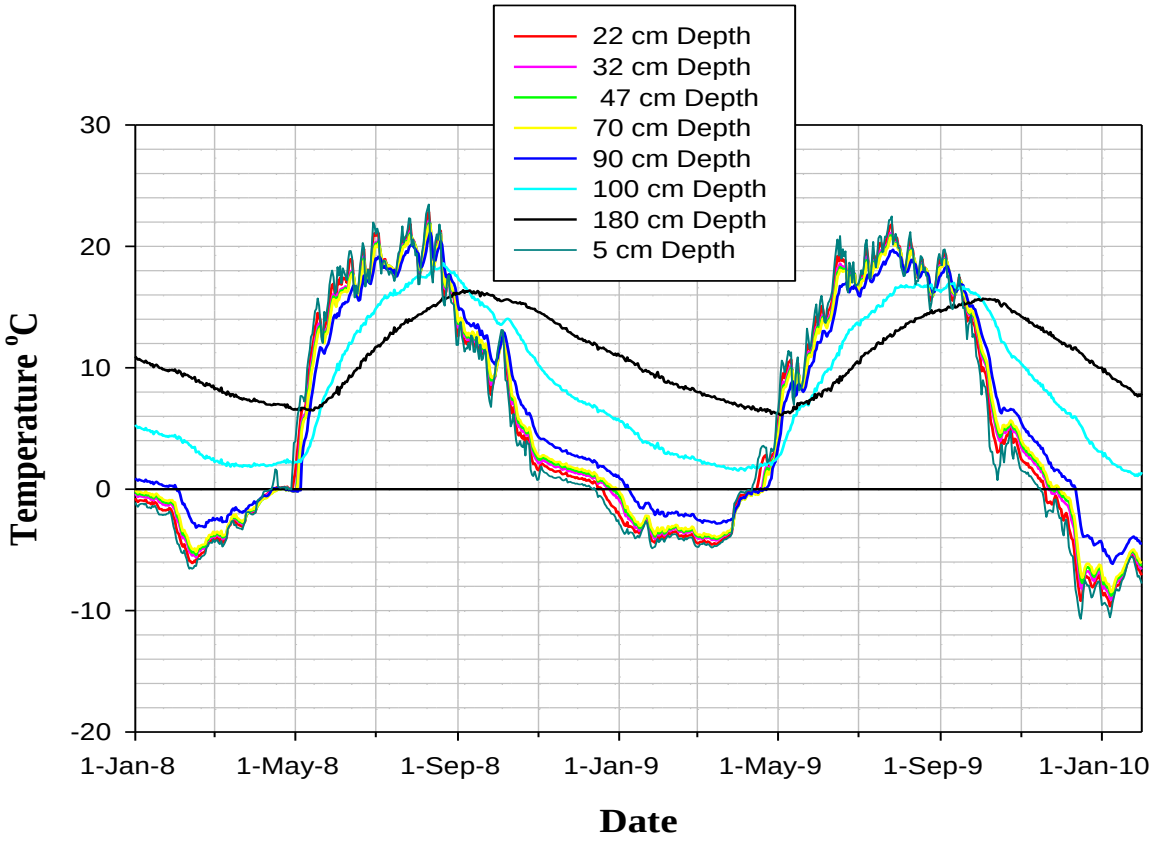

Figure A.1: Measured Soil Temperature of Soil Profile for the Shallow Cover (2008-2010)

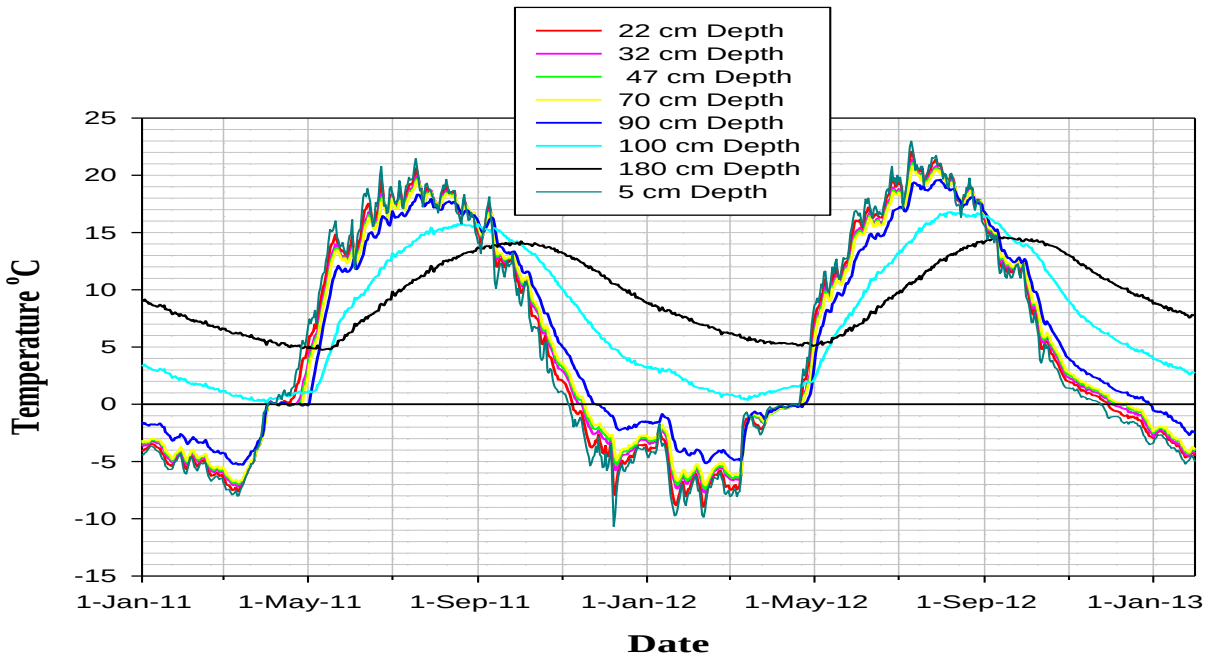

Figure A.2: Measured Soil Temperature of Soil Profile for the Shallow Cover (2011-2013)

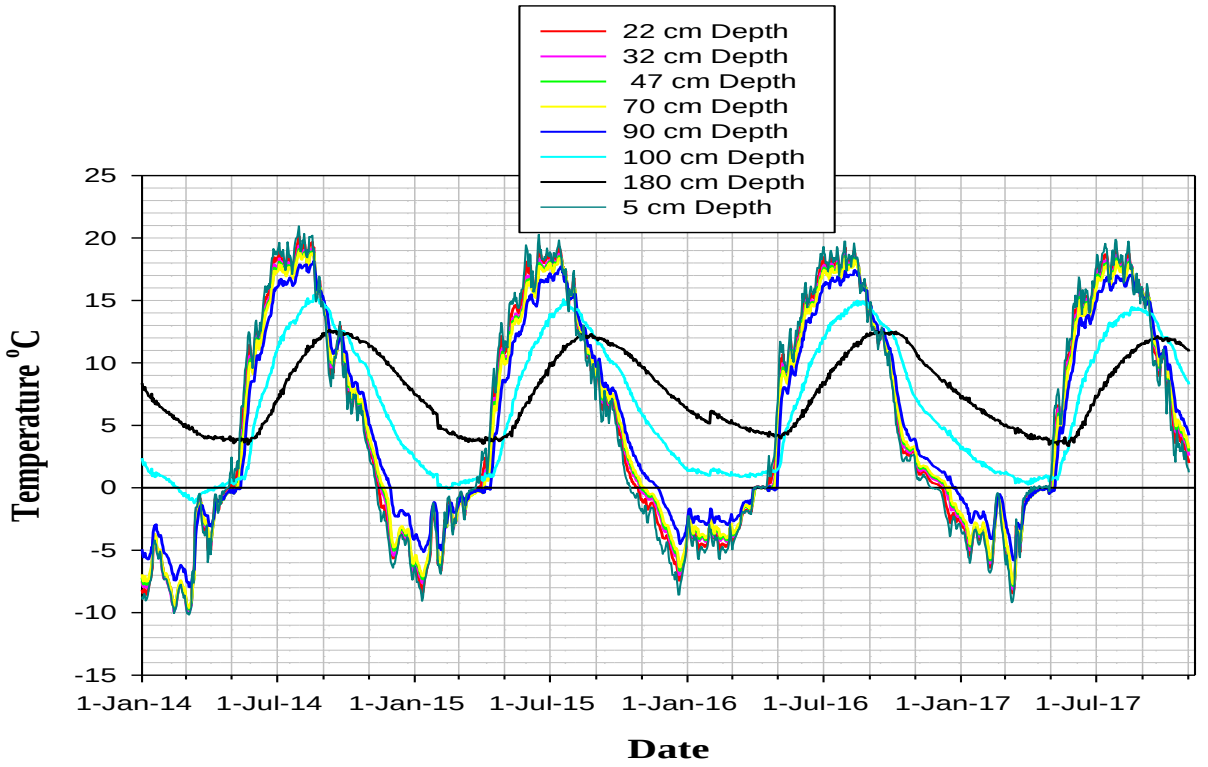

Figure A.3: Measured Soil Temperature of Soil Profile for the Shallow Cover (2014-2017)

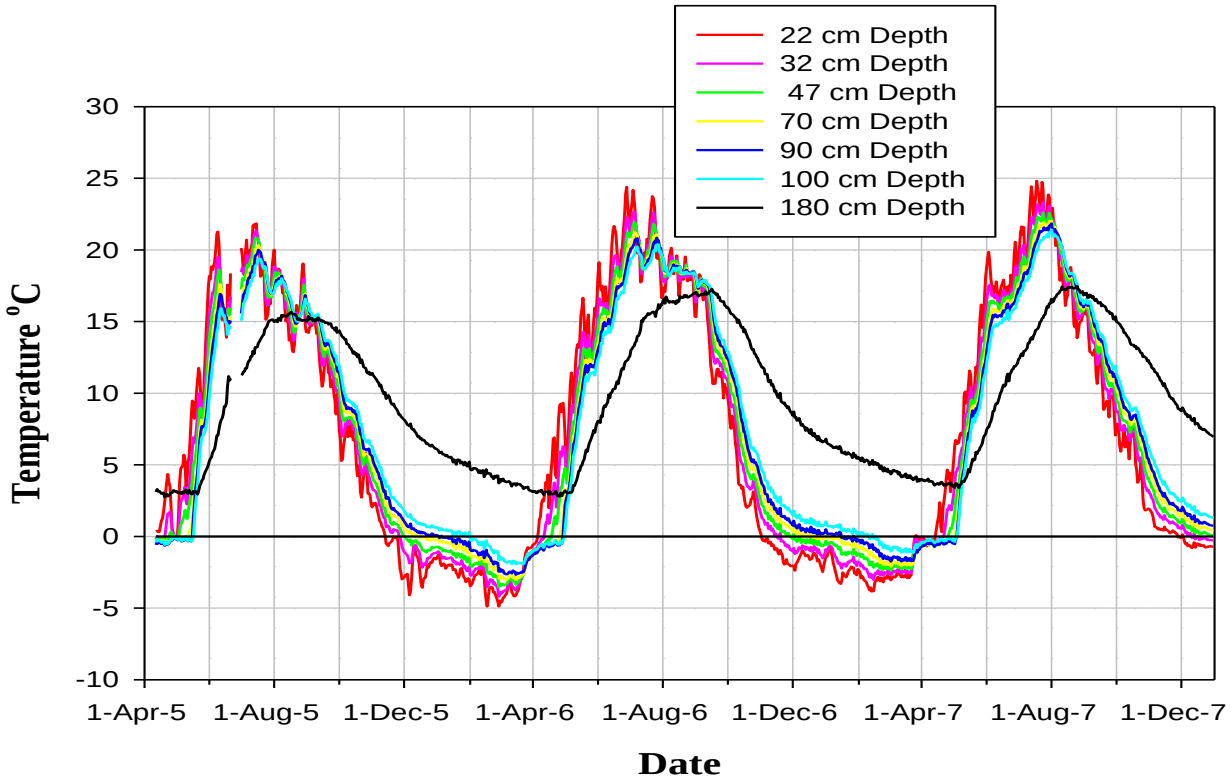

Figure A.4: Measured Soil Temperature of Soil Profile for the Deep Cover (2005-2007)

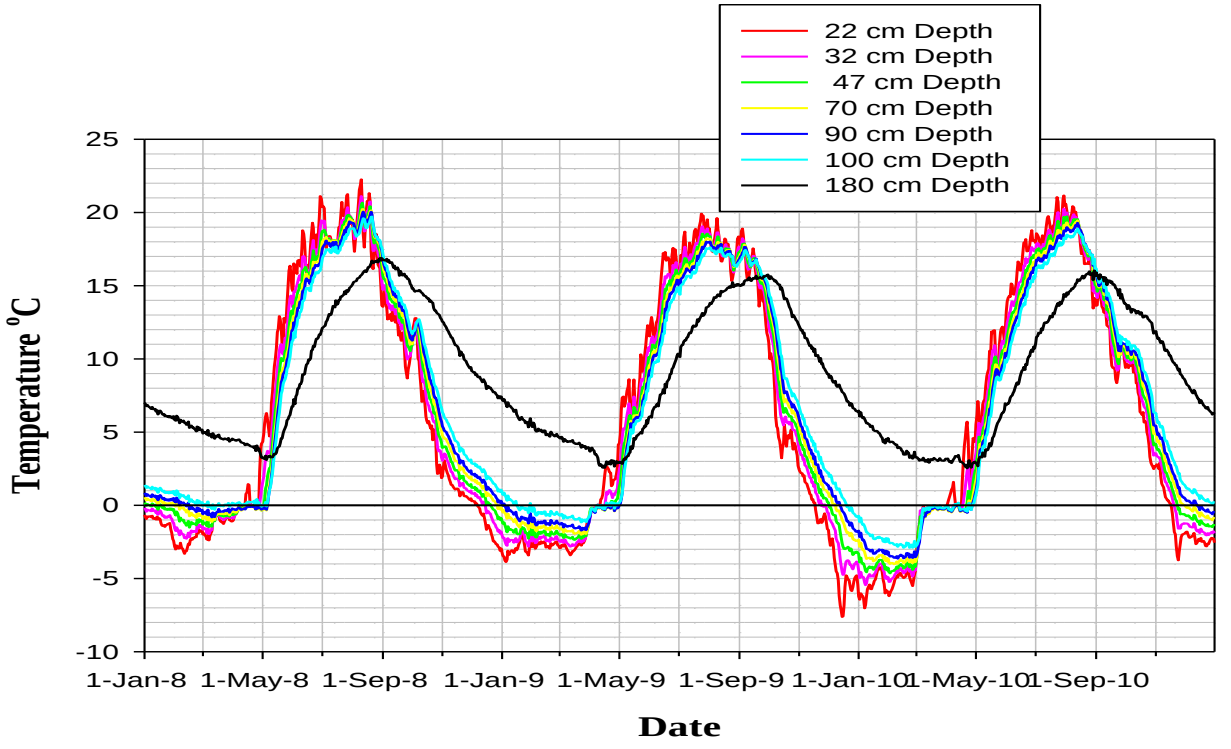

Figure A.5: Measured Soil Temperature of Soil Profile for the Deep Cover (2008-2010)

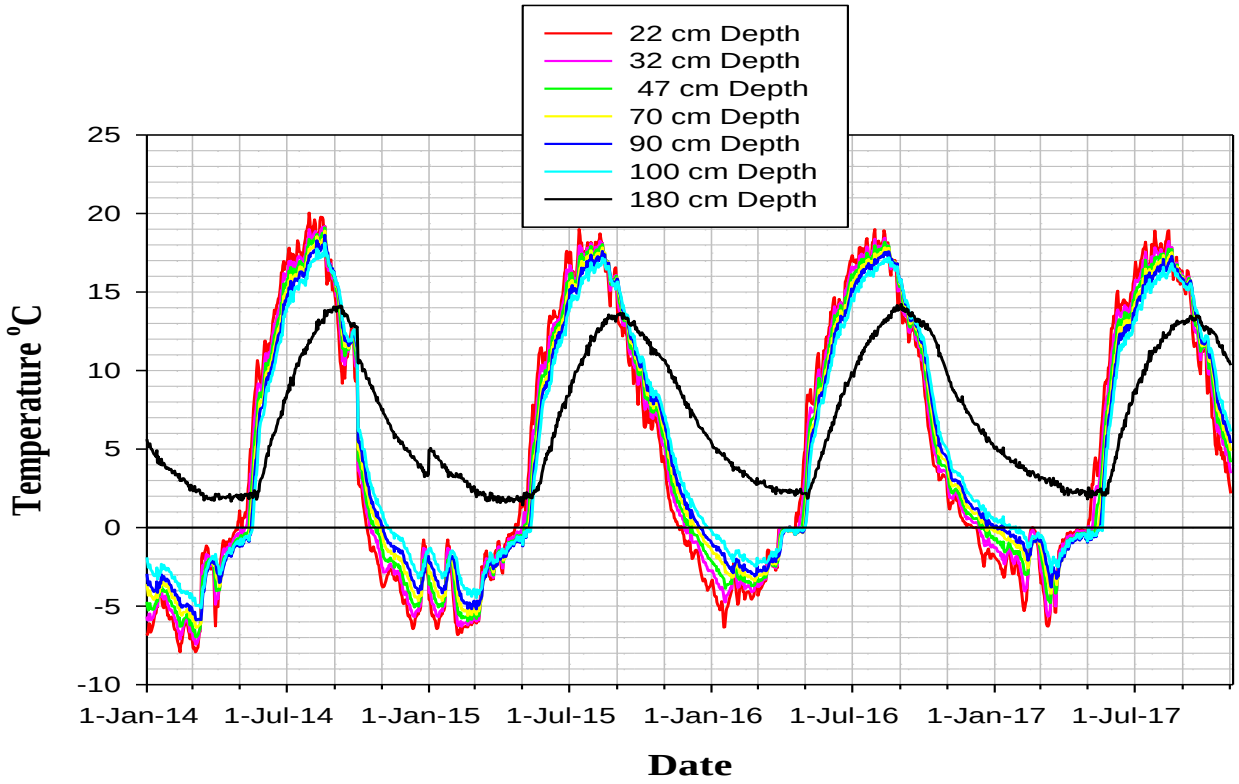

Figure A.6: Measured Soil Temperature of Soil Profile for the Deep Cover (2014-2017)

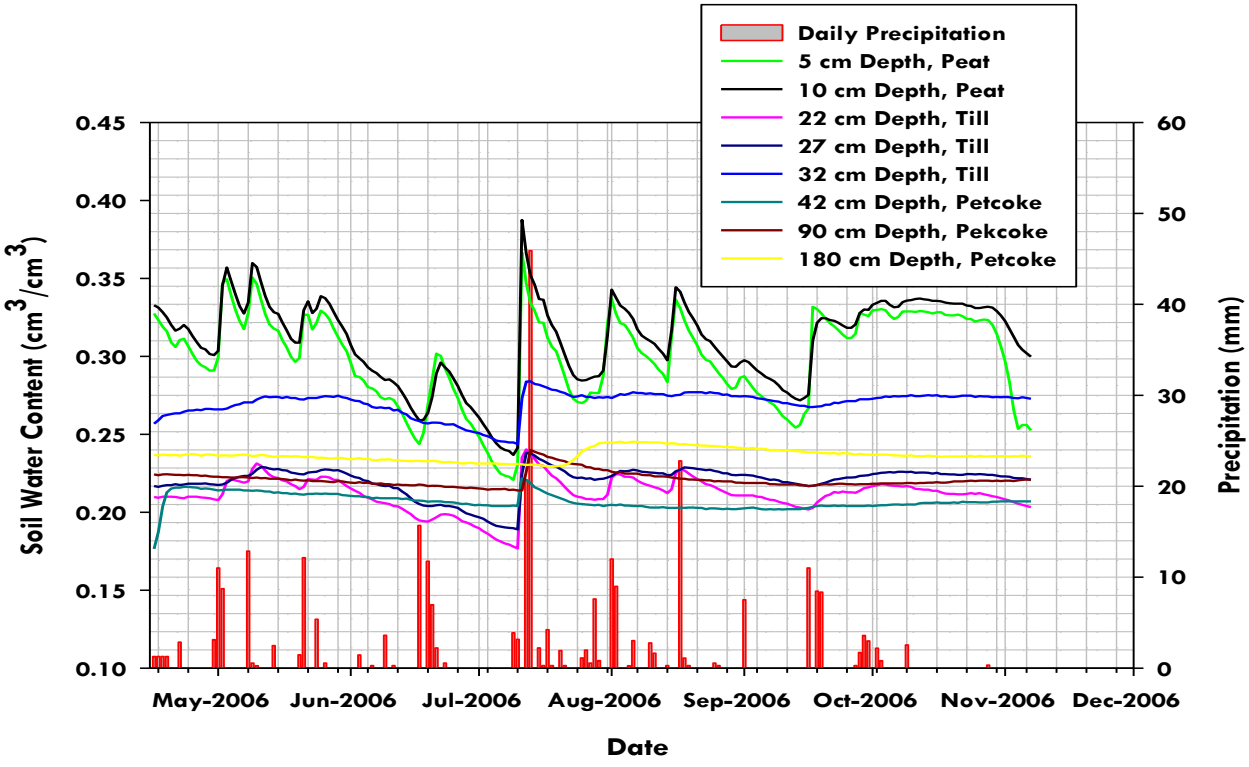

Figure A.7: Volumetric Soil Water Content with Precipitation for the Shallow Cover (2006)

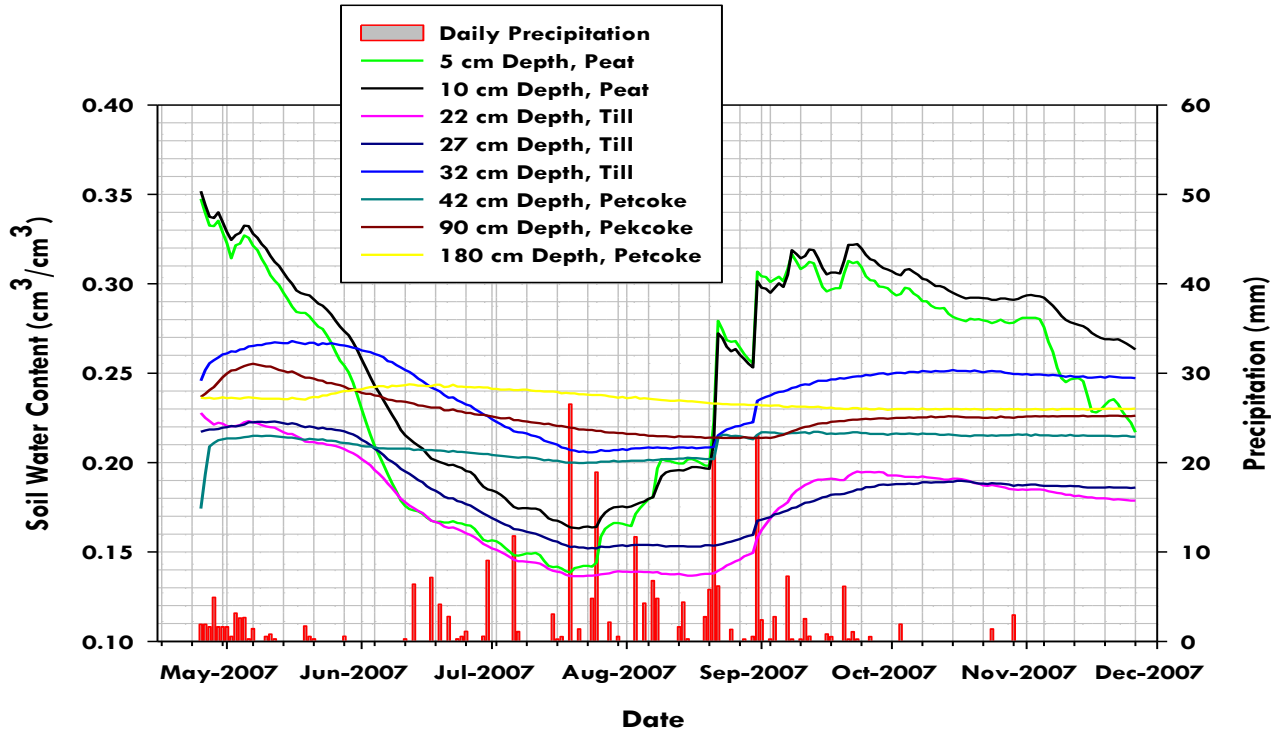

Figure A.8: Volumetric Soil Water Content with Precipitation for the Shallow Cover (2007)

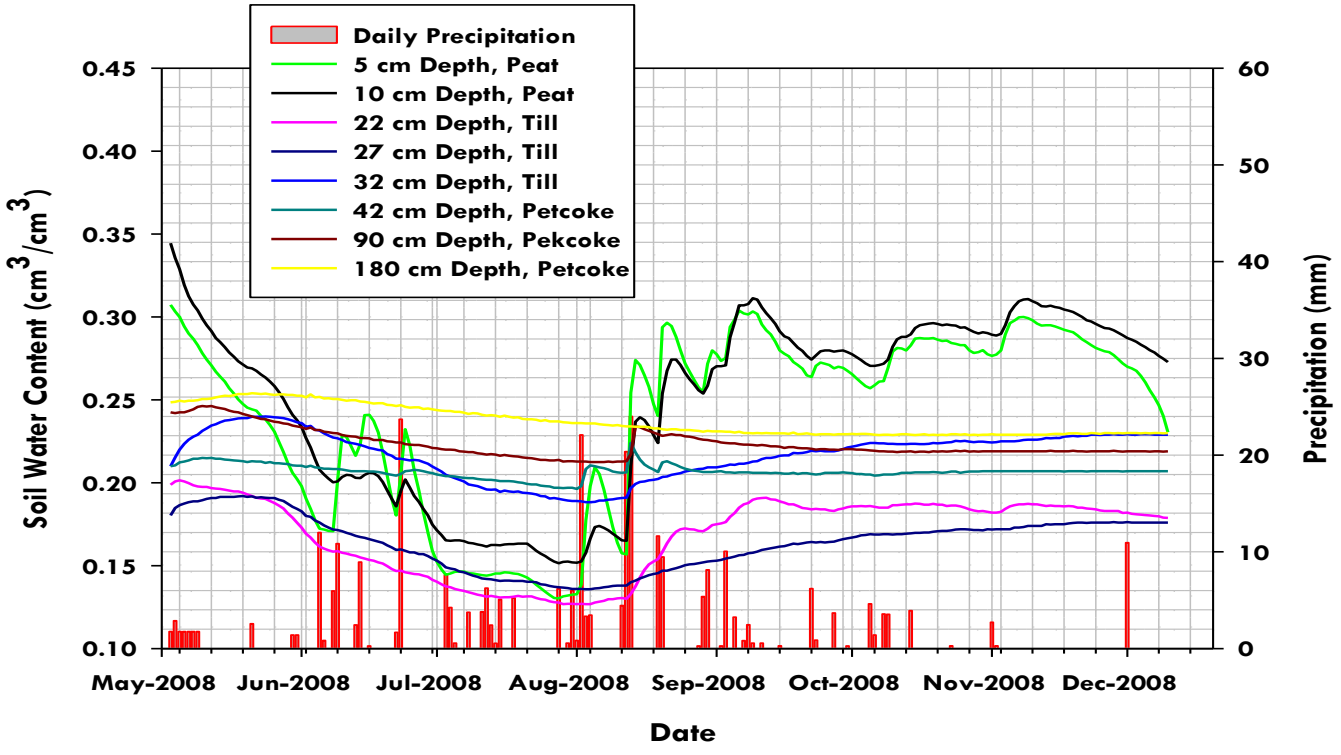

Figure A.9: Volumetric Soil Water Content with Precipitation for the Shallow Cover (2008)

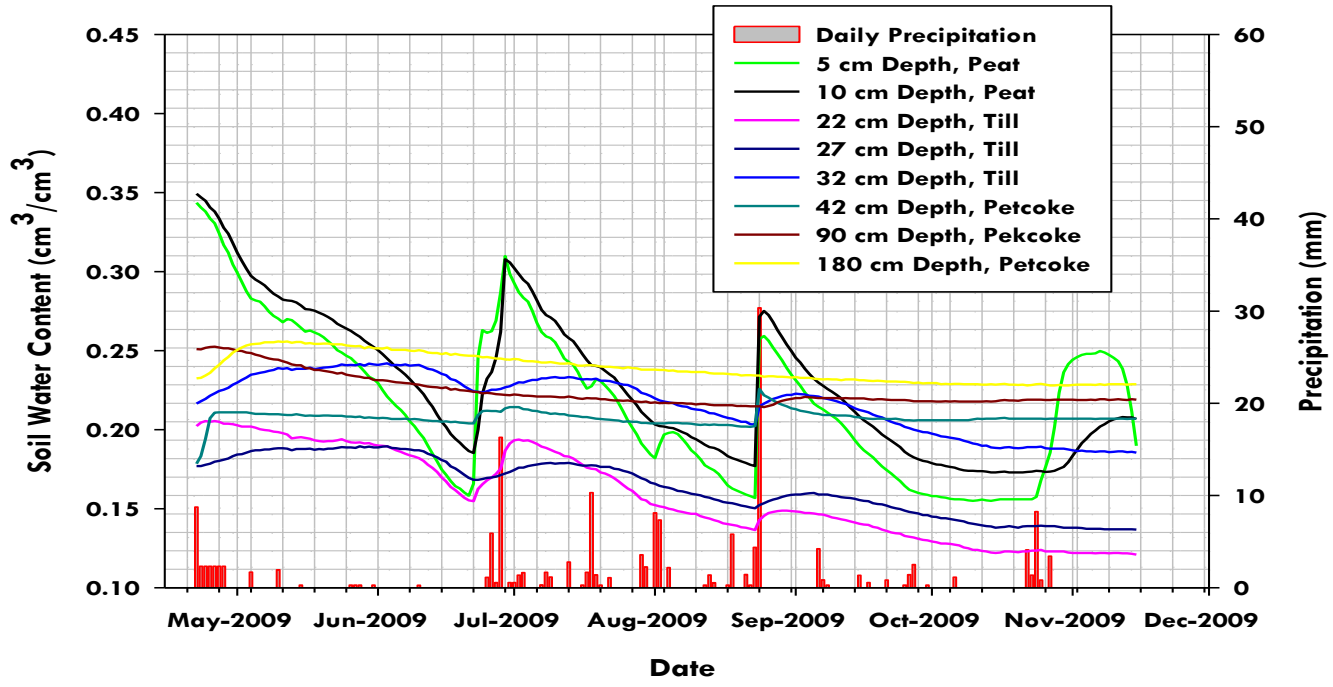

Figure A.10: Volumetric Soil Water Content with Precipitation for the Shallow Cover (2009)

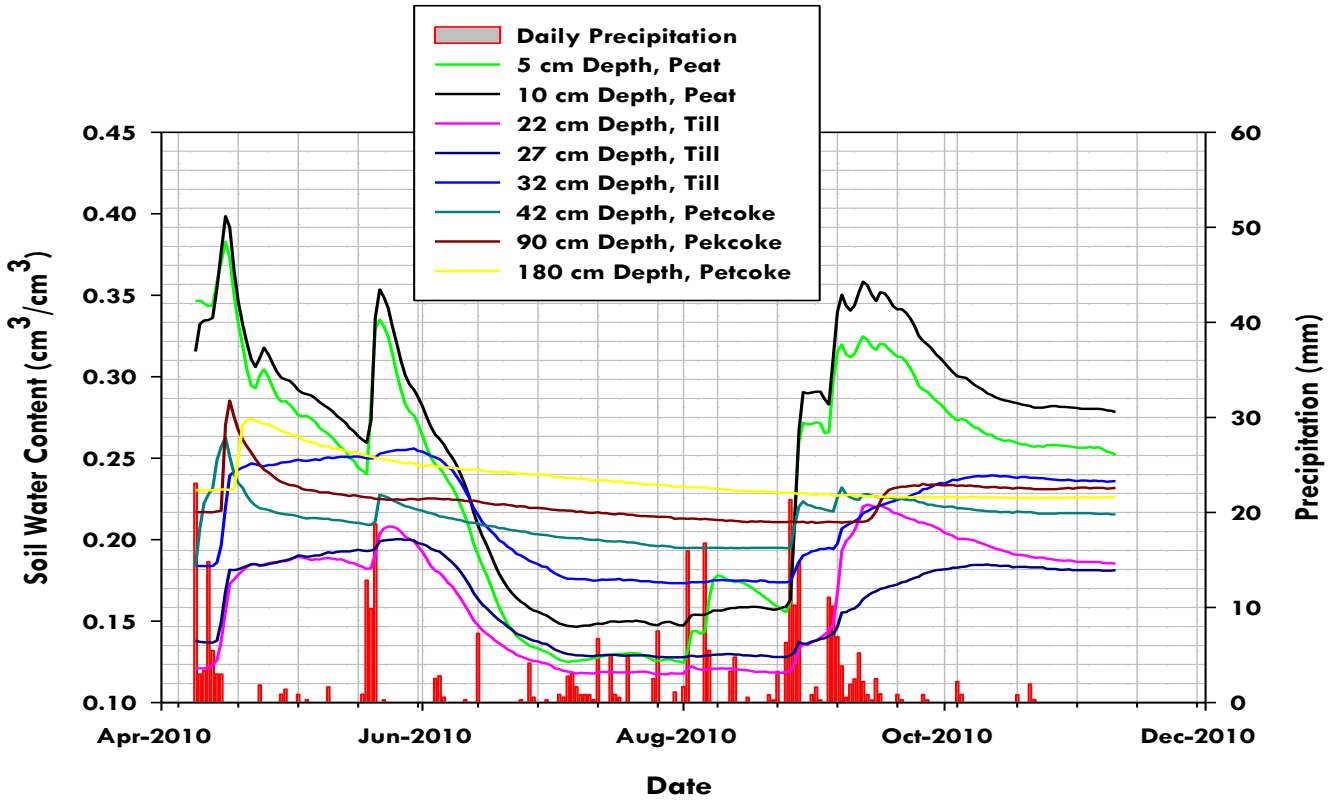

Figure A.11: Volumetric Soil Water Content with Precipitation for the Shallow Cover (2010)

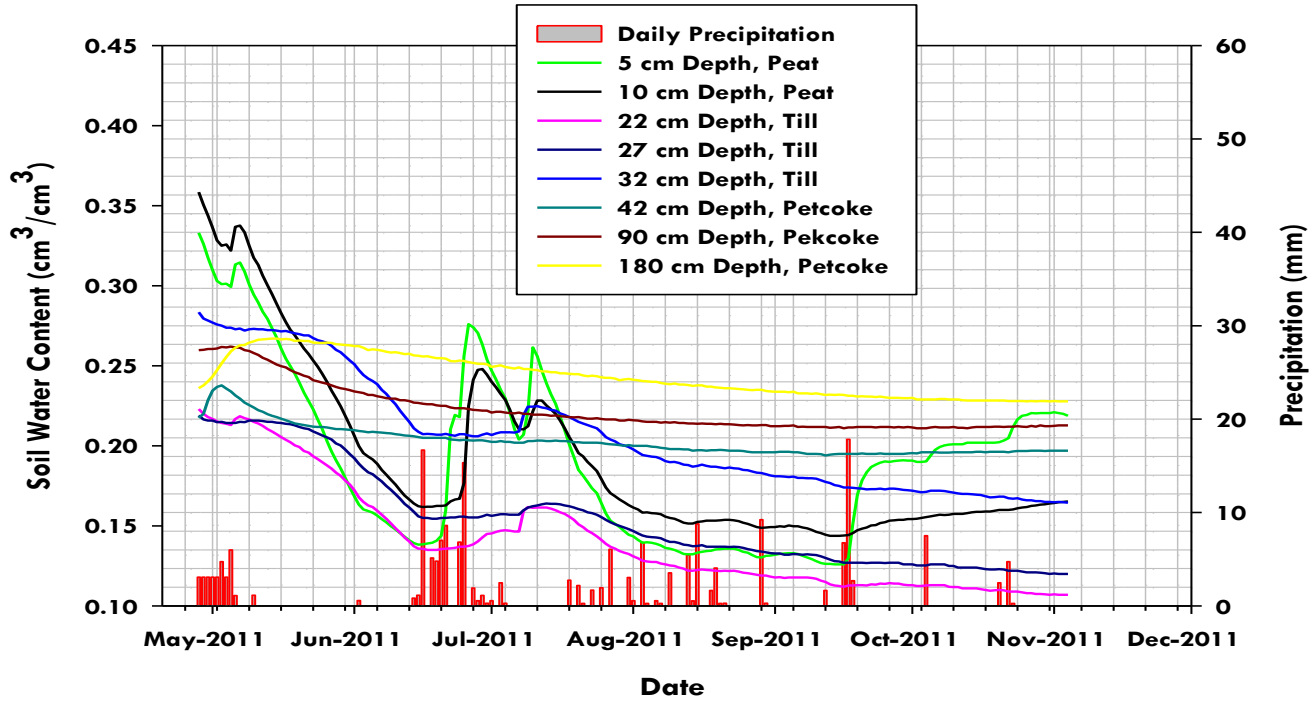

Figure A.12: Volumetric Soil Water Content with Precipitation for the Shallow Cover (2011)

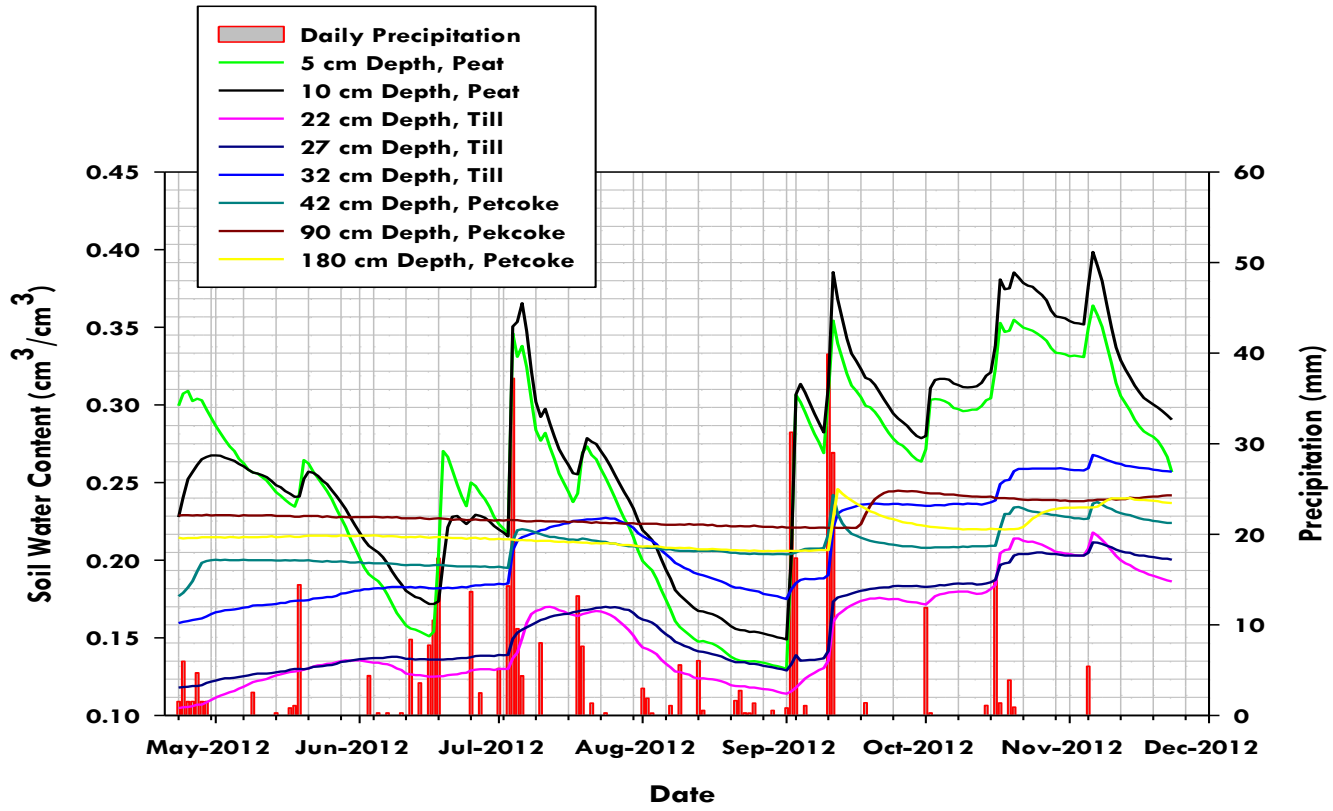

Figure A.13: Volumetric Soil Water Content with Precipitation for the Shallow Cover (2012)

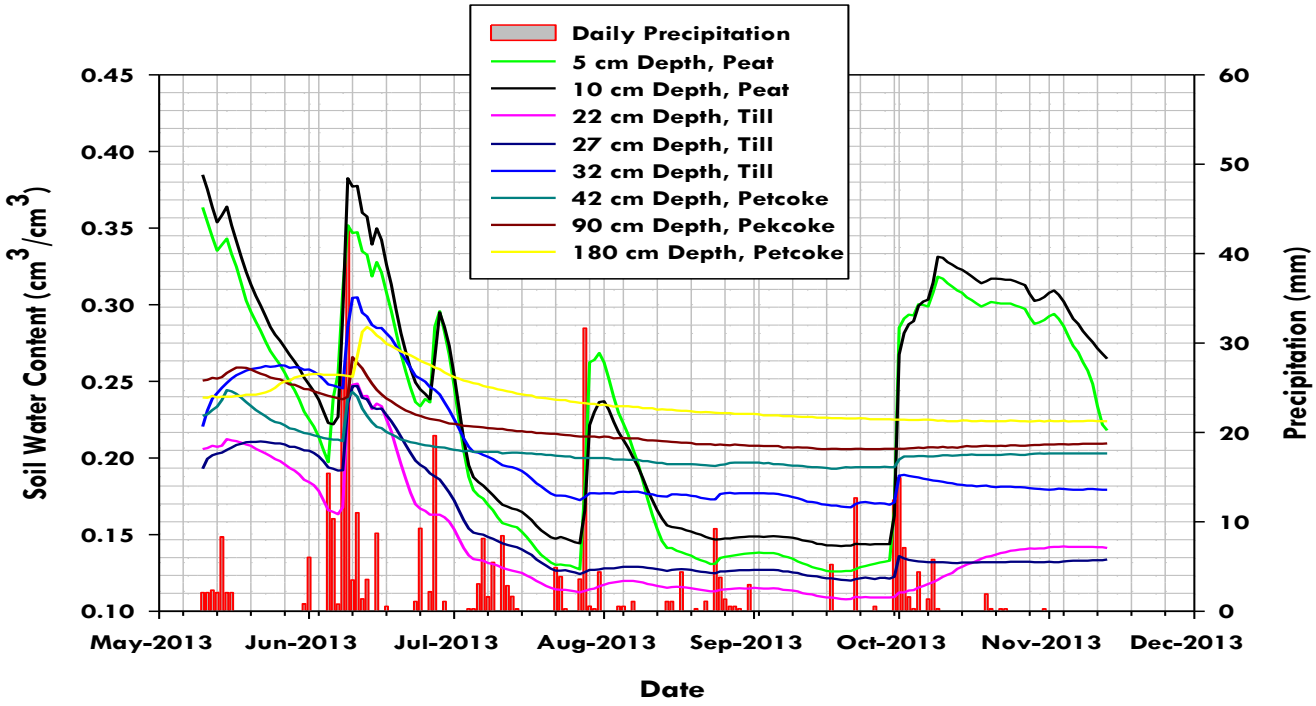

Figure A.14: Volumetric Soil Water Content with Precipitation for the Shallow Cover (2013)

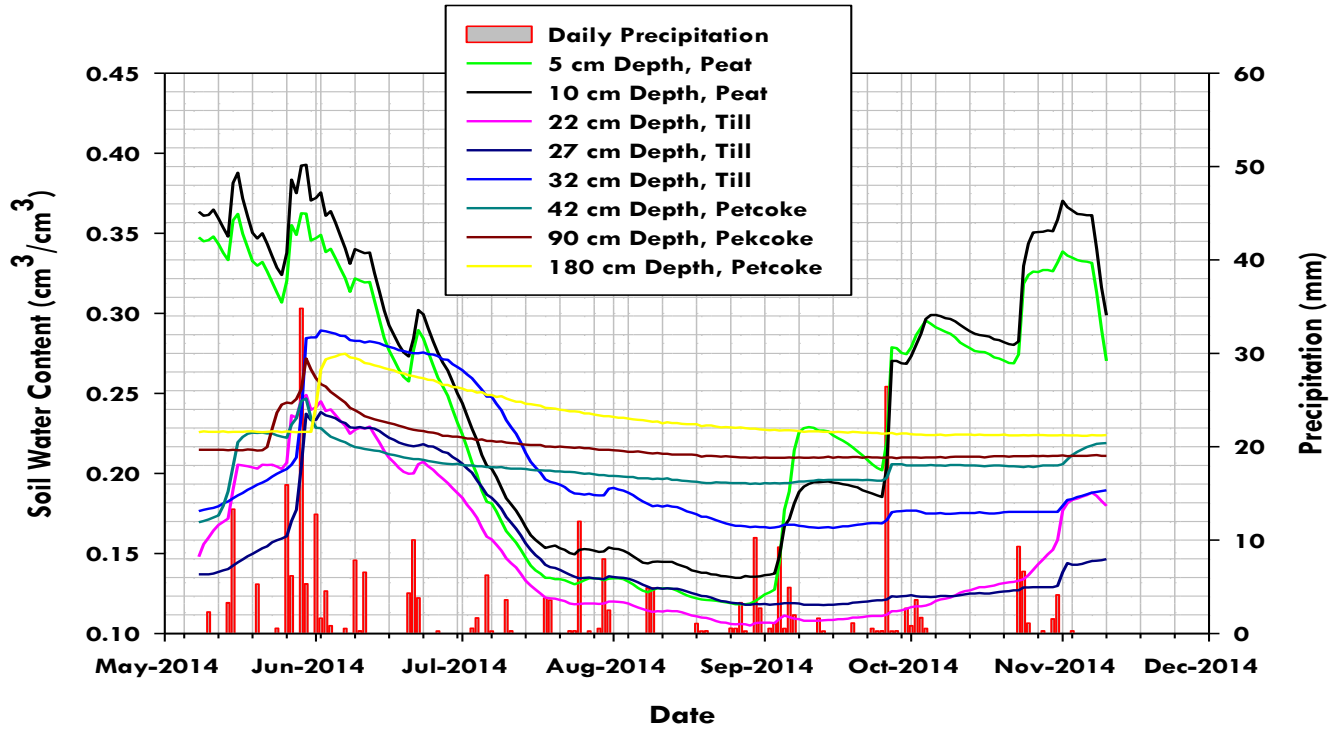

Figure A.15: Volumetric Soil Water Content with Precipitation for the Shallow Cover (2014)

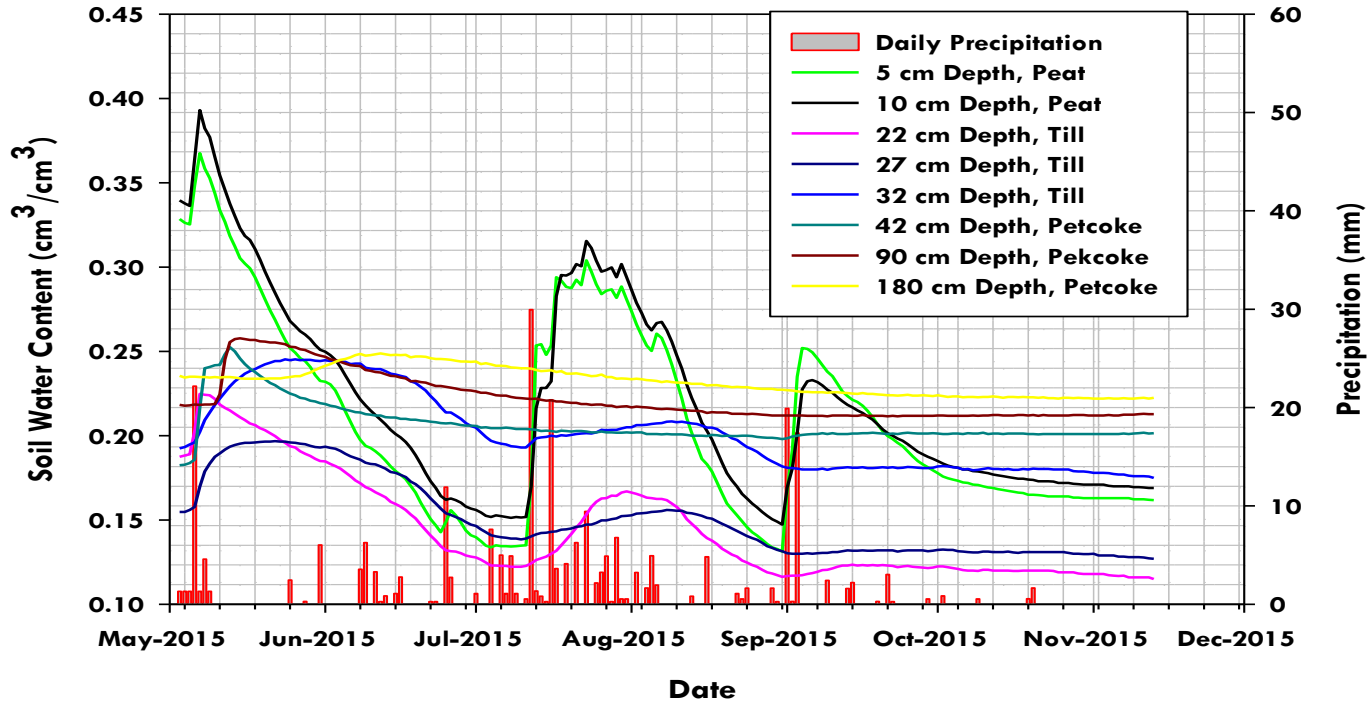

Figure A.16: Volumetric Soil Water Content with Precipitation for the Shallow Cover (2015)

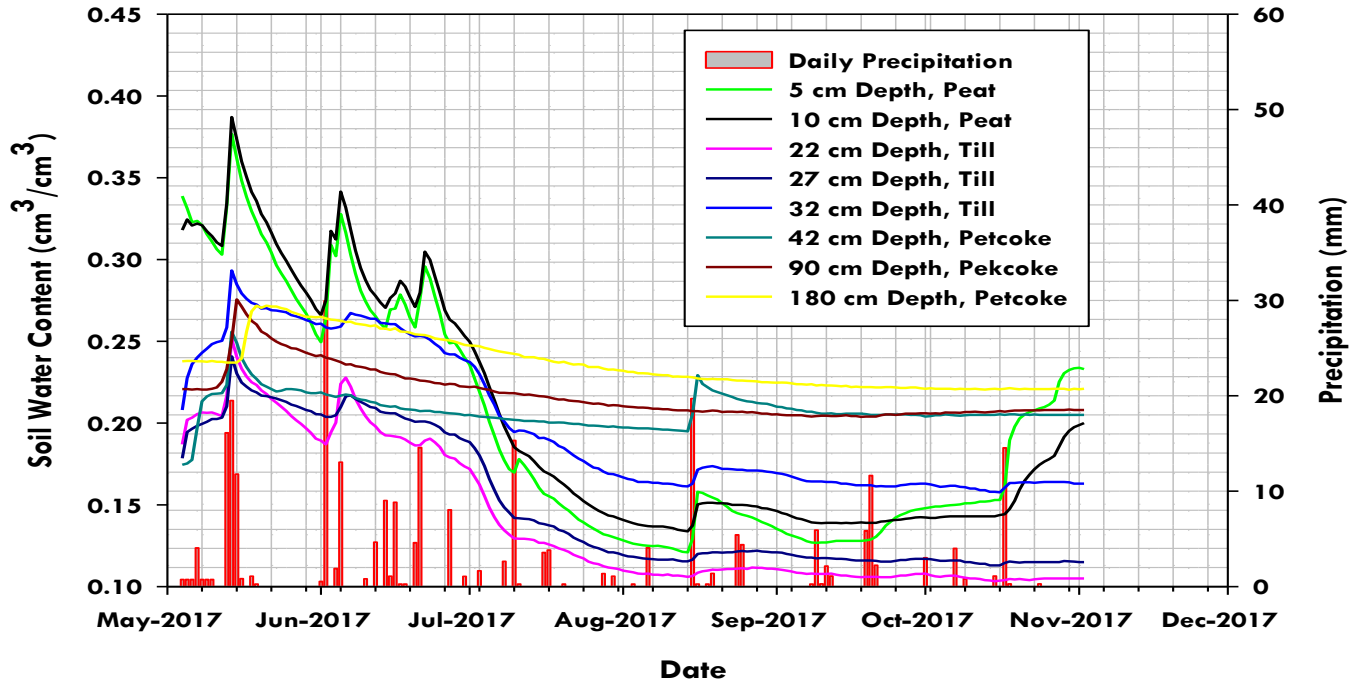

Figure A.17: Volumetric Soil Water Content with Precipitation for the Shallow Cover (2017)

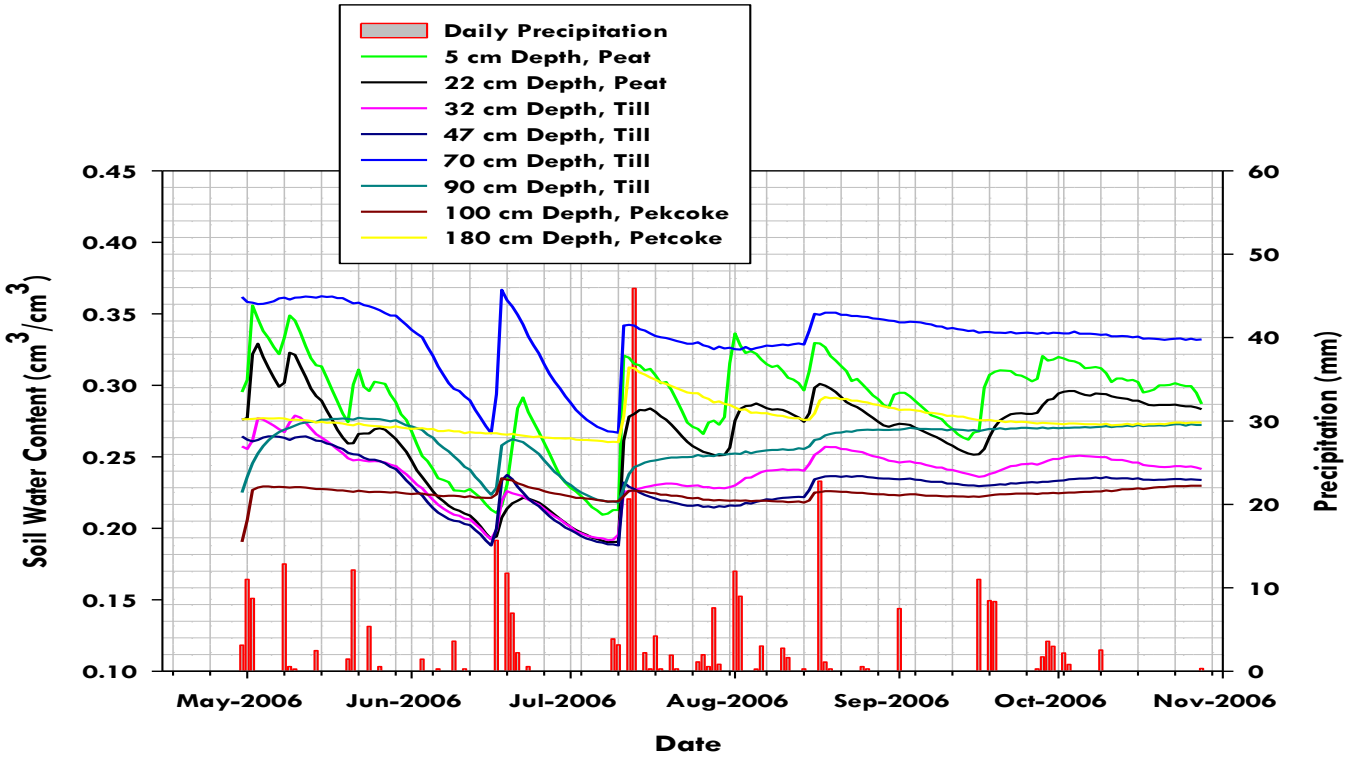

Figure A.18: Volumetric Soil Water Content with Precipitation for the Deep Cover (2006)

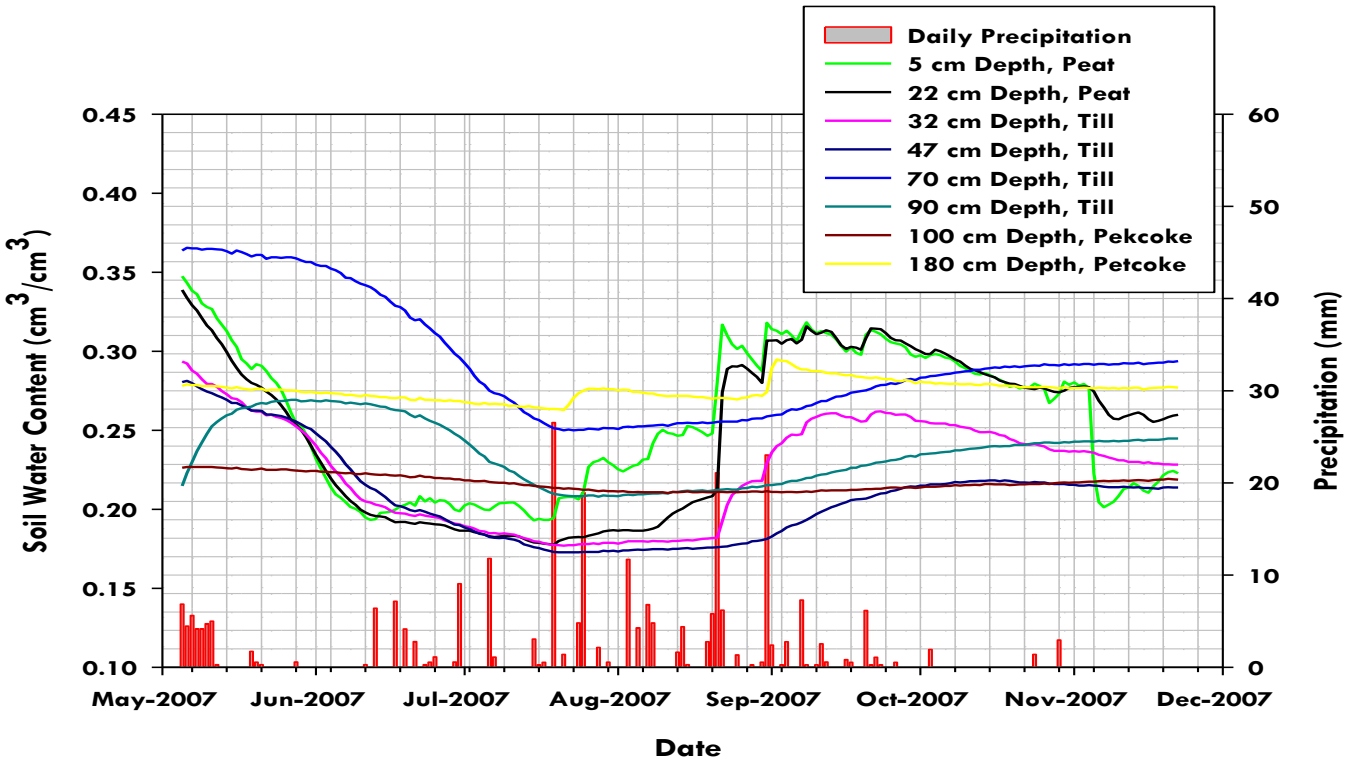

Figure A.19: Volumetric Soil Water Content with Precipitation for the Deep Cover (2007)

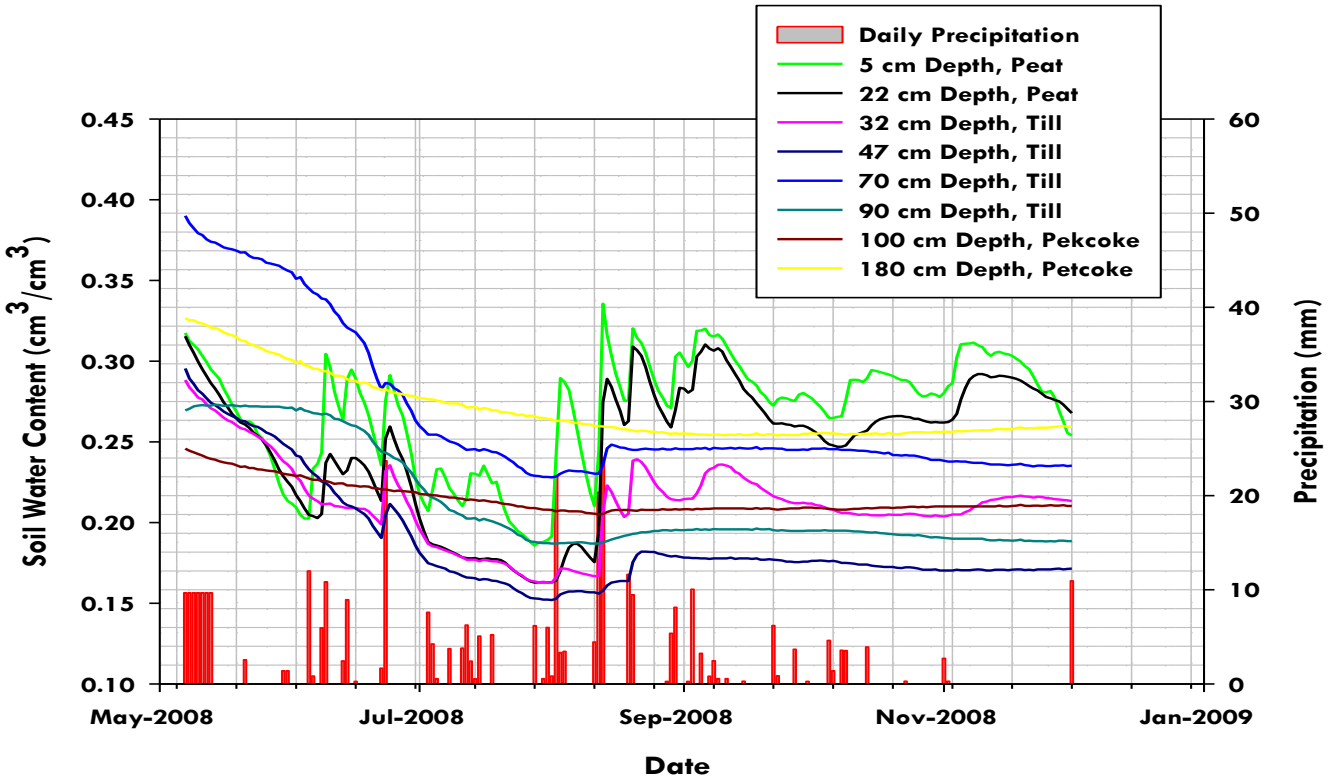

Figure A.20: Volumetric Soil Water Content with Precipitation for the Deep Cover (2008)

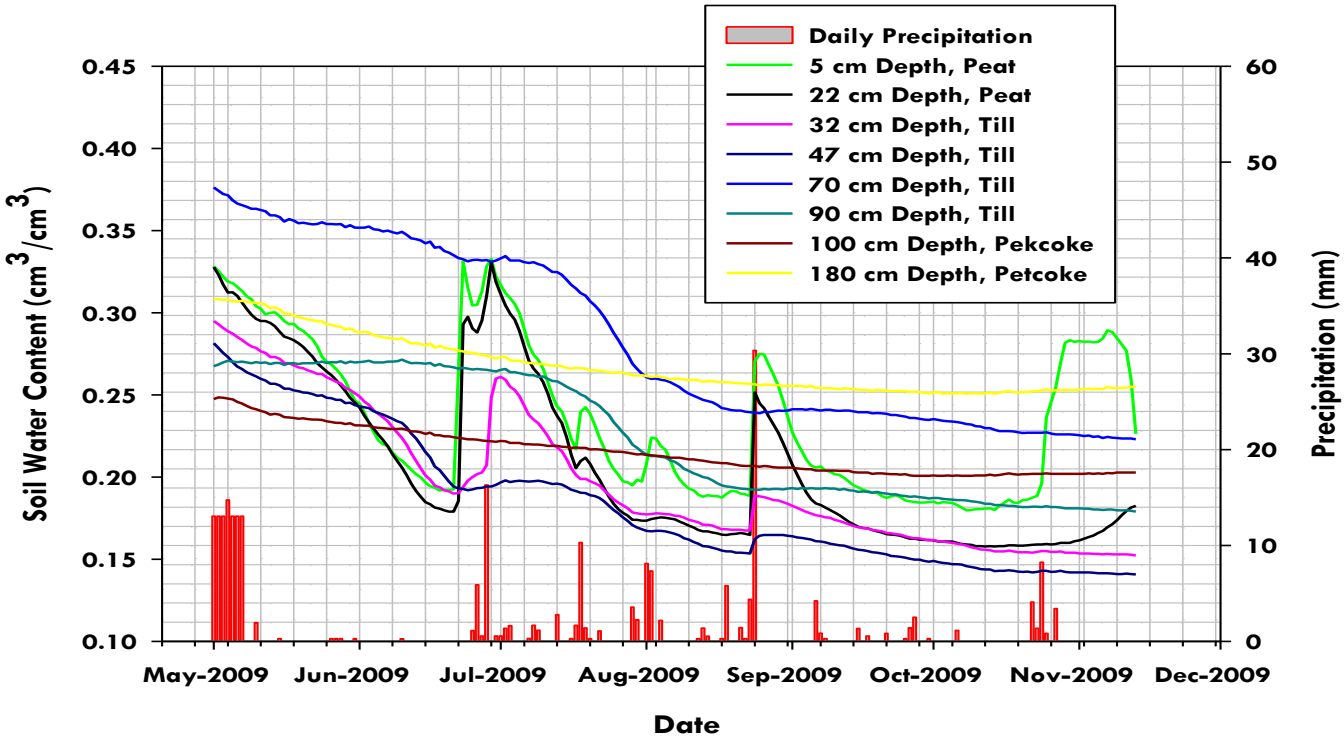

Figure A.21: Volumetric Soil Water Content with Precipitation for the Deep Cover (2009)

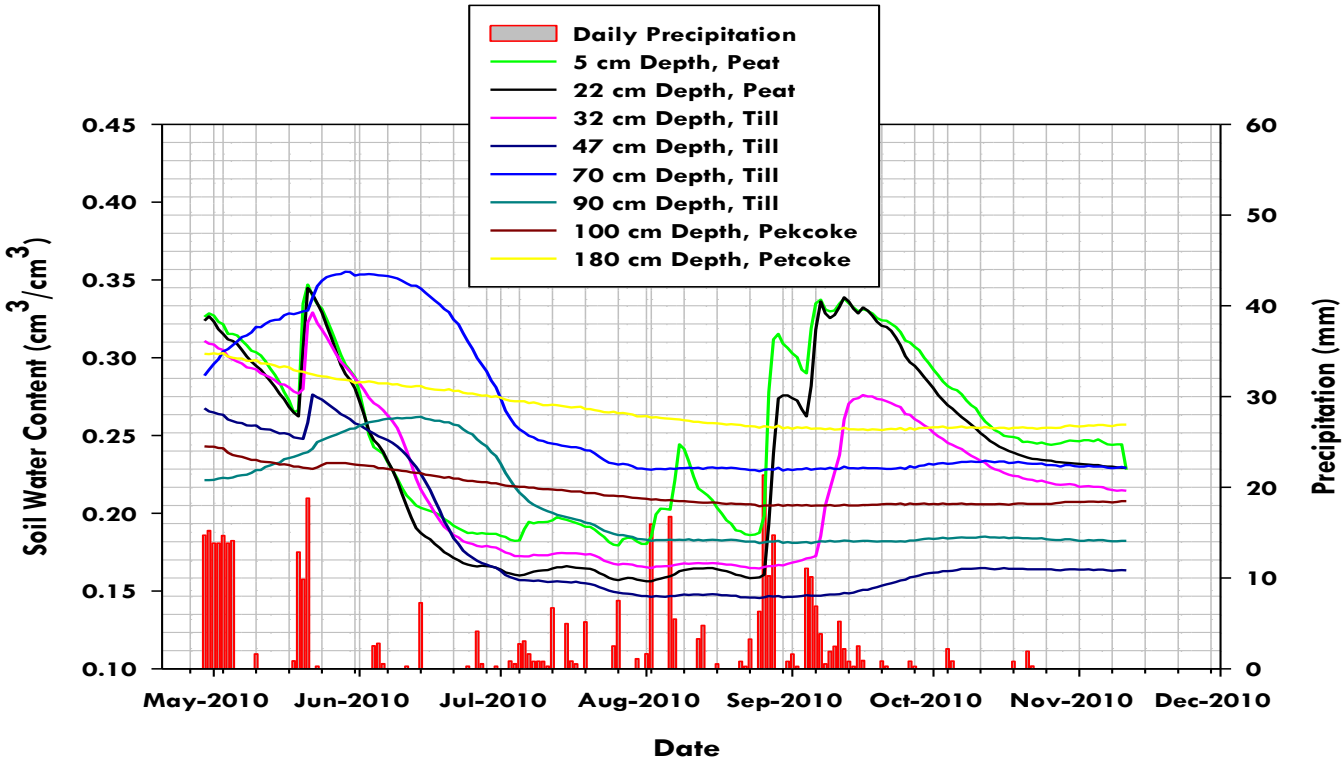

Figure A.22: Volumetric Soil Water Content with Precipitation for the Deep Cover (2010)

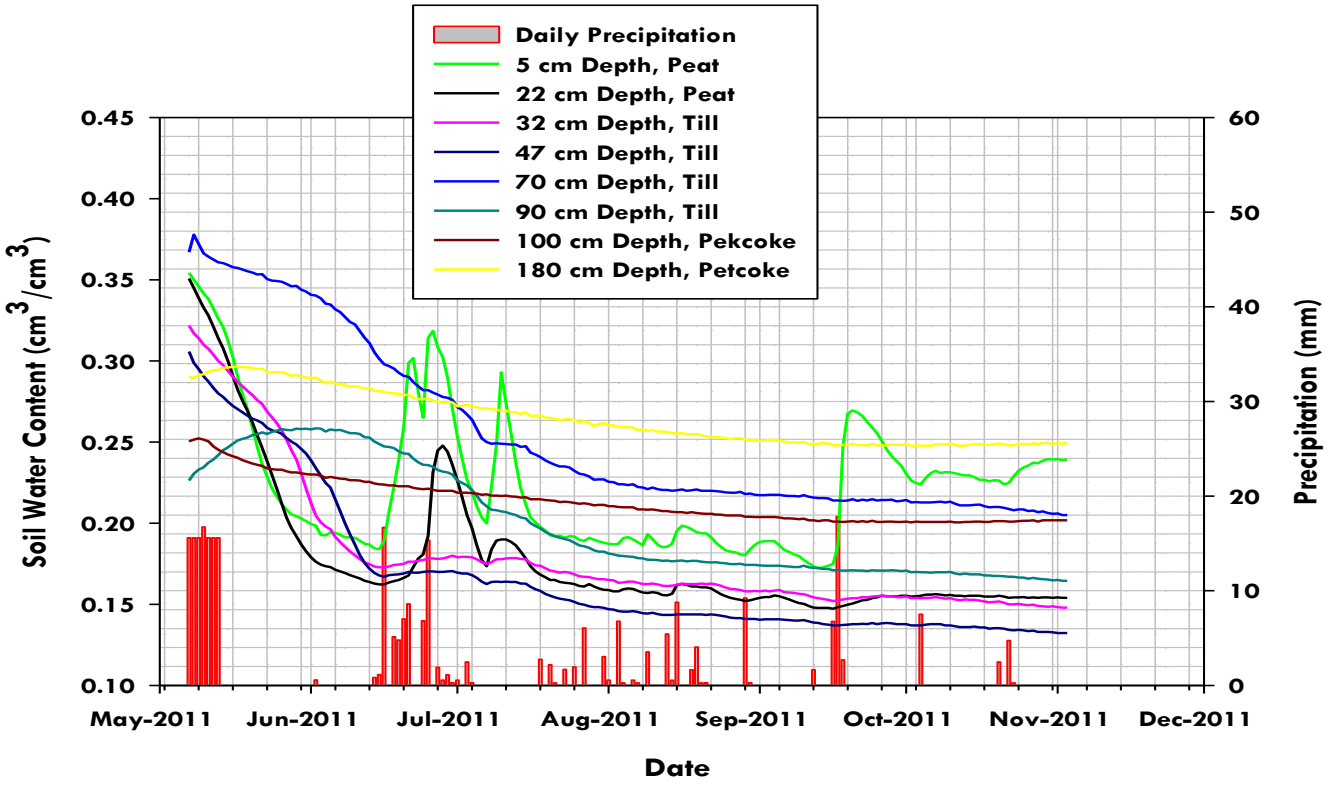

Figure A.23: Volumetric Soil Water Content with Precipitation for the Deep Cover (2011)

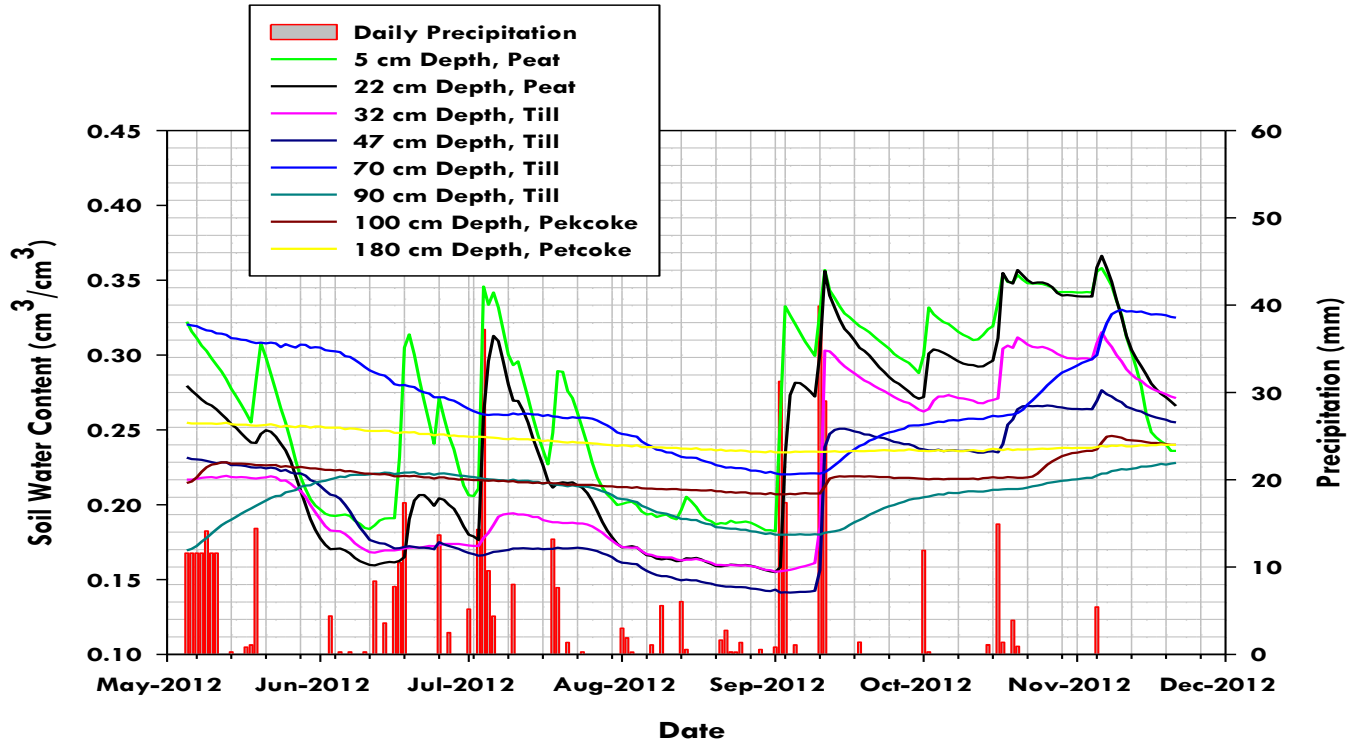

Figure A.24: Volumetric Soil Water Content with Precipitation for the Deep Cover (2012)

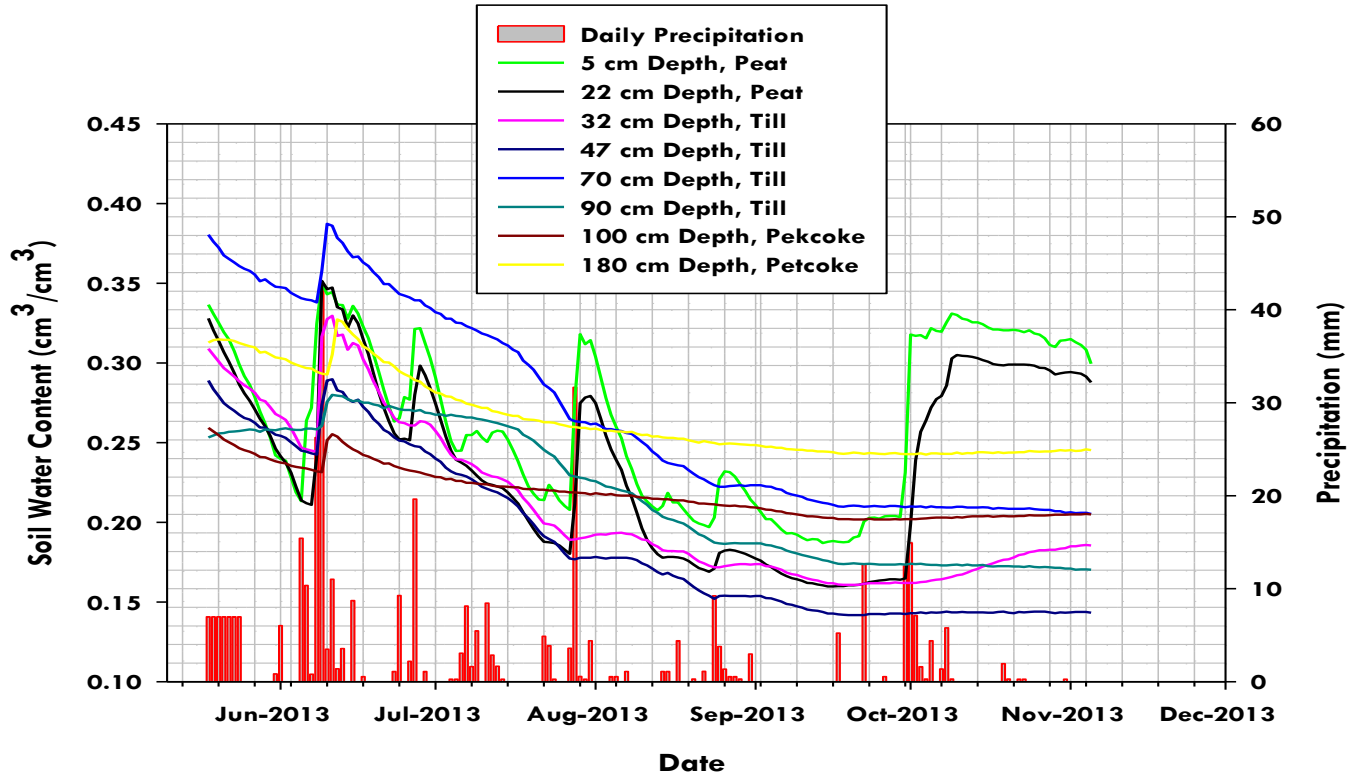

Figure A.25: Volumetric Soil Water Content with Precipitation for the Deep Cover (2013)

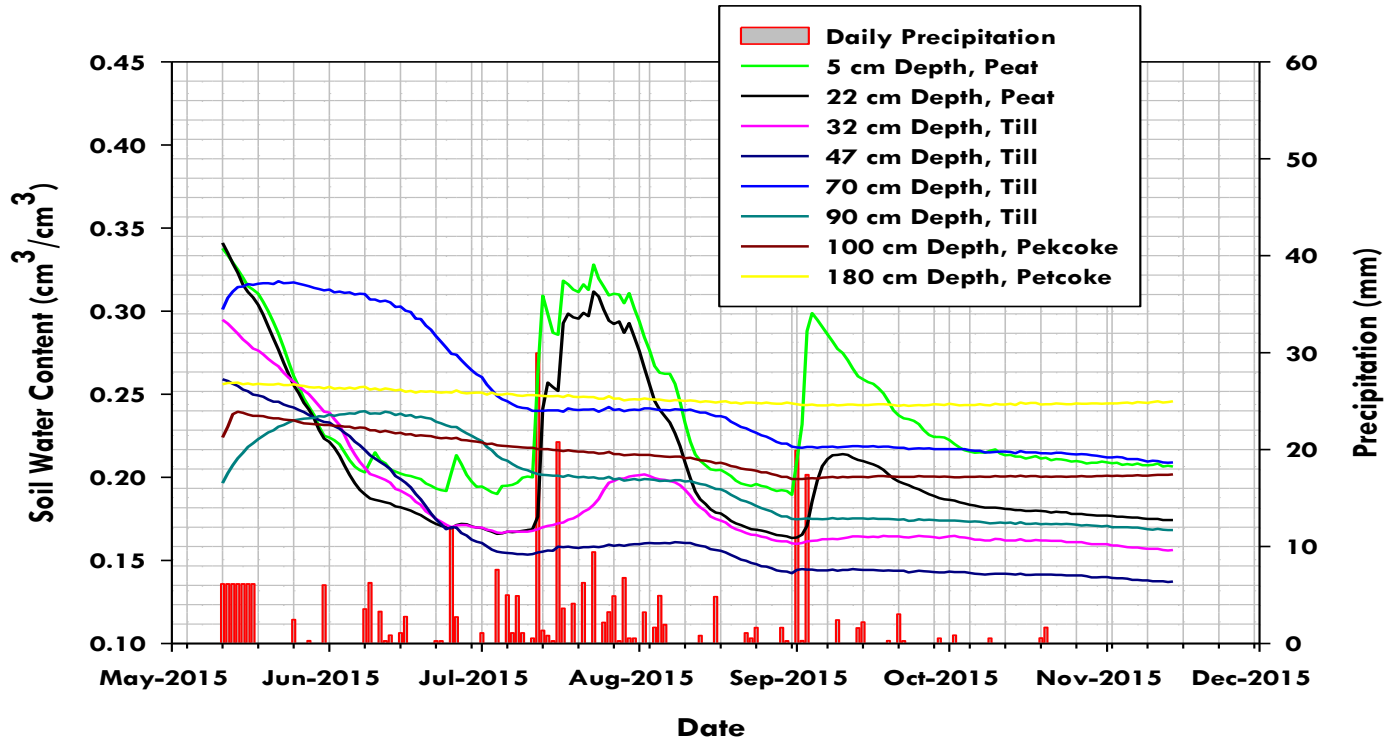

Figure A.26: Volumetric Soil Water Content with Precipitation for the Deep Cover (2015)

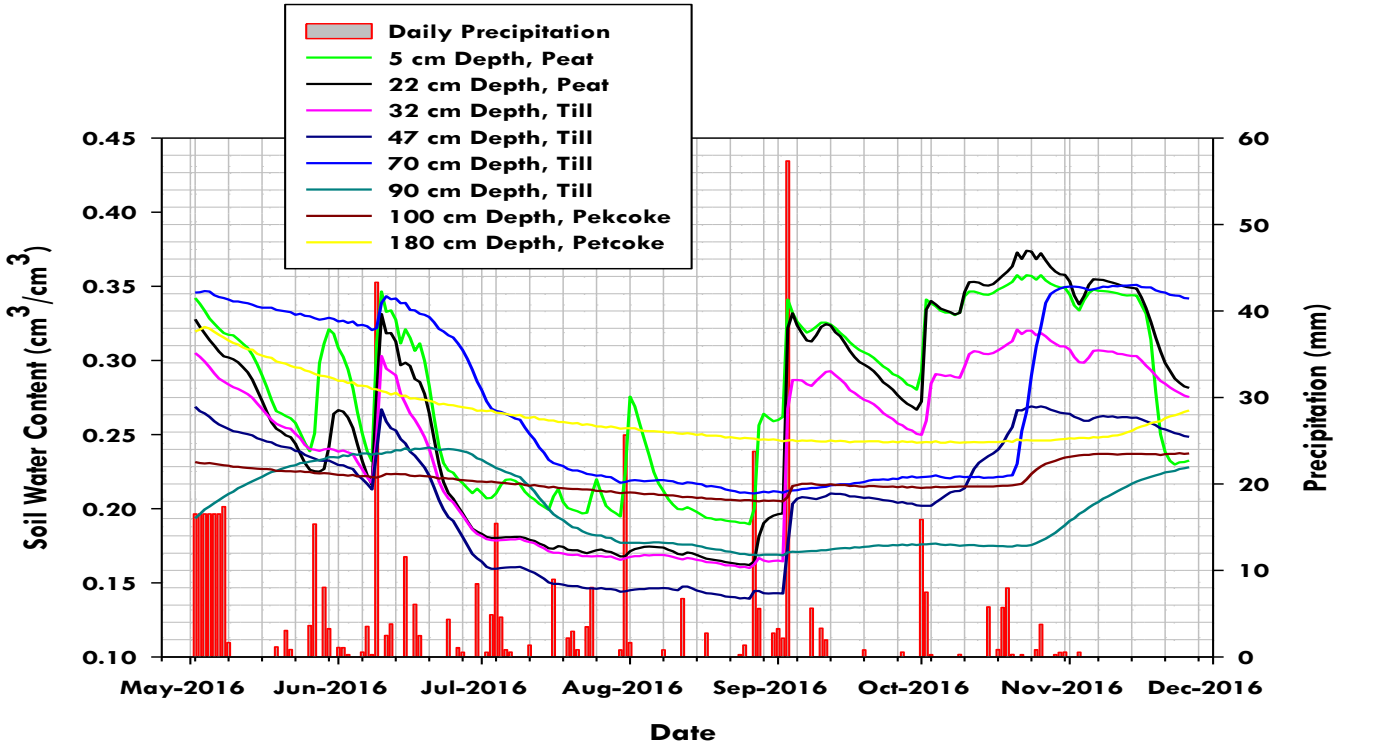

Figure A.27: Volumetric Soil Water Content with Precipitation for the Deep Cover (2016)

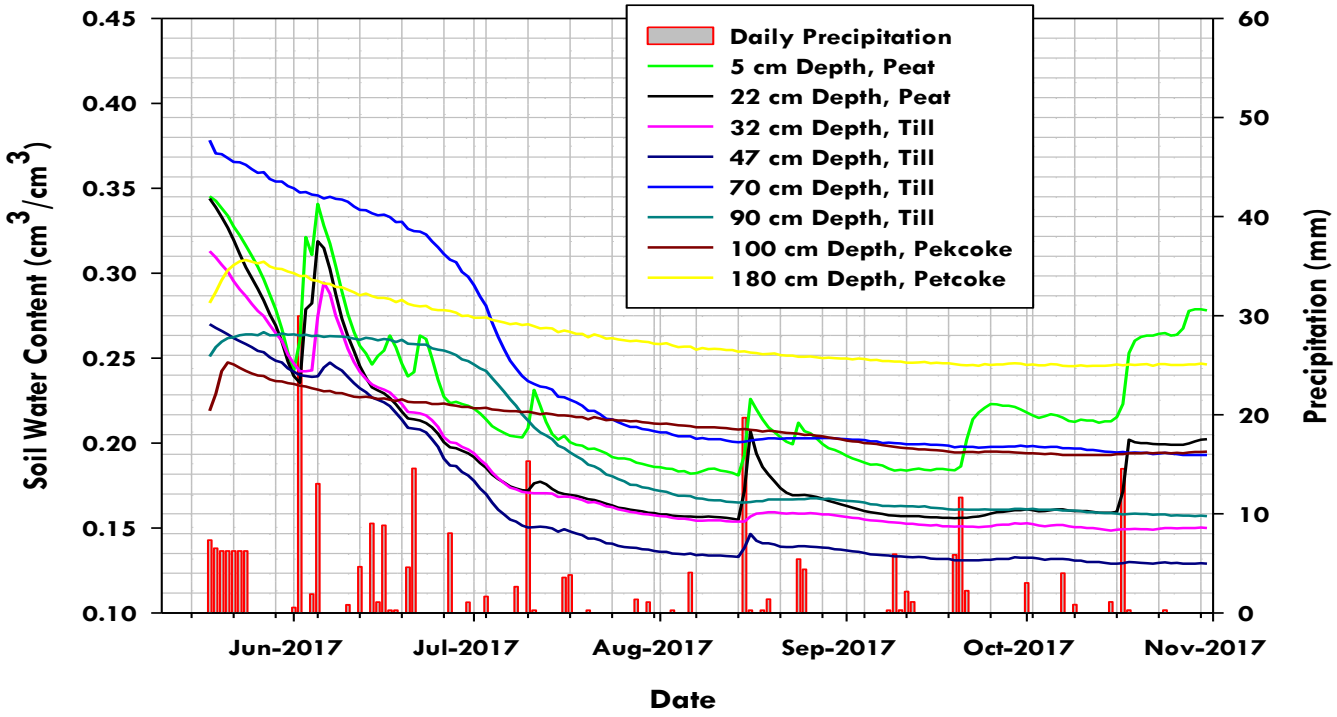

Figure A.28: Volumetric Soil Water Content with Precipitation for the Deep Cover (2017)

APPENDIX B

System Dynamics and Simulated Water Balance Component for the Shallow and the Deep Covers

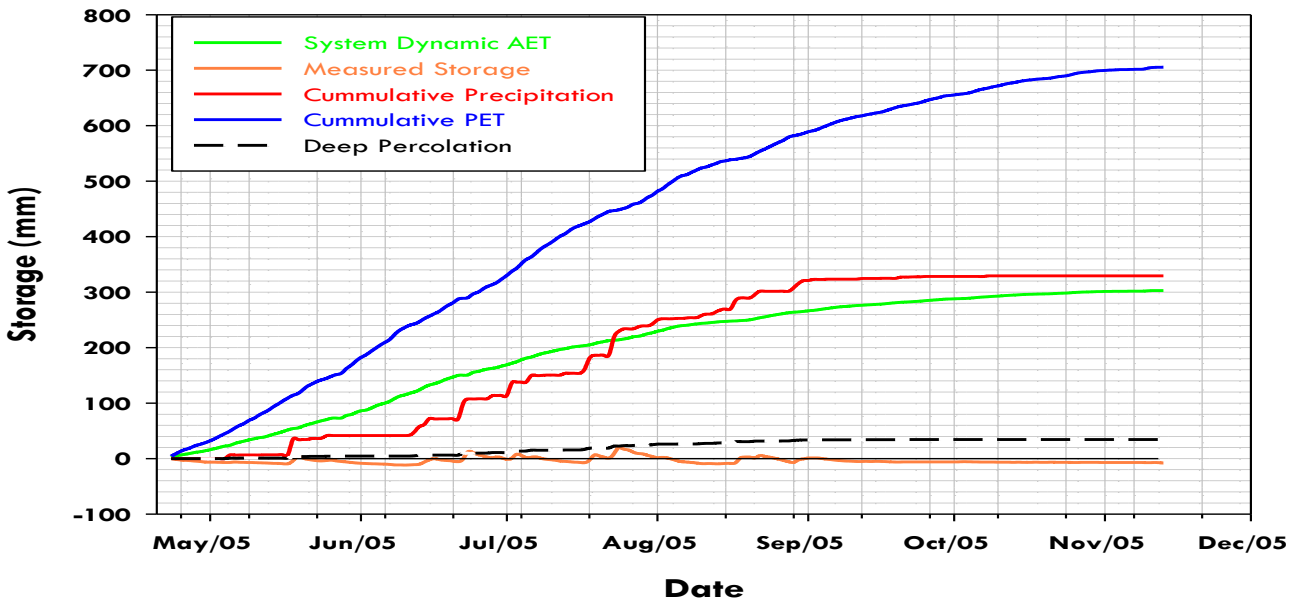

Figure B.1: System Dynamic Water balance for Shallow Cover System for 2005

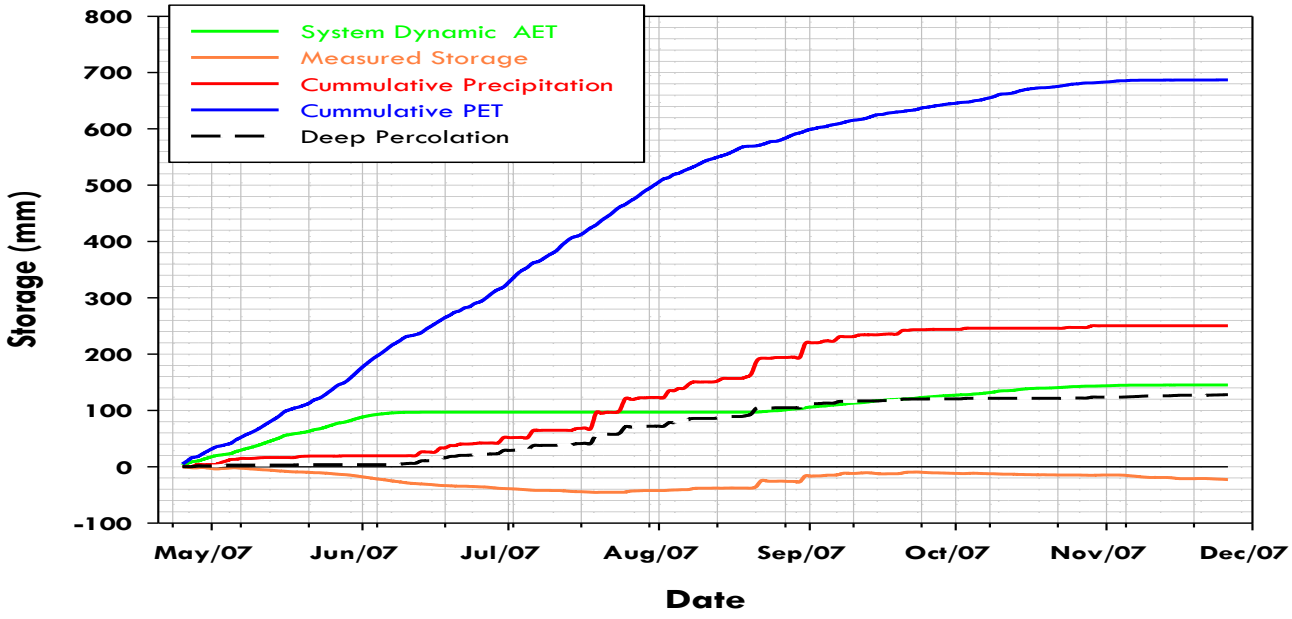

Figure B.2: System Dynamic Water balance for Shallow Cover System for 2007

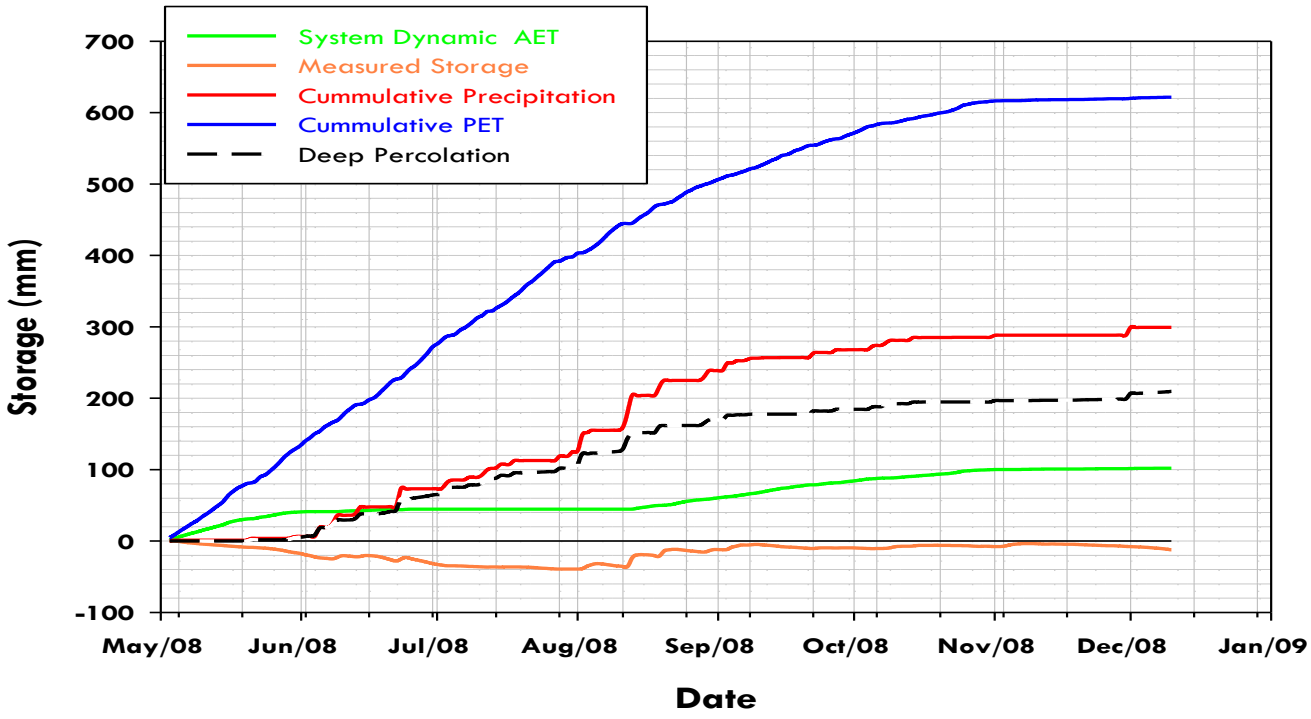

Figure B.3: System Dynamic Water balance for Shallow Cover System for 2008

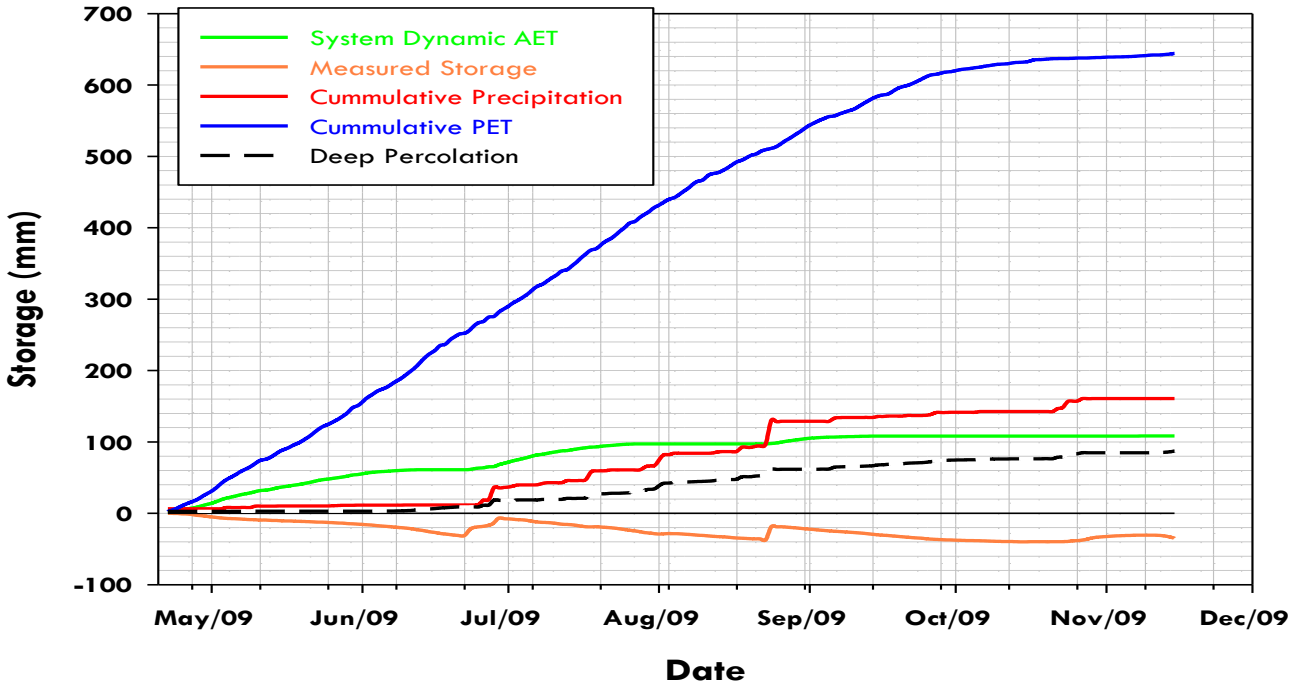

Figure B.4: System Dynamic Water balance for Shallow Cover System for 2009

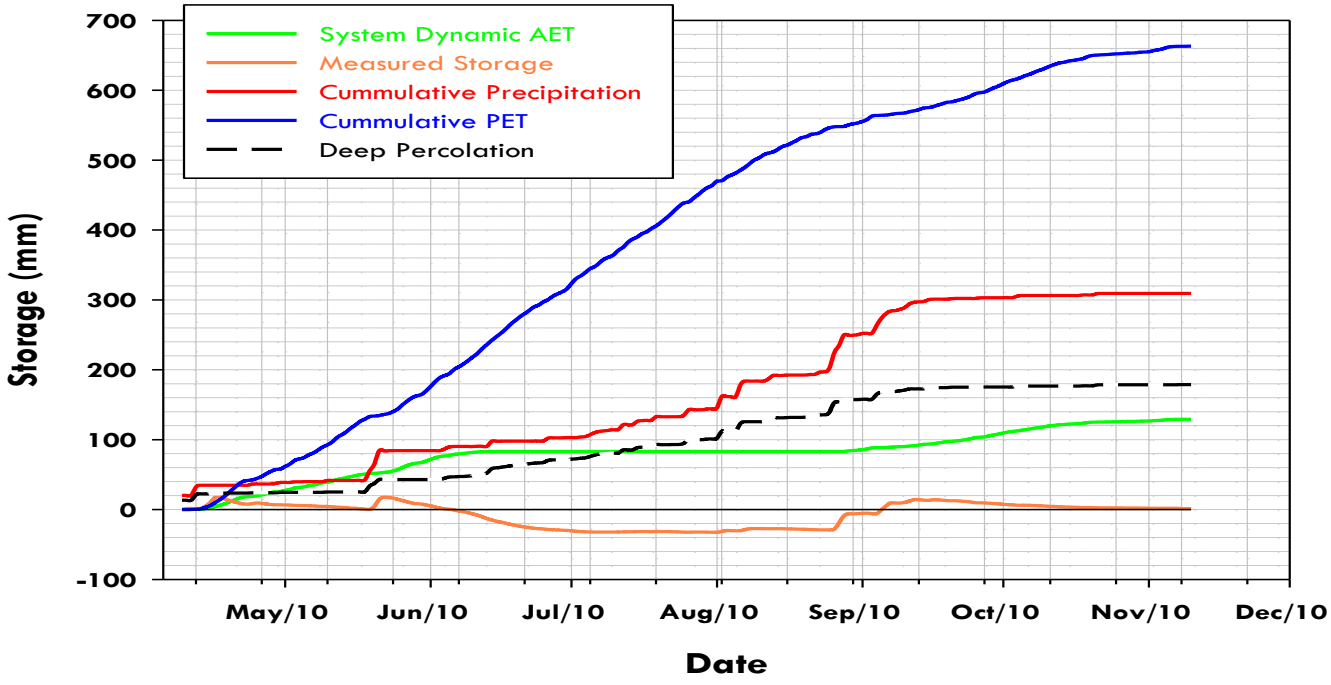

Figure B.5: System Dynamic Water balance for Shallow Cover System for 2010

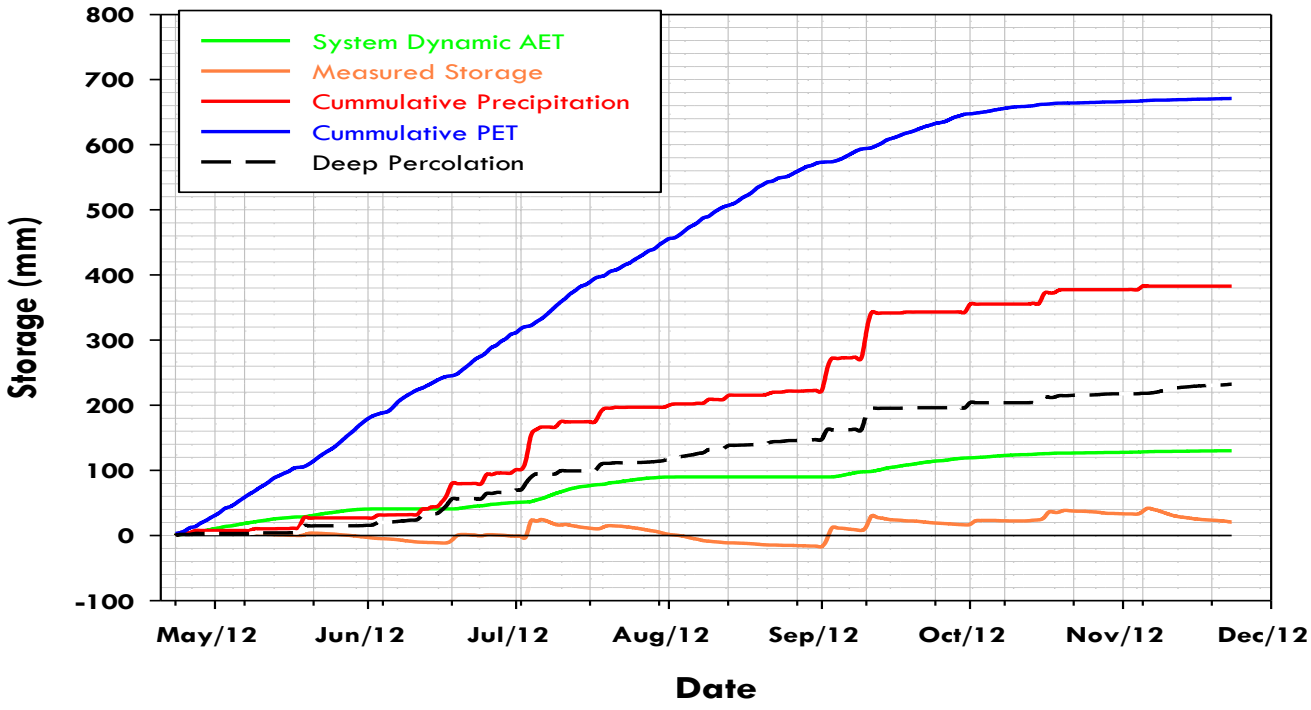

Figure B.6: System Dynamic Water balance for Shallow Cover System for 2012

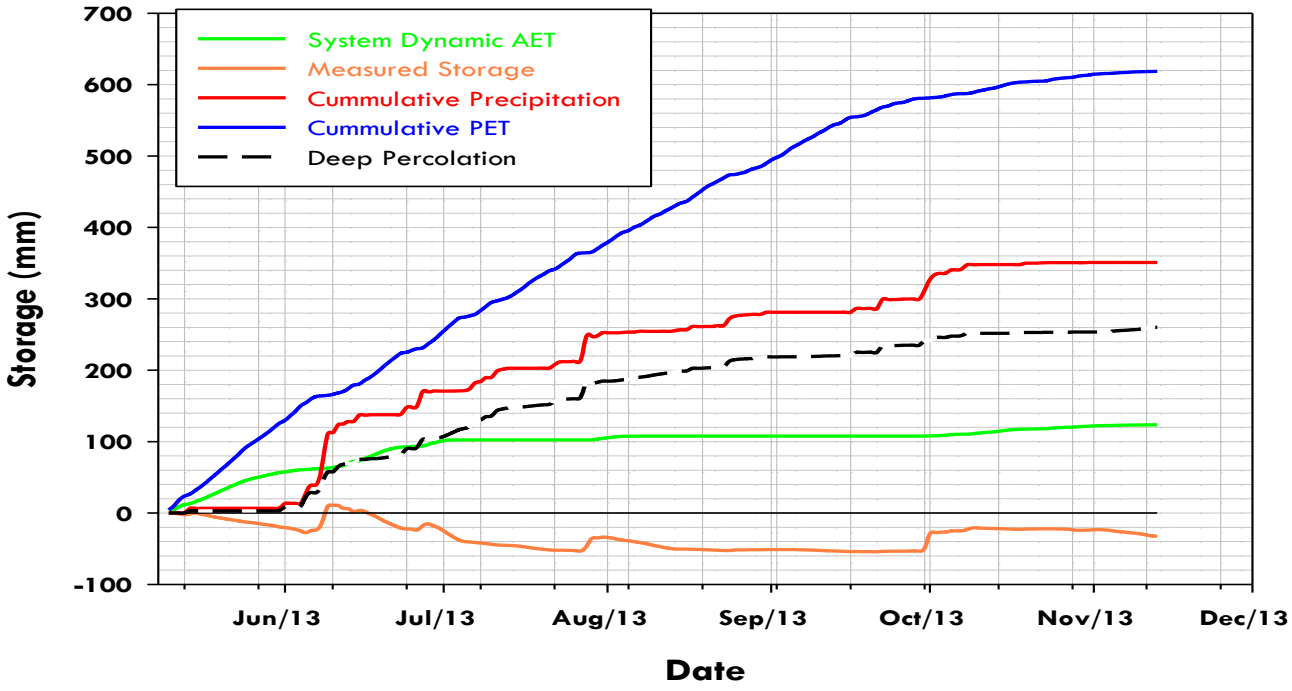

Figure B.7: System Dynamic Water balance for Shallow Cover System for 2013

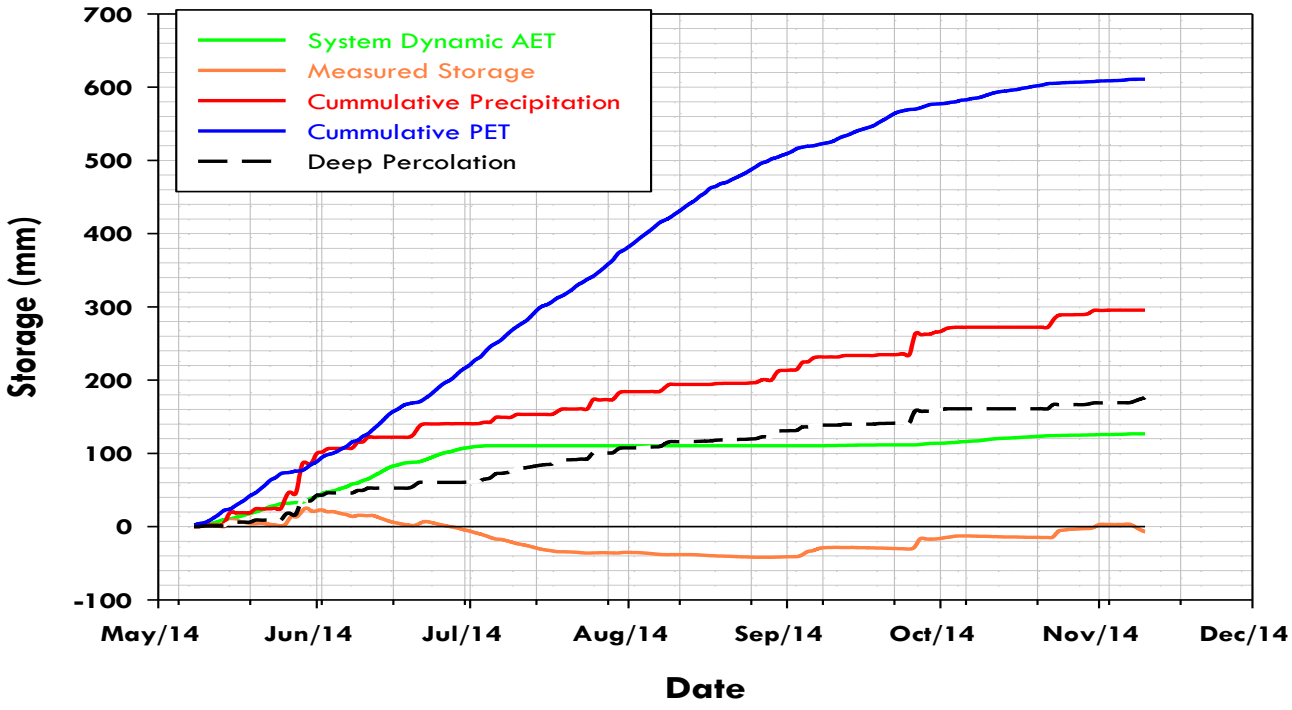

Figure B.8: System Dynamic Water balance for Shallow Cover System for 2014

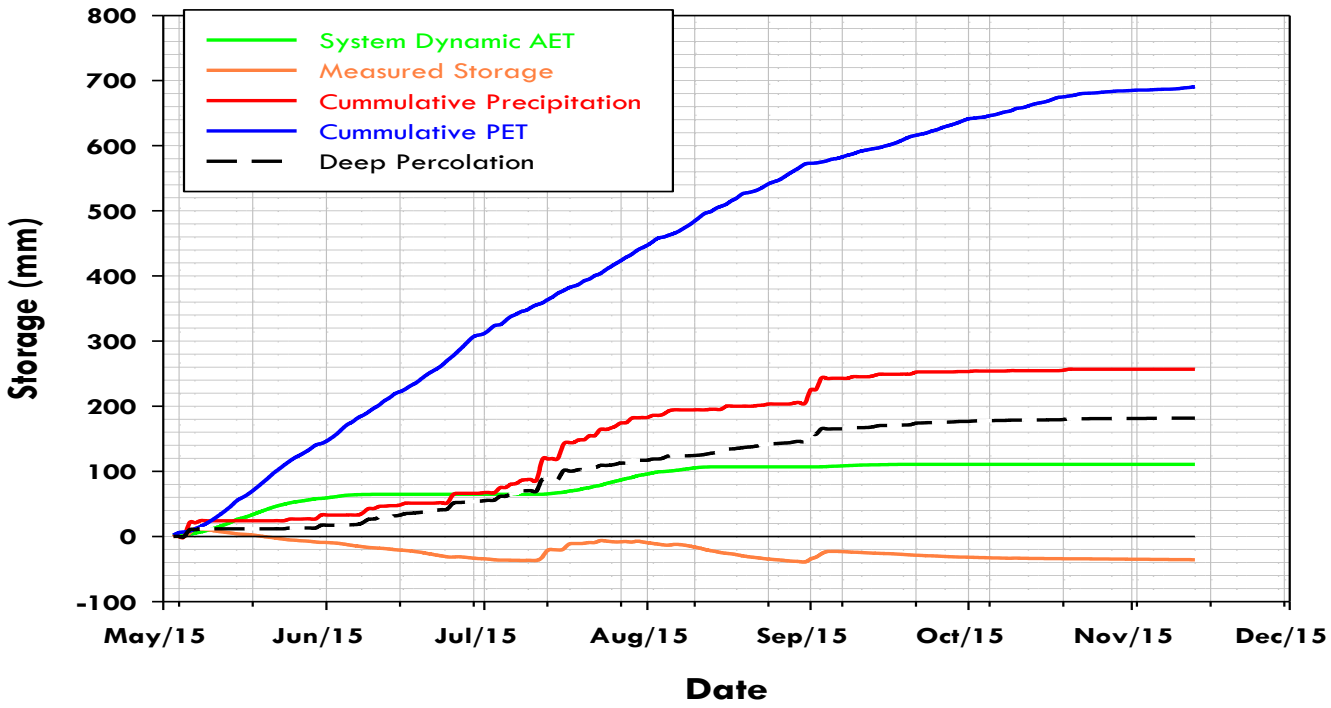

Figure B.9: System Dynamic Water balance for Shallow Cover System for 2015

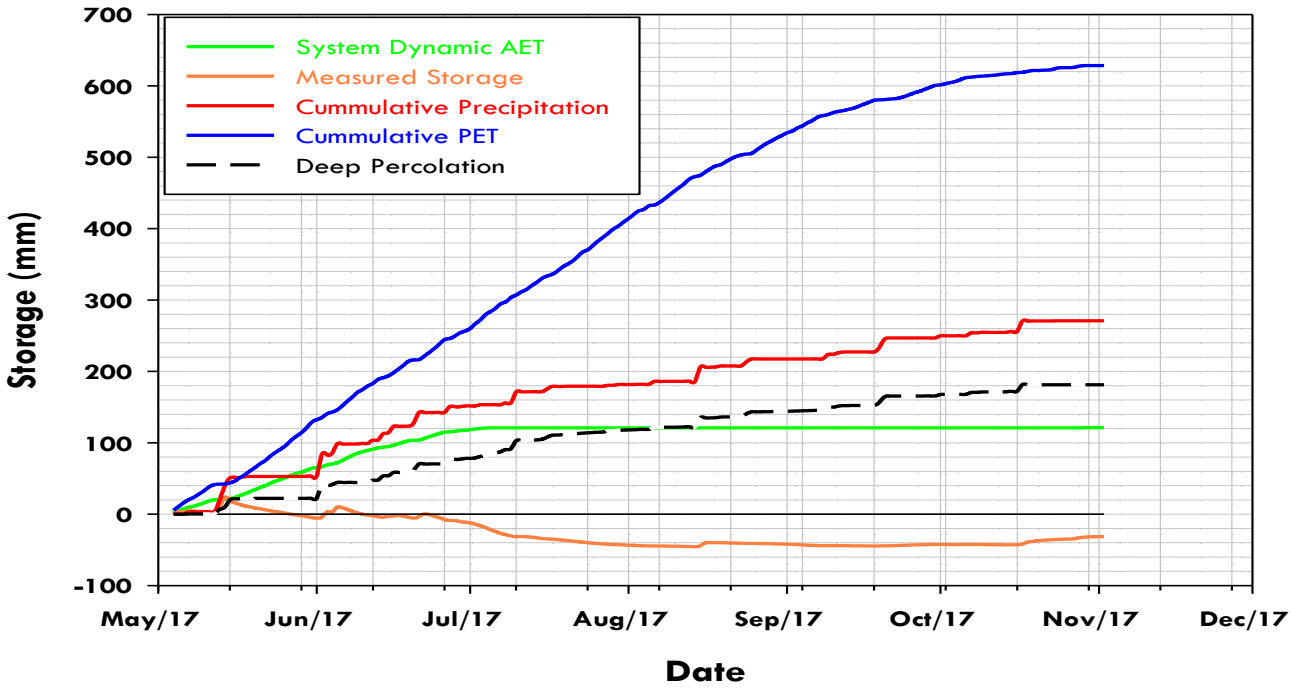

Figure B.10: System Dynamic Water balance for Shallow Cover System for 2017

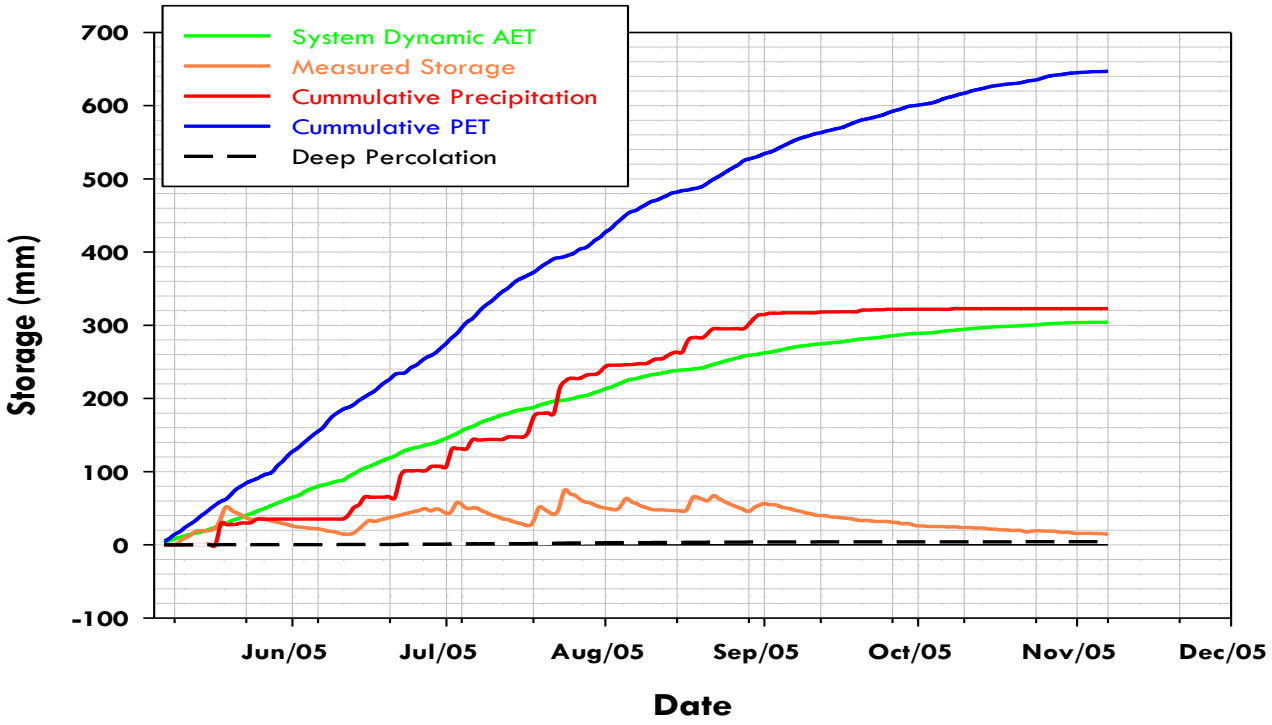

Figure B.11: System Dynamic Water balance for Deep Cover System for 2005

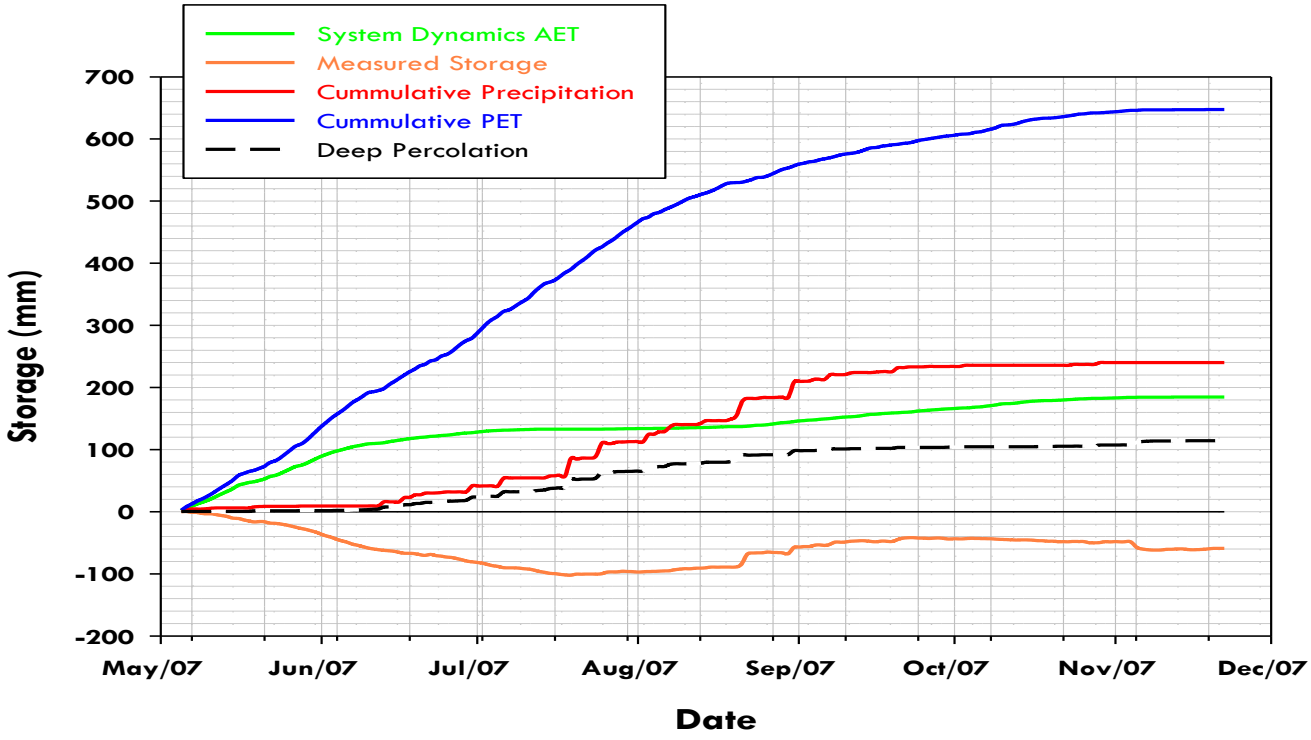

Figure B.12: System Dynamic Water balance for Deep Cover System for 2007

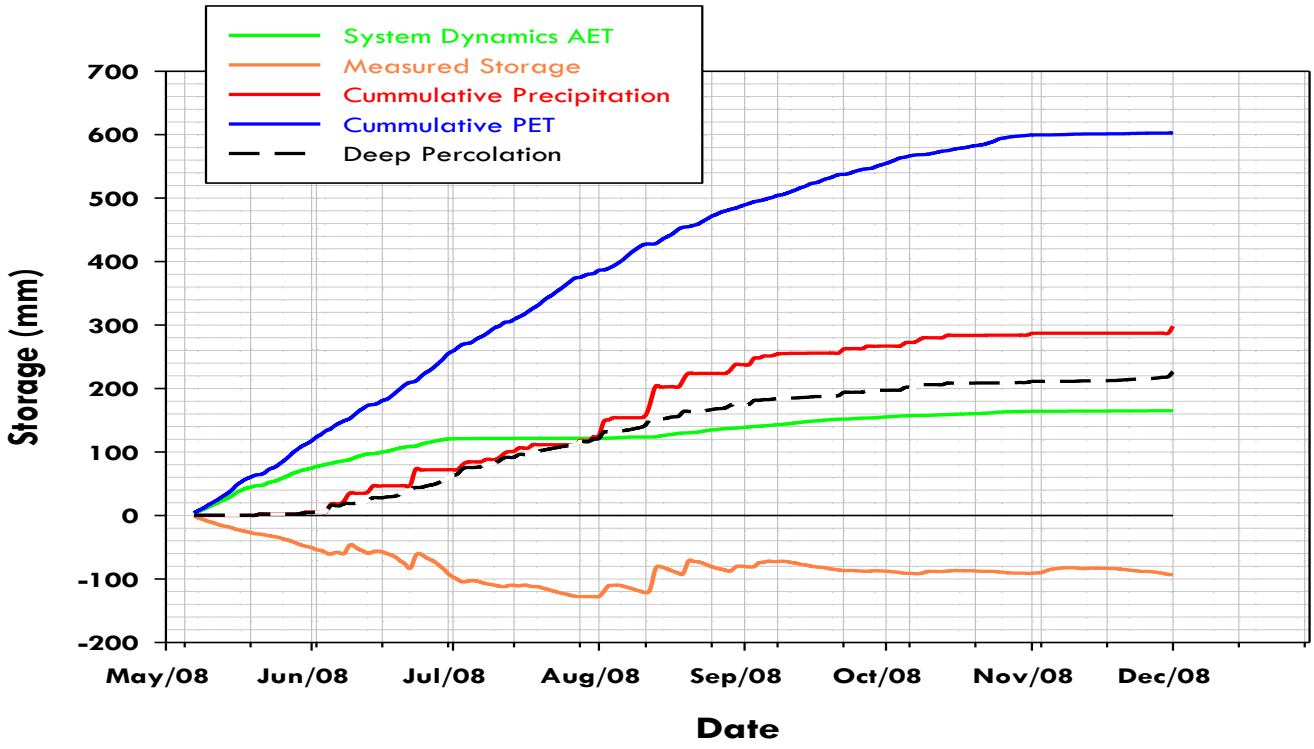

Figure B.13: System Dynamic Water balance for Deep Cover System for 2008

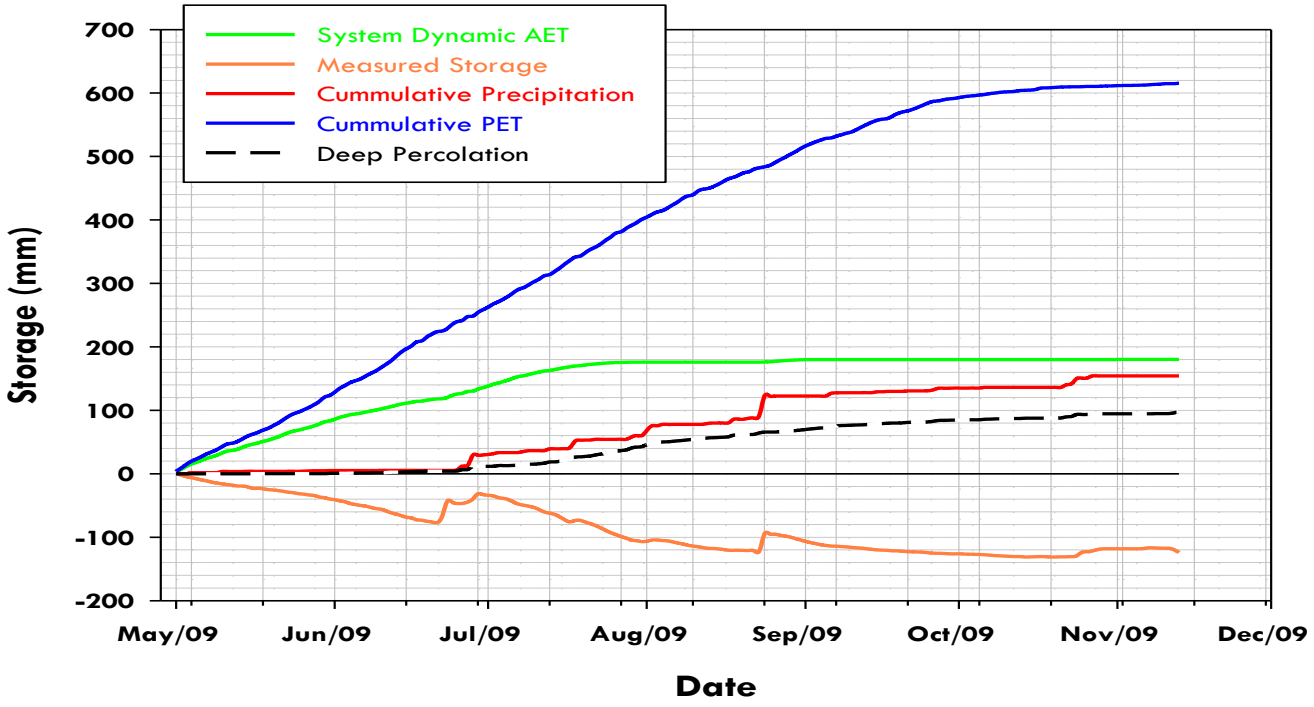

Figure B.14: System Dynamic Water balance for Deep Cover System for 2009

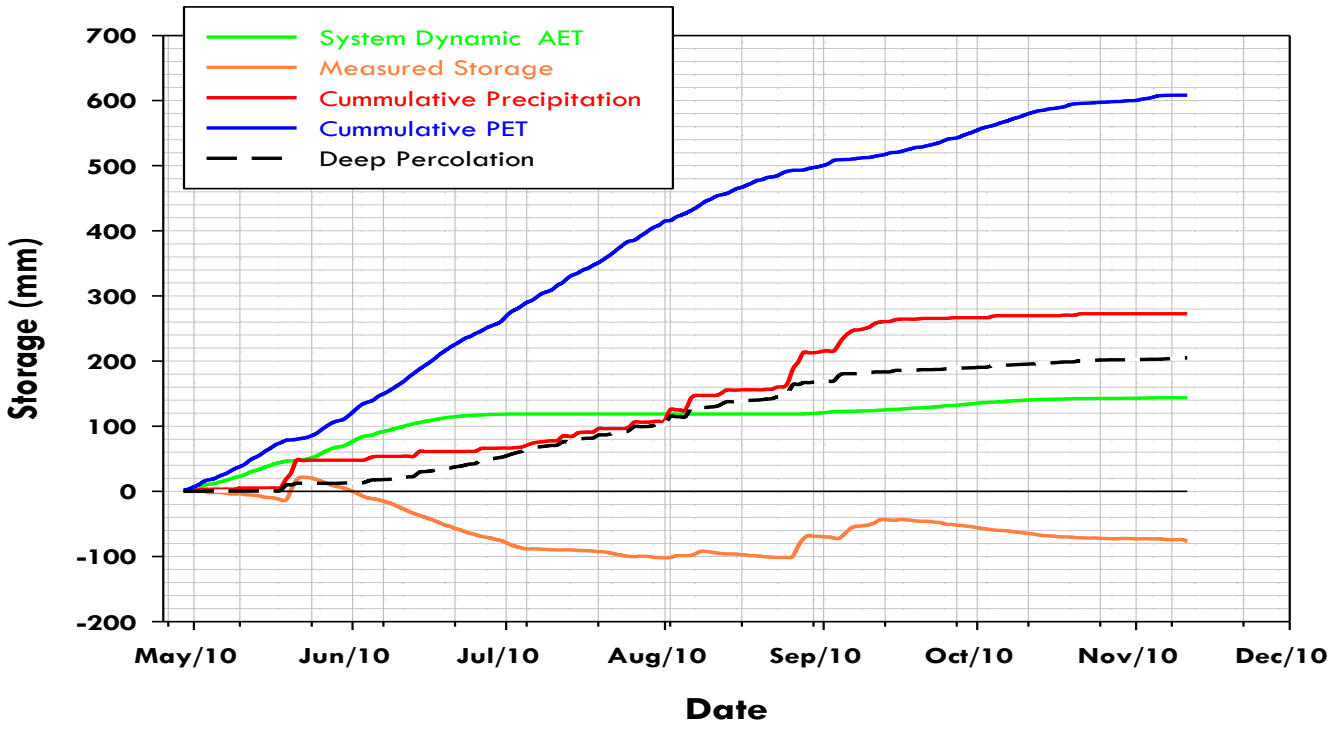

Figure B.15: System Dynamic Water balance for Deep Cover System for 2010

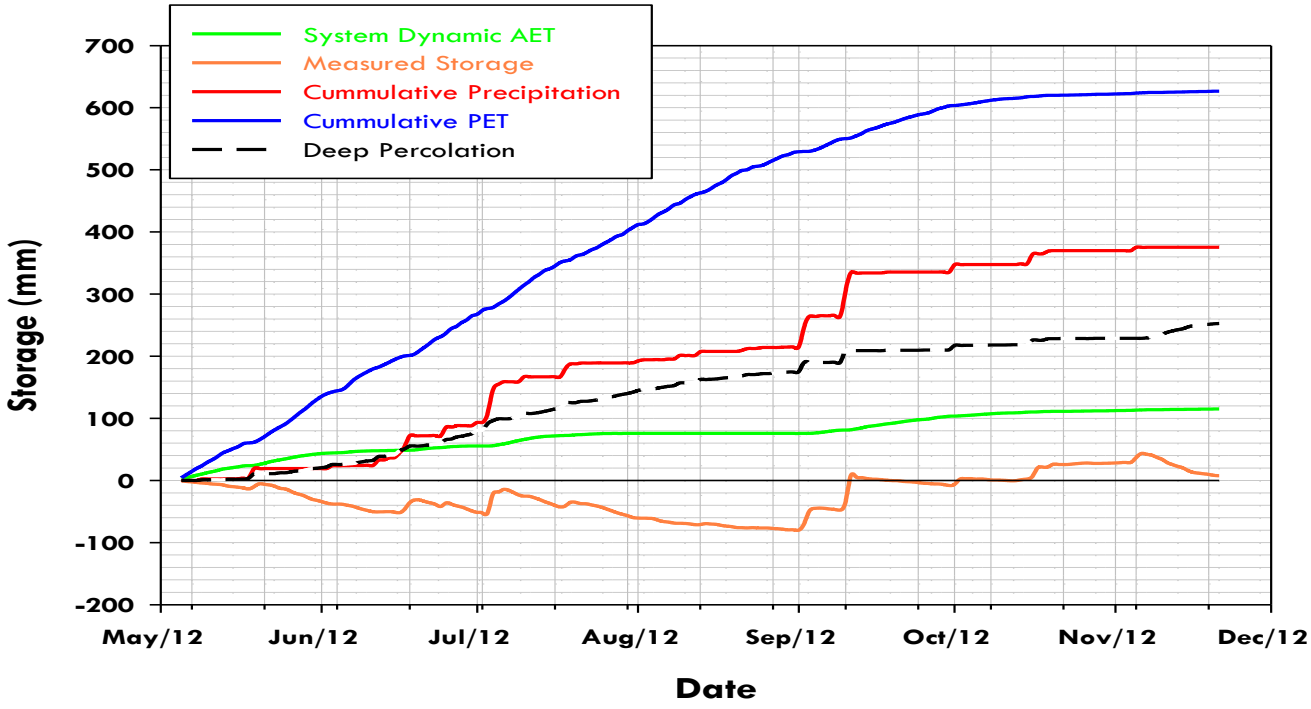

Figure B.16: System Dynamic Water balance for Deep Cover System for 2012

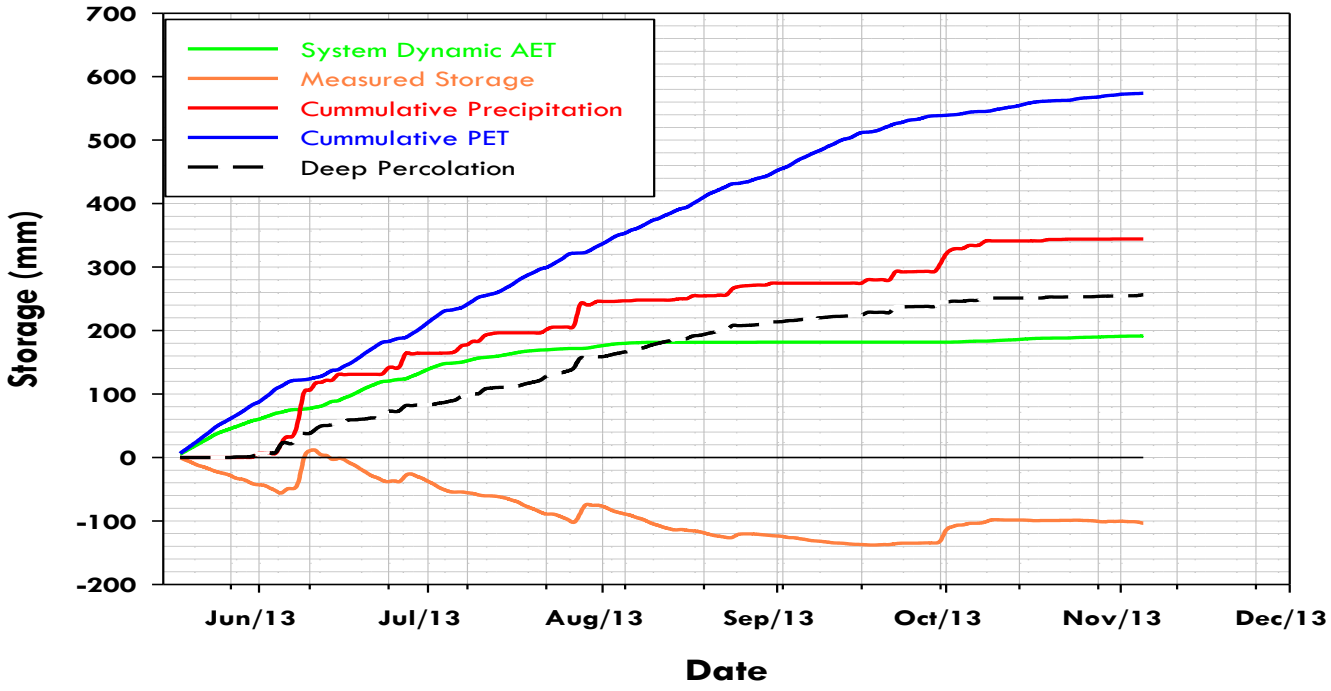

Figure B.17: System Dynamic Water balance for Deep Cover System for 2013

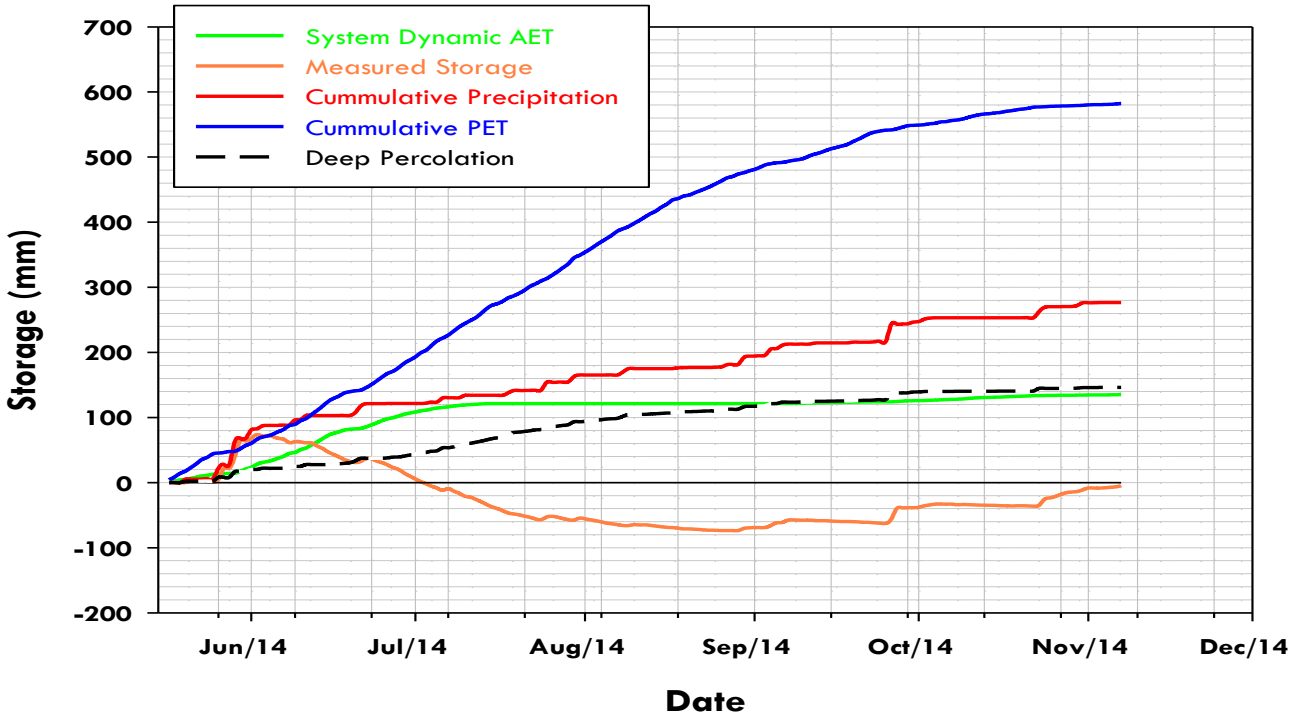

Figure B.18: System Dynamic Water balance for Deep Cover System for 2014

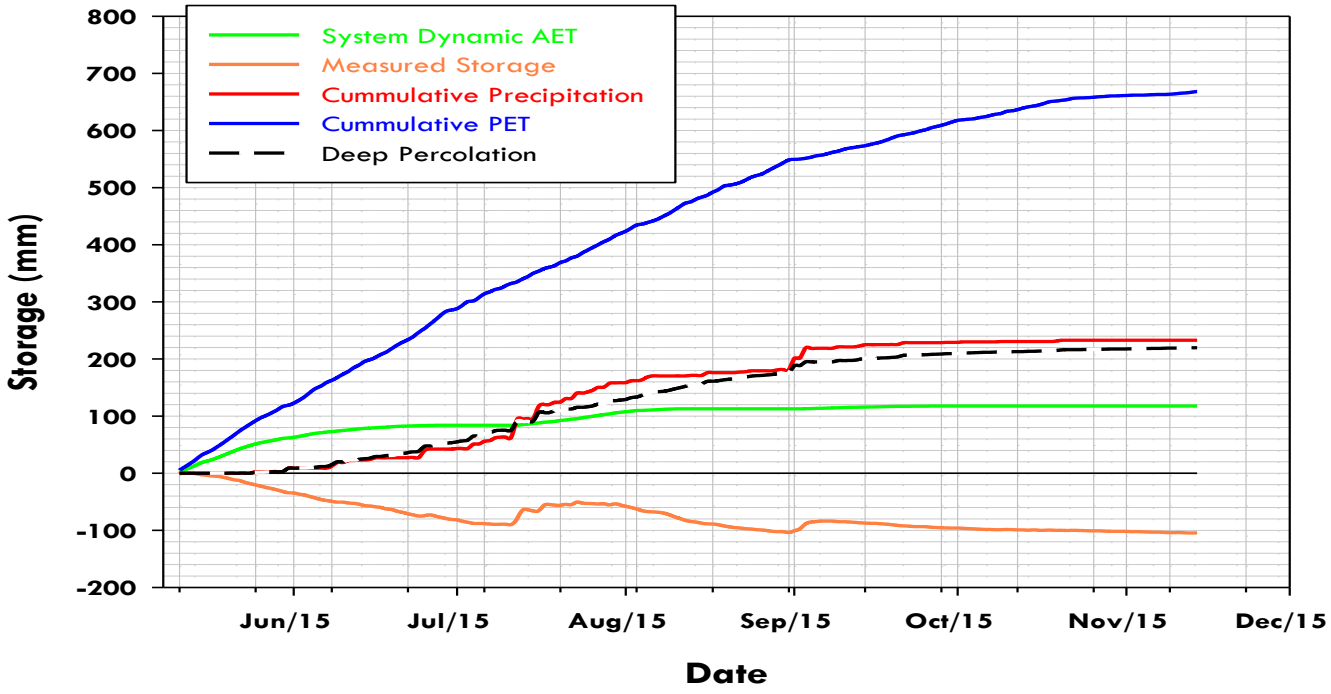

Figure B.19: System Dynamic Water balance for Deep Cover System for 2015

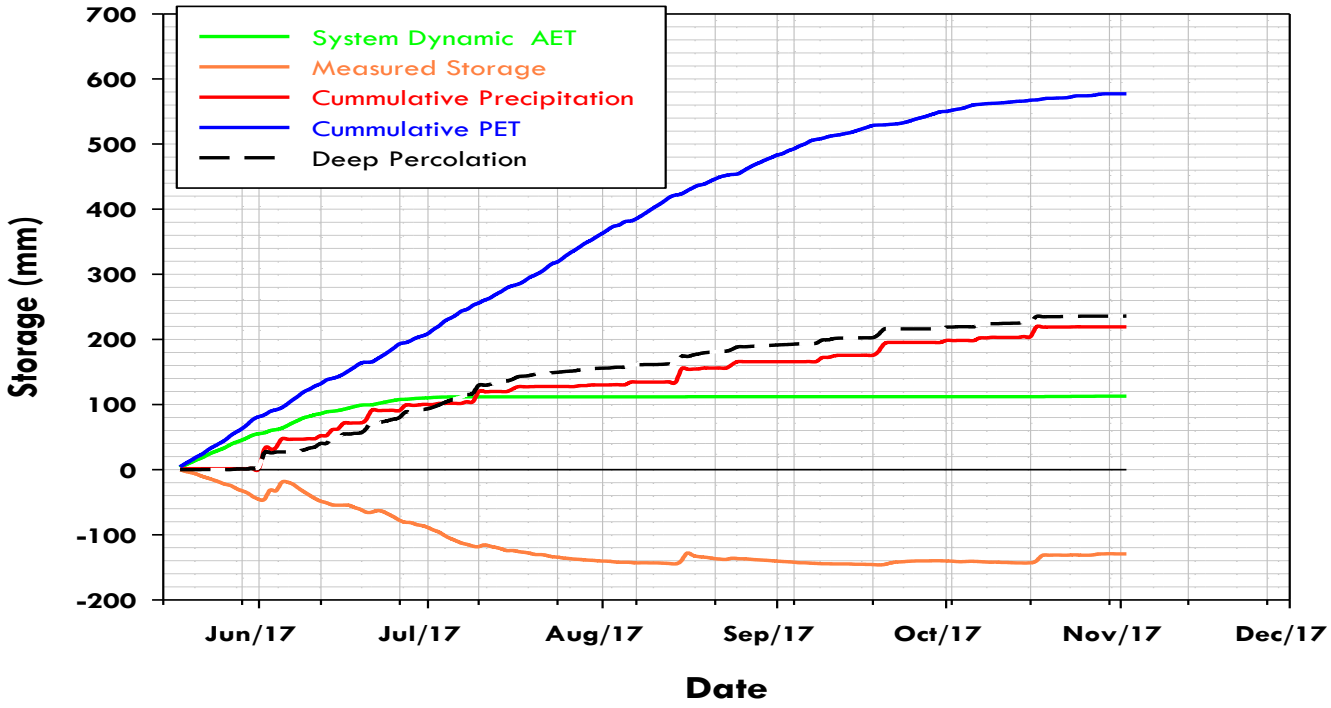

Figure B.20: System Dynamic Water balance for Deep Cover System for 2017

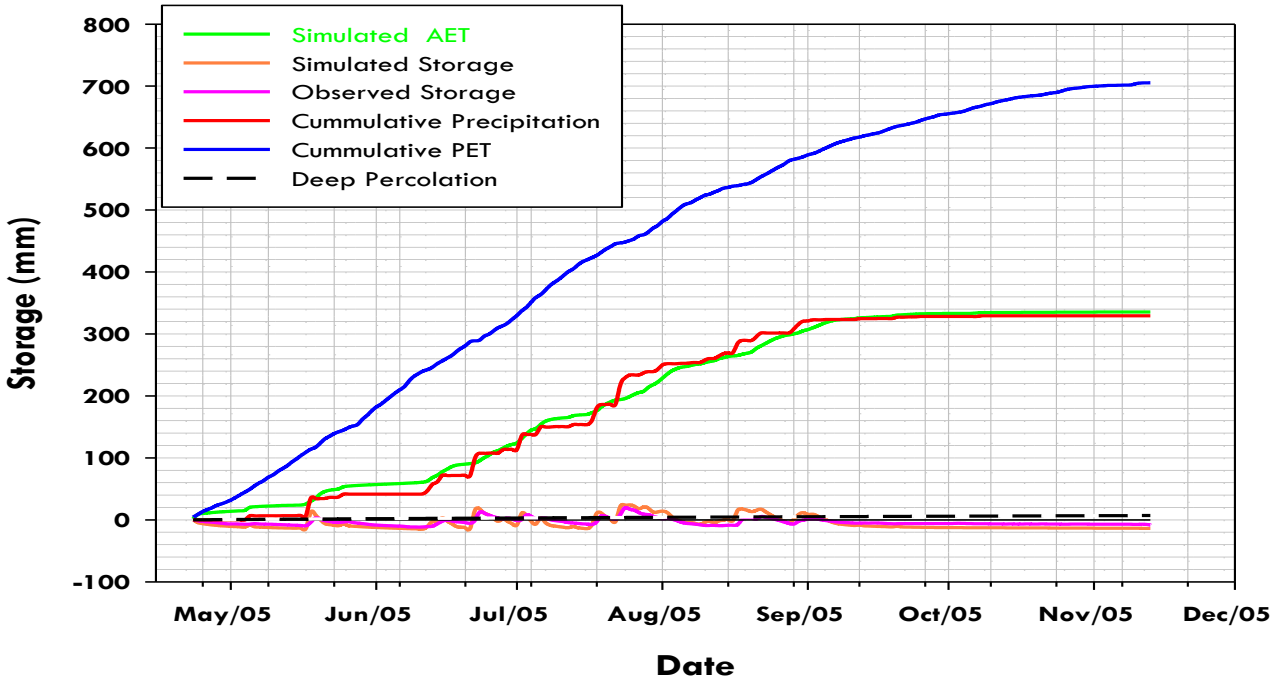

Figure B.21: Simulated Water balance for Shallow Cover System for 2005

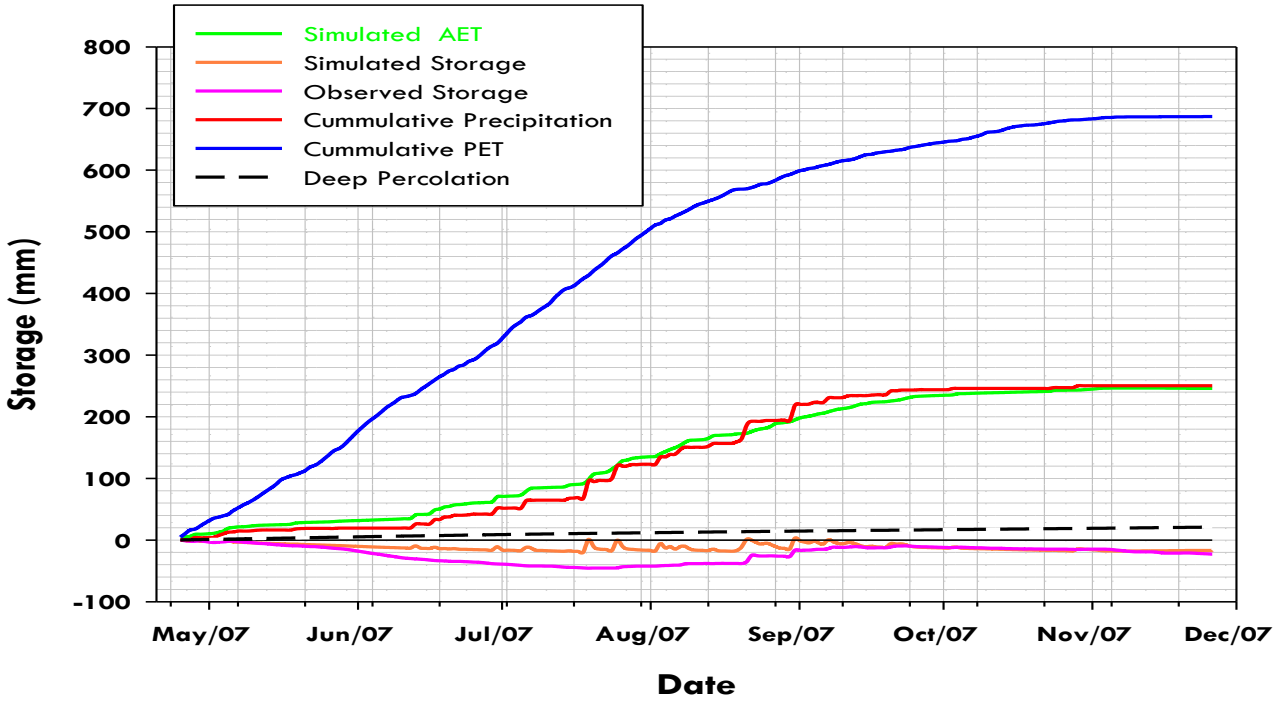

Figure B.22: Simulated Water balance for Shallow Cover System for 2007

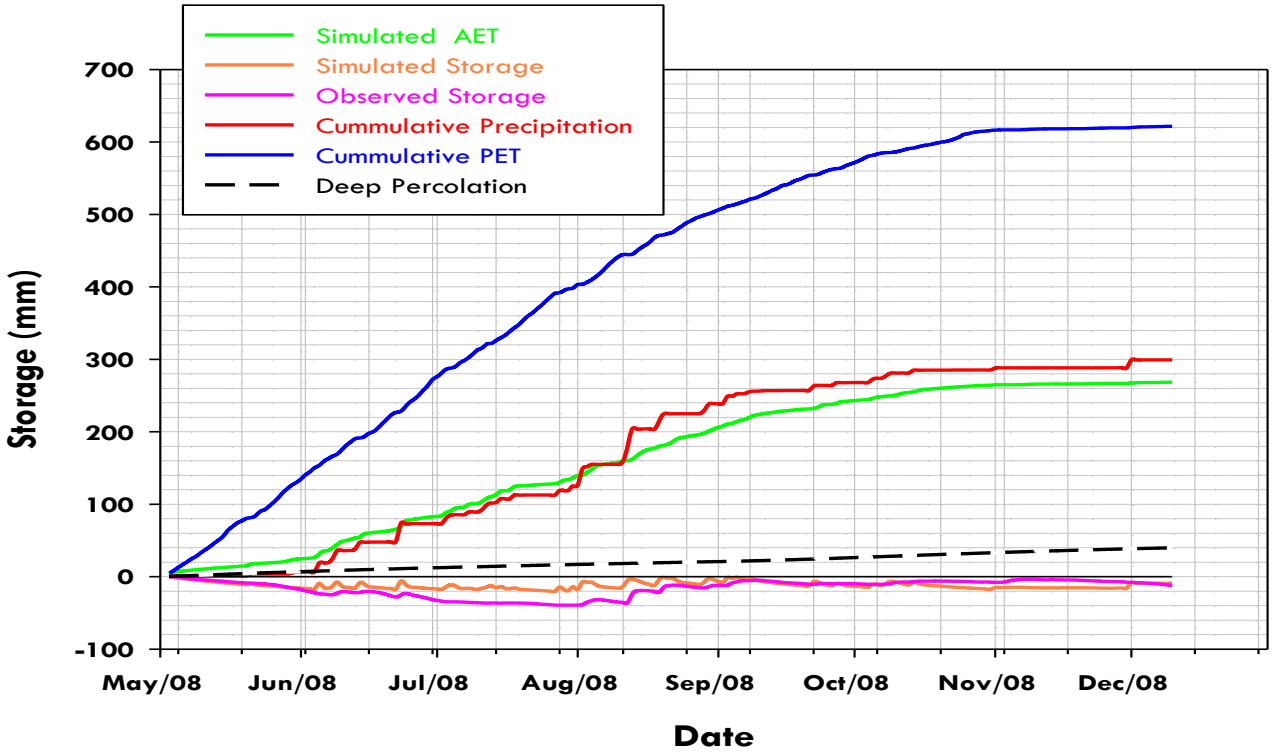

Figure B.23: Simulated Water balance for Shallow Cover System for 2008

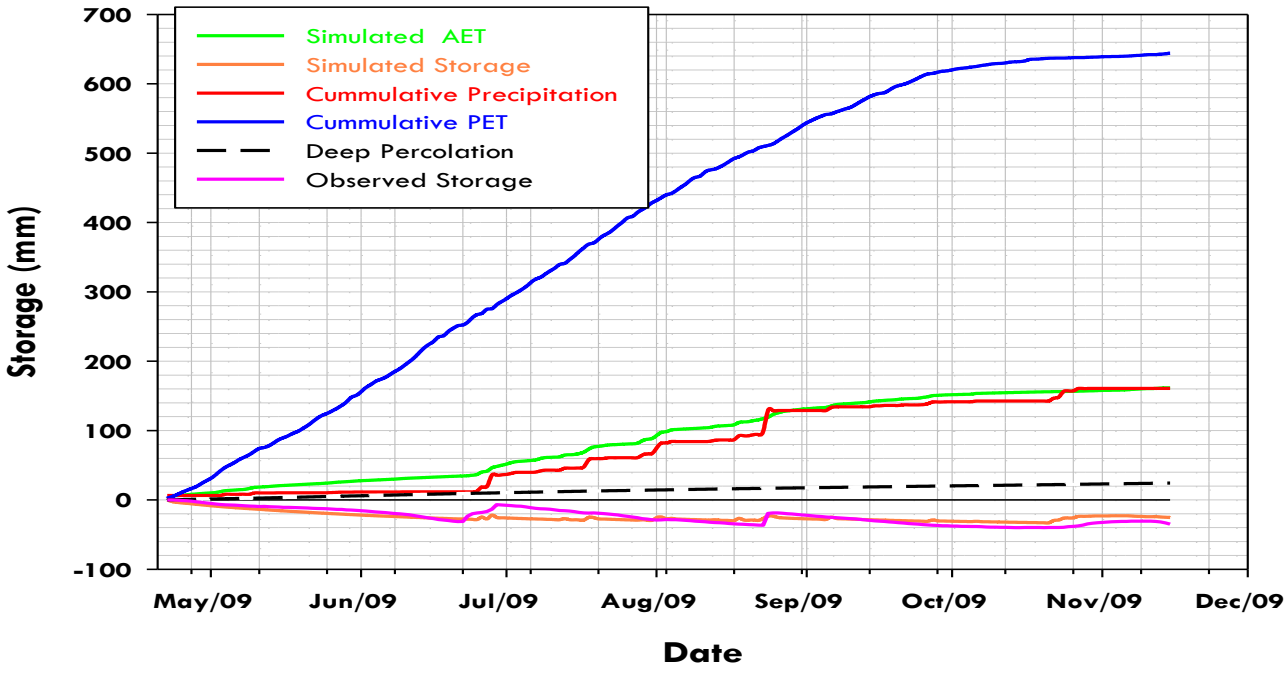

Figure B.24: Simulated Water balance for Shallow Cover System for 2009

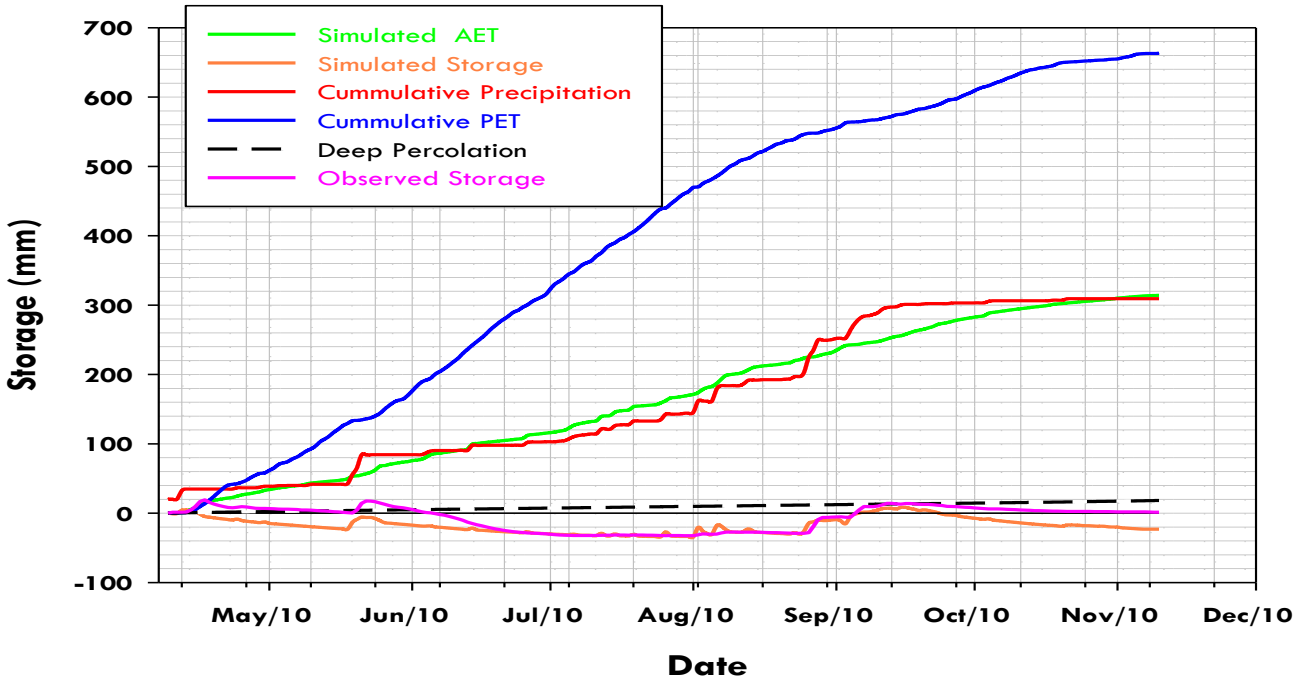

Figure B.25: Simulated Water balance for Shallow Cover System for 2010

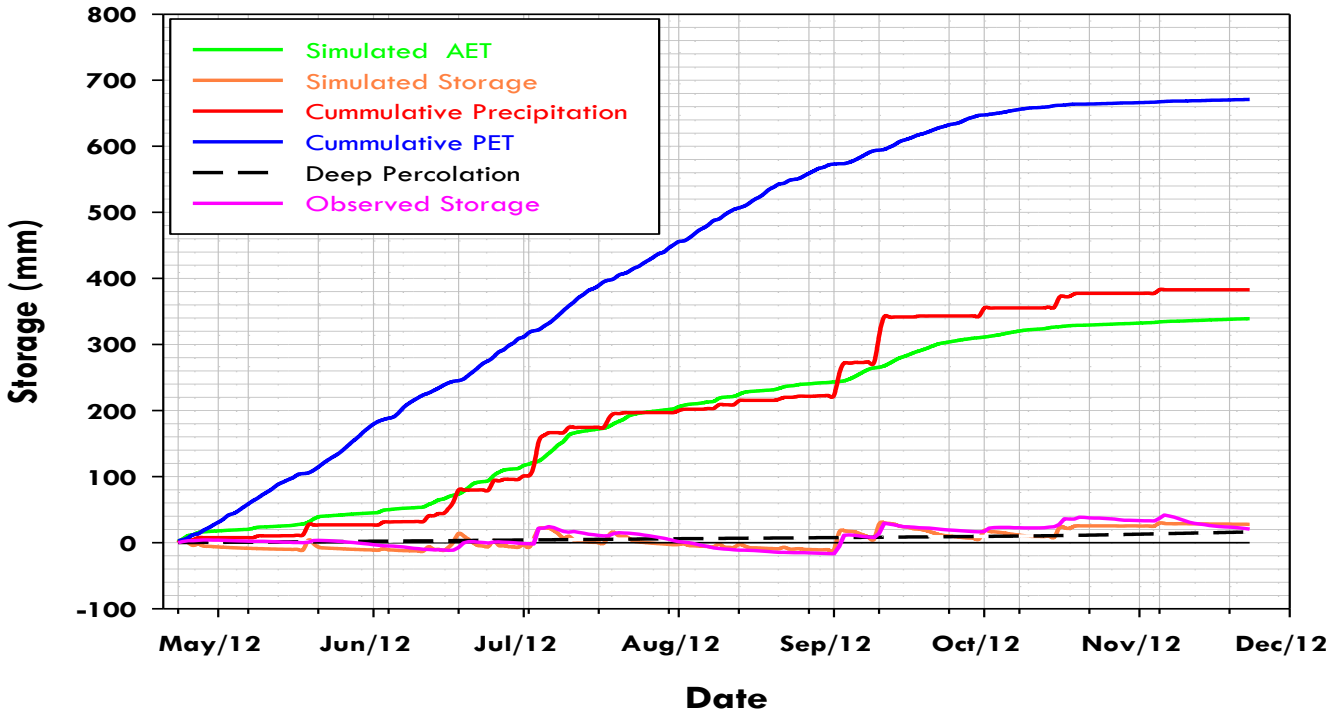

Figure B.26: Simulated Water balance for Shallow Cover System for 2012

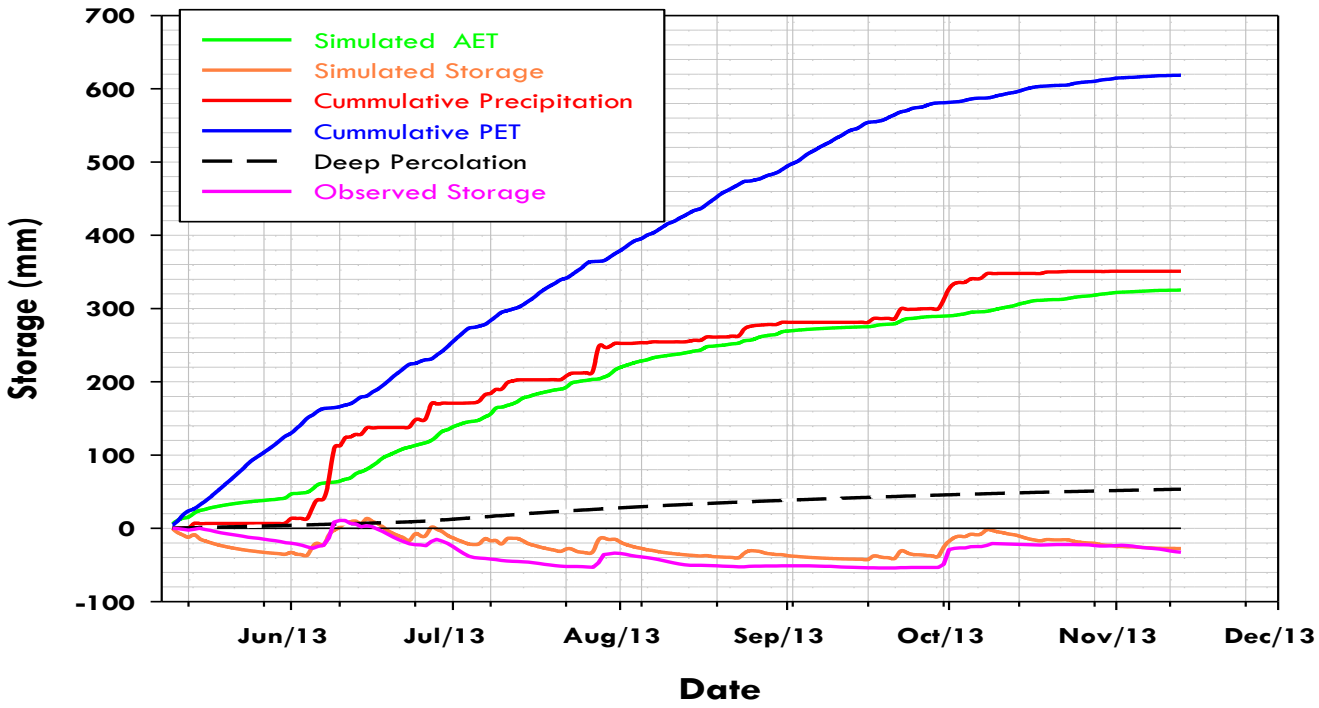

Figure B.27: Simulated Water balance for Shallow Cover System for 2013

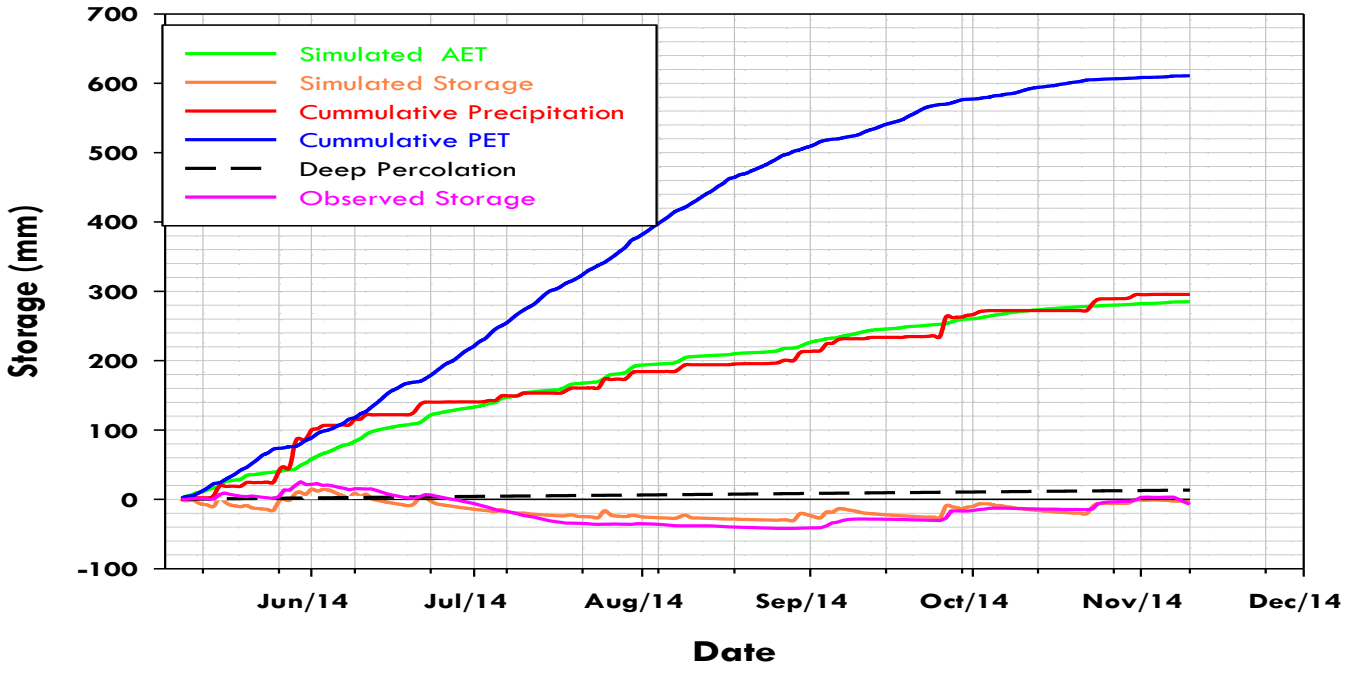

Figure B.28: Simulated Water balance for Shallow Cover System for 2014

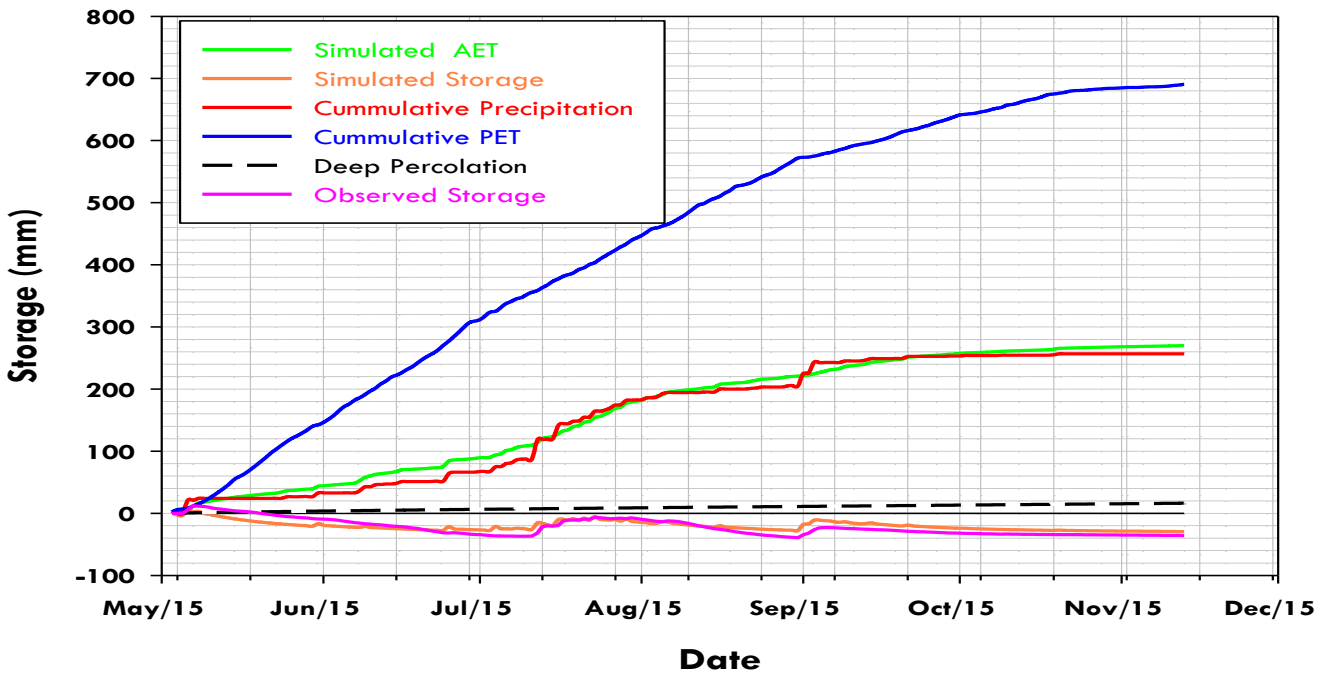

Figure B.29: Simulated Water balance for Shallow Cover System for 2015

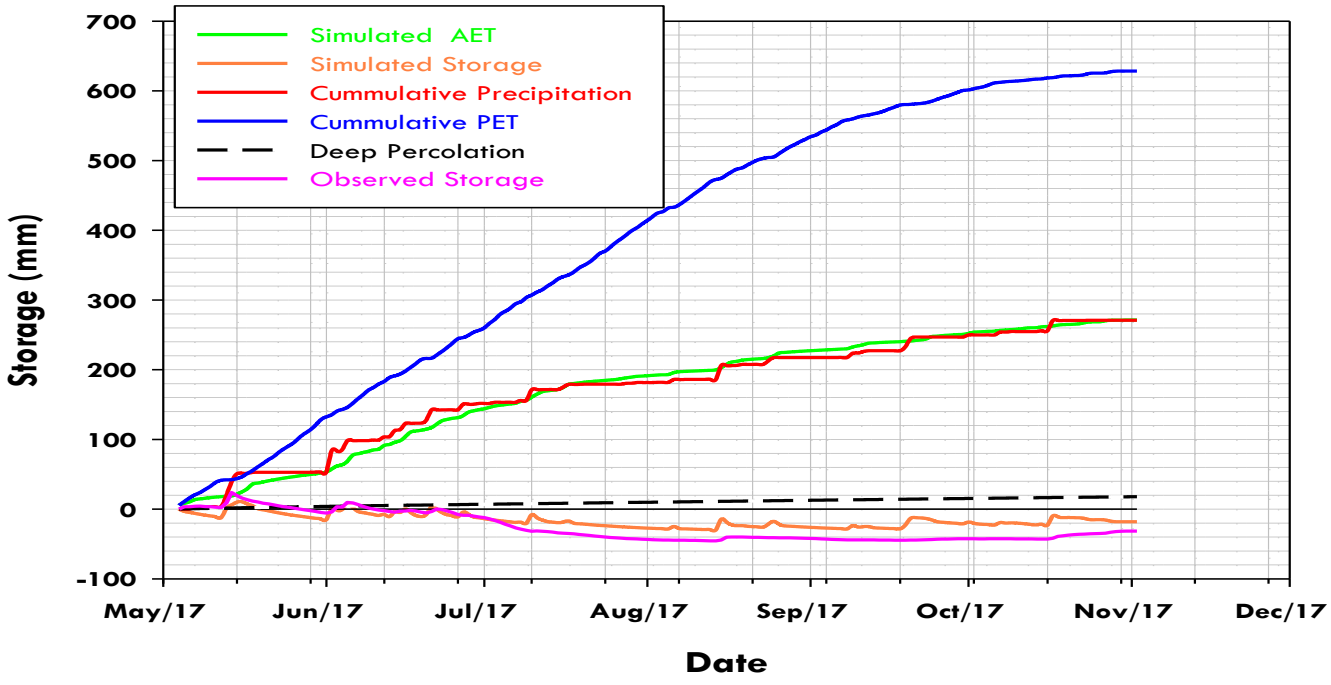

Figure B.30: Simulated Water balance for Shallow Cover System for 2017

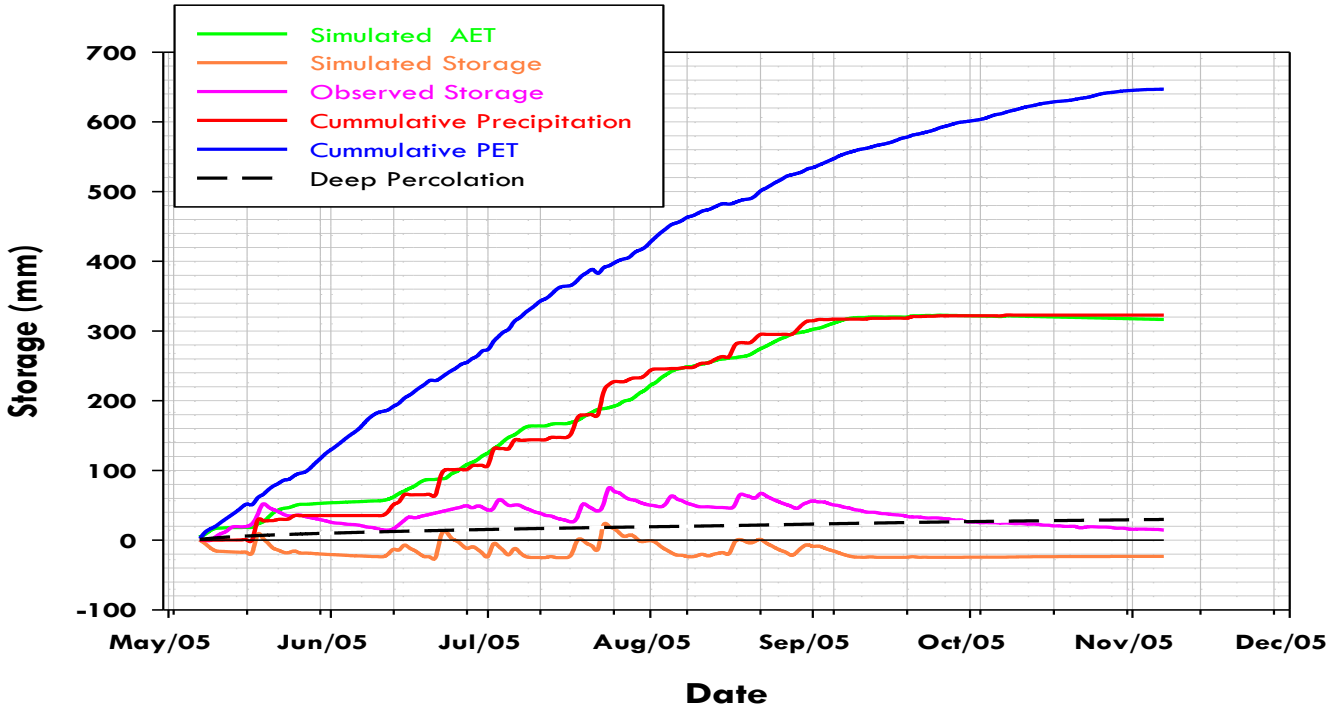

Figure B.31: Simulated Water balance for Deep Cover System for 2005

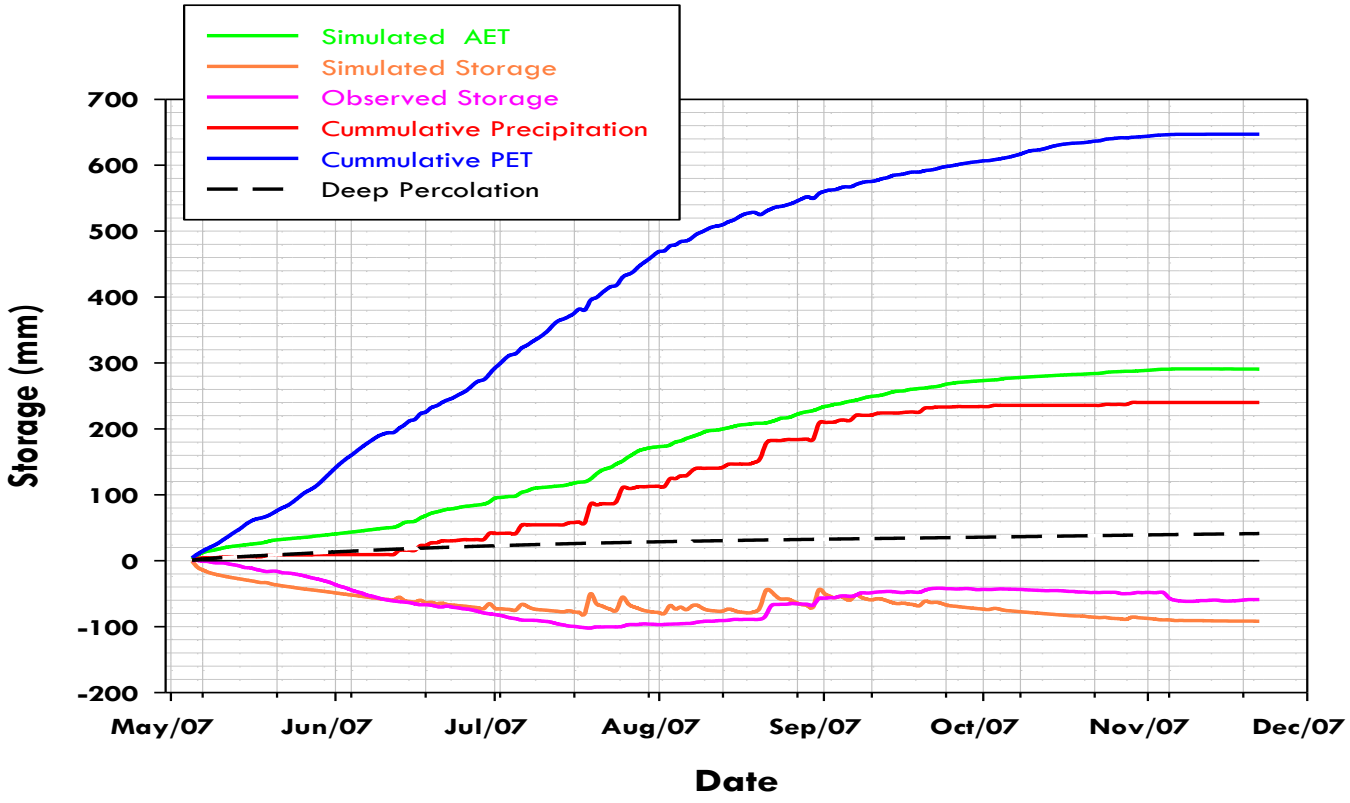

Figure B.32: Simulated Water balance for Deep Cover System for 2007

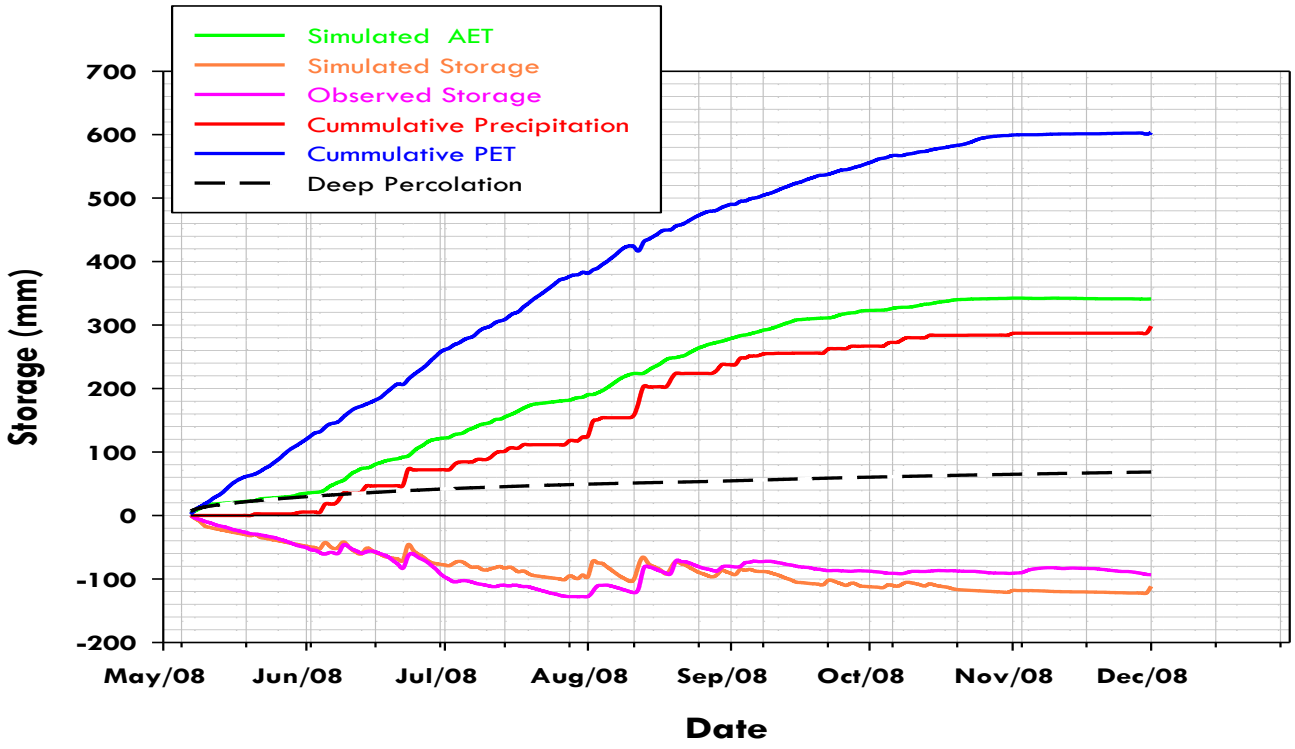

Figure B.33: Simulated Water balance for Deep Cover System for 2008

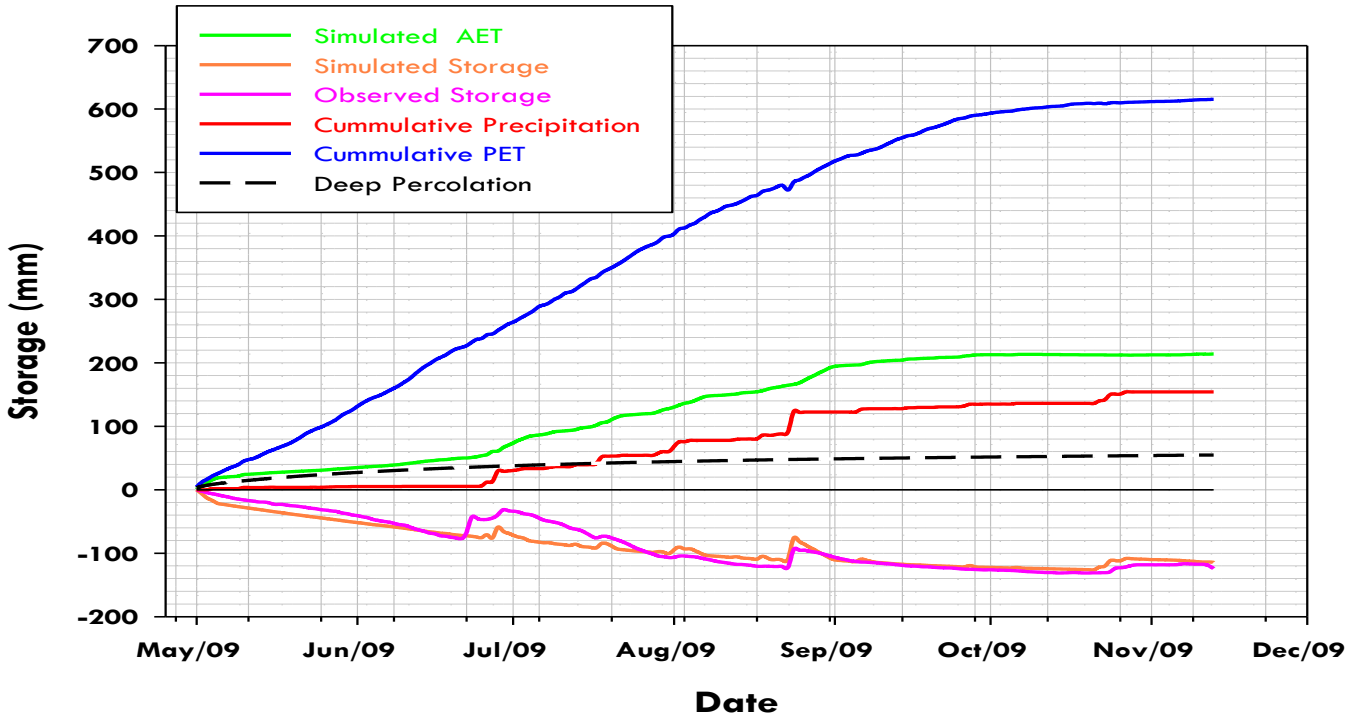

Figure B.34: Simulated Water balance for Deep Cover System for 2009

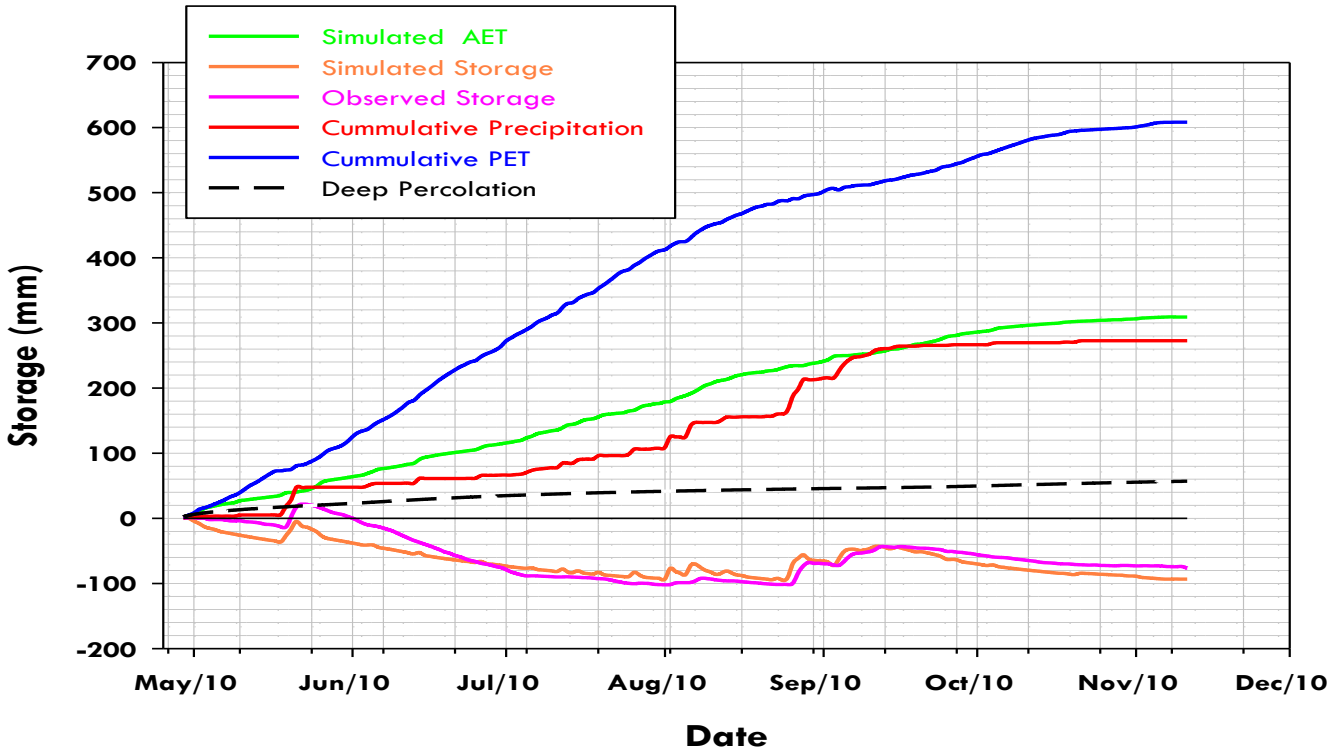

Figure B.35: Simulated Water balance for Deep Cover System for 2010

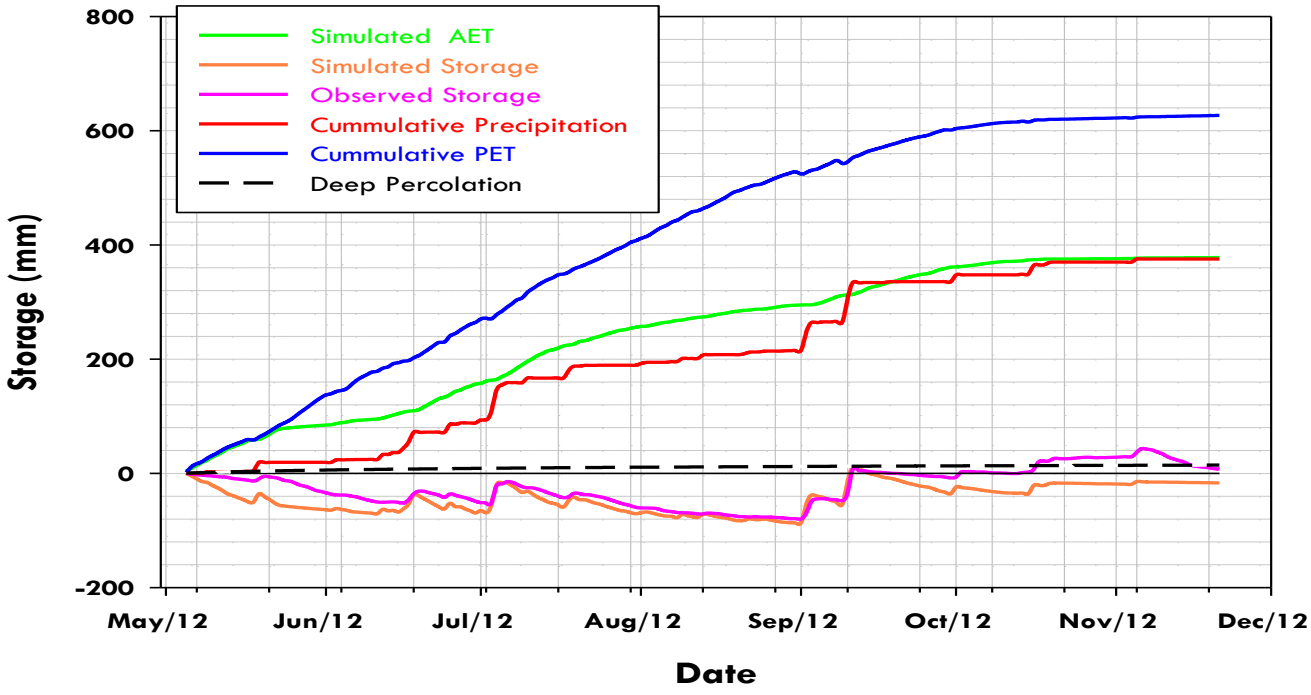

Figure B.36: Simulated Water balance for Deep Cover System for 2012

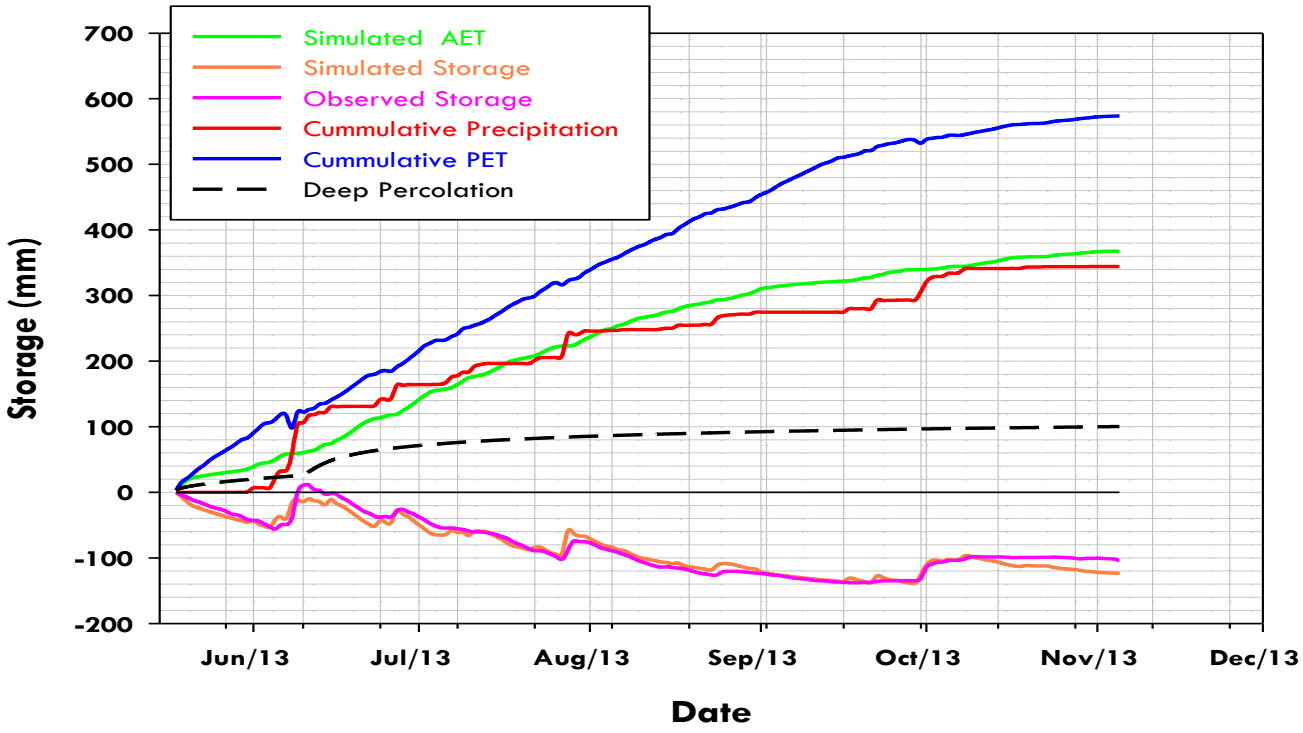

Figure B.37: Simulated Water balance for Deep Cover System for 2013

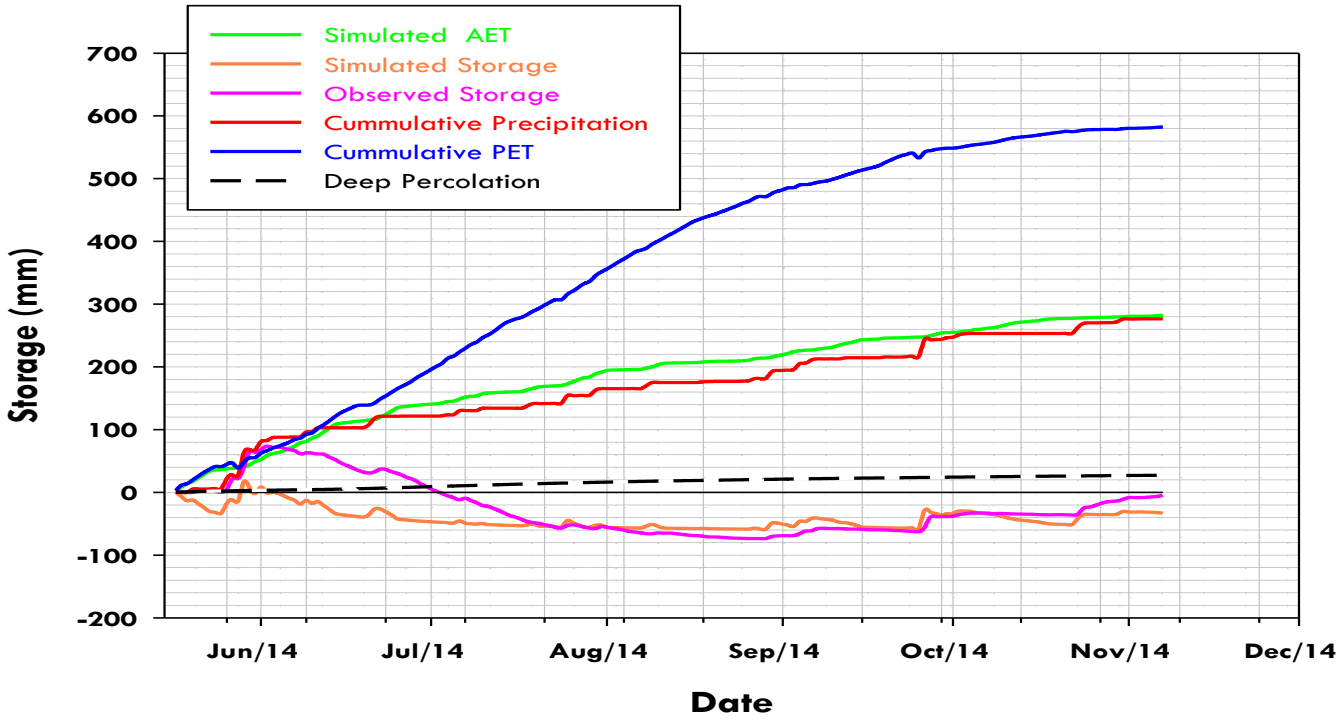

Figure B.38: Simulated Water balance for Deep Cover System for 2014

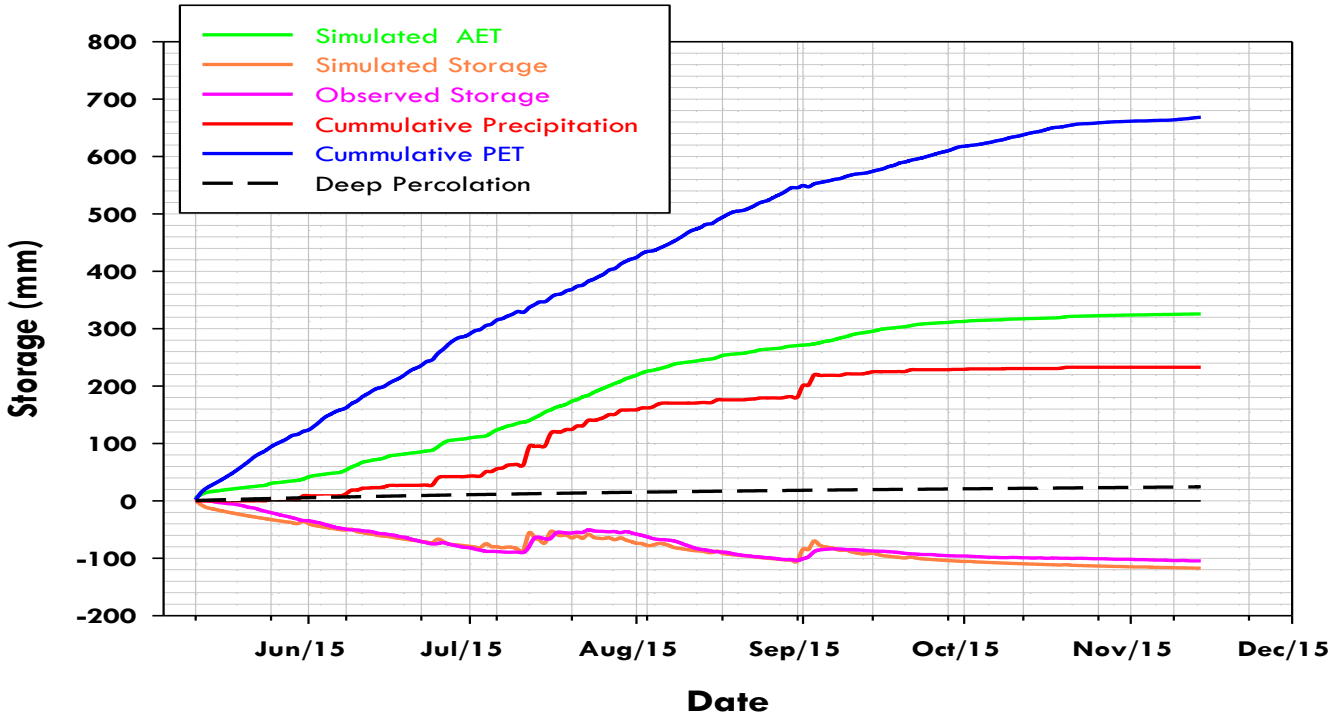

Figure B.39: Simulated Water balance for Deep Cover System for 2015

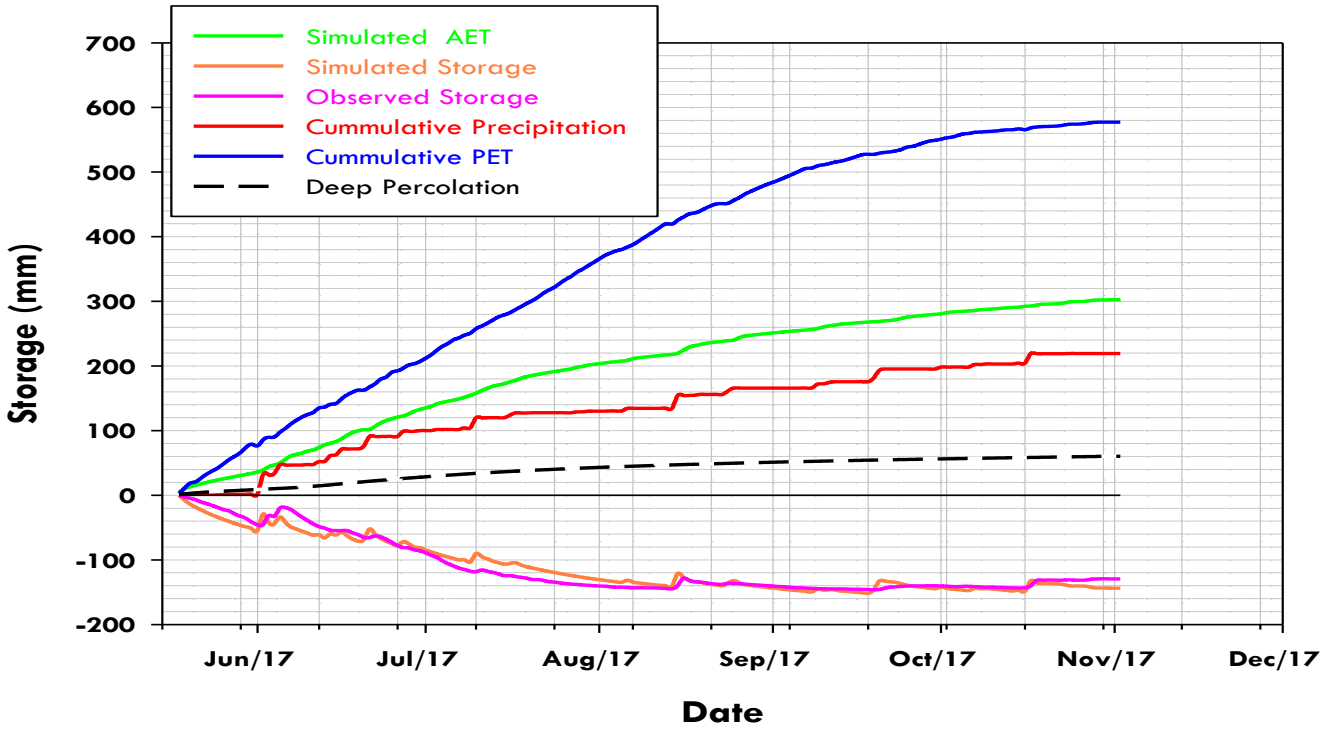

Figure B.40: Simulated Water balance for Deep Cover System for 2017

APPENDIX C

Potential Evapotranspiration and Summary of Growing and Frozen Season Precipitation Component for Both Covers

Table C.1: Potential Evapotranspiration Data for both Covers

Year	Shallow Cover (mm)	Deep Cover (mm)
2005	705	647
2006	719	653
2007	687	647
2008	622	603
2009	644	615
2010	663	608
2011	673	642
2012	671	627
2013	619	574
2014	611	582
2015	691	668
2016	641	618
2017	628	577
Mean	**660**	**620**

Table C.2: Summary of Water Components for the Study Period

Year	Annual Rainfall (mm)	SWE (mm)	Annual Precipitation (mm)	Growing Season Rainfall, Shallow Cover (mm)	Frozen Season PPT, Shallow Cover (mm)	Growing Season Rainfall, Deep Cover (mm)	Frozen Season PPT, Deep Cover (mm)
2005	397	67	464	329	135	323	141
2006	322	43	365	303	62	300	65
2007	274	120	394	250	143	240	154
2008	304	103	407	299	108	298	109
2009	169	92	262	161	101	154	107
2010	314	45	358	309	49	273	86
2011	193	67	260	188	72	180	80
2012	396	45	441	383	58	375	66
2013	357	72	429	351	78	344	85
2014	307	35	342	295	47	277	66
2015	270	39	309	257	52	233	77
2016	397	46	443	385	58	382	61
2017	291	25	316	271	45	219	96
Mean	**307**	**62**	**369**	**291**	**78**	**277**	**92**

Table C.3: Summary of Growing Season and Frozen Season Precipitation, Shallow Cover

Date	Captured Growing Season PPT (mm)	% of Captured Growing Season PPT	Missing Growing Season PPT (mm)	% of Missing Growing PPT	Frozen Season PPT (mm)	Frozen Season storage (mm)	% of Frozen Season storage	Frozen Season NP (mm)	% Frozen Season NP
2005	121	37	208	63	135	40	29	95	71
2006	105	35	198	65	62	4	6	58	94
2007	52	21	199	79	143	11	8	132	92
2008	57	19	242	81	108	12	11	96	89
2009	49	31	111	69	101	16	16	85	84
2010	62	20	247	80	49	21	43	28	57
2011	34	18	155	82	72	22	30	50	70
2012	124	32	259	68	58	11	18	48	82
2013	102	29	249	71	78	15	19	64	81
2014	90	30	205	70	47	0	0	47	100
2015	58	22	199	78	52	9	17	43	83
2016	96	25	289	75	58	48	82	11	18
2017	71	26	200	74	45	5	12	40	88
Mean	**79**	**27**	**212**	**73**	**78**	**16**	**22**	**61**	**78**

Table C.4: Summary of Growing Season and Frozen Season Precipitation, Deep Cover

Date	Captured Growing Season PPT (mm)	% of Captured Growing Season PPT	Missing Growing Season PPT (mm)	% of Missing Growing PPT	Frozen Season PPT (mm)	Frozen Season storage (mm)	% of Frozen Season storage	Frozen Season NP (mm)	% Frozen Season NP
2005	220	67	109	33	141	42	30	99	70
2006	200	66	103	34	65	0	0	65	100
2007	108	43	143	57	154	29	19	124	81
2008	185	62	114	38	109	68	62	42	38
2009	129	80	32	20	107	91	85	16	15
2010	104	37	195	63	86	97	113	-11	-13
2011	90	48	98	52	80	109	136	-29	-36
2012	226	59	157	41	66	81	123	-15	-23
2013	176	50	176	50	85	49	57	36	43
2014	175	59	121	41	66	34	52	31	48
2015	111	43	147	57	77	43	56	34	44
2016	223	58	162	42	61	116	190	-55	-90
2017	141	52	130	48	96	44	45	53	55
Mean	**161**	**56**	**130**	**44**	**92**	**62**	**75**	**30**	**25**

APPENDIX D

Summary of Water balance Component Volumes for Both Covers

Table D.1: Summary of System Dynamics Seasonal Water Balance Components Results, Shallow Cover

Year	Total PPT (mm)	Total PET (mm)	Total AET (mm)	ΔS (mm)	NP (mm)	AET as a Percentage of PET (%)	AET as a Percentage of PPT (%)	NP as a Percentage of PPT (%)	ΔS as a Percentage of PPT (%)
2005	329	705	303	-8	34	43	92	10	-2
2006	303	719	206	-8	104	29	68	34	-2
2007	250	687	145	-23	128	21	58	51	-9
2008	300	622	102	-12	210	16	34	70	-4
2009	160	644	108	-35	87	17	68	54	-22
2010	309	663	129	1	179	19	42	58	0
2011	188	673	77	-49	160	11	41	85	-26
2012	383	671	130	20	232	19	34	61	5
2013	351	619	123	-33	260	20	35	74	-9
2014	295	611	127	-7	176	21	43	60	-2
2015	257	691	111	-36	182	16	43	71	-14
2016	385	641	150	-15	250	23	39	65	-4
2017	271	628	121	-31	181	19	45	67	-12
Mean	**291**	**660**	**141**	**-18**	**168**	**21**	**49**	**58**	**-7**

Table D.2: Summary of System Dynamic Annual Water Balance Components Results Including Frozen Period Precipitation and NP, Shallow Cover

Year	Annual PPT (mm)	Annual PET (mm)	Annual AET (mm)	Annual ΔS (mm)	Annual NP (mm)	AET as a Percentage of PET (%)	Annual AET as a Percentage of PPT (%)	Annual NP as a Percentage of PPT (%)	Annual ΔS as a Percentage of PPT (%)
2005	470	705	303	32	129	43	65	28	7
2006	368	719	206	-4	162	29	57	44	-1
2007	404	687	145	-12	260	21	37	66	-3
2008	409	622	102	0	306	16	25	75	0
2009	268	644	108	-19	172	17	41	66	-7
2010	395	663	129	22	207	19	36	58	6
2011	269	673	77	-27	210	11	30	81	-10
2012	449	671	130	31	280	19	29	63	7
2013	436	619	123	-18	324	20	29	75	-4
2014	361	611	127	-7	223	21	37	65	-2
2015	333	691	111	-27	225	16	36	73	-9
2016	446	641	150	33	260	23	34	59	7
2017	367	628	121	-26	221	19	38	70	-8
Mean	**383**	**660**	**141**	**-2**	**229**	**21**	**38**	**63**	**-1**

Table D.3: Summary of System Dynamics Seasonal Water Balance Components Results, Deep Cover

Year	Total PPT (mm)	Total PET (mm)	Total AET (mm)	ΔS (mm)	NP (mm)	AET as a Percentage of PET (%)	AET as a Percentage of PPT (%)	NP as a Percentage of PPT (%)	ΔS as a Percentage of PPT (%)
2005	329	705	310	14	4	44	94	1	4
2006	303	719	208	-7	102	29	69	34	-2
2007	250	687	196	-59	112	29	78	45	-24
2008	299	622	170	-93	222	27	57	74	-31
2009	161	644	187	-124	98	29	116	61	-77
2010	309	663	180	-77	205	27	58	66	-25
2011	188	673	114	-141	215	17	60	114	-75
2012	383	671	123	8	253	18	32	66	2
2013	351	619	205	-104	250	33	58	71	-30
2014	295	611	155	-5	146	25	52	49	-2
2015	257	691	142	-105	220	21	55	86	-41
2016	385	641	167	-24	242	26	43	63	-6
2017	271	628	165	-129	236	26	61	87	-48
Mean	**291**	**660**	**179**	**-65**	**177**	**27**	**64**	**63**	**-27**

Table D.4: Summary of System Dynamics Annual Water Balance Components Results Including Frozen Period Precipitation and NP, Deep Cover

Year	Annual PPT (mm)	Annual PET (mm)	Annual AET (mm)	Annual ΔS (mm)	NP (mm)	AET as a Percentage of PET (%)	Annual AET as a Percentage of PPT (%)	Annual NP as a Percentage of PPT (%)	Annual ΔS as a Percentage of PPT (%)
2005	464	647	304	56	103	47	66	22	12
2006	365	653	189	-7	183	29	52	50	-2
2007	394	647	185	-30	239	29	47	61	-8
2008	407	603	165	-26	268	27	40	66	-6
2009	262	615	180	-33	114	29	69	44	-13
2010	358	608	144	20	194	24	40	54	6
2011	260	642	105	-32	187	16	40	72	-12
2012	441	627	115	89	237	18	26	54	20
2013	429	574	191	-55	293	33	45	68	-13
2014	342	582	135	29	177	23	40	52	9
2015	309	668	118	-62	253	18	38	82	-20
2016	443	618	161	92	190	26	36	43	21
2017	316	577	113	-86	288	20	36	91	-27
Mean	**368**	**620**	**162**	**-3**	**210**	**26**	**44**	**58**	**-2**

Table D.5: R2 and RMSE for Simulated Soil Water Content to Measured Soil Content for Both Shallow and Deep Covers

Year	R^2		RMSE	
	Shallow Cover	Deep Cover	Shallow Cover	Deep Cover
2005	0.8	0.3	0.01	0.05
2006	0.8	0.4	0.01	0.03
2007	0.3	0.4	0.02	0.03
2008	0.5	0.5	0.02	0.02
2009	0.7	0.6	0.02	0.02
2010	0.7	0.6	0.02	0.02
2011	0.7	0.7	0.02	0.02
2012	0.7	0.5	0.02	0.02
2013	0.7	0.7	0.02	0.02
2014	0.8	0.5	0.02	0.02
2015	0.7	0.6	0.02	0.02
2016	0.7	0.5	0.02	0.02
2017	0.7	0.7	0.02	0.02
Mean	**0.7**	**0.5**	**0.02**	**0.02**

Table D.6: Summary of Simulated Seasonal Water Balance Components Results, Shallow Cover

Year	Total PPT (mm)	Total PET (mm)	Total AET (mm)	ΔS (mm)	NP (mm)	AET as a Percentage of PET (%)	AET as a Percentage of PPT (%)	NP as a Percentage of PPT (%)	ΔS as a Percentage of PPT (%)
2005	329	705	336	-14	7	48	102	2	-4
2006	303	719	284	-6	25	40	94	8	-2
2007	250	687	246	-17	21	36	98	8	-7
2008	299	622	268	-9	40	43	90	13	-3
2009	161	644	162	-25	24	25	101	15	-16
2010	309	663	314	-23	18	47	102	6	-7
2011	188	673	192	-39	35	28	102	19	-21
2012	383	671	339	28	16	51	89	4	7
2013	351	618	325	-28	53	53	93	15	-8
2014	295	611	285	-3	13	47	96	4	-1
2015	257	691	270	-29	16	39	105	6	-11
2016	385	641	348	0	37	54	90	10	0
2017	271	628	271	-18	18	43	100	7	-7
Mean	**291**	**660**	**280**	**-14**	**25**	**43**	**97**	**9**	**-6**

Table D.7: Summary of Simulated Annual Water Balance Components Results Including Frozen Period Precipitation and NP, Shallow Cover

Year	Annual PPT (mm)	Annual PET (mm	Annual AET (mm)	Annual ΔS (mm)	Annual NP (mm)	Annual AET as a Percentage of PET (%)	Annual AET as a Percentage of PPT (%)	Annual NP as a Percentage of PPT (%)	Annual ΔS as a Percentage of PPT (%)
2005	464	705	336	26	102	48	72	22	6
2006	365	719	284	-2	83	40	78	23	-1
2007	394	687	246	-5	153	36	62	39	-1
2008	408	622	268	3	136	43	66	33	1
2009	262	644	162	-9	109	25	62	42	-3
2010	358	663	314	-2	46	47	88	13	-1
2011	260	673	192	-17	85	28	74	33	-7
2012	441	671	339	38	64	51	77	14	9
2013	429	618	325	-13	117	53	76	27	-3
2014	342	611	285	-3	60	47	83	17	-1
2015	309	691	270	-20	60	39	87	19	-7
2016	443	641	348	47	48	54	79	11	11
2017	316	628	271	-13	57	43	86	18	-4
Mean	**368**	**660**	**280**	**2**	**86**	**43**	**76**	**24**	**0**

Table D.8: Summary of Simulated Seasonal Water Balance Components Results, Deep Cover

Year	Total PPT (mm)	Total PET (mm)	Total AET (mm)	ΔS (mm)	NP (mm)	AET as a Percentage of PET (%)	AET as a Percentage of PPT (%)	NP as a Percentage of PPT (%)	ΔS as a Percentage of PPT (%)
2005	323	647	316	-23	30	49	98	9	-7
2006	300	653	295	-29	34	45	98	11	-10
2007	240	647	291	-92	41	45	121	17	-38
2008	298	603	341	-112	68	57	114	23	-37
2009	154	615	214	-114	55	35	139	36	-74
2010	273	608	309	-93	57	51	113	21	-34
2011	180	642	269	-154	65	42	150	36	-86
2012	375	627	378	-17	14	60	101	4	-4
2013	344	574	368	-124	100	64	107	29	-36
2014	277	582	282	-33	27	48	102	10	-12
2015	233	668	326	-117	24	49	140	10	-50
2016	382	618	400	-53	36	65	105	9	-14
2017	219	577	303	-144	60	52	138	28	-66
Mean	**277**	**620**	**315**	**-85**	**47**	**51**	**117**	**19**	**-36**

Table D.9: Summary of Simulated Annual Water Balance Components Results Including Frozen Period Precipitation and NP, Deep Cover

Year	Annual PPT (mm)	Annual PET (mm)	Annual AET (mm)	Annual ΔS (mm)	Annual NP (mm)	Annual AET as a Percentage of PET (%)	Annual AET as a Percentage of PPT (%)	Annual NP as a Percentage of PPT (%)	Annual ΔS as a Percentage of PPT (%)
2005	464	647	316	19	129	49	68	28	4
2006	364	653	295	-29	98	45	81	27	-8
2007	394	647	291	-63	166	45	74	42	-16
2008	407	603	341	-44	110	57	84	27	-11
2009	262	615	214	-23	71	35	82	27	-9
2010	358	608	309	3	46	51	86	13	1
2011	260	642	269	-45	36	42	104	14	-17
2012	441	627	378	64	-1	60	86	0	15
2013	429	574	368	-75	136	64	86	32	-17
2014	342	582	282	1	59	48	83	17	0
2015	309	668	326	-74	58	49	105	19	-24
2016	443	618	400	62	-19	65	90	-4	14
2017	316	577	303	-100	113	52	96	36	-32
Mean	**368**	**620**	**315**	**-23**	**77**	**51**	**86**	**21**	**-7**

Table D.10: Mean Water Balance Components Results for the MLSB Site

Mean Results of Water Balance Components	Shallow Cover		Deep Cover	
	System Dynamics Approach (mm)	Simulated Approach (mm)	System Dynamics Approach (mm)	Simulated Approach (mm)
Annual PPT	368	368	368	368
Annual AET	141	280	162	315
Growing season, NP	168	25	180	47
Frozen season, NP	61	61	33	33
Annual NP	229	86	213	80
Annual ΔS	-2	2	-3	-23

APPENDIX E

Site Photographs


2008.07.25 06:52


June 2009


September 2010


October 2012


July 31, 2013


May 2014


August 2015


June 2016


February 2017